UNIVERSITÉ DE MONTRÉAL

FLUIDIZED BED BIOMASS GASIFICATION

RAMIN RADMANESH
DÉPARTEMENT DE GÉNIE CHIMIQUE
ÉCOLE POLYTECHNIQUE DE MONTRÉAL

THÉSE PRÉSENTÉE EN VUE DE L'OBTENTION
DU DIPLOME DE PHILOSOPHIAE DOCTOR
(GÉNIE CHIMIQUE)
JANVIER 2006

Your file Votre référence
ISBN: 978-0-494-17013-7
Our file Notre référence
ISBN: 978-0-494-17013-7

UNIVERSITÉ DE MONTRÉAL

ÉCOLE POLYTECHNIQUE DE MONTRÉAL

Cette thése intitulée:

FLUIDIZED BED BIOMASS GASIFICATION

présentée par : RADMANESH Ramin
en vue de l'obtention du diplôme de: Philosophiae Doctor
a été dûment acceptée par le jury d'examen constitué de:

M. LEGROS Robert, Ph.D., président
M. CHAOUKI Jamal, Ph.D., membre et directeur de recherche
M. GUY Christophe, Ph.D., membre et codirecteur de recherche
M. PATIENCE Gregory-S., Ph.D., membre
M. BERRUTI Franco, Ph.D., membre

ACKNOWLEDGEMENTS

I wish to express my sincere gratitude to those who helped me in the completion of this thesis. First of all, I am indebted to my supervisors, *Professor Jamal Chaouki* and *Professor Christophe Guy*, for their kind guidance, helpful suggestions, encouragement and confidence in me.

I would like to extend my thanks to my friends and colleagues for sharing with me their friendship and knowledge. I am thankful to *Mr. Pierre Sauriol* for his generous nature and help during the first years of my Ph.D at École polytechnique. The interesting discussions I had with *Dr. Yann Courbariaux* were always useful in my research and I am thankful to him. I also need to thank *Mr. Rachid Mabrouk* for his assistance in particle tracking experiments. My thanks also go to *Mr. Babak Esmaile* and *Mr. Nick Virgilio* for carrying out SEM and X-ray tests on my behalf, *Ms. Tania Tzakova* for translating the extended abstract into French, and *Dr. Gregory Kennedy* and *Mr. Jean St. Pierre* for activating the tracers.

A special thanks goes to the entire technical staff of the Chemical Engineering Department. In particular, I wish to thank *Mr. Daniel Dumas* for installing the reactor and his help during the course of experiments and *Mr. Jean Huard* for his technical support. I am also equally thankful to *Robert*, *Carol* and *Éric*.

RÉSUMÉ

La gazéification de la biomasse a été étudiée dans un lit fluidisé à bulles. De nombreuses réactions chimiques sont impliquées dans une réaction de gazéification. La pyrolyse constitue la première étape d'une réaction de gazéification ou de combustion de combustibles solides tels que le charbon et la biomasse. Dans les lits fluidisés à bulles de biomasse (LFBB), les produits des réactions de pyrolyse subissent d'autres réactions chimique. Tout ceci a lieu à l'intérieur même d'un lit fluidisé qui présente une température élevée ($T \geq 800^{o}C$) ou bien dans l'espace libre au dessus du lit. Deux aspects des LFBB, c'est à dire la pyrolyse et l'hydrodynamique des lits fluidisés à haute température sont les sujets principaux de cette étude.

Dans une première étape, la réaction de pyrolyse de plusieurs types de biomasse a été étudiée. La TGA ou analyse thermogravimétrique a été utilisée en conjonction avec des techniques de chromatographie en phase gazeuse (GC). La TGA permet de générer la dévolatilisation de la biomasse alors que le GC permet l'analyse de la composition des gaz issus de la pyrolyse. L'utilisation simultanée des deux techniques permet d'obtenir une représentation complète de la pyrolyse et des produits générés lors de cette dernière. Faire varier les rampes de température a permis d'étudier leurs effets sur la composition des gaz émis. Les résultats expérimentaux montrent que le rendement des différents produits dépend des rampes de chauffage que la biomasse subit dans la thermobalance.

A partir de ces résultats, des modèles cinétiques ont été développés pour décrire la cinétique de dévolatilisation globale et les émissions individuelles de gaz. Le modèle cinétique a été subséquemment modifié pour prendre en compte le changement de rendement d'émissions selon la rampe de chauffage.

Dans une seconde étape, la dynamique de phases et le mélange de particules solides ont été étudiées dans un lit fluidisé à hautes températures (25-700°C). Les LFBB sont des bons exemples de réacteurs qui opèrent à des températures élevées. Pour la première fois la technique de Traçage d'une Particule Radioactif (TPR) a été employée à haute température pour étudier l'hydrodynamique d'un lit fluidisé. Un traceur particulaire constitué d'oxyde de scandium et d'une densité et taille proche de celles de la taille des particules du lit a été utilisé. Le traceur a été placé dans le lit fluidisé à haute température après avoir été activé à 200-300 μCi dans le réacteur nucléaire de l'École Polytechnique de Montréal.

Les rayons gamma émis par le traceur ont été détectés par 8 détecteurs NaI à scintillation placés autour du lit. Les rayons gamma reçus par les détecteurs sont utilisés pour localiser le traceur dans le lit fluidisé. Larachi *et al.* (1995) ont décrit les détails de la reconstruction de la position du traceur par TPR. La distribution des vitesses du traceur indique la dynamique de phase dans le lit. A plus haute température, le traceur passe plus de temps dans les bulles et moins dans l'émulsion. Ce résultat est cohérent avec le travail précédemment effectué dans notre laboratoire sur la structure

de l'écoulement dans un lit fluidisé de particules de FCC (Cui et Chaouki, 2004) des concentrations de particules plus faibles dans la phase dense ont été trouvées à haute température. Le changement de la dynamique de phase affecte le mélange des particules solides. Le mélange des particules a aussi été étudié en utilisant un modèle de mélange à contre-courant à haute température (CCBM) (May, 1950). L'unique paramètre ajustable du modèle (le coefficient de transfert entre la phase ascendante et descendante (K_w)) a été calculé en ajustant le modèle CCBM sur le réponse de concentration de particules lors de l'injection d'un traceur.

L'injection d'une grande quantité de traceurs a été rendue possible par l'application de la théorie d'ergodicité (Cassanello *et al.*, 1996; Mostoufi et Chaouki, 2001; Larachi *et al.*, 2003). Le coefficient de transfert de masse entre les deux phases à contre-courant (K_w) calculé dans ce travail à une température de 25-400°C était de l'ordre de 0.7-1.6 s^{-1}.

L'effet de la température sur certaines caractéristiques de la fluidisation a aussi été étudié. La méthode présentée par Mostoufi et Chaouki (2004) a été utilisée pour dériver la vitesse des bulles à partir de données de TPR. Il a été trouvé qu'à hautes températures (T>400°C) des déviations existent entre la vitesse des bulles calculées avec les corrélations et celles calculées à partir des données de TPR. Cela implique que la vitesse des bulles ne peut être estimée seulement en considérant les propriétés physiques du gaz interstitiel. Les temps caractéristiques montrent des changements

significatifs avec la température pour des particules de sable. Le nombre de saut (déplacements rapides) (Stein *et al.*, 1997, 2000) est plus important en augmentant la température ce qui montre une augmentation du nombre de bulles.

La dernière étape de ce travail est une tentative de modéliser la gazéification de la biomasse dans un lit fluidisé à bulles. Deux modèles de cinétique de pyrolyse différents (Nunn *et al.*, 1985; Radmanesh *et al.*, 2005a) incluant celui développé lors de la première étape de ce travail, en conjonction avec le modèle de mélange (CCBM) pour des particules solides (charbon) ont été utilisés à cette étape. Certains des paramètres hydrodynamiques requis tels que le coefficient de transfert de masse (K_w) ont été obtenus par TPR (Radmanesh *et al.*, 2005b). En plus de la pyrolyse, d'autres réactions homogènes et hétérogènes ont été prises en compte dans le modèle de LFBB. Les expériences ont été menées sur du bois de hêtre dans un lit fluidisé en utilisant de l'air comme agent gazéifiant. Le modèle permet de prédire la composition et le rendement de différents gaz pour des conditions d'opérations variées. Une analyse de sensibilité a été faite sur certains paramètres d'opération importants de la gazéification tels que la proportion air/biomasse, la température du lit et la localisation de l'alimentation du lit (alimentation par le haut ou le bas).

ABSTRACT

In this thesis, biomass gasification was studied in a bubbling fluidized bed reactor. Many chemical reactions are involved in gasification. Pyrolysis is the first step that takes place in gasification and combustion of solid fuels such as biomass and coal. In bubbling fluidized bed gasifiers (BFBG) of biomass materials, the products of pyrolysis are subject to further chemical reactions. This takes place in a bed that is at a high temperature of $T \geq 800^{o}C$ or in the freeboard area of the reactor. Two aspects of BFBGs, i.e. pyrolysis and hydrodynamics of a fluidized bed at high temperatures, are the main subjects of this study.

In the first step, pyrolysis of three biomass materials was studied. Thermogravimetry analysis (TGA) was employed alongside with gas chromatography (GC) technique. TGA provides the overall devolatilization of biomass and GC accounts for the individual gases released during pyrolysis. The ensemble use of these two techniques provides a complete picture of pyrolysis and the range of products in it. Different heating rates were used in the TGA experiments to investigate its effect on product distribution in pyrolysis. Experimental results show that yield of different gases depends on the heating rate that the biomass experiences during the pyrolysis in the thermobalance. Based on the obtained experimental results, kinetic models were developed for overall devolatilization and individual gas releases. The kinetic model

for the individual gas release was then modified to account for the change in the yield of gases with heating rates.

In the second step, phase dynamics and solids mixing were studied in a fluidized bed at high temperatures (25-700°C). BFBGs are an example of reactors that operate at relatively high temperatures. For the first time, Radioactive Particle Tracking (RPT) was employed at high temperatures to study the hydrodynamics of a fluidized bed reactor. A single solid tracer was made of scandium oxide with density and size close to those of the bed particles. The tracer was placed in the fluidized bed at high temperature after being activated to 200-300 μCi in the SLOWPOKE nuclear reactor at the nuclear engineering department of the École Polytechnique de Montréal. The γ-rays emitted from the tracer were detected by eight NaI scintillation detectors located around the bed. The γ-rays counts received by the arrays of detectors were used to locate the tracer in the fluidized bed. Larachi *et al.* (1995) have described the details of tracer position reconstruction in RPT. The distribution of the tracer velocity shows a change in the dynamics of the phases in the bed. At higher temperatures, the tracer spends more time in the bubbles phase and less in emulsion. This was consistent with previous work done in our lab on the flow structure of FCC particles at high temperature using fiber optics (Cui and Chaouki, 2004), where lower solid concentration of the dense phase was found at higher temperatures. The change in phase dynamics affects the mixing of solids phase. The latter was studied as well, using a counter-current back mixing model (CCBM) (May, 1950) at high temperatures. The

sole adjustable parameter of the model, i.e. transfer coefficient between the ascending and descending phases (K_w), was calculated by fitting the CCBM model to the solid concentration response to a pulse injection of tracers. The pulse injection of a large number of tracers was doable by benefiting from ergodicity theory (Cassanello *et al.*, 1996; Mostoufi and Chaouki, 2001; Larachi *et al.*, 2003). The transfer coefficient between the counter-current phases (K_w) calculated in this work at a temperature range of 25-400°C was in the range of 0.7-1.6 s^{-1}.

The effect of temperature on some characteristics of fluidization was also investigated. The method presented by Mostoufi and Chaouki (2004) was used to infer bubble (wake) velocity from RPT experiments. It was found that at high temperatures (T>400°C), there exist deviations between the bubble velocities calculated from correlation and those calculated from RTP experiments. This implies that bubble velocity cannot be estimated solely by taking into account the physical properties changes of interstitial gas. The characteristic times (jump and cycle times) show significant changes with temperature for silica sand particles. The number of jumps (Stein *et al.*, 1997, 2000) increases by increasing the temperature which shows an increase in bubble frequency with temperature.

The last step of this work was an attempt to model a biomass BFBG. Two different pyrolysis kinetic models (Nunn *et al.*, 1985; Radmanesh *et al.*, 2005), including the one developed in the first step, along with a mixing model (CCBM) for solid particles

(char), were used in this stage. Some required hydrodynamic parameters such as transfer coefficient between the phases (K_w) were chosen based on RPT experiments at high temperatures (Radmanesh *et al.*, 2005b). Apart from pyrolysis, other heterogeneous and homogeneous reactions were taken into account to model BFBG. Experiments were carried out on beech wood gasification in the bubbling fluidized bed using air as a gasifying agent. The model was able to predict the compositions and yields of different gases for different conditions. A sensitivity analysis was done on some important operational parameters in gasification such as equivalent ratio (ER), bed temperature, and biomass feed location (top and bottom feeding).

CONDENSÉ EN FRANÇAIS

La concentration du dioxyde de carbone dans l'air a considérablement augmentée ces dernières décennies. Cette concentration qui était de 290 ppm pendant la période préindustrielle et qui est passée à 370 ppm de nos jours, provient principalement de la combustion de combustibles fossiles. Les changements climatiques des dernières années sont dus aux gaz à effet de serre et en particulier le dioxyde de carbone (CO_2). Le rôle du CO_2 dans les changements climatique a longtemps été un sujet de discussion dans la communauté scientifique. Aujourd'hui il est reconnu que les émissions de CO_2 dans l'air sont d'une grande importance dans les changements climatiques. Selon le Global Climate Change Initiatives (GCCI), les Etats-Unis doivent diminuer les émissions de CO_2 de 18% pour la fin l'année 2012 (Granite et O'Brien, 2005). L'Union Européenne (EU) a lancé une politique de réduction de l'émission de gaz à effets de serre avant certains pays comme les États-Unis et le Canada (Maniatis et Millich, 1998). Le livre blanc sur l'énergie de la Commission européenne prévoit la réduction des émissions de gaz à effet de serre en faveur des sources d'énergie renouvelables de 5 % en 1997 à 12 % en l'an 2010. Le protocole de Kyoto exige que les pays industrialisés réduisent leurs émissions de gaz à effet de serre de 6 pour cent du niveau de 1990 en 2012. Le Canada compte atteindre cet objectif durant la période 2008 à 2012.

Les efforts de développement de technologies et de stratégies visant à la réduction des émissions de CO_2 se sont intensifiés récemment. Deux stratégies principales pour limiter le niveau de l'émission de CO_2 se sont développées simultanément :

- La séquestration et le captage du CO_2 (Varma *et al.*, 2005; Eide *et al.*, 2005)

- L'utilisation de sources alternatives d'énergies qui ne produisent aucune ou très peu d'émissions de CO2 par unité d'énergie produite

Parmi tous les choix d'énergie renouvelable, la biomasse est celle qui a le potentiel le plus élevé. La biomasse est rapidement produite par des processus naturels, aussi elle est abondante et elle est considérée comme la troisième ressource énergétique après le pétrole et le charbon (Vamvuka *et al.*, 2003; Liang et Koziski, 2000). De plus, le CO_2 qui est émis par la conversion thermique de la biomasse est naturellement séquestré par le processus de photosynthèse.

Il est non seulement important d'utiliser la biomasse comme source d'énergie, mais aussi de sélectionner le bon procédé thermique qui la transformera. La transformation de biomasse en électricité à partir d'un procédé de gazéification présente plus d'avantages que la combustion. La gazéification est un processus thermique qui convertit les combustibles solides en combustibles gazeux par oxydation partielle en présence de l'air ou de vapeur d'eau.

L'efficacité du procédé de gazéification est plus élevée que celle de la combustion directe. D'ailleurs, en raison d'un rendement plus élevé des turbines à gaz comparées à celui des turbines à vapeur, la production d'électricité par l'intermédiaire de la gazéification de biomasse dans un cycle combiné de gazéification à gaz (IGCC) augmente l'efficacité de génération d'électricité de 22 à 37 pour cent. Le gaz produit par le gazéifieur à biomasse, cependant, doit être nettoyé du goudron et de la matière particulaire avant d'entrer dans la turbine à gaz.

Beaucoup de réactions sont impliquées dans la gazéification. Ces réactions peuvent être classifiées par types: pyrolyse primaire, pyrolyse secondaire ou craquage de goudrons et différentes réactions homogènes et hétérogènes. Dans un lit fluidisé, ces réactions sont importantes ainsi que le transfert de chaleur et de masse qui a lieu dans le lit fluidisé et la zone de désengagement. La pyrolyse primaire est la première étape qui est quasiment instantanée comparée aux autres réactions chimiques impliquées dans la gazéification. Les substances volatiles, le charbon de bois et le goudron libérés pendant la pyrolyse sont sujets à d'autres réactions chimiques dans le lit fluidisé ou dans la zone de désengagement. Par conséquent, les points suivants sont très importants dans la modélisation et la prédiction de la production de gaz dans un gazéifieur à lit fluidisé à bulles:

- La réaction de pyrolyse qui détermine le rendement en gaz provenant de cette étape. Puisqu'il y a une présence élevée des composés volatils dans la biomasse, la pyrolyse est une étape prédominante comparée aux autres combustibles solides.

- L'hydrodynamique du lit et plus particulièrement le mélange du solide à des températures élevées.

La cinétique de la pyrolyse primaire de biomasse a été étudiée activement dans le passé. Les produits principaux issus de la pyrolyse sont les gaz volatils (H_2, CH_4, CO et CO_2), ainsi que le goudron et le résidu solide (charbon). Un modèle cinétique, qui peut prévoir le rendement des tous les produits est essentiel dans le design et la mise à l'échelle des réacteurs de combustion et des gazéifieurs. Cette compréhension du modèle cinétique est importante parce que dans la gazéification la valeur calorifique finale du gaz produit dépend de sa composition. Le goudron produit durant la pyrolyse primaire se décompose thermiquement dans le secteur de la zone de désengagement et de cette manière les gaz formés présents dans le mélange final sont plus stables. En outre, si le produit final de la pyrolyse est de la bio-huile dans ce cas une prédiction précise du goudron sera importante.

La plupart des études effectuées sur la pyrolyse se concentrent seulement sur la dévolatilisation totale (Shafizadeh *et al.*, 1977; Varhegyi *et al.*, 1989; Gronli *et al.*, 2002). Ces modèles peuvent prévoir seulement le rendement en résidu solide bois et la période finale de dévolatilisation, et ils ne sont pas suffisants pour la modélisation ou la mise à l'échelle. Des modèles semi globaux ont été également présentés (Di Blasi, 1998). Bien que les modèles semi-globaux puissent prévoir le rendement des réactions de carbonisation, le goudron et le mélange de gaz, ils ne peuvent pas prévoir le rendement des différents gaz. Peu de travaux ont été consacrés à la prédiction de la gamme complète de produits, y compris le rendement des gaz stables finaux tels que H_2, CH_4, CO et CO_2 (Nunn *et al.*, 1985; Bilbao *et al.*, 1995; González *et al.*, 2005) et le goudron. Le premier objectif de la première partie de cette étude est donc de fournir une représentation plus complète de la pyrolyse de la biomasse en tenant compte de la gamme entière des produits de la pyrolyse.

Pour l'étude de la pyrolyse de la biomasse deux méthodes sont utilisées: l'analyse par thermogravimétrie (ATG) et la chromatographie en phase gazeuse (GC). La première méthode permet l'étude de la dévolatilisation globale de la biomasse, tandis que la deuxième se consacre à l'évolution des gaz pendant la pyrolyse. L'évolution des quatre gaz principaux, c.-à-d. H_2, CH_4, CO et CO_2, peut être détectée par la chromatographie en phase gazeuse. Ces derniers sont les produits les plus abondants pendant la pyrolyse. Le goudron et l'eau, qui sont la partie condensable du produit ne peuvent pas être détectés par la chromatographie en phase gazeuse et pour cette raison ils sont analysés

par un bilan de matière dans le système. Suite à l'analyse par les deux méthodes, une gamme complète des produits de biomasse pendant la pyrolyse est fournie en utilisant le système de TGA/GC.

Pour pouvoir faire la présente étude, différentes biomasses ont été choisies. Ces biomasses se composent de deux types de bois : bois de meuble et bois de hêtre canadien ainsi que des écorces de riz. La cellulose en tant que produit commun a été employée également comme standard pour la comparaison et la calibration du système de mesure. Pour pouvoir faire l'étude de l'effet du taux de chauffage avec une thermo-balance sur le rendement des gaz et les produits de carbonisation, différents taux de chauffage sont choisis (5, 10, 20, 30, 50 K/min).

Un modèle cinétique est mis au point à partir des résultats expérimentaux. Un modèle basé sur trois réactions en parallèle est utilisé pour la prédiction de la dévolatilisation totale de la biomasse tandis qu'une cinétique de premier ordre est employée pour la formation des gaz de pyrolyse. Une analyse non linéaire des moindres carrés est employée comme critère d'évaluation pour déterminer les paramètres cinétiques. Afin d'obtenir une cinétique plus fiable qui permet la prédiction du rendement global de la pyrolyse, l'effet de la rampe de chauffage sur la pyrolyse a été pris en considération en adaptant une cinétique simple aux expériences exécutées à différents taux de chauffage. Les résultats de l'évolution de la concentration du gaz ont prouvé que le rendement de gaz augmente en augmentant le taux de chauffage. Ceci a été aussi été observé dans

d'autres travaux (Gonzalez *et al.*, 2005; Bilbao *et al.*, 1995). La rapidité de l'augmentation de la température de la biomasse dans le réacteur dépend du type du réacteur et varie selon les conditions d'opération. Par conséquent, il est important de relier le taux de chauffage dans la particule de biomasse au rendement de gaz. Pour cette raison, un changement simple a été mis en application dans le modèle cinétique et qui tient compte des changements du taux de chauffage. Il est également démontré dans ce travail, que le modèle développé pour une condition de chauffage était capable de prévoir le rendement total de dévolatilisation à une condition de chauffage modérée différente.

Il a été mentionné plus haut que l'arrangement complexe de la réaction durant la gazéification doit être couplé à l'hydrodynamique du lit fluidisé. Pour cette raison, la deuxième partie de ce travail est consacrée à l'étude hydrodynamique des lits fluidisés à température élevée. La gazéification et la combustion, comme beaucoup d'autres processus industriels, ont lieu à des températures élevées. Néanmoins, la plupart des études hydrodynamiques dans des réacteurs à lit fluidisé ont été effectuées à température ambiante. Il y a un manque certain de données obtenues à des températures élevées.

Puisque les réactions hétérogènes dans la gazéification se passent en phase solide, un modèle de mélange de particules peut s'avérer utile dans la modélisation d'un gazéifieur à lit fluidisé à bulles. Le mélange du solide dans un lit fluidisé à température

élevée est étudié en utilisant la technique de traçage de particules radioactives. Cette technique non intrusive permet de suivre le mouvement d'un traceur radioactif dans un lit chaud rempli avec des particules solides. Le réacteur à lit fluidisé utilisé dans cette étude est fait en acier inoxydable et résiste aux températures élevées. Il se compose d'un lit et d'un d'une zone de désengagement de 0.078 m et 0.75 m de hauteur respectivement, de trois bandes de chauffage, d'une boîte à vent, qui sert également au préchauffage, et d'une zone de dégagement de 0.15 m et de 0.90 m de hauteur. Les surfaces externes du de la boîte à vent, et du lit sont enveloppées avec des bandes chauffantes qui permettent de maintenir la température du lit à 800°C. Le gaz de fluidisation dans toutes les expériences est de l'air. La phase solide est composée de particules du groupe B de la classification de Geldart (sable et alumine). Un traceur radioactif, composé d'oxyde de scandium avec une densité et une taille proches de celles du matériel du lit, est placé dans le réacteur à lit fluidisé. Huit détecteurs, placés à distance de la surface chaude du réacteur, ont été utilisés pour détecter les rayons γ émis par la particule radioactive. Les quantités de rayons γ qui sont comptés par le détecteur sont enregistrées et employées pour déterminer la position de la particule du traceur dans le lit. Les différentes expériences sont effectuées à des températures variables du lit de 25 à 700°C et à des vitesses superficielles de gaz de 0.16 à 0.78 m/s. Chaque expérience dure environ 4 à 5 heures.

Pour procéder à la modélisation du mélange solide dans le lit composé de particule de sable chaud, un modèle du rétromélange à deux phases et à contre courant est employé

(May, 1950). Ce dernier modèle est connu pour être plus robuste et décrivant mieux les phénomènes étudiés comparé que le modèle de dispersion (Lim *et al.*, 1995). Du fait du nombre restreint de données expérimentales sur les phases en contre courant, le modèle de rétromélange à deux phases en contre courant n'a pas été employé aussi souvent que le modèle de dispersion.

La technique de traçage de particules radioactives qui est utilisée dans ce travail a fournit des informations sur les phases en contre courant et de cette manière il est possible de trouver le seul paramètre du modèle qui n'est pas connu et qui est le coefficient de transfert entre les phases (K_w). Ce paramètre peut être ajusté et il est calculé en adaptant le modèle du rétromélange à deux phases en contre courant à la concentration du solide résultant d'une injection pulsée de traceur. Cela est rendu possible grâce à la théorie d'ergodicité (Cassanello *et al.*, 1996; Mostoufi et Chaouki, 2001; Larachi *et al.*, 2003). Dans le présent travail K_w a été calculé à des températures élevées du réacteur à lit fluidisé et ses valeurs se situaient dans la gamme de 0.7-1.6 s^{-1}.

La distribution de la vitesse des particules solides dans le lit suit une tendance gaussienne avec une vitesse moyenne de zéro. Il est constaté qu'en augmentant la température, dans la gamme de 25 à 400°C, la distribution des particules solides à proximité de zéro diminue. Cette dernière remarque démontre que le temps passé par les particules solides dans la phase d'émulsion, là où la vitesse des particules solides est

proche de zéro à cause du mouvement brownien, a diminué. Cette découverte est conforme avec les résultats présentés par Cui et Chaouki (2004).

Certaines caractéristiques de la fluidisation à température élevée sont également calculées en utilisant les résultats de RPT. La vitesse de bulle a été éstimée à partir des résultats de RPT basés sur la méthode de calcul présentée par Mostoufi et Chaouki (2004). La vitesse de bulle lors de la fluidisation des particules de sable de silice dévie de la valeur prévue par les corrélations existantes pour des températures de 500 à 700°C, ce qui suggère que la vitesse de bulle ne peut pas être prédite en tenant compte seulement du changement, en fonction de la température, des propriétés physiques du gaz. Il a été trouvé que le saut et la durée du cycle (Stein *et al.*, 2000) changent aussi avec la température.

Chacune des deux premières parties de ce travail ont éclaircissent les différents aspects de la gazéification dans un lit fluidisé. Dans la dernière partie de cette étude, ces deux parties sont combinées ensemble pour former un modèle de gazéification de biomasse pour un gazéifieur à lit fluidisé à bulles. Les résultats de la pyrolyse de biomasse servent durant la première étape qui a lieu dans un gazéifieur à lit fluidisé à bulles, et le modèle du rétromélange à deux phases en contre courant est employé comme modèle de mélange des particules de résidus solide dans le lit. La sensibilité du modèle du rapport équivalent (RE), la température du lit ainsi que la localisation de l'alimentation au réacteur est étudiée. Également, le modèle est comparé aux résultats expérimentaux

de cette étude (avec une l'alimentation de bois de hêtre) mais aussi avec d'autres travaux expérimentaux tirés de la littérature. Ce modèle permet de prédire la composition et la valeur calorifique du gaz produit par la gazéification de la biomasse dans un gazéifieur à lit fluidisé à bulles.

TABLE OF CONTENTS

LIST OF TABLES

LIST OF FIGURES

LIST OF APPENDICES

LIST OF SYMBOLS

CHAPTER 5

E	Activation energy (kJ/mol)
i	Each component in the biomass (Cellulose, hemicellulose or lignin)
k_0	Pre-exponential constant (s^{-1})
$k_{v:}$	Constant in Equation (5.9) (min/K)
N	Number of data points in experiments
Obj	Objective function in optimization
P	Number of adjustable parameters
t	Time (s)
T	Temperature (K)
V	Volatile released during pyrolysis
V^*	Total volatile available for a gas component
W	Weight of the biomass (mg)
Y	Total yield of devolatilization

Greek letters

β Heating rate in TGA experiments (K/min)

Subscripts

c	Cellulose
hc	Hemicellulose

l	Lignin

CHAPTER 6

C	Concentration of particles
d	Diameter, m
f	Fraction of the ascending/descending phases in the bed
H	Height of the bed, m
K	Exchange coefficient between the countercurrent phases, 1/s
Re	Reynolds number
U	Velocity of the particles in the ascending or descending phases, m/s
u	Gas velocity, m/s

Greek letters

ε	Voidage
δ	Bubble fraction in bed

Subscripts

as	Ascending phase
b	Bubble
ds	Descending phase
m	Maximum
mf	Minimum fluidization
w	Wake

CHAPTER 7

Ar	Archimedes Number
u	Gas velocity (m/s)
d	Bubble diameter (m)
Re	Reynolds number

Greek letter

Θ	Granular Temperature (m^2/s^2)
σ	Variance
ε	Bubble fraction in bed

Subscript

mf	Minimum fluidization condition
w	Wake
g	Interstitial gas
b	Bubble

APPENDIX A

C_i	concentration of component i, kmol/m^3
C_p	heat capacity, J/kg K
d	diameter, m
E	activation Energy, kJ/mol
h_{conv}	convective heat transfer coefficient, W/m^2 K
K_g	thermal conductivity of gas, W/m K
$k_{0,i}$	frequency factor for component i, 1/s
M_i	molecular weight of component I, kg/kmol
N	Total number of data points in TGA experiments
n_p	parameter in Equation (A.6)
r_i	rate of reaction for component i
r_{w-g}	water gas shift's reaction rate
Re	Reynolds number
Pr	Prandtl number
T_b	bed temperature, K
T_p	particle temperature, K
u	gas velocity in the freeboard, m/s
V_i	release volatile matter, wt%
V_i^*	ultimate final yield for component i in pyrolysis
V_p	volume of the wood particle, m^3
X_{tar}	mass fraction of the tar in the gas stream, wt%

X_{vm}	volatile content in the wood, wt%
y_i	total volatile yield for component i
Z	height of the freeboard, m

Greek letters

α_i	contribution coefficient in Equation (A.9)
ε	emissivity coefficient
φ	Parameter in Equation (A.6)
ρ_i	density of component i, kg/m^3
υ	stoichiometric coefficient

CHAPTER 1

INTRODUCTION

The concentration of CO_2 during the past decades has risen drastically. The observed increase of CO_2 in the atmosphere, from about 290 ppm in the pre-industrial era to the current 370 ppm, has come mainly from fossil fuel combustion. The dramatic climate changes in recent years have pinpointed greenhouse gas emissions and in particular CO_2, as the main contributors. Despite the debates of the last years, there is now a broad consensus among the scientific community about the role played by CO_2 in climate change. Even in the United States, according to the Global Climate Change Initiatives (GCCI), the greenhouse gas intensity should be decreased by 18 percent by the year 2012 (Granite and O'Brien, 2005). The European Union (EU) initiated a policy to reduce the emission of CO_2 long before the USA and Canada (Maniatis and Millich, 1998). A European Commission White Paper on energy included a plan for reducing greenhouse gas emissions from 5 in 1997 up to 12 percent in the year 2010, through the promotion of renewable energy sources. The Kyoto Protocol mandates that industrialized countries reduce greenhouse gas emissions to 6 percent below 1990 levels by the year 2012. Canada has aimed to achieve this goal by the period between 2008 and 2012.

Technologies and strategies aimed at reducing the emission of CO_2 have gained momentum recently. Two main strategies have been followed simultaneously to curb the level of emissions:

- The sequestration and capture of CO_2 (Varma *et al.*, 2005; Eide *et al.*, 2005).

- The use of alternative energy sources that give off no-- or less-- CO_2 per unit of produced energy.

Among all the renewable energy sources, biomass material undoubtedly represents the highest potential. Biomass materials are rapidly replenished by natural processes. They are also abundant and stand as the third energy resource after oil and coal (Vamvuka *et. al.*, 2003; Liang and Koziski 2000). Moreover, the CO_2 emitted from the thermal conversion of biomass material is naturally sequestered by the photosynthesis.

Apart form the advantages of using biomass as a source of energy, choosing the right and suitable thermal process to convert biomass into energy has vital importance. The biomass-to-electricity system based on gasification has been proved to be a promising conversion technology and has certain advantages over combustion. Gasification is a thermal process that converts solid fuels to combustible gaseous fuel through partial oxidation in the presence of air and/or steam. The efficiency of gasification is higher than direct combustion. Moreover, due to higher efficiency of gas turbines compared

to steam turbines, power generation via biomass gasification in an Integrated Gasification Combined Cycle (IGCC) increases the electrical efficiency by 22-37 percent. Product gas from a biomass gasifier, however, must be cleaned from the tar and particulate matter before entering the gas turbine.

Many reactions are involved in gasification. These reactions can be summarized as primary pyrolysis, secondary pyrolysis or tar cracking and different homogeneous and heterogeneous reactions. In a fluidized bed, these reactions should be taken into consideration in conjunction with the heat and mass transfers that take place in the bed and freeboard. Primary pyrolysis is the first step that takes place instantaneously, compared to the other chemical reactions involved in gasification. The volatile matter, char and tar released during the pyrolysis are subject to other chemical reactions in the fluidized bed or the freeboard of the reactor. Therefore, understanding the following points is essential in modeling and predicting the product fuel gas composition from a bubbling fluidized bed gasifier (BFBG):

- Pyrolysis kinetics is important in biomass gasification because it determines the gas yields. Due to larger volatile content in biomass compared to the other solid fuels, pyrolysis is an even more influential step in the case of biomass materials.

- Hydrodynamics of the bed and in particular solids mixing at elevated temperatures.

The kinetics of biomass primary pyrolysis has been studied extensively in the past. The main product of pyrolysis can be lumped into volatile gases (H_2, CH_4, CO and CO_2), tar and char. A kinetic model, which can predict the yield of the products, is essential in modeling and scale-up of combustors and gasifiers. This is because, in gasification, the final heating value of the product gas depends on its composition. Tar material resulting from the primary pyrolysis decomposes thermally in areas such as the freeboard of fluidized beds and thus contributes to the formation of more stable end-product gases. Furthermore, if the final product of the pyrolysis is bio-oil, then the accurate prediction of the tar is important.

Most studies carried out on biomass pyrolysis focus only on the total devolatilization (Shafizadeh and Chin, 1977; Varhegyi *et al.*, 1989; Gronli *et al.*, 2002). These kinds of models can predict only the final char yield and time of devolatilization, which are insufficient for modeling or scale-up. Semi-global models have also been presented (Di Blasi, 1998). Although these models can predict the yield of char, tar, and gas, they cannot predict the yield of individual gases. Fewer studies have been devoted to prediction of the total range of products, including stable end-product gases such as H_2, CH_4, CO and CO_2 (Nunn *et al.*, 1985; Bilbao *et al.*, 1995; González *et al.*, 2005) and tar.

Thermogravimetry analysis (TGA) and gas chromatography (GC) are used simultaneously in this work to explore pyrolysis of biomass. The former leads to the

overall devolatilization of biomass, whereas the latter provides the evolution of the gases during the pyrolysis. The evolution of four main gases, i.e. H_2, CH_4, CO and CO_2 can be detected by GC; these are the most abundant gases produced during the pyrolysis. Tar and water, which are the condensable part of the product and cannot be detected by GC, are determined through a mass balance in the system. Therefore, a complete picture of biomass pyrolysis is provided using the system of TGA/GC.

In modeling BFBGs, the reaction scheme of gasification should be coupled with the hydrodynamics of the fluidized bed. This necessitates a hydrodynamic study of the fluidized bed at high temperatures. Gasification and combustion, like many other processes, take place at elevated temperatures. Nevertheless, most hydrodynamic studies on fluidized bed reactors are carried out at ambient temperatures. There is certainly a lack of data for high temperatures. Since the heterogeneous reactions in gasification come about in the solid phase, a solids mixing model can be helpful in the modeling of a FBG.

It is well known that the mixing of solids in a gas fluidized bed is induced by bubbles. Bubbles carry solids up in their wakes. The rising of the bubbles also causes solids to drift in the bed. This upward movement of solids is known as the bubble-induced drift of solids. A downward movement of solids also takes place to compensate for the upward movement of solids. These ascending and descending phases are responsible for the mixing in the bed.

Radioactive particle tracking (RPT) was used in this work to study solids mixing and phase dynamics in the fluidized bed at high temperatures. The local position of a single tracer, which is placed in the bed at high temperature, is provided in a non-intrusive manner. The tracer has a density and diameter close to the bed material. Its position in the bed provides extensive information on fluidization, including the ascending (descending) phase, bubble (wake) and instantaneous (and time average) velocities.

Dispersion model (DM) (May, 1959) and two- or three-phase counter-current back-mixing models (CCBM) (van Deemter, 1967) are the most important models used in the literature on the study of solids mixing. While the DM model has demonstrated less satisfactory results, the CCBM model is known to be a more robust and phenomenological model (Lim *et al.*, 1995). Unlike the dispersion model, the CCBM model considers the underlying mechanism involving solids mixing in the bed. The model considers the bed as a multiple-phase system with an upward flow of solids in the wake and drift phases and a downward flow in the dense phase. Mass exchange occurs between these counter-current phases. A mass balance between the phases results in a system of partial differential equations that describes phenomena. The use of the CCBM model to study solids mixing has been impeded due to the scarcity of experimental data on counter-current phases and bubble phases. RPT, however, provides enough information on both ascending and descending phases over a long period of time and this can be used to derive the mixing parameter (exchange coefficient) in the CCBM model.

CHAPTER 2

LITERATURE REVIEW

2.1 Introduction:

Gasification is the thermal conversion of solid fuels such as coal, municipal solid waste (MSW) and biomass to gaseous fuel. It takes place at temperatures higher than T>800 in the presence of a gasifying agent that can be oxygen, air, steam/air or even carbon dioxide/air. Unlike combustion, however, it takes place in an atmosphere lean in oxygen.

The main products of gasification are stable gases such as H_2, CH_4, CO, CO_2, H_2O, and heavy hydrocarbons with low dew points known as tar. The high heating value of the product gas depends on the gasifying agent and it may vary from 4-6 MJ/Nm^3 in air gasification to 10-18MJ/Nm^3 in steam or oxygen gasification. Oxygen gasification is not economically attractive because it requires pure oxygen. Moreover, for small units with limited flow rate of biomass feed, it may not be feasible. Steam gasification stimulates the water-gas shift reaction which, in turn, increases the concentration of hydrogen in the product gas and leads to a higher heating value. The typical concentration of fuel gas in air-blown gasification is H_2 10%, CH_4 4%, C_2H_2 2%, CO 12 %, CO_2 15%, N_2 55% and in steam-blown gasification, H_2 45-55%, CH_4 10-5%, CO 30- 5 %, CO_2 15-26% on a dry basis.

Table 2.1 depicts the gasification mechanism and the involved reactions. The first step in gasification (and combustion) is drying and pyrolysis of biomass. The products of this step - char, stable gases and tar - undergo further homogeneous and heterogeneous reactions. In a combustion environment, the combustion of volatile gases is complete. However, in a gasification environment, where the gas is lean in oxygen, complete

Table 2.1: Gasification mechanism and reactions

Step	Chemical Reactions	ΔH (kJ/mol)
Pyrolysis	Biomass→ $H_2 + CO + CO_2 + CH_4 + H_2O$ + tar + char + ash	Endothermic
Gasification reactions	$\lambda C + O_2 \rightarrow 2(\lambda-1)CO + (2-\lambda)CO_2$	-111
Boudouard reaction	$C + CO_2 \leftrightarrow 2CO$	+172
Water-gas reaction	$C + H_2O \rightarrow CO + H_2$	+131
Methanation	$C + 2H_2 \rightarrow CH_4$	-75
Tar Cracking	Tar $\rightarrow \upsilon_{H2}H_2 + \upsilon_{CH4}CH_4 + \upsilon_{CO}CO + \upsilon_{CO2}CO_2$	Endothermic
Homogeneous reactions	$H_2 + 1/2O_2 \leftrightarrow H_2O$	-242
	$CH_4 + 2O_2 \rightarrow CO_2 + 2H_2O$	
	$CO + 1/2O_2 \rightarrow CO_2$	-283
Water-gas Shift reaction	$CO + H_2O \rightarrow H_2 + CO_2$	-41
Steam methane reforming	$CH_4 + H_2O \leftrightarrow CO_2 + 2H_2$	+206

combustion does not occur. As Table 2.1 shows, some of the reactions involved in gasification, namely pyrolysis, are endothermic. Gasification, however, is an autothermal process, which means that the heat required for thermal decomposition of biomass and tar cracking is provided by the combustion of char and some part of the volatiles. The ratio of the biomass-to-oxidizing agent should be adjusted in such a way

that, on the one hand, the autothermicity of the whole process is guaranteed and, on the other hand, maximum heating value is obtained for the fuel gas. The equivalence ratio, defined as the ratio of the actual air-to-biomass to the air-to-biomass mass flow rate required for combustion is, hence, an important parameter in biomass gasification.

The heating value of the fuel gas from air-blown biomass gasifiers is diluted with nitrogen and, as a result, the heat content of the gas is low. This makes combustion of this gas in a regular furnace close to impossible. As a result, co-processing of biomass with another feedstock such as coal has gained attention (Andre *et al.*, 2005; McLenndon *et al.*, 2004). Some industries produce large volumes of seasonal waste. The co-gasification of coal and biomass is advantageous in this case because it replaces some of the fossil fuel in the season when the waste is available without needing to shut down the plant. The co-combustion of product gas, from air-blown biomass gasification with natural gas in a regular furnace, is another option that helps replace some of the natural gas with a renewable energy source.

The route from biomass to syngas is another promising application of gasification (Panigrahi *et al.*, 2003; Chaoudhari *et al.*, 2003). In a recent article, Levenspiel (2005) has suggested coal as a substitute to oil for syngas production. The process involves steam gasification of coal followed by the use of existing Fischer-Tropsch reactions to produce synthetic fuels. Unfortunately, there is no mention of biomass material in the

article. Likewise, the same route presented for coal-to-syngas, can be adopted for biomass-to-syngas:

$$Biomass + Steam \longrightarrow CO + H_2 \xrightarrow{fischer-tropsch} gasoline \quad (2.1)$$

In fact, the challenge in syngas production, from either biomass or coal, lies in the separation of CO_2 and N_2 from the CO/H_2, as well as conversion of CH_4, tar and other hydrocarbons to H_2. This necessitates that further reactions, such as catalytic steam reforming of the hydrocarbons, gas shift reaction step and CO_2 sequestration (Varma *et al.,* 2005; Eide *et al.*, 2005) be undertaken.

2.2 Biomass Pyrolysis

As mentioned earlier, pyrolysis is an important step in both gasification and combustion of biomass materials. The kinetic information of pyrolysis, hence, is crucial in modeling and scale-up of gasifiers. A large number of studies have addressed the kinetics of biomass pyrolysis. In fact, the literature on this subject is voluminous. Many models were initially developed for coal and were later extended to biomass. This is not surprising because biomass is actually nothing but young coal. Biomass material, however, constitutes higher volatile content and less fixed carbon, which makes the prediction of gases and tar yields resulting from pyrolysis more important.

Kinetic models of biomass pyrolysis range from simple, first order, one-step models (Di Felice *et al.*, 1999) to more complicated two- or three-steps with parallel or series reactions (Thurner and Mann, 1981; Koufopanos *et al.,* 1989)

Kinetic parameters have often been determined by fitting the experimental data, usually obtained by thermogravimetric analysis (TGA), to the model. Since biomass is composed of cellulose, hemicellulose and lignin, some kinetic models have been proposed, which are the superposition of kinetic models for each constitute of biomass materials (Cozzani *et al.*, 1997; Orfao *et al.*, 1999; Vamvuka *et al.* 2003).

Miller and Bellan (1997) have classified pyrolysis kinetic models into two primary categories: micro- and macro-particle models.

Micro-particle models: In micro-particle models, the sample size is so small that heat transfer and diffusion effect on pyrolysis of biomass particle can be neglected and pyrolysis is controlled by kinetics alone.

Different kinetic schemes have been suggested to describe pyrolysis. The products of pyrolysis in all these kinds of modeling are generally lumped to char, tar or vapors and volatiles. The majority of the models can only predict the total volatile yield or char yield. These types of models are not useful in applications such as gasification and combustion, where individual gas yield is important in design and scale-up. Kinetic

schemes are proposed based on experimental evidence. Table 2.2 shows some kinetic schemes available in the literature.

Table 2.2: Kinetic schemes of the biomass pyrolysis (V=Virgin biomass, AC=Active Cellulose)

Model #	**Biomass**	**Kinetic scheme**	**Reference**
1	Cellulose	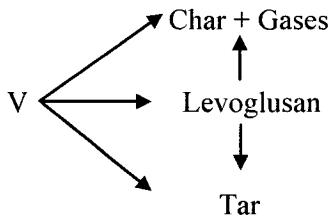	Shafizadeh (1968)
2	Cellulose	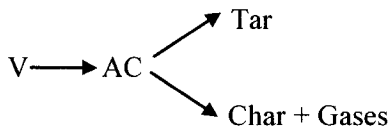	Bradbury and Shafizadeh (1979)
3	wood	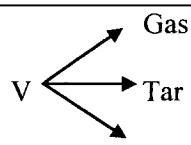	Thurner and Mann (1981)
4	Wood	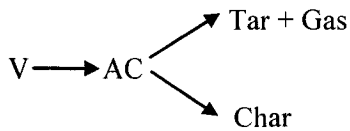	Koufopanos *et al.* (1989)
5	Wood	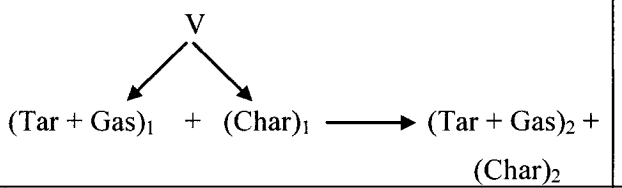	Koufopanos *et al.* (1991)
6	Cellulose	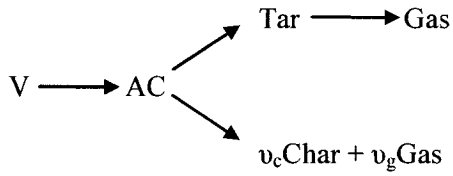	Di Blasi (1996)

Anthony and Howard (1976) proposed an interesting kinetic scheme that is called the distributed activation energy model (DAEM). It was originally introduced to model coal pyrolysis. DAEM is more complicated than the other kinetic models because it assumes that devolatilization occurs through an infinite number of first order reactions. Each reaction has the same pre-exponential value but a different activation energy. If the number of reactions is large enough, which is reasonable in the case of biomass gasification, the change in activation energy can be considered continuous and, as a result, there is a distribution of activation energy. The integration of all the weight losses due to each reaction, by taking into account the distribution of the activation energy, gives the overall weight loss or char yield of the pyrolysis.

Macro-particle models: In macro-particle models, pyrolysis is strongly affected by heat transfer and diffusion limitations, which cause a temperature gradient inside the particle (Di Blasi, 1996b; Di Blasi, 1997; Koufopanos, 1991). This effect has been observed at a critical limit of particle size, which is reported to be around d_p>1 mm. Macro-particle models are more sophisticated because they deal not only with reaction kinetics but also with heat and mass transfer, and particle thermal properties. It is well known that both endothermic and exothermic reactions are involved during pyrolysis. Pyle and Zaror (1984) and Koufopanos *et al.* (1991) have reported the primary pyrolysis as the endothermic and the secondary pyrolysis, which is the reaction between the gas product and solid phase, as the exothermic reaction. The heat release and consumption in large particle sizes cause an important temperature gradient, which affects the kinetics.

Pyle and Zaror (1984) have coupled a kinetic scheme for pyrolysis with all the mass and energy balances for a single particle of biomass. They have developed criteria to classify four different regimes in the pyrolysis process. These are: 1) external heat transfer control; 2) internal heat transfer control; 3) kinetic control and; 4) a general model when the rates of all three processes are important. To classify the regimes the authors have introduced two dimensionless numbers: the internal pyrolysis number $P = k/(\rho c d_p^2 r)$ which is the ratio between conduction heat transfer and pyrolysis rate as well as Biot number B= $(h_c d_p)/k$, which signifies the relative importance of external to internal heat transfer. For P<<1 the process is under heat transfer control and, for P>>1, it is under kinetic control. Biot numbers greater than 1 result in internal heat transfer limitation while Biot numbers smaller than 1 lead to external heat transfer limitation.

Di Blasi and her associates at the Universita di Napoli have studied single biomass particle pyrolysis with considering the effect of transport phenomena in a series of papers (Di Blasi, 1996a, 1996b, 2002; Di Blasi and Branca, 2003). Di Blasi and Brance (2003) in an experimental attempt have measured the temperature of the lateral, top and center of wood particles inserted into a high temperature fluidized bed. The results show a time lag between the particle center and the surface temperature for particles larger than 2 mm in diameter.

Individual gas formation kinetics: Despite the importance of individual gas evolution in pyrolysis, only a few studies on the kinetics study of gas formation during pyrolysis can be found. Suuberg *et al.* (1978) have reported yields of different gas evolution in fast pyrolysis of lignite. Later on, using the same methodology, they calculated kinetic parameters for the major gas evolution in the fast pyrolysis of sweet gum hardwood in a batch reactor (Nunn e*t al.*, 1985). Hajalligol *et al.* (1982) and Bilbao *et al.* (1995) have derived kinetic parameters for the major gas released in the fast pyrolysis of cellulose and pine wood separately. The kinetic model used by these investigators was a single- step first order reaction. The effect of heating rate on gas yields, however, has not been addressed.

Secondary pyrolysis or tar cracking: Like gas formation kinetics in pyrolysis, only a few studies have been done on secondary pyrolysis reactions which involve the fate of tar and its thermal or catalytic cracking. Boroson and Howard (1989) and Liden *et al.* (1988) have reported separately kinetic parameters of the tar cracking derived from the wood. Their kinetic models are based on single-step, first order decomposition of tar into gas molecules. Their results show comparable rates and are the most used. Cozzani *et al.* (1995) have followed the same approach to find a kinetic model for the homogeneous tar cracking of Refused Derived Fuel (RDF) material.

2.3 Gasification Reactors

The reactors used for biomass gasification can be grouped into four categories: moving bed (MBG), bubbling fluidized bed (BFBG), circulating fluidized bed (CFBG) and entrained-flow gasifiers (EFG). Ciferno and Marano (2002) have recently listed fifteen commercialized technologies of biomass gasification at various stages of development. Seven of the technologies listed are BFBG, six are CFBG and only two are moving bed gasifiers.

Moving bed gasifiers are characterized by a moving bed of biomass that undergoes drying, pyrolysis, gasification and combustion in different zones of the reactor. The MBG can be categorized as counter-current (updraft) and co-current (downdraft). In the counter-current, the gas leaves the reactor at low temperature, resulting in both high thermal efficiency and low tar content. The capacity of this type of MBG is usually lower than 10 MWt (Beenackers, 1999). In the co-current MBG, the tar content is lower but it is difficult to scale-up and hence its maximum size is limited to 1 MWt. In general, the main drawbacks of MBG are the small installation size and poor mixing between feed and oxidant that result in poor heat and mass transfers.

Entrained-flow gasifiers have been used mostly for coal gasification. They are characterized by very high gas velocity and low residence time which, consequently, need a higher gasifier temperature to achieve reasonable carbon conversion. The high temperature and low residence time is advantageous because it leads to no-- or less-- tar

compared to other types of gasifiers. Nonetheless, high temperature gives rise to slagging of the ash. Higman and Van der Burgt (2003) have reported that although the ash content in the biomass has a low melting point compared to that of coal, at the same time it is very aggressive in the molten state. This disadvantage, along with the necessity of small particle size of biomass in the entrained-flow gasifier, has restricted

the use of this type of reactor for biomass gasification. No attempts at commercializing the biomass EFG have been reported (Ciferno and Marano, 2002).

Bubbling fluidized bed and *circulating fluidized bed* are the more appealing reactors for biomass gasification. The advantage of fluidized bed reactors are: better solid mixing, improved heat transfer in the bed, uniform temperature (in BFBG), high carbon conversion, and the possibility of in-bed use of a catalyst for tar cracking.

Most studies in pilot scales have been devoted to these two types of reactors. Table 2.3 summarizes some of the important biomass gasification studies in pilot bubbling and circulating fluidized beds.

Different biomass materials have been used in gasification experiments. They range from wood (Geyer *et al.*, 2000; Li *et al.*, 2004; Narvaez *et al.*, 1996; Gil *et al.*, 1999; Corella *et al.*, 1991; Herguido *et al.*, 1992), manure (Beck *et al.*, 1980), rice husk

Table 2.3: Biomass pilot plant gasifiers

Gasifier type	Biomass type	Gasifying agent	Temperature (°C)	Catalyst	Reference
CFBG	wood residues	air	800	N/A**	Li *et al.* (2004)
BFBG	wood	air-steam	750	N/A	Beck and Wang (1980)
BFBG	Pure cellulose	steam	600-800	High Temperature	Hoveland *et al.* (1985)
CFBG	Not specified	steam	850	N/A	Walawender *et al.* (1985)
BFBG	Pine sawdust	air	800	N/A	Narvaez *et al.* (1996)
BFBG	-Pine sawdust -cereal straw -thistle	steam	650-780	N/A	Herguido *et al.* (1992)
BFBG	Not specified	air	780-920	Fixed bed of dolomite catalyst	Olivares *et al.* (1997)
BFBG	-pine flakes -bagasse	steam	750	Fluidized bed Nickel catalyst	Baker *et al.* (1987)
BFBG	Cellulosic waste	steam	660-810	Fixed bed Calcined silica sand	Corella *et al.* (1991)
BFBG	Lignocellulose	Steam/ air	720-760	Fixed bed Steam reforming catalyst	Caballero *et al.* (2000, 1997)
BFBG	Pine sawdust	steam	800-880	Fixed bed Calcined dolomite ,magnesite and calcite	Delgado *et al.* (1996)

Table 2.3: Biomass pilot plant gasifiers, cont.

BFBG	Almond Shell	steam	800-850	Olivine Calcined dolomite	Rapagna *et al.* (2000)
BFBG	Small chips of pine	air/steam steam/O_2	750-780	N/A	Gil *et al.* (1999)
CFBG	Different agricultural waste	air	850	N/A	Van der Drif *et al.* (2001)
CFBG	char	CO_2 CO_2/O_2	900-970	N/A	Fang *et al.* (2001)
BFBG	Pine chips and coal blend	steam/air	840-910	N/A	Padban *et al.* (2000)
BFBG	Poplar clones	steam	595-617	N/A	Geyer *et al.* (2000)
Twin CFBG (gasification and combustion)	RDF wood	air	650-1000	N/A	Paisley *et al.* (1990)

*ICFBG: Internally Circulating Fluidized Bed Gasifier

**N/A: No Catalyst was used

(Mansaray *et al.*, 1999; Mansaray *et al.*, 2000), plastic material, cellulose (Hoveland *et al.*, 1985; Walawender *et al.*, 1985) and biomass-derived char (Chaudhari *et al.*, 2001).

Beck *et al.* (1979, 1980) at Texas Tech University were among the first to initiate biomass gasification experiments. They succeeded in producing a medium calorific gas (8-11 MJ/Nm^3) by feeding wood and manure separately in an air-blown fluidized bed reactor. The energy balance of the reactor shows that the reaction can be performed

auto-thermally without the need for an external source of energy. However, their experimental setup lacks a suitable technique to separate and measure tar quantity.

Walwender *et al.* (Walawender *et al.*, 1985; Hoveland *et al.*, 1985) at Kansas State University have carried out steam gasification of cellulose in a bubbling fluidized bed. They have showed that bed and freeboard temperatures are the most important parameters that affect the yields of gases. In the first part of their experimental work, they showed two different gasification regimes. The first regime is dominated by cracking of tar and takes place in the temperature range of 500 to 660°C. The second regime is dominated by water-gas shift reaction at temperatures above 660°C. The effect of freeboard temperature on gas yield and composition was also studied by implementing a uniform high temperature in the freeboard area. The results show drastic changes in gas composition when the freeboard temperature is 83°C higher than the bed temperature.

In Canada the research group of Esteban Chornet at Université de Sherbrooke initiated some gasification experiments of biomass material (Bilodeau *et al.*, 1993). Mansaray *et al.* (1999) at Dalhousie University have carried out gasification of rice husk in a dual-distributor bubbling fluidized bed gasifier. Li *et al.* (2004) at the University of British Columbia have carried out gasification of different wood residues in a pilot plan CFBG.

Spain has been the leading European country in studying biomass gasification. Several research groups throughout Spain have studied various aspects of biomass gasification in bubbling fluidized beds. Herguido *et al.* (1992) have gasified different biomass and lignocellulosic residues (sawdust, straw, chips, thistle) in a BFBG. They have reported difficulties in feeding this type of material. In order to overcome this problem, they have recommended crushing the material to a size under about 5 mm and using agitator in the feeding system.

Narvaez *et al.* (1997) have studied the effect of six operational variables on the quality of the produced gas in an atmospheric BFBG of pine sawdust. They have also modified the feeding system of the reactor to make feeding of biomass fuel directly into the bed (bottom feeding) possible. They have studied the effect of bed temperature, equivalence ratio (ER), H/C ratio fed to the gasifier, additional gas injection into the freeboard as well as the effect of dolomite in the bed on produced gas composition, higher heating value (HHV) of the gas, tar and gas yields. The produced gas composition in the air-blown gasifers is highly affected by ER. The results show that by increasing the ER, the HHV of produced fuel gas decreases. The best value for the ER was reported to be around 0.25 but tar production is very high at this value. In-bed use of dolomite shows a minimum of 40% reduction in tar content of the produced fuel gas.

Tar cracking: Developments in biomass-to-electricity conversion relies on the cracking of tar and production of a tar-free fuel gas. Moreover, up-grading of the product gas is important in biomass-to-syngas conversion. Many studies have been devoted to tar cracking and up-grading (Arauzo *et al.*, 1997; Aznar *et al.*, 1993; Baker *et al.*, 1987; Caballero *et al.*, 1997; Caballero *et al.*, 2000; Corella *et al.*, 1998; Delgado *et al.*, 1996; Narvaez *et al.*, 1997; Rapagna *et al.*, 2000; Corella *et al.*, 2004; Wang *et al.*, 2005). Both in-bed use of catalysts (Olivares *et al.*, 1997; Orio *et al.*, 1997; Rapagna *et al.*, 2000) and secondary catalytic reactor (Aznar *et al.*, 1993; Caballero *et al.*, 1997; Caballero *et al.*, 2000; Corella *et al.*, 1998; Corella *et al.*, 2004; Narvaez *et al.*, 1997) have been reported. Sutton *et al.* (2001) have classified the catalysts used in cracking and up-grading of tar in three categories: dolomite ($MgCO_3.CaCO_3$), alkali metals and nickel catalysts. Dolomite has been reported to be effective in increasing gas yield and hence heating value of the gas (Orio *et al.*, 1997; Corella *et al.*, 1999), while the other two groups are effective for up-grading and composition adjustment of the gas (Aznar *et al.*, 1993; Caballero *et al.*, 1997; Corella *et al.*, 1998).

2.4 Modeling of Fluidized Bed Gasifiers

In general, two different approaches can be identified in modeling biomass gasification in BFBG. The first approach is a kinetic-free equilibrium calculation to estimate the final gas composition of product gas (Bacon *et al.*, 1985; Double *et al.*, 1985; Ruggiero and Manfrida, 1999; Mansaray *et al.*, 2000; Altafini *et al.*, 2003; Li *et al.*, 2004). The second approach, however, is more robust and takes into account the kinetics of the

reactions along with the hydrodynamics of the fluidized bed (de Souza-Santos, 1989; Hamel, 2001; Fiaschi and Michelini, 2001). The first approach is not a dynamic modeling and does not take into account the underlying chemical and transport phenomena, particularly pyrolysis and tar formation.

Double *et al.* (1989) have classified modeling of biomass gasification in BFBGs based on the equilibrium approach. In some studies, the whole gasifier has been considered as an equilibrium stage (Mansaray *et al.*, 2000; Li *et al.*, 2004) and, in other studies, only pyrolysis has been the equilibrium stage (Bilodeau *et al.*, 1993; Sadaka *et al.*, 2002). Mansaray *et al.* (2000) have used an ASPEN simulator to model rice husk gasification in a BFBG with a specially designed distributor. Bilodeau *et al.* (1993) and Sadaka *et al.* (2002) have used a semi-equilibrium model in which the gases resulting from pyrolysis have been accounted for through equilibrium calculations. The BFBG has been simulated by a two-phase model of fluidization (Kunii and Levenspiel, 1999). These models can predict the variations of temperature and gas concentration in the reactor but they lack the tar formation and its cracking.

The kinetic non-equilibrium models that couple pyrolysis, homogeneous and heterogeneous reactions (including tar formation and cracking) with transport phenomena in the fluidized bed are few. Corella *et al.* (2005) have recently and briefly reviewed the existing models for BFBGs.

In kinetic modeling of bubbling fluidized bed gasifiers (BFBGs), one needs the hydrodynamics of the bed along with the kinetics of pyrolysis and various homogeneous and heterogeneous reactions. Hydrodynamics of fluidized beds has been well studied. Most hydrodynamic characteristics of fluidized beds, however, have been derived at ambient temperature.

2.5 Solids Mixing in Fluidized Bed Reactors:

Gasification reactions take place in both gas and solid phases. The kinetic expressions of gasification reactions, when coupled with the flow models of the gas and solid phases in fluidized beds, lead to modeling of fluidized bed gasifiers. Moreover, mixing of solids in gas fluidized beds has a crucial impact on the reaction, heat and mass transfer in the bed. In gasification and combustion, poor mixing of solids leads to hot-spots in the bed and an abrupt change in temperature. Solid mixing also can affect the overall conversion of carbon in the bed. Furthermore, feeding biomass material into the reactor is a crucial issue. Solid mixing studies can be helpful in finding the best location to feed the biomass. This may reduce operational problems associated with feeding and can also improve the quality of mixing in the bed. In reactions such as exothermic catalytic reactions, the hot spots caused by poor mixing of solids may damage catalysts or cause operational failures.

It is well known that solids mixing in a gas-solid fluidized bed is induced by bubbles. Bubbles carry solids up in their wakes. The rising bubbles also cause solids to drift in

the bed. This upward movement of solid is known as the bubble-induced drift of solids. The downward movement of solids also takes place in the zones where there are fewer bubbles. These ascending and descending phases are responsible for the axial mixing in the bed. Lateral mixing also takes place in the bed through periodic disposal and replenishment of the wake, wake shedding and the bursting of bubbles at the surface of the bed.

The dispersion model and two- or three-phase counter-current back mixing models (CCBM) are the most important models used in the literature for solids mixing. May (1959) was among the first to use the dispersion model to study solid mixing in a large-scale fluidized bed by injecting radioactive solid tracers in the bed. While the DM model has demonstrated less satisfactory results, the CCBM model, first introduced by van Deemter (1967), is known to be more robust and phenomenological. Unlike the dispersion model, the CCBM model considers the aforementioned mechanism involving solids mixing in the bed. Although Lim *et al.* (1995) have reported the second approach to be more robust, its use has been restricted. The main hurdles in applying this model can be summarized as follows: 1) CCBM is a more complex model, which results in parabolic partial differential equations; 2) unlike the dispersion model which consists of only one model parameter i.e. the dispersion coefficient, the number of model parameters in the CCBM model can be as high as 6, depending on the number of phases considered in the model. This is a shortcoming of the model, especially when these hydrodynamic parameters are difficult to measure and are treated

as adjustable parameters; 3) the scarcity of the experimental data is another reason which have impeded the use of the CCBM model.

Several studies on the parameter estimation of the CCBM model can be found in the literature (Sitnai, 1981; Lakshmanan and Potter, 1990; Basesme and Levy, 1992; Lim *et al.*, 1993; Shen and Zhang, 1998; Hull *et al.*, 1999; Grasa and Abanades, 2002). Two types of experimental data are needed to appropriately estimate the exchange coefficient between the counter-current phases in the model. The first type of data can be obtained by pulse injection of solid tracers and it provides information on the solids gross behavior in the bed. Positron emission and γ-ray particle tracking (Dechsiri *et al.*, 2005; Mostoufi and Chaouki, 2001), digital image analysis (Grasa and Abanades, 2002; Lim *et al.*, 1993), and magnetic tracer injection (Sitnai, 1981) are some of these experimental techniques. The second type provides local instantaneous motion of individual particles and, consequently, provides information on ascending and descending phases in the bed. Radioactive particle tracking and image processing technique have been employed for the second type of data. In the absence of instantaneous data, some authors have treated the hydrodynamic parameters of the ascending and descending phases as adjustable parameters (Sitnai, 1989; Grasa and Abanades, 2002) while others have used hydrodynamic correlations or a measuring technique to estimate these parameters (Lim *et al.*, 1993).

Most studies on the mixing of solid based on CCBM model are lumped. For instance, Sitnai (1981), Grasa and Abanades (2002), as well as Lakshmanan and Potter (1990), have lumped the drift and bubbles wake into one ascending phase. Lim *et al.* (1993), Shen *et. al.* (1998) and Hull *et al.* (1999) have used only the wake (ascending) and emulsion phase (descending) in their study, which is again a lumped approach.

Despite the fact that industrial reactors operate at high temperatures, all the studies have been carried out at ambient temperature. The effect of temperature on the global solids mixing is still unexploited and missing.

CHAPTER 3

METHODOLOGY AND MATERIALS

Based on the literature review presented in Chapter 2, the following missing aspects in the gasification of biomass materials in bubbling fluidized bed reactors can be identified:

- *In the pyrolysis of biomass:* The majority of the studies on biomass pyrolysis account only for the total devolatilization and there are fewer studies on gas formation during pyrolysis. Moreover, the effect of heating rates on the gas formation has not been addressed. This is especially important in modeling biomass gasifiers, where biomass materials undergo different heating rates depending on the type of gasifiers and their operating conditions.

- *In the hydrodynamics of fluidized bed:* Fluidized bed combustion and gasification of solid fuels take place at the high temperature range of 800-1000°C. Bed particles in these types of fluidized beds usually consist of inert sand particles which belong to Group-B Geldart classification. The hydrodynamics of the fluidized bed, however, has been mostly studied at ambient temperature. There is certainly a lack of data for high temperatures.

3.1 Objectives

The primary objective of this work is to develop a model for biomass gasification in fluidized bed reactors. Based on the preceding literature review, two different but equally influential aspects of biomass gasification in a bubbling fluidized bed gasifier (BFBG) merge and give rise to a comprehensive model of a biomass BFBG. These two aspects are as follows:

1. Biomass pyrolysis

2. Gas-solid fluidization hydrodynamics at elevated temperatures

The specific objectives of the present study are as follows:

- To develop a kinetic model for the pyrolysis of biomass that can be used in the modeling of bubbling fluidized bed gasifiers (BFBG).

- To investigate the effect of temperature on the hydrodynamics of fluidized beds. Various hydrodynamic parameters are studied in this part:

    - Change in the phase dynamics with temperature.

- Solids mixing using a two-phase counter-current back-mixing model (CCBM).

- Effect of temperature on wake and bubble phase velocities.

- The effect of temperature on the characteristics of gas-solid fluidization. This includes characteristic times (i.e. jump and cycle time) and granular temperature.

- To develop a comprehensive modeling of a fluidized bed gasifier based on pyrolysis kinetic model and solids mixing studies. The model should be capable of predicting the composition of fuel gas products. The following characteristics should be part of the model:

  - Pyrolysis takes place instantaneously, compared to other chemical reactions and transport phenomena, and it provides the yield of different individual gases, char and tar.

  - The products of pyrolysis undergo further chemical reactions in the bed and freeboard.

  - A two-phase model (Kunii and Levenspiel, 1991) describes the flow of the gas phase in the bed.

- A counter-current back-mixing model (CCBM) describes the flow of the solid phase (char).

- Homogeneous and heterogeneous reactions take place in both solid and gas phases.

The originality of this work lies on the fact that it unifies two important aspects in fluidized bed gasification, which are the pyrolysis kinetics and hydrodynamics at elevated temperature.

3.2 Methodology

To tackle the aforementioned objectives, the following experimental strategies are undertaken:

- Thermogravimetry analysis and gas chromatography (TGA/GC) are used to study pyrolysis of biomass. TGA/GC provides the evolution of total mass loss and individual gas formations during pyrolysis at different heating rates. First order single-step kinetics for different gases and char are fitted to the experimental results to determine the kinetic parameters of the model.

- Radioactive particle tracking (RPT) at high temperatures (25-700°C) is used to investigate the hydrodynamics of the bed. Mixing of the solid phase and hydrodynamic characteristics of the bed are studied at high temperatures.

3.3 Characteristic of Materials

3.3.1 Biomass gasification

Table 3.1 shows the proximate and ultimate analysis of the biomass used in this work to study pyrolysis. Beech wood is selected as well for the gasification experiments in a bubbling fluidized bed reactor. The bed materials in the gasification experiments are silica sand particles that belong to Group-B Geldart classification. The characteristics of these particles are presented in the next section.

3.3.2 Hydrodynamic Study

Solids mixing is studied in a fluidized bed at high temperature using radioactive particle tracking (RPT). Silica sand and alumina particles (Group-B Geldart classification) are used in this study. Figure 3.1 shows the particle size distribution of the sand and alumina particles used in this work.

Table 3.1: Chemical analysis and heating values of the biomass used in this work

Analysis	Sawdust	Beech wood	Rice Husk
Elemental Wt%			
C	48.3	48.27	35.7
H	6.22	6.36	4.6
O	45.2	45.2	59.3
N	0.22	0.14	0.34
S	0.0	0.0	0.0
Proximate Wt%			
Char	16	18	17
Volatile matter	81	81	65
Ash	2.90	0.8	18
Heating value MJ/kg			
	19	19.4	11

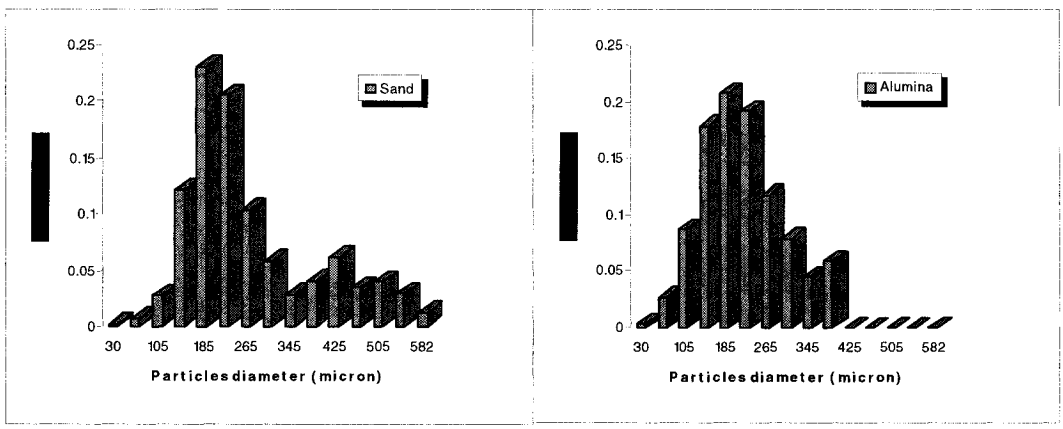

Figure 3.1: Particle size distributions of sand and alumina particles

CHAPTER 4

ORGANIZATION OF ARTICLES AND THESIS STRUCTURE

The thesis outline is as follows: Chapter 1 and 2 consist of an introduction and a literature review on biomass pyrolysis, as well as fluidized bed hydrodynamics at high temperatures. Chapter 3 presents the objectives, methodology and materials used in this study. Chapters 5 to 8 give shape to the main body of this thesis and corresponding scientific findings. Each of these chapters consists of an article. The following is a brief description of each chapter and the link between them:

- Chapter 5 deals with biomass pyrolysis. Pyrolysis, as mentioned in Chapter 2, is the first step in all thermochemical conversions of solid fuels, including *combustion* and *gasification*. Pyrolysis of three different types of biomass is studied in a system of TGA/GC. These include: Canadian beech wood, saw dust and rice husk. Cellulose is also used when it is needed for comparison or calibration purposes. The main objective of this part is to investigate the evolution of all products during the pyrolysis of the selected biomass. Kinetic models are also developed for total devolatilization and gaseous species (H_2 CH_4, CO and CO_2).

- Chapter 6 is devoted to solids mixing at elevated temperatures. Mixing of solid particles can be very influential in fluidized bed reactors. In *gasification* and

combustion, in particular, poor mixing may cause hot spots in the bed. Radioactive particle tracking at high temperature, for the first time, is employed to investigate solids mixing at high temperature. A two-phase counter-current back mixing model (CCBM) is used to describe mixing of solids. The parameter of the model is calculated by fitting the experimental data to the model.

- Chapter 7 explores the effect of temperature on some hydrodynamic characteristics of the bed at elevated temperatures (25–700°C).

- The results from Chapters 5 and 6 are used in Chapter 8 to model a bubbling fluidized bed gasifier of biomass materials. The model takes into account the mixing of char particles in the bed using the CCBM model and primary pyrolysis. The output of the model, which is the composition of the product fuel gas, is compared with the result obtained in this work and other studies in the literature.

Chapter 9 is a general discussion and a summary of results obtained in this study. Finally, the thesis presents a conclusion and options for future work in Chapter 10.

CHAPTER 5

A UNIFIED LUMPED APPROACH IN KINETIC MODELING OF BIOMASS PYROLYSIS*

5.1 Presentation of the Article

The objective of the first article is to study pyrolysis kinetics of some selected biomass materials in moderate heating rates (5, 10, 20, 30, 50 K/min). Two measuring techniques, i.e. thermogravimetric analysis (TGA) and gas chromatography (GC), are used simultaneously in order to explore the evolution of various products during pyrolysis. A kinetic model is fitted to the experimental results and the model parameters are calculated. The experiments reveal that gas yields depend on the heating rates that biomass particles undergo in the thermobalance furnace. An increase in the heating rate results in a rise in the gas yield of stable end-product gases and a decrease in tar yield. A modified kinetic model for gas formation during pyrolysis is presented that accounts for the change in gas yield by increasing the heating rate.

*Accepted in *FUEL*

5.2. A Unified Lumped Approach in Kinetic Modeling of Biomass Pyrolysis

Ramin Radmanesh, Yann Courbariaux, Jamal Chaouki*, Christophe Guy
Department of Chemical Engineering, École Polytechnique de Montréal,
P.O. Box 6079, Station Centre-ville, Montréal, QC H3C 3A7, Canada
Fax*: 514 340 4159; e-mail: *jamal.chaouki@polymtl.ca*

5.2.1 Abstract

Thermogravimetry analysis and gas chromatography techniques are used at different heating rates (from 5K/min to 50K/min) to map all the products and to develop suitable kinetic models of biomass pyrolysis. A three-independent-parallel-reactions model is used to model kinetic of total devolatilization. This part accounts for the total char yield and devolatilization time. The evolutions of condensable vapors (tar and H_2O) and non-condensable gases (H_2, CH_4, CO and CO_2) are also studied using gas chromatography. It is shown that the final total yield of gases increases by increasing the heating rate, whereas those of tar decrease by increasing the heating rate. A kinetic model was then proposed and the parameters were calculated that can predict the change of the gas yield at different heating rates. The performance of the kinetic models was evaluated for other experimental studies available in the literature or by exposing the biomass to a different heating program.

Keywords: Biomass; pyrolysis; kinetic model; gas evolution

5.2.2 Introduction

Fossil fuels have been considered as the main culprit for the recent climate changes. The accumulation of CO_2 in the atmosphere, the emissions of NO_X and SO_2 and other contaminants are all consequences of using non-renewable fossil fuels as energy resources. Biomass on the other hand, is a clean and renewable energy source. It is also abundant and stands as the third energy resource after oil and coal [1, 2]. Moreover, the burden of biomass waste management diminishes when it is used as an energy resource. Thermal conversion of biomass such as pyrolysis, combustion and gasification are the major route toward cleaner energy production. Pyrolysis is, however, the initial step in all the thermal conversions of biomass materials including combustion and gasification. The kinetic information of pyrolysis is essential in the modeling or scale up attempts of waste to energy production.

Kinetic of biomass primary pyrolysis has been studied extensively in the past. The main product of pyrolysis can be lumped into volatile gases (H_2, CH_4, CO, and CO_2), tar and char. A kinetic model, which can predict all the products yield, is essential in modeling and scale-up of combustors and gasifiers. This is because in gasification the final heating value of the product gas depends on its composition. Tar material resulting from the primary pyrolysis decomposes thermally in area such as freeboard of the fluidized bed and thus contributes to the formation of more stable end-product gases. Furthermore, if the final product of the pyrolysis is bio-oil then the accurate prediction of the tar is important.

Most studies carried out on pyrolysis focus only on total devolatilization [1-12]. These kinds of models can predict only the final char yield and time of devolatilization, which are insufficient for modeling or scale up. Semi-global models have also been presented [10-12]. Although the semi-global models can predict the yield of char, tar and gas, but, they cannot predict the yield of individual gases. Few works have been devoted to predict total range of products, including stable end-product gases such as H_2, CH_4, CO and CO_2 [13-18] and tar. The primary objective of this work is therefore to provide a more complete picture of biomass pyrolysis by taking into account the total devolatilization and gas evolution.

5.2.3 Literature Review

Thermogravimetry analysis has been used extensively to study pyrolysis of different carbonaceous materials, including biomass. Studies on biomass pyrolysis have been carried out in low and medium heating rates [3, 4, 7, 19], high heating rates and isothermal conditions [5, 8, 12, 20, 21]. The kinetic models and consequently the corresponding parameters depend on the experimental condition, especially heating rates in the dynamic experiments and final temperatures in isothermal operations.

Different kinetic models have been introduced by authors to describe pyrolysis kinetics. These models range from single step kinetics to parallel and consecutive reaction schemes [10, 11]. An appropriate kinetic model depends on the final application. Many

authors have reported a three independent parallel reaction model as the best kinetic model to describe the pyrolysis of wood at moderate heating rates [3, 4, 7, 9, 19, 22]. In this model the pyrolysis in wood is considered to be the result of thermal decomposition in each component of the wood (i.e. cellulose, hemicellulose and lignin).

Most studies based on the three independent parallel reactions model have been performed at a single heating rate [3, 4, 7, 9, 19, 22]. Since the effect of the heating rate on the devolatilization is eminent, the parameters calculated by fitting the model to a single heating rate experiment does not represent a lump kinetic parameters. Moreover, the applicability of such model to other heating conditions has not been yet verified.

Unlike total devolatilization kinetics, paucity in the kinetic study of gas formation in pyrolysis is evident. In general, most of the few studies on the gas evolution from biomass pyrolysis have been carried out at high heating rate [18, 17, 23, 24]. Bilbao et al. [15, 16] have studied the formation of gases from cellulose and pine sawdust pyrolysis in thick regime, where the effect of mass and heat transfer inside the particles are significant. Gonzalez et al [13, 14] have recently studied the pyrolysis of residual biomasses such as almond shell and cherry stones again in the thick regime. They have reported the effect of heating rate, in dynamic experiments, and final temperature in isothermal experiments on the formation of different end-product gases.

In all the studies done at moderate heating rates and mentioned above [13-16], it has been observed that yield of gases evolving during the pyrolysis, increases by increasing the heating rate (in dynamic experiments) or final temperature (in non-dynamic isothermal experiments). The traditional first order kinetic model in this case, results in a constant final yield for each gas, which does not depend on the heating rate experienced by the biomass particles. Therefore, it is not capable of predicting the variation of gaseous product yield with heating rate.

Based on the aforementioned literature review the specific objectives of the present work are as follows:

1. To apply three-independent-parallel-reactions model for char production or total devolatilization to three different biomasses and exploit the capability of this model in predicting total gas and volatile release during pyrolysis.

2. To test this model when the experimental conditions in TGA, notably the heating rate, differs from those with them the model parameters were derived.

3. To generate a complete picture of pyrolysis by taking into account the formation of volatile gases and tar during pyrolysis and develop a kinetic model which accounts for variation of product gases yields at different heating rates.

5.2.4 Experimental

5.24.1 Samples

Three different types of plant biomass were used in this study: two types of wood; Canadian beech wood and saw dust; and Chinese rice husk. Table 5.1 shows the proximate and ultimate analysis of the biomasses used in this study. Cellulose Avicel PH-101 was also selected, beside the mentioned biomass, as a standard material merely for the sake of comparison.

Table 5.1: Chemical analysis and heating values of the biomass used in this work

Analysis	Sawdust	Beech wood	Rice Husk
Elemental Wt%			
C	48.3	48.27	35.7
H	6.22	6.36	4.6
O	45.2	45.2	59.3
N	0.22	0.14	0.34
S	0.0	0.0	0.0
Proximate Wt%			
Char	16	18	17
Volatile matter	81	81	65
Ash	2.90	0.8	18
Heating value MJ/kg			
	19	19.4	11

5.2.4.2 Apparatus, Procedures and Calibration

Experiments have been carried out in a TGA/GC system. A Mettler-Toledo thermobalance, with a precision of 1 μg, was hooked up to a Varian micro-GC to study pyrolysis of biomass materials. The sample pan size in all the experiments was 4.5 mm ID × 4.5mm (~71μL). The temperature of the thermobalance furnace and sample were measured by means of two R-Type thermocouples, located on the furnace wall and beneath the sample holder, respectively. The difference between furnace temperature and that of sample were in the range of few degrees in all the experiments. Argon, with a flow rate of 45 ml/min, was used in all the experiments as the carrier gas. Experiments were performed at different heating rates (i.e. 5, 10, 20, 30 and 50K/min). The exiting gases from thermobalance were sucked by the sampling pump of the GC and injected into two parallel columns of the GC. Molecular sieve and Porapak columns were used simultaneously to separate the resulting gases. Two thermal conductivity detectors, at the end of each column, were used to detect quantity of Ar, H_2, CH_4, CO and CO_2 in the effluent gas. A two point external calibration, using standard gases composed of five gas components at different concentration, was employed for all the GC experiments.

Prior to the experiments, synchrony between the thermobalance and GC was tested using calcium oxalate. Calcium oxalate at high temperature decomposes to CO and CO_2. A comparison between the CO and CO_2 peaks, detected by GC, and weight loss peak, given by TGA, showed a lag time of 60 seconds. This time lag corresponds to the

traveling time of the gas stream between the thermobalance and GC. Thus, throughout the experiments, this time lag was considered and the temperature was corrected accordingly. The calcium oxalate decomposition is also a means to verify the accuracy of the GC measurement. A sample of 4mg of calcium oxalate ($CaC_2O_4.H_2O$) was used in the experiment. Figure 5.1 shows the decomposition curve obtained by TGA and evolution of CO and CO_2 detected by GC. The first drop in the mass loss curve is due to water release. The second and third mass losses are CO and CO_2 release, respectively. Good agreements between the theoretical yields and the ones measured by GC are found in this work.

Cellulose Avicel PH-101 was used as a standard material to verify the consistency of the results obtained in this study with other studies. Gronli et al. [25] in a round-robin study for the Cellulose pyrolysis have reported the TGA results from eight different laboratories in Europe. Table 5.2 compares the results obtained in this study with those reported by Gronli et al. [25]. A good agreement between the temperature peaks which is the temperature at maximum rate of devolatilization can be observed. The kinetic parameters also show a good consistency between the two studies

5.2.5 Kinetic Modeling

5.2.5.1 Total Devolatilization

Different models were employed in this work, among them the three-independent parallel reactions model fits well with the experimental results. This model considers

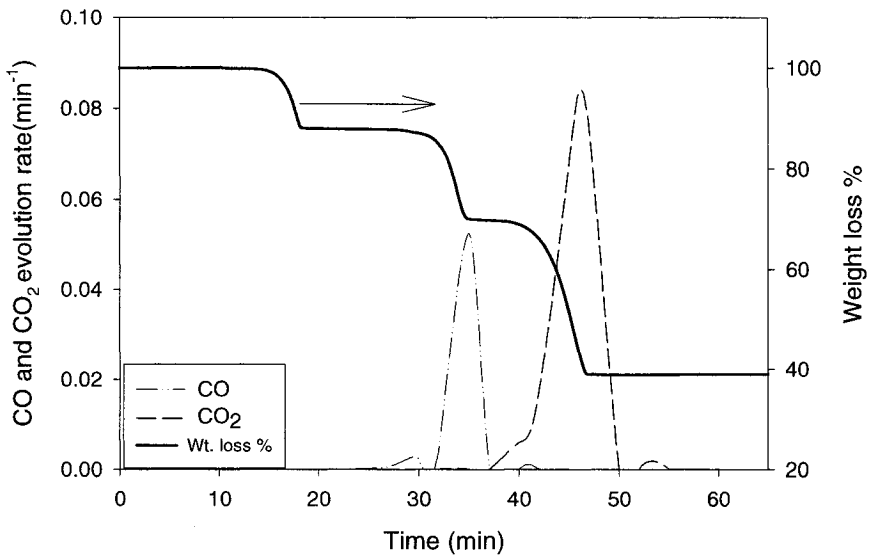

Figure 5.1: Decomposition of 4 mg of calcium oxalate in argon atmosphere. Line represents the weight loss from TGA and line-symbols represent CO and CO_2 mass flow rate calculated from GC results.

Table 5.2: Kinetic parameters for cellulose Avicel PH-101

Parameters	m_o (mg)	β (K/min)	T_{peak} (K)	log(k) (1/s)	E (kJ/mole)	Y_f (%)	Deviation %
This study	5.9	5	605	21.5	270	10	1.09
Gronli et al. [25]	___	5	592-609	17.8-21.1	234-263	5.2-13	_____

that the decomposition of the biomass takes place through the decomposition of its main components in a way that there is no interaction between the components. For each three components, one can write the following kinetic which relates the volatile release at time t to the activation energy and pre-exponential value for each component:

$$\frac{d\left(V_i/V_i^*\right)}{dt} = k_{0i}e^{-E_i/RT}\left(1-\frac{V_i}{V_i^*}\right) \tag{5.1}$$

where, V* is the total volatile available for each component in the virgin biomass. The total volatile release for the biomass is given by a linear correlation:

$$\left(\frac{V}{V^*}\right)_{Total} = \sum_i C_i \times \left(\frac{V}{V^*}\right)_i \tag{5.2}$$

C_i in the above equation corresponds to the contribution of each component to the total volatile release. One can relate the parameters V and V* to the weight of the sample which is a more relevant parameter in thermogravimetry by the following equation:

$$\frac{V}{V^*} = \frac{W_0 - W(t)}{W_0 - W(\infty)} = \frac{1-Y(t)}{1-Y(\infty)} \tag{5.3}$$

Where, $Y(t)$ and $Y(\infty)$ are instantaneous and final yield of devolatilization and W_o and $W(\infty)$ stand for the initial and final weight of the sample, respectively. At $t=\infty$, the right hand side of the above equation is 1 and thus:

$$\sum_i C_i \times \left(\frac{V}{V^*}\right)_i = 1 \; or \; \sum_i C_i = 1 \tag{5.4}$$

Total yield of the devolatilization is expressed then by the following equation:

$$Y(t)=1-(1-Y(\infty))\sum C_i \frac{V_i}{V_i^*} \tag{5.5}$$

The objective function used in this study is a quadrupled of error between experimental and calculated TG. Nonlinear least square analysis is used as the estimation criterion and is given by:

$$Obj=\frac{1}{N-P}\sum_{j=1}^{m}\sum_{i=1}^{N}\left(Y_i^{cal}-Y_i^{\exp}\right)^2 \tag{5.6}$$

where, m is the number of experiments done at different heating rate and N is the number of data points for each experiments. The deviation between the model and the experimental result was calculated using the following equation throughout this study:

$$\text{deviation}=100\times(\text{obj})^{1/2}. \tag{5.7}$$

5.2.5.2 Gas Release

A simple one step reaction has been used for the kinetics of each gas evolution during the pyrolysis [15, 17]. The presentation of the kinetic model is as follows:

$$\frac{d(V_i)}{dt}=k_{0i}e^{-E_i/RT}\left(V_i^*-V_i\right) \tag{5.8}$$

where, V_i is the yield of gas component at time t and V_i* is the ultimate attainable yield for each gas. This model is consistent with the total devolatilization model described earlier by Equation (5.1). As mentioned before and the experimental results show, the final yield of each gas increases by increasing heating rate. However, the kinetic model

described by Equation (5.8) results in the same final gas yield (V_i*) for different heating rates. In order to make the kinetic model more versatile and applicable for different heating rates we consider the dependency of the V_i* on the heating rare. This is done by using a simple first order kinetic which describes the change in the concentration of convertible precursor in the virgin biomass to a certain gas component i. This can be described as follows:

$$\frac{dV^*}{d(1/\beta)} = -K_v V^* \quad \text{or} \quad V^* = V_\infty^* \exp(-K_v/\beta) \tag{5.9}$$

where, β is the heating rate and $V_\infty{}^*$ is the maximum attainable yield at $\beta \rightarrow \infty$.

5.2.6 Results and Discussion

5.2.6.1 Total Devolatilization Kinetic

The same approach as presented by Courbariaux [26] was used to study the possible interference of transport processes on the kinetics of devolatilization. Experiments at different heating rates, initial sample weight and particle size were carried out. The results show no distinct change in weight loss curves from one experiment to the others done at different initial weight (5, 10 and 15 mg) and particles size (d_p<1 mm, 355 μm<d_p<600 μm and d_p<355 μm). This proves that transport processes, in the range of sample weight and particle size of this study, do not interfere with the kinetics of devolatilization, which is in agreement with previous investigations [27, 28]. Knowing that the sample weight and size are well below the limit where the inter and intra-

particle transportation may affect the kinetics, an initial weight of 5 mg and size of d_p<1 mm was chosen in this study. The approximate height of the biomass sample inside the sample pan at this condition was close to 1-2 mm. Figure 5.2 shows the DTG curve obtained for the pyrolysis of the three samples of biomass listed in Table 5.1 at a heating rate of 30 K/min. The same type of curves has been found at different heating rates of 5, 20 and 50 K/min. The curves have the typical appearance of pyrolysis of lignocellulose materials. Two distinct peaks are distinguished clearly in all the DTG curves. The first peak, which occurs at lower temperatures, is related to the hemicellulose. The decomposition of the hemicellulose starts at 504-515 K for each biomass samples. The second peak, which starts at temperatures in the range of 580-615 K, corresponds to cellulose decomposition. The decomposition of cellulose attains its maximum at temperatures in the range of 620-650K. The lignin, as the third major component in the all the biomass samples, decomposes slowly in a broader temperature range thus, it can not be distinguished as a distinct peak in any of the DTG curves.

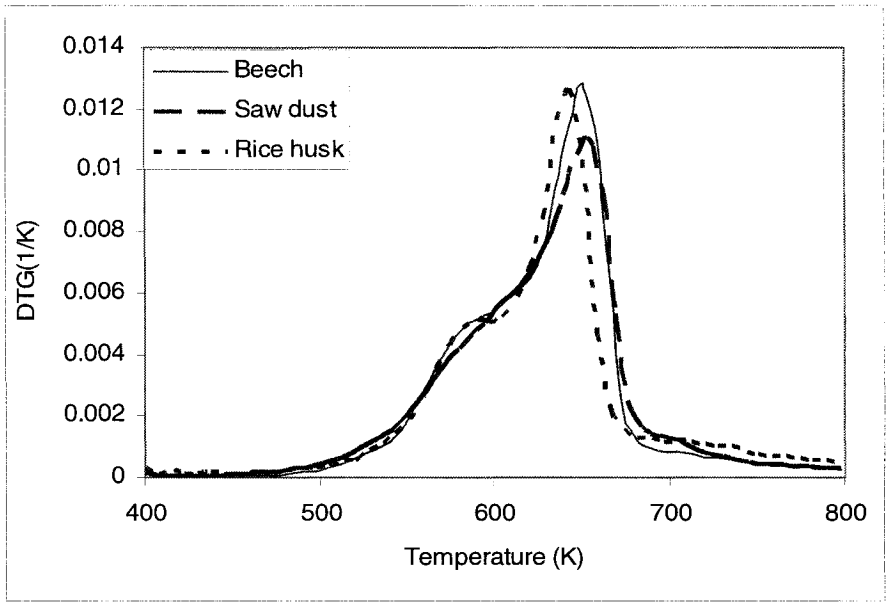

Figure 5.2: DTG curve for three biomass samples at heating rate of 30K/min.

In order to obtain a more reliable kinetics, which can predict the overall yield of the pyrolysis, the effect of heating rate on the pyrolysis should be taken into account. Gronli et al. [3] have characterized degradation of wood samples by introducing some parameters. These parameters are calculated from the weight loss curves and its first and second derivatives. We use here the same parameters and notations introduced by them to evaluate the effect of heating rate on the devolatilization characteristics. Table 5.3 summarizes the effect of heating rates on the onset temperature of devolatilization for the hemicellulose and cellulose ($T_{onset(hc)}$ and $T_{onset(c)}$) and also the temperature of the peak, which corresponds to the maximum devolatilization rate (T_{peak}). As Table 5.3 shows, an increase in the heating rate increases the onset of the devolatilization and

Table 5.3: Effect of heating rate on the devolatilization characteristic

Biomass	Heating Rate (K/min)	$T_{onset(hc)}$ (K)	$T_{onset(c)}$ (K)	T_{peak} (K)
Beech wood	5	504	579	620
	20	508	607	644
	30	514	611	652
Saw dust	5	504	579	617
	20	508	612	646
	30	514	615	653
Rice Husk	5	504	577	618
	20	508	600	637
	30	514	605	641

peak temperature for all the biomass samples. Teng and Wei, [19] have reported the same trend in the T_{peak} for rice husk. Because these events describe the way devolatilization and the release of different products during devolatilization proceed, thus, a suitable kinetic model should take into considerations their changes with heating rate.

In order to determine kinetic parameters which are suitable for different heating rates and can account for the change in the abovementioned characteristics, experimental results at 3 heating rates (5, 20 and 30K/min) were fitted to the model presented by Equations (5.1)-(5.5). Figures 5.3 and 5.4 compare the experimental results with the kinetic models for beech wood, and rice husk respectively. As the figures show, the model can follow the changes in the peak temperatures and onset of devolatilization successfully at different heating rates. It is believed that the degree of confidence in utilizing model parameters developed for various heating rate increases because it has the capability to predict the global yield of devolatilization at different heating rates.

As shown in Figure 5.2, beech wood and saw dust exhibit very similar pyrolysis behavior. Thus, for further evaluation of the kinetic model at this stage, the kinetic parameters derived for the beech wood is used to predict the pyrolysis of saw dust. Figure 5.5 shows the prediction of the kinetic model and experimental data for the saw dust. The deviation between the model and experiments for all three heating rates, although higher than those of beech wood (5.14%), still demonstrates a reasonable agreement.

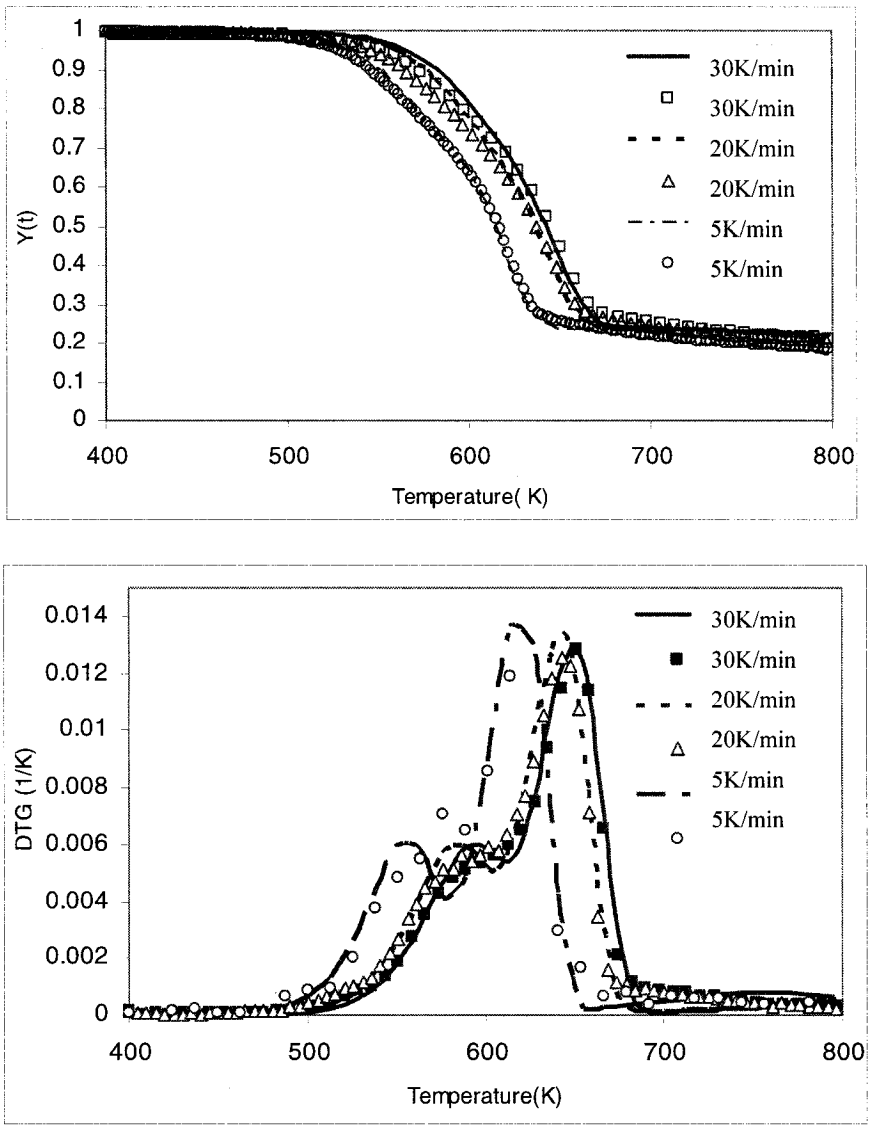

Figure 5.3: experimental versus model results for beech wood at different heating rates. Lines represent the model and the symbols are the experimental points.

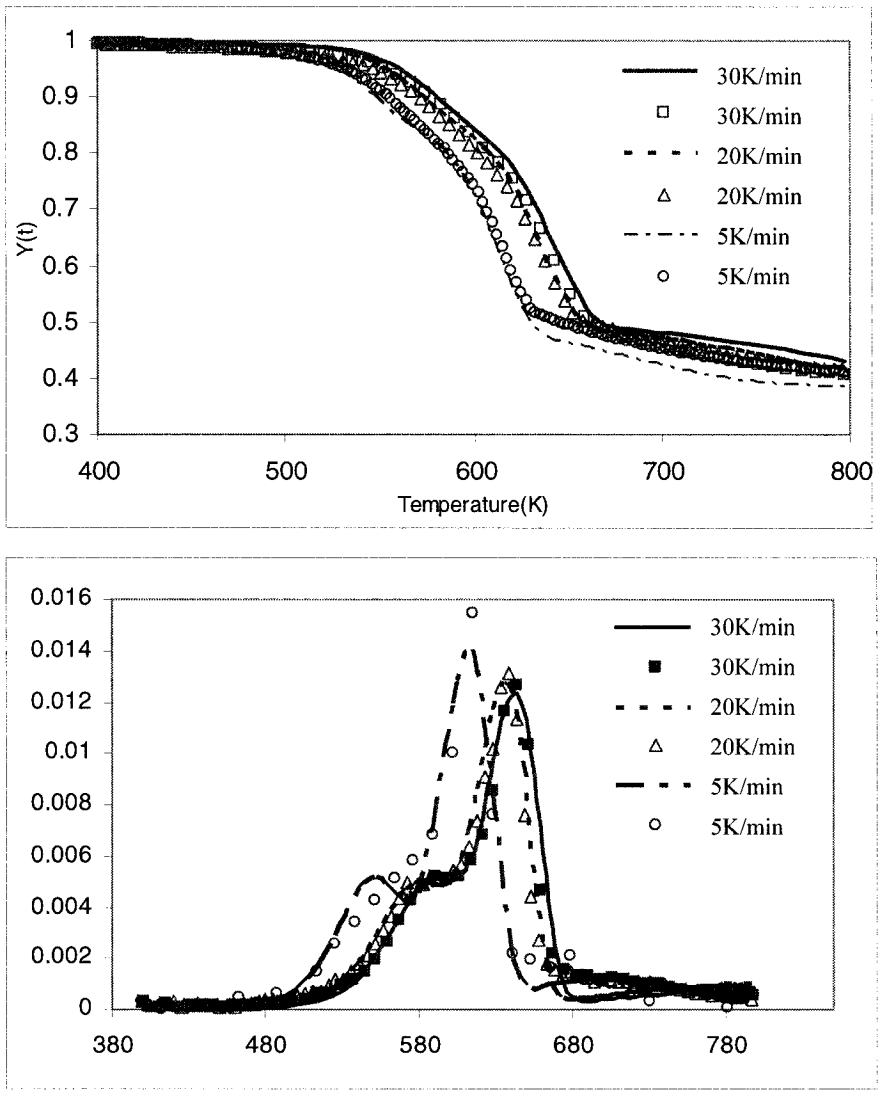

Figure 5.4: experimental versus model results for rice husk at different heating rates. Lines represent the model and the symbols are for the experimental points.

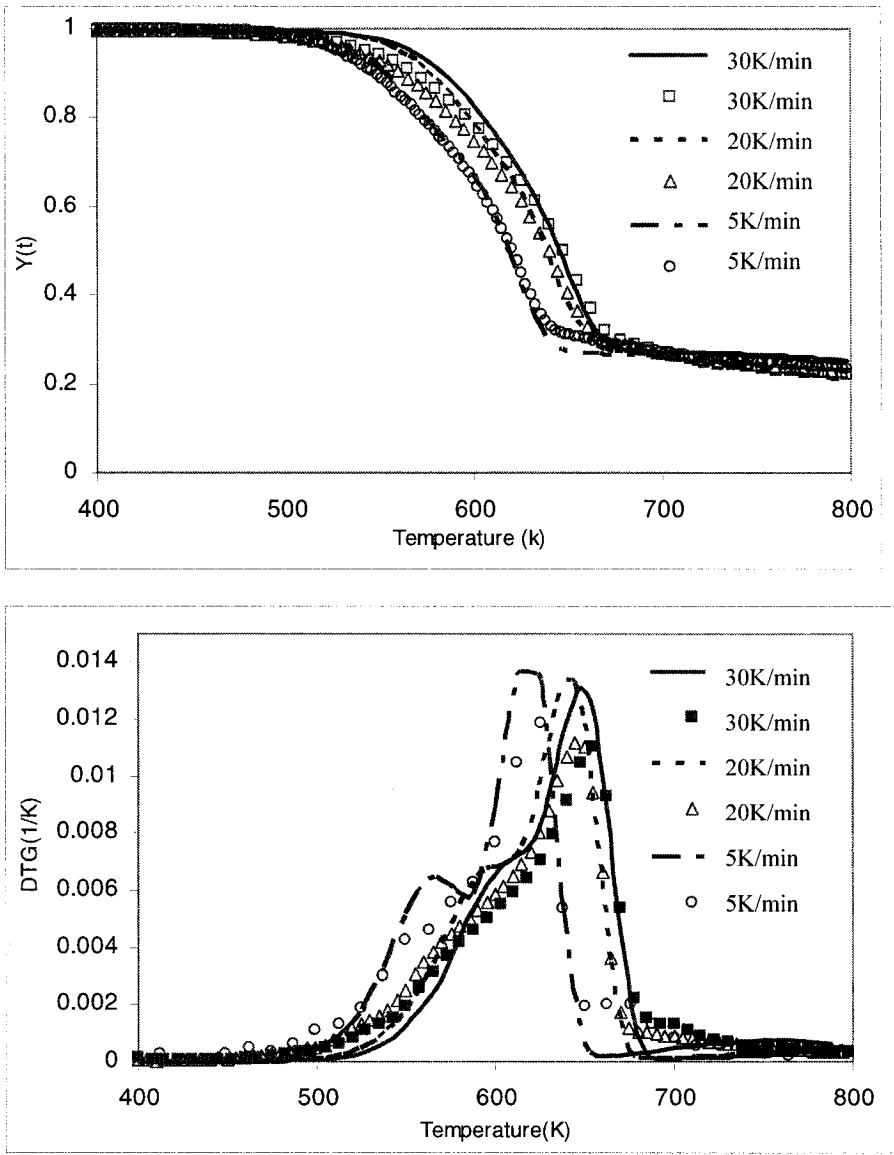

Figure 5.5: Kinetic model evaluation by applying the model parameters derived for beech wood to saw dust. Lines represent the model and the symbols are the experimental points.

Table 5.4 presents the model parameters for different biomass samples and the deviation between the model and experiments. The deviation was calculated according to Equation (5.7).

Table 5.4: kinetic parameters found in this work for the different biomass material

Kinetic Parameters	Beech Wood	Rice Husk
E_c, (kJ/mol)	192	184
E_{hc}, (kJ/mol)	133	129
E_l, (kJ/mol)	87	64
$\log(k_{0,c})$, s^{-1}	13.9	13.4
$\log(k_{0,hc})$, s^{-1}	10.2	9.9
$\log(k_{0,l})$, s^{-1}	3.1	1.80
C_c	0.61	0.59
C_{hc}	0.27	0.22
C_l	0.11	0.18
Deviation %	1.71	2.4

5.2.6.2 Model Evaluation at Other Heating Conditions

In order to scrutinize the performance of the kinetic model at other heating conditions, the kinetic parameters developed in the previous section was directly applied to other heating conditions. The experimental conditions such as flow rate of the inert gas and size and initial weight of the biomass samples remained unchanged as explained in the experimental section. The heating program, in this part, consists of two isothermal and two non-isothermal sections. The non-isothermal parts constitute two separate heating ramps each at 50K/min. This heating rate is totally different from the heating rates used to determine the model parameters.

The details of the heating program are shown in Figure 5.6. This figure compares the experimental result and the model prediction for beech wood particles. As these figures demonstrate, the model is capable of predicting the overall yield of devolatilization successfully for the whole region of interest. The deviation between the model and the experiment, however, increases at the higher temperatures and at the end of the pyrolysis. The weight loss in this section corresponds to only 20% of the total weight loss. The correlation coefficient between the model and the experiments beside the larger deviation at the last course of the pyrolysis is 0.98. The same trend was found in the prediction of the other biomasses.

5.2.6.3 Gas Evolution during Pyrolysis

5.2.6.3.1 Effect of Heating Rate on the Gas Distribution

Evolution of different stable gases, at different heating rates (10, 20, 30K/min), were studied using the GC. The evolution of flow rates of each gas component was calculated simply by a mass balance over the inert gas (argon). The mass flow rate of each gas was normalized based on the initial weight of the biomass used in each TGA experiments to eliminate the effect of change in the initial mass in various experiments.

Figure 5.7 shows the evolution of H_2, CH_4, CO, and CO_2 for the beech wood at different heating rates. The same type of curves was obtained for other biomass. CO_2 is always the most abundant gas in all the experiments. The evolution of both CO_2 and

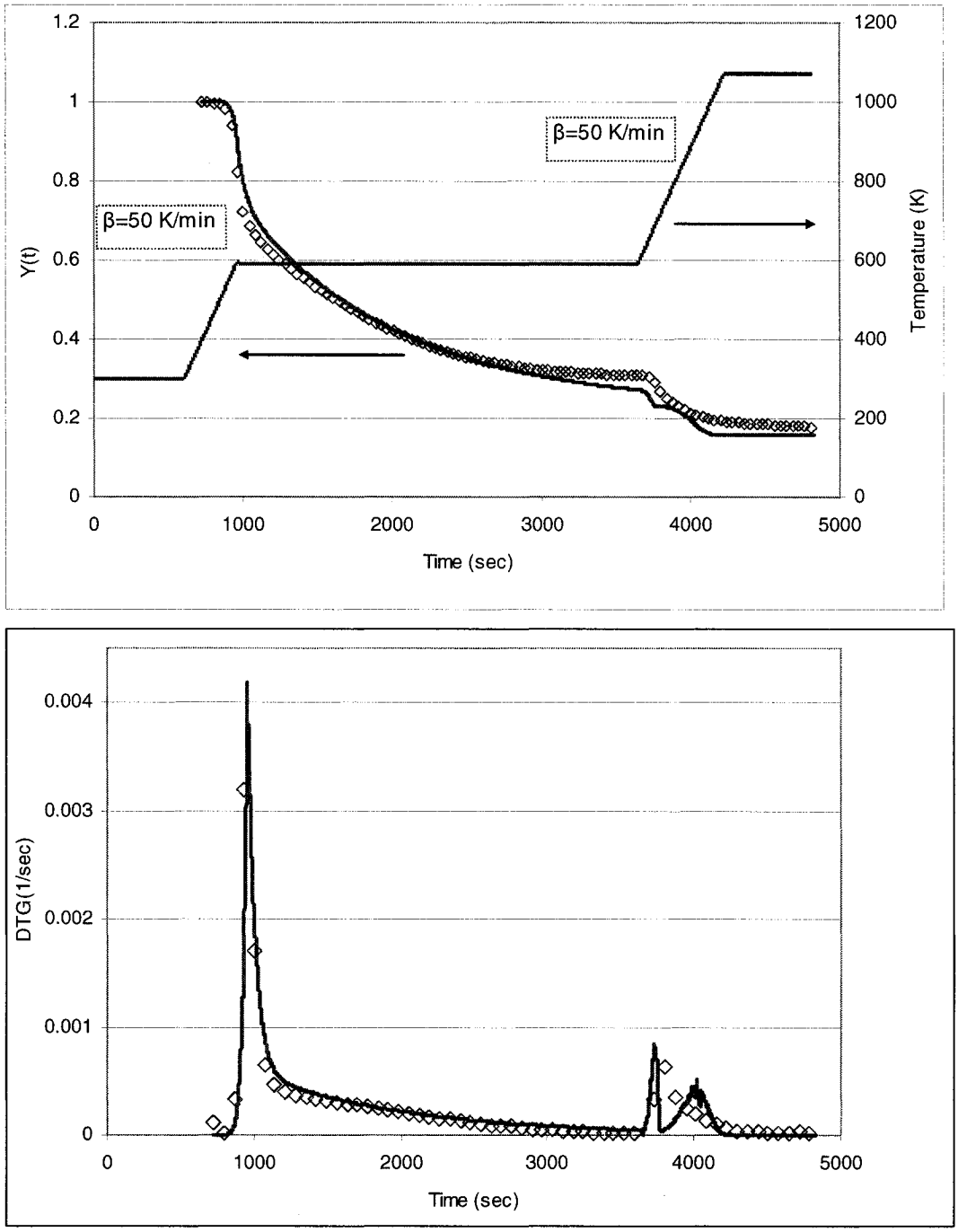

Figure 5.6: Model evaluation for beech wood at different heating rates. Line for the model and symbols for the experiments

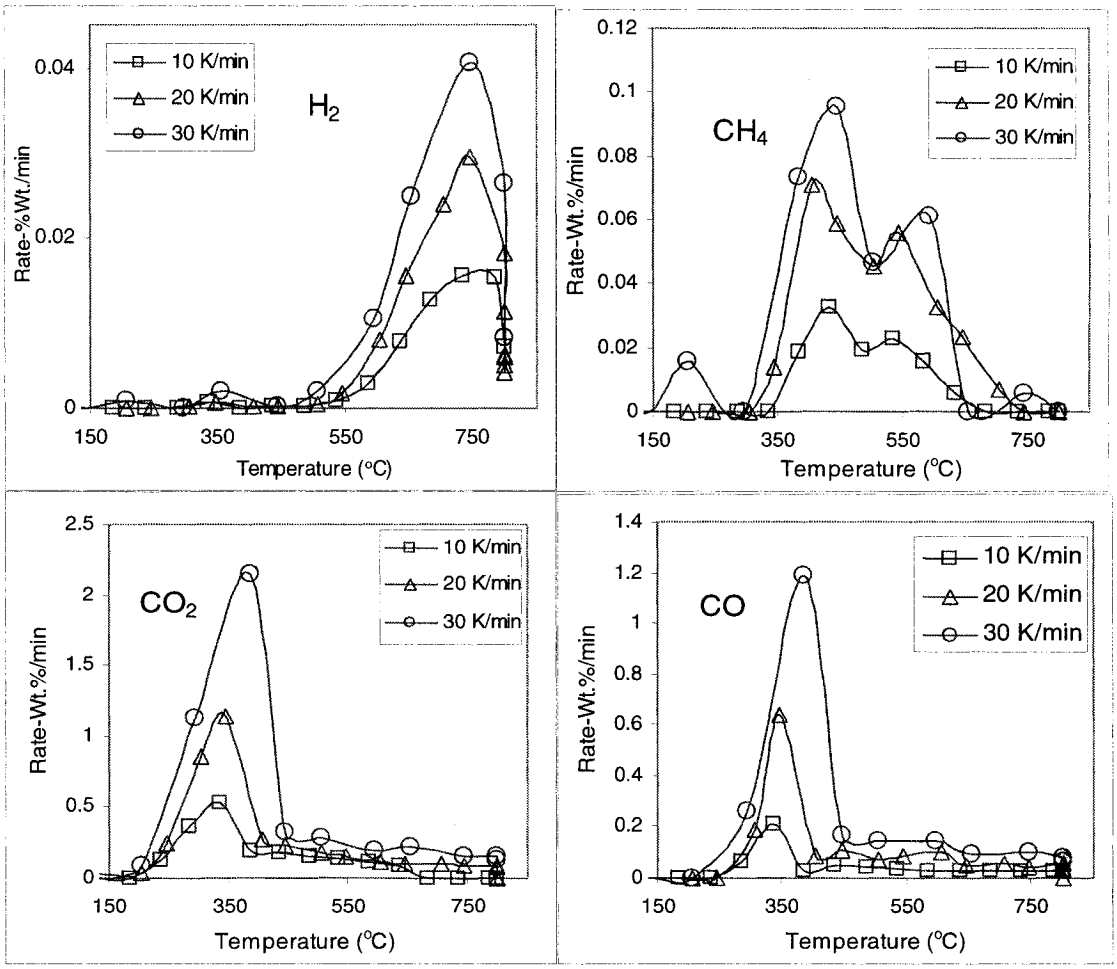

Figure 5.7: Evolution of gases at different heating rates in the pyrolysis of beech wood. The experimental points are connected by lines.

CO commence at around 250°C and it reaches its maximum at a temperature of 350°C. CH_4 and H_2 on the other hand are the less abundant components in the gas and their evolution starts at higher temperatures. The evolution of CH_4 takes place at the temperature range of 350-750°C and that of H_2 at an even higher temperature range of 550-800°C. This suggests the possibilities of the heavier hydrocarbons cracking as the heating rate increases. Most studies on the H_2 evolution from the different biomasses show the same range of temperature for H_2 release [13, 14, 29]. Gonzalez et al. [13] have reported two maxima in the evolution of H_2 in almond shell pyrolysis, the first one at temperature of 350°C and the second one with higher rate of evolution at 750°C. Bilbao et al. [15], on the other hand, have reported the formation of H_2 at temperatures close to 300°C.

In the study of the gas evolution it is not easy to relate a gas evolution to one of constitutes in the biomass (i.e. hemicellulose, cellulose and lignin). The CH_4 evolution is, however, an exception because in both beech wood and saw dust and for all the heating rates it manifests two peaks at two different temperatures. These peaks are observed at the temperature of 450° C and 550°C. In the case of cellulose only one peak at the peak temperature of 550°C was observed. This indicates the first evolution of CH_4 at lower peak temperature of 450°C is associated to the hemicellulose decomposition. In fact, both cellulose and hemicellulose have contribution in the evolution of CH_4. The same conclusion can not be made for the other gases because a

clear distinction between the gases evolving from cellulose and hemicellulose can not be seen.

Table 5.5 presents the yields of the different gases for the biomass used in this study and at different heating rate. It also compares the data of this study with other results performed at different heating rates. Table 5.5 also shows that the yields of gases increase by increasing the heating rate. This also can be seen in Figure 5.7, which shows the effect of heating rates on the evolution rate of different gases in pyrolysis. Apart from stable end-product gases (H_2, CH_4, CO and CO_2) a large portion of the product gas is devoted to the tar and water. The last column in the Table 5.5 indicates the yield of the condensable vapors or tar and water, derived from the mass balance. As Table 5.5 shows, the yield of the condensable vapors decreases by increasing the heating rate. This can be explained by the result presented in Table 5.3, which shows T_{onset} and T_{peak} of devolatilization increase by increasing the hearing rate.

5.2.6.3.2 Kinetics of gas evolution

A simple kinetic model was employed to model evolution of gases in pyrolysis. This model is described by the Equation (5.9). Yields of the different gases, calculated and presented in the previous section, were fitted to the model and the parameters were calculated for each biomass. Different heating rates were fitted to a single kinetic model to obtain the best lumped model possible. As Table 5.5 shows, V^*, or total

Table 5.5: A comparison between the fractional yields of products in pyrolysis obtained in his work with other published results

Run	Biomass type	Reactor type	Particle size/weight	β °C/min	Char %	H_2 %	CH_4 %	CO %	CO_2 %	Total gas yield	Liquids (tar+H_2O)
This study	Beech Wood	TGA	<1 mm, 5mg	10	18.2	0.23	0.5	2.9	9	11.7	67
This study	Beech Wood	TGA	<1 mm, 5mg	20	18.5	0.9	0.70	3.9	9.7	15.5	66
This study	Beech Wood	TGA	<1mm, 5 mg	30	17.6	0.6	0.74	5.6	12.8	20	62.4
This study	Saw Dust	TGA	<1 mm, 5 mg	10	20.9	0.2	0.64	2.5	10.0	13.3	65.8
This study	Saw Dust	TGA	<1 mm, 5 mg	20	20.8	0.3	0.8	3.7	12	16.8	62.4
This study	Saw Dust	TGA	<1 mm, 5 mg	30	19.2	0.28	0.9	5	14	20	60.8
Nunn et. al. [17]	Sweet gum Hardwood	Captive sample	<88 μm, 100 mg	1000	7.0	nd*	2.3	17.0	6.1	41	51
Bilbao et al. [15]	Cellulose	Tubular	2.5g <0.25 mm	31	NA	0.7	nd*	4.75	12.36	17.8	NA
	saw dust		<1.6 mm	31	NA	0.7	nd*	6.51	14.47	22.4	NA
Gonzalez et al. [13]	Almond shell	Fixed bed	10 g	20	22.1	0.63	3.5	9.8	18.5	32.5	49.1
Zanzi et. al. [30]	Wood brich	Free fall	0.8-0.1 mm	500	27.6	0.54	8.2	23.8	17	51.8	21.6

*nd=not detected

attainable yield for each gas presented in Equation (5.8), changes with heating rate. This has been neglected in the previously developed kinetic models for the gas release but has been reflected in our model. Table 5.6 shows calculated parameters of the kinetic model for the saw dust and beech wood and for different gases and the corresponding error. No parameters were presented for the condensable part of the gases, because this part encompasses both tar and water which may in fact exhibit different chemical kinetics.

Table 5.6: Kinetic parameters for the evolution of gases

Biomass	Component	$Log(k_{01})$ (1/min)	E_i (kJ/mol)	k_v	V_∞^*	Deviation %
Beech wood	H_2	8.9	93	14.5	1.0	0.27
	CH_4	2.87	45	8.2	1.1	0.10
	CO	6.5	50	11	7.5	0.55
	CO_2	4.7	34	6.2	15	2.41
Saw Dust	H_2	8.9	110	12.3	0.9	0.03
	CH_4	2.7	51	7.2	1.1	0.08
	CO	5.5	41	8.9	6.7	0.4
	CO_2	6.3	55	6.15	16	0.4

Figure 5.8 compares the kinetic model in this work with the experimental result for beech wood particles. Considering the fact that the model is lumped and derived for all the heating rates in the range of this experimental work, it relatively fits well to the experimental result.

In order to further evaluate the performance of the model presented in this study, the yield of the four stable end-product gases predicted by the model at different heating

rates are compared in Figure 5.9 with other experimental results. This figure compares the data obtained by Bilbao et al. [15] for the pyrolysis of saw dust; and the results obtained in this work extended to a heating rate of 50K/min with the model prediction. As Figure 5.9 demonstrates, the model is capable of predicting the final gas yields at different heating rates relatively well. It is also follows the increasing trend of the gas yield by increasing heating rate. The result obtained by Bilbao et al. [15], also, shows a relatively good agreement with the model. The more deviation observed in the prediction of model with the experimental result of Gonzalez et al. [13]. This must be related to the kinetic regime of that study. The initial mass of biomass used in that work is large (10g) compared to the present work. Consequently, a secondary reaction between the tar exiting from the biomass particles and the char is inevitable. This reaction leads to tar cracking and production of more end-product gases such as H_2 and CH_4. This reaction is less important in the case of Bilbao et al. [15] experiments where the initial weight of the captive sample is less (2.5 g).

Table 5.5 also compares the result of this work with other pyrolysis experiments at very high heating rates [17, 30]. Although the model works relatively well for the CH_4 and H_2, it cannot predict the concentration of CO and CO_2 at very high heating rates. This shows that although the model prediction is well at low and moderate heating rates, more work still needs to be done to extend the applicability of such kinetic model to very high heating rates.

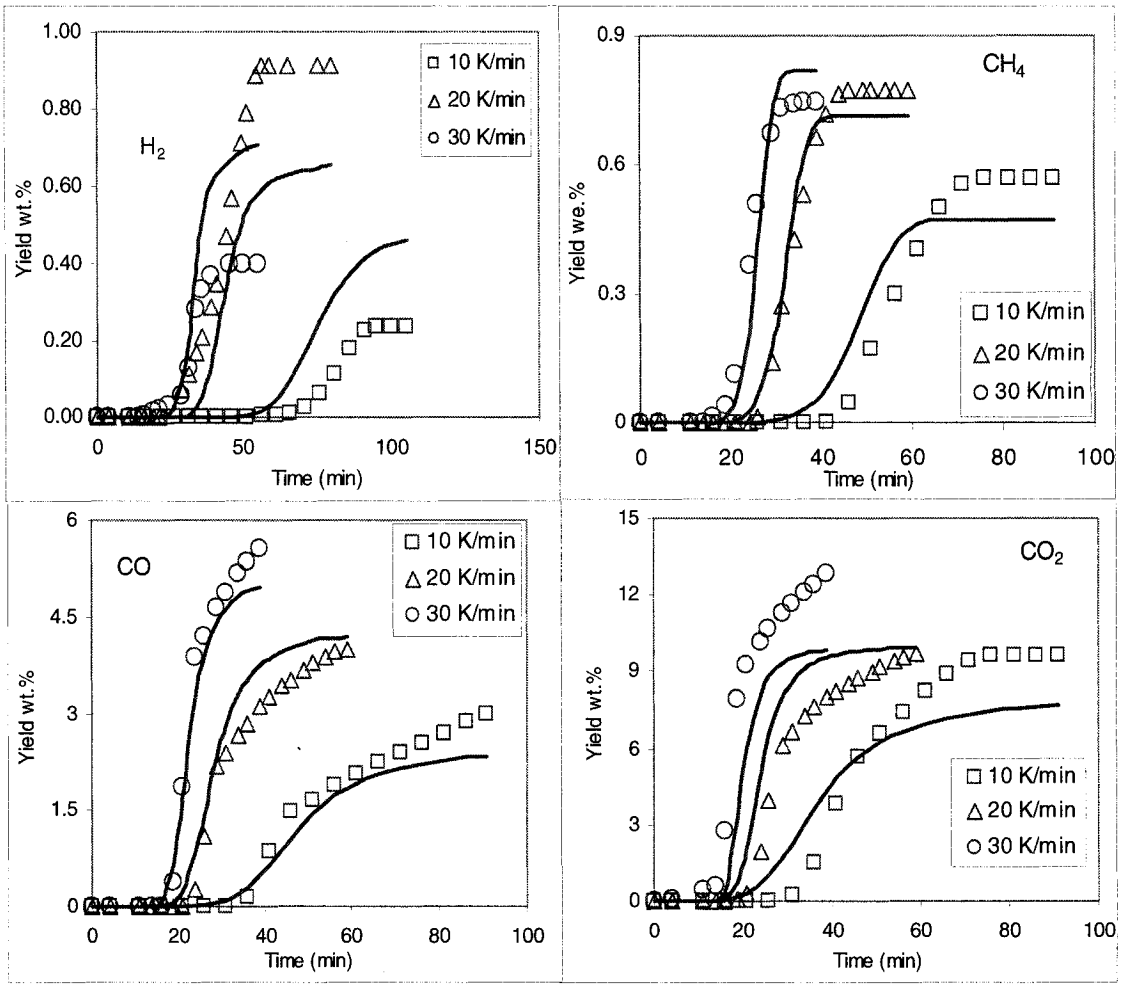

Figure 5.8: Kinetic model versus experiments for beech wood at different heating rates. Lines represent the evolution of yield predicted by the model and the symbols are the experimental points.

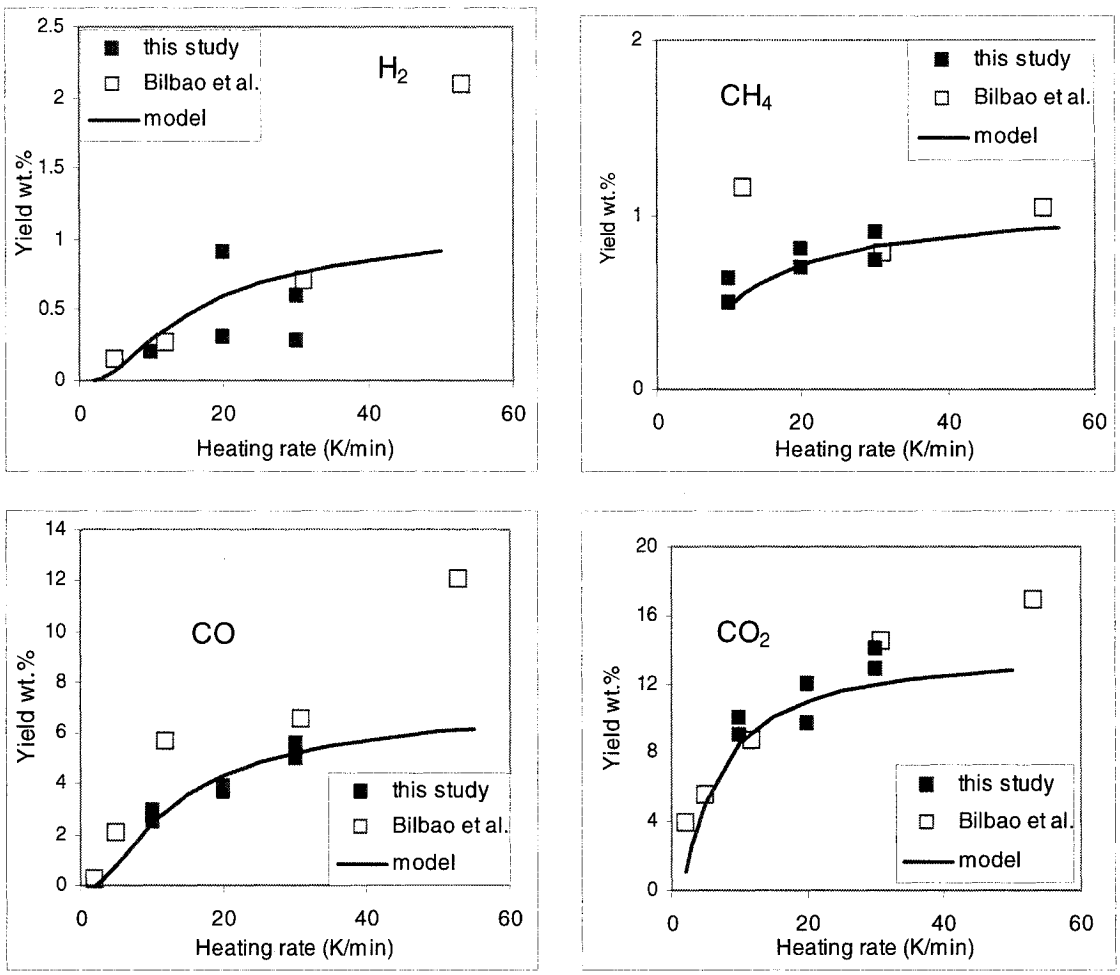

Figure 5.9: comparison of the final attainable yields at different heating rates and final temperature of T=800°C. Lines represent the model prediction and the symbols are the experimental points.

5.2.7 Conclusions

A complete map of the different products during pyrolysis of woody biomass was demonstrated. This includes the char, H_2, CH_4, CO, CO_2 and liquids (tar and water). CO_2 and CO were identified as the most abundant gases resulting from pyrolysis. Suitable kinetic models were also developed for all the range of products. This kind of kinetics would be useful for modeling the gasification processes, where the final gas composition and consequently its heat content is significant, or, in pyrolysis, where the goal is to produce liquid tarry material known as bio-oil. It was shown that the heating rate has an impact on the final attainable gas yields. The kinetic models in this study were improved in order to extend their applicability to other heating conditions or even other biomass samples. This makes the model more versatile especially in applying it to different reactors where the operating conditions are different from the thermobalnce.

5.2.8 Notations

C: contribution factor for each component in the biomass

E: activation energy (kJ/mol)

i: each component in the biomass (Cellulose, hemicellulose or lignin)

k_0: Pre-exponential constant (s^{-1})

k_v: Constant in Equation (5.9) (min/K)

N: number of data points in experiments

Obj: objective function in optimization

P : number of adjustable parameters

t : time (s)

T : Temperature (K)

V : volatile released during pyrolysis

V^* : total volatile available for a gas component

W: weight of the biomass (mg)

Y: total yield of devolatilization

Greek letters

β: heating rate in TGA experiments (K/min)

Subscripts

c: Cellulose

hc: Hemicellulose

l: Lignin

5.2.9 References

[1] Vamvuka D, Kakaras E, Kastanaki E, Grammelis P. Fuel 2003; 82:949-1960.

[2] Liang XT, Koziski JA. Fuel 2000; 79:1477-1486.

[3] Gronli MG, Varhegyi G, Di Blasi C. Ind Engng Chem Res 2002; 41:4201-4208.

[4] Meszaros E, Varhegyi G, Jakab E, Marosvolgyi B. Energy Fuels 2004; 18:497-507.

[5] Reina J, Velo E Puigjaner L. Ind Engng Chem Res 1998; 37: 4290-4295.

[6] Varhegyi G, Antal MJJ, Jakab E, Szabo P. J Anal Appl Pyrol 1997; 42:73-87.

[7] Varhegyi G, Antal MJJ, Szekely T, Szabo P. Energy Fuels 1989;3:329-335.

[8] Branca, C.; Di blasi, C., J Anal Appl Pyrol 2003; 67:207-219.

[9] Orfao J M Antunes FJA Figueiredo JL. Fuel 1999; 78: 349-358.

[10] Shafizadeh F, Chin PPS. ACS symposium series 1977; 43:57-81.

[11] Koufopanos CA, Mashio G, Lucchesi A. Can J chem eng 1989; 67: 75-84.

[12] Di blasi C. J Anal Appl Pyrol 1998; 47:43-64.

[13] González JF, Ramiro A, González-García CM, Gañán J, Encinar JM, Sabio E, Rubiales J. Ind Engng Chem Res 2005; 44:3003-3012.

[14] González JF., Encinar JM, Canito JL, Sabio E, Chacon M. J Anal Appl Pyrol 2003; 67:165-190.

[15] Bilbao R, Arauzo J, Salvador ML. Ind Engng Chem Res 1995; 34:786-793.

[16] Bilbao R, Arauzo J, Murillo MB, Salvador ML. J Anal Appl Pyrol 1997; 43: 27-39.

[17] Nunn TR, Howard JB, Longwell JP, Peters WA. Ind Engng Chem Proc Des Dev 1985; 24:836-844.

[18] Hajaligol MR, Howard JB, Longwell JP, Peters WA. Ind Engng Chem Proc Des Dev 1982; 21:457-465.

[19] Teng H, Wei YC. Ind Engng Chem Res 1998; 37:3806-3811.

[20] Di blasi C. Branca, C., Ind Engng Chem Res 2001; 40:5547-5556.

[21] Pyle DL, Zaror CA. Chem Eng Sci 1984; 39:147-158.

[22] Sorum L, Gronli MG, Hustad JE. Fuel 2001; 80:1217-1227.

[23] Simmons, G.; Gentry, M., J Anal Appl Pyrol 1986;10:129-138.

[24] Banyasz JL, Lyons-Hart J, Shafer KH. Fuel 2001; 80:1757-1763.

[25] Gronli M, Antal MJJ, Varhegyi G. Ind Engng Chem Res 1999; 38:2238-2244.

[26] Courbariaux, Y, Ph.D thesis École polytechnique de Montréal 2004; 93-98.

[27] Chang WR, Kelbon M., Krieger-Brockett B. Ind Engng Chem Res 1988; 27:2261

[28] Encinar JM, González JF, González J. Fuel processing technology 2000; 68:209.

[29] Blanco Lopez M.C, Blanco CJ, Martinez-Alonso A, Tascon, J.M.D., J. Anal Appl Pyrol 2002; 65:313-322.

[30] Zanzii R, Sjostrom K, Bjornbom E. Biomass Bioenergy 2002; 23:357-366.

CHAPTER 6

EFFECT OF TEMPERATURE ON SOLIDS MIXING IN A BUBBLING FLUIDIZED BED REACTOR*

6. 1 Presentation of the Article

The objective of the second article is to investigate the effect of temperature on the mixing of the solid phase in a bubbling fluidized bed. Most industrial fluidized bed reactors operate at high temperatures. Fluidized bed *combustion* and *gasification* are two relevant examples of high temperature operation of fluidized bed reactors. Poor mixing of solids in fluidized bed *gasifiers* may lead to hot spots and operational difficulties. In this article, Radioactive Particle Tracking (RPT) is employed to investigate solids mixing using a counter-current back mixing model in a bubbling fluidized bed at a temperature range of 25-400°C (CCBM). The bed material is silica sand which belongs to Group-B Geldart classification. The transfer coefficient (K_w) between the counter-current phases in CCBM model is found to be in the range of K_w=0.7-1.6s^{-1}.

*Published online in International Journal of Chemical Reactor Engineering, 2005, A16.http://www.bepress.com/ijcre/vol3/A16/

6.2 Effect of Temperature on Solids Mixing in a Bubbling Fluidized Bed Reactor

Ramin Radmanesh, Rachid Mabrouk, Jamal Chaouki, Christophe Guy
Department of Chemical Engineering, l'École Polytechnique,
P.O. Box 6079, Station Centre-ville, Montréal, QC H3C 3A7, Canada
Fax: 514 340 4159; e-mail: jamal.chaouki@polymtl.ca

6.2.1 Abstract:

Solid mixing in fluidized bed reactors has a great impact on the transport phenomena in the reactor. Most studies, concerning solid behavior and hydrodynamic correlations of fluidized bed reactors, have been done at ambient temperature. Industrially, however, fluidized bed reactors operate at high temperatures. The lack of studies at higher temperatures is due to difficulties associated with measuring techniques under these conditions. In extrapolating hydrodynamic parameters derived at ambient temperature to higher temperatures, only the physical property changes of gas and solid phases, such as density and viscosity are taken into consideration. On a microscopic scale, however, change of temperature strongly affects the interaction between particles, which in turn has a substantial impact on the hydrodynamics of a fluidized bed.

In this study and for the first time, the Radioactive Particle Tracking (RPT) is used to investigate the effect of temperature on the fluidization of silica sand particles (Geldat-B) in a bubbling fluidized bed reactor. Experiments have been carried out at different temperatures (25-400°C) and superficial gas velocities (0.17-0.75 m/s). The effect of temperature on the global mixing is studied in conjunction with the changes found in

the dynamic of the ascending and descending phases. A two-phase countercurrent back-mixing model (CCBM) was used to investigate global solid mixing at different temperatures. The wake exchange coefficient, in the CCBM model, is calculated and compared with the values obtained from different correlations. For various experiments, the exchange coefficient is found to be in the range of 0.6-1.7 s^{-1}. The correlations can predict the trend of the wake exchange coefficient change with temperature, but they all overestimate it. The correlations developed by Hoffmann et al. (1993) and Lim et al. (1993) were found to give a better agreement with the results at high temperatures.

6.2.2 INTRODUCTION

Mixing of solids in gas fluidized beds has a crucial impact on the reaction, heat and mass transfer. In fast catalytic reactions, a good gas-solid contact is deterministic in achieving the desirable yields for the products. In gasification and combustion, poor solids mixing leads to hot-spots and an abrupt increase in temperature. In exothermic catalytic reactions the hot spots caused by poor mixing of solids, may damage catalyst or cause operational failures.

It is well known that mixing of solids in a gas fluidized bed is induced by bubbles. Bubbles carry solids up in their wakes. The rising bubbles also cause solids to drift in the bed. This upward movement of solid is known as the bubble-induced drift of solids. The downward movement of solids also takes place in the zones where there are less

bubbles. These ascending and descending phases are responsible for the axial mixing in the bed. Lateral mixing also takes place in the bed through periodic disposal and replenishment of the wake, wake shedding and the bursting of the bubbles at the surface of the bed.

The dispersion model and two or three phase counter-current back-mixing models (CCBM) are the most important models used in the literature for solids mixing study. May (1959) is among the first who used dispersion model to study solid mixing in a large scale fluidized bed by injecting radioactive solid tracers in the bed. While the DM model has demonstrated less satisfactory results, the CCBM model is known to be a more robust and phenomenological model, which was first introduced by van Deemter (1967). Unlike the dispersion model, the CCBM model considers the aforementioned mechanism involving solids mixing in the bed. Although Lim et al. (1995) have reported the second approach to be more robust, its use has been restricted. The main hurdles in applying this model can be summarized as: 1) CCBM is a more complex model, which results in parabolic partial differential equations; 2) Unlike the dispersion model that consists of only one model parameter i.e. the dispersion coefficient, the number of model parameters in the CCBM model can be as high as 6 parameters depending on the number of phases considered in the model. This is a shortcoming of the model especially when these hydrodynamic parameters are difficult to measure and are treated as adjustable parameters; 3) The scarcity of the experimental data is another reason which have impeded the use of the CCBM model.

Several studies on the parameters estimation of the CCBM model can be found in the literature (Sitnai, 1981; Lakshmanan and Potter, 1990; Basesme and Levy, 1992; Lim et al., 1993; Shen and Zhang, 1998; Hull et al., 1999; Grasa and Abanades, 2002). Two types of experimental data are needed to estimate appropriately the exchange coefficient between the countercurrent phases in the model. The first type of data can be obtained by pulse injection of solid tracers and it provides information on the solid's gross behavior in the bed. Positron emission and γ-ray particle tracking (Dechsiri et al., 2005; Mostoufi and Chaouki, 2001), digital image analysis (Grasa and Abanades, 2002 and Lim et al., 1993) and magnetic tracer injection (Sitnai 1981) are some of these experimental techniques. The second type provides local instantaneous motion of individual particles and, consequently, provides information on ascending and descending phases in the bed. Radioactive particle tracking and image processing technique have been employed for the second type of data. In the absence of instantaneous data some authors have treated the hydrodynamic parameters of the ascending and descending phases as adjustable parameters (Sitnai,1989; Grasa and Abanades, 2002) while some others have used hydrodynamic correlations or a measuring technique to estimate these parameters (Lim et al., 1993).

Most studies on the mixing of solid based on CCBM model are lumped. For instance, Sitnai, (1981), Grasa and Abanades (2002), Lakshmanan and Potter (1990), have lumped the drift and bubbles wake into one ascending phase. Lim et. al. (1993), Shen

et. al. (1998), Hull et al (1999) have used only wake (ascending) and emulsion phase (descending) in their study, which is again a lumped approach.

Despite the fact that industrial reactors operate at high temperatures, all the studies have been carried out at ambient temperature. The effect of temperature on the global solids mixing is still unexploited and missing. Moreover, most experiments have been performed in 2-D fluidized beds (Sitnai, 1981; Lim et al., 1993; Basesme and Levy, 1992; Grasa and Abanades 2002).

In this work, radioactive particle tracking at high temperatures is used to study the global mixing of solids using the CCBM model. It is believed that temperature affects the interparticle-hydrodynamic forces and, accordingly, the dynamics of the phases in the fluidized bed. It is also believed that the effect of temperature on interparticle forces is more conspicuous for Geldart-A particles. However, it is also interesting to study this effect on Geldart-B particles. Therefore, the objective of this study is to investigate the effect of temperature on solid mixing and in particular, the exchange coefficient between the phases in the CCBM model. The comparison of the exchange coefficient found in this work and the one given by correlations can give insight into the effect of temperature on interparticle force changes.

6.2.3 THEORY

The CCBM model has already been discussed in several papers (van Deemter 1967, Sitnai 1981, Lim et al., 1993, Grasa and Abanades, 2002). Two or three phases have been considered in different studies in the literature. Sinai (1981) has introduced three phases: the main drift phase of solid, the descending phase of emulsion and another descending phase close to the wall. The model consists of 6 adjustable parameters which were calculated by fitting the model to experimental work. The large number of adjustable parameters is one of the drawbacks of most modeling attempts using the CCBM model. Figure 6.1 demonstrates a two-phase CCBM model. This model can be described by the following equations:

$$\frac{\partial(C_{as} f_{as})}{\partial t} + \frac{\partial(U_{as} C_{as} f_{as})}{\partial z} + K_w (C_{as} - C_{ds}) f_{as} = 0 \tag{6.1}$$

$$\frac{\partial(C_{ds} f_{ds})}{\partial t} + \frac{\partial(U_{ds} C_{ds} f_{ds})}{\partial z} + K_w (C_{ds} - C_{as}) f_{as} = 0 \tag{6.2}$$

where, U_{as} and U_{ds} are the velocities of ascending and descending phases respectively, C_{as} and C_{ds} are the solid concentration in both phases, and K_w is the exchange coefficient between the phases. The boundary conditions for these equations are:

$$\frac{dC_{as}}{dz} = \frac{dC_{ds}}{dz} = 0 \qquad \text{at } z=0 \text{ and } z=H_{db} \tag{6.3}$$

The initial concentration of the tracers, in both the ascending and descending phases, is given by the pulse injection of solid tracers to the reactor.

As mentioned earlier, most studies on solid mixing are lumped. In this study also the drift and wake velocities are lumped into one velocity (u_{as}). The descending velocity, on the other hand, lumps the descending phases in the emulsion and close the wall. Thus, the transfer coefficient (k_w) is simply between these countercurrent phases. Thus, the ascending solid velocity in Equations (6.1) and (6.2) is the average ensemble velocity of the particle in the wake and drift phases. The descending solid velocity is also the average ensemble velocity of the descending phase in the emulsion and the one close to the wall. All the parameters in the above equations, except K_w, are derived form the RPT experiments as described below.

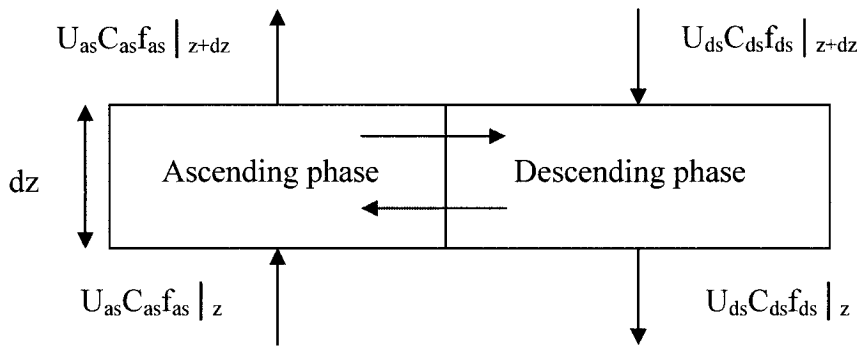

Figure 6.1: A demonstration of the CCBM model.

Solving Equations (6.1) and (6.2) gives the theoretical concentration profile ($C(z,t)$) for a pulse injection of solid tracers. This concentration should be compared with the experimental results of the concentration response of the bed to a pulse injection. We benefit from the ergodic nature of the RPT experiments (Cassanello et al., 1996; Mostoufi and Chaouki, 2001; Larachi et al., 2003) to virtually inject a large number of particles in certain location in the bed.

It is worth noting that the driving force for the mass transfer between the ascending and descending phases in the CCBM model, according to Equations (6.1) and (6.2), are the difference in concentrations of solids in the two phases. However, this does not fully represent the underlying physics. In fact, the solids exchange between the two phases is a result of continuous shedding and replenishment of the bubble wake into the emulsion phase. In that sense, the third term in Equations (6.1) and (6.2) can be considered as a plain approximation of a more complicated phenomena.

6.2.4 EXPERIMENTAL

Figure 6.2 is a schematic representation of the reactor and detectors around the bed. The fluidized bed is made of stainless steel and capable of withstanding high temperatures. It consists of a bed and freeboard of 0.078 m ID and 0.75 m in height, three heating bands, a windbox, which also serves as a pre-heater, and a disengagement zone of 0.15 m ID and 0.90 m in height.

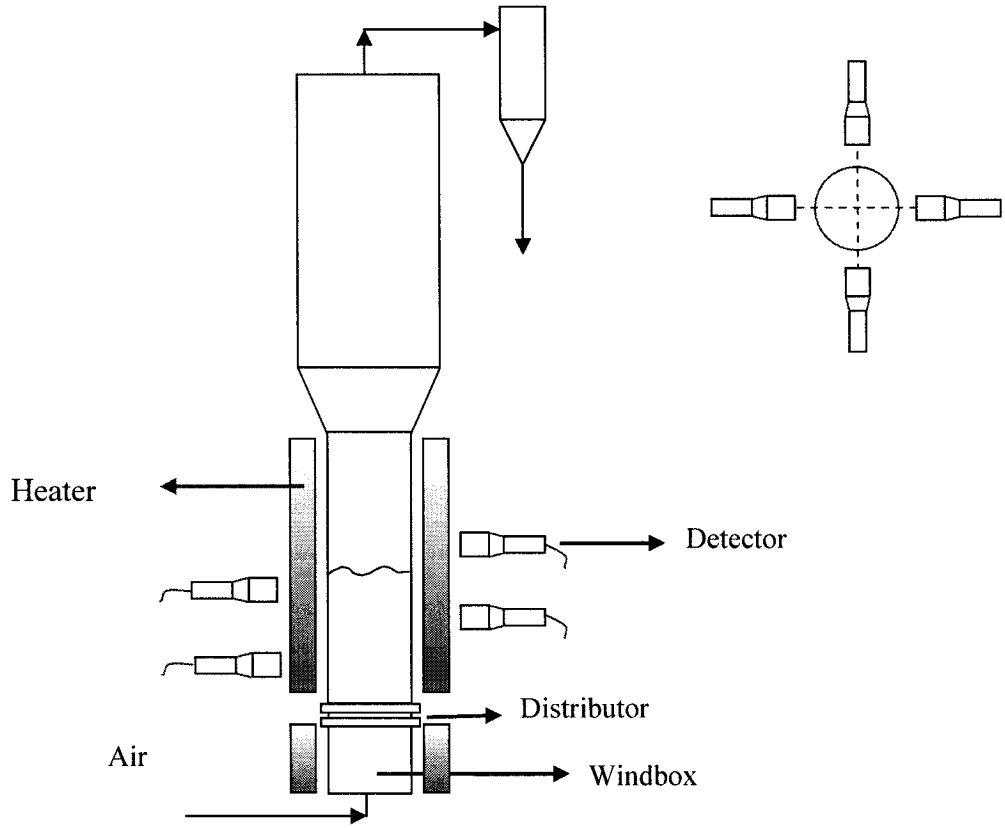

Figure 6.2 Schematic illustration of fluidized bed reactor and the detector's locations

The external surface of the windbox and bed are wrapped with heating bands which allow the temperature in the bed to be maintained as high as 800°C. The gas flow rate to the reactor is measured by means of a rotameter, at low gas velocities, and an orifice plate, at high gas velocities. The fluidizing gas in all the experiments was air.

Air at ambient temperature first passes through the windbox or preheating zone and then enters the bed through a distributor. The distributor is a perforated plate made up of 1-mm holes and a total free area of 0.5%. The temperatures in the bed and at various locations in the freeboard are measured using thermocouples. A controller was used to

maintain the temperature in the bed at the desired set point value. The bed material consists of sand particles with an average particle size of 250μm and solid density of 2650 kg/m^3. The static height of the bed was 20 cm for all the experiments. Experiments were carried out at 4 different temperatures and 4 different superficial gas velocities. When changing the temperature from one experiment to another, the flow rate of the air was readjusted to maintain the same superficial gas velocity at the bed temperature. The range of temperature in these experiments were 25-400°C and that of superficial gas velocity 0.17-0.78 m/s. Table 6.1 shows the experimental conditions. The tracer was made of scandium oxide with a density and size close to those of the bed material. It was activated to 300 μ Ci in the SLOWPOKE nuclear reactor at École Polytechnique de Montréal. Eight detectors were located around the fluidized bed to track the particle in the hot bed of sand. The sampling time in the experiments was 20 ms.

6.2.5 RESULTS AND DISCUSSION

6.2.5.1 Dynamics of Phases

The primary objective of this work was to study the effect of the temperature on the global mixing and in particular on the exchange coefficient between the phases. Mixing of solids, however, is affected by dynamics of the phases and their change with temperature. Thus, this issue is addressed here briefly.

Table 6.1 Experimental conditions in bubbling fluidized bed and calculated result

Run	Bed material	u (m/s)	T (°C)	u_{mf} (m/s)	u_b (m/s)	u_{as} (m/s)	u_{ds} (m/s)	f_{as} Cal.	f_{as} Exp.	K_w (1/s)
1	Sand	0.17	25	0.09	0.32	0.03	0.05	0.61	0.53	1.6
2	Sand	0.29	25	0.09	0.38	0.04	0.08	0.66	0.53	0.7
3	Sand	0.38	25	0.09	0.42	0.07	0.07	0.51	0.54	0.93
4	Sand	0.52	25	0.09	0.51	0.08	0.01	0.53	0.52	1.4
5	Sand	0.75	25	0.09	0.7	0.14	0.17	0.54	0.54	1.7
6	Sand	0.17	200	0.067	0.34	0.03	0.03	0.54	0.51	1.0
7	Sand	0.29	200	0.067	0.37	0.05	0.11	0.70	0.55	0.58
8	Sand	0.38	200	0.067	0.49	0.06	0.16	0.73	0.58	0.90
9	Sand	0.52	200	0.067	0.62	0.09	0.10	0.52	0.59	0.74
10	Sand	0.75	200	0.067	0.77	0.14	0.22	0.61	0.53	1.2
11	Sand	0.29	300	0.058	0.46	0.06	0.10	0.64	0.53	0.72
12	Sand	0.38	300	0.058	0.5	0.07	0.10	0.59	0.53	0.63
13	Sand	0.52	300	0.058	0.66	0.09	0.10	0.53	0.52	0.68
14	Sand	0.29	400	0.052	0.43	0.06	0.07	0.53	0.51	0.64
15	Sand	0.38	400	0.052	0.48	0.06	0.17	0.70	0.60	0.85
16	Sand	0.52	400	0.052	0.63	0.08	0.17	0.68	0.59	0.86

The effect of temperature on the dynamics of phases in a fluidized bed has been investigated before in our lab. Cui and Chaouki (2004) have reported a change in the local flow structure and phase dynamics in the fluidization of FCC (Geldart-A) particles. They found that the local concentration of FCC particles in the dense phase decreases by increasing temperature and that solid particles tend to be distributed more homogenously in the two phases by increasing the temperature. Formisani et al. (2002) using the bed collapse technique, also, reported a change in the global bed voidage and bubble hold-up for silica sand (Geldart-B) and FCC particles. The change in the flow structure eventually affects the global mixing of solids, which is the subject of this study.

Figure 6.3 shows the effect of superficial gas velocity on the phase dynamic changes at two different temperatures. Total number of 80,000 data points was used in each experimental run. As this figure demonstrates, the distribution of velocities exhibits a Gaussian function with an average velocity of zero. The maximum distribution takes place at the vicinity of zero velocity. This suggests that particles spend more time wandering in the emulsion phase where due to random walking or the Brownian motion of the particles the velocity is very close to zero (Mostoufi and Chaouki, 2004; Stein *et al.*, 2000).As it was expected, by increasing the superficial gas velocity the effect of the bubbles in the bed becomes more vigorous and more particles are being picked up by the bubbles. By increasing the probability of particles being caught in the bubbles and move with bubbles in the wake the distribution of velocity close to zero decreases. This is again due to Brownian motion of particles in the emulsion phase which causes an average velocity very close to zero. The velocity of particles in the wake or drift of bubbles strongly deviates from zero and thus a reduction in the distribution of the velocity in the vicinity of zero is observed by `increasing the probability of the particles being picked up by bubbles.

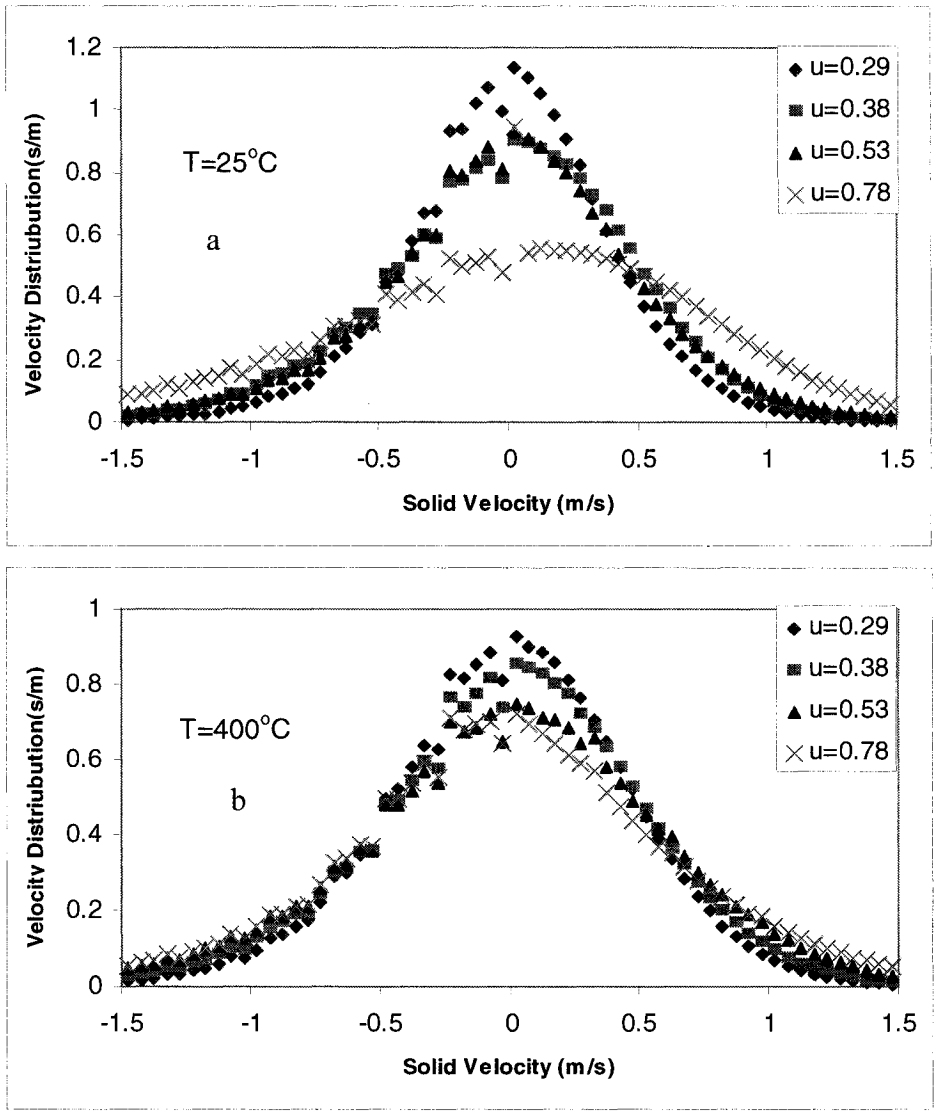

Figure 6.3 Effect of superficial gas velocity on solid velocity distribution

Figure 6.4 shows the distribution of tracer velocity at two different superficial gas velocities and at different bed temperatures for sand particles (see Table 6.1). Figure 6.4 unveils the effect of temperature on the phase dynamics. The temperate seems to have the same effect on the phase distribution in the bed as the velocity. By increasing

the temperature the intensity of the peak changes at velocities close to zero and is lower at higher temperatures. As Figures 6.3-a and 6.3-b show, by increasing the temperature at the same superficial gas velocity the distribution of the velocity in the vicinity of zero decreases. This indicates that by increasing the temperature more particles move to the dilute phase where they move more rapidly in the wake, drift or descending phase.

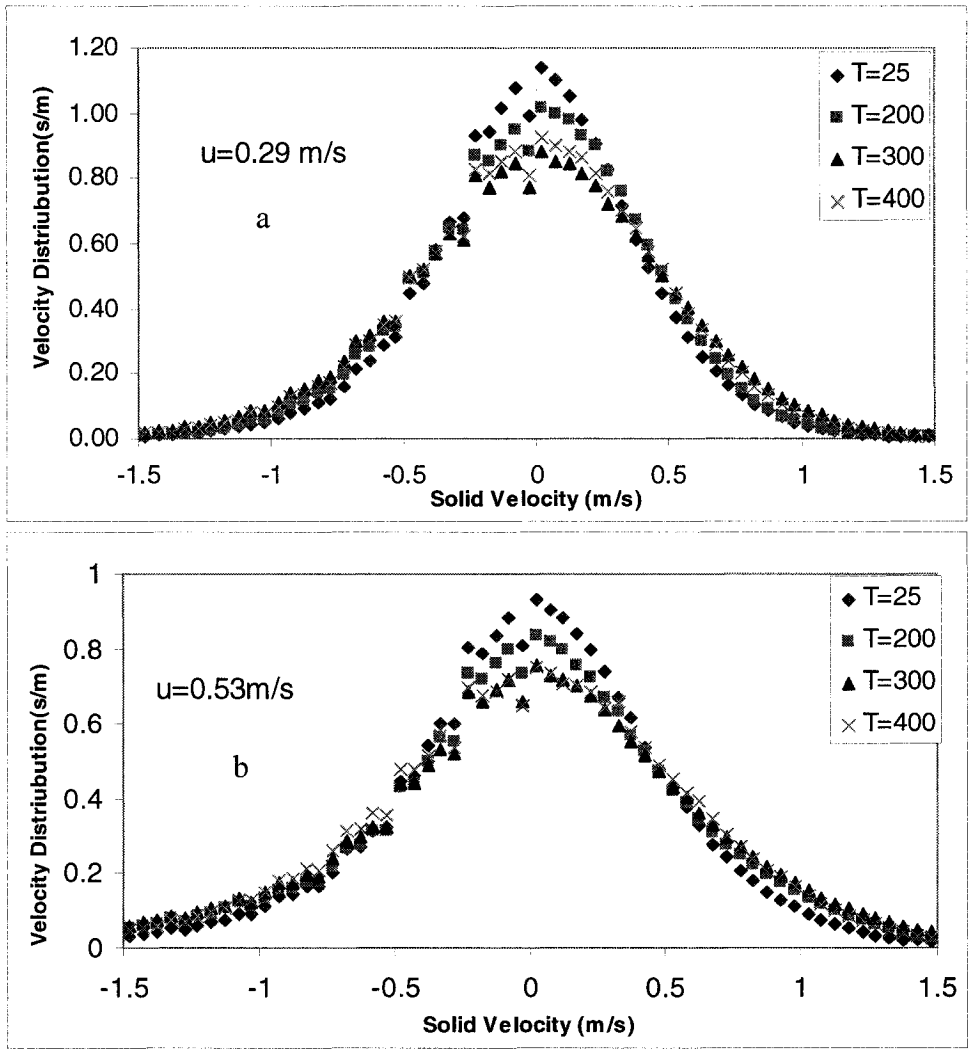

Figure 6.4: Effect of temperature on solid velocity distribution

In other words, by increasing the temperature, particles have more of a chance to be picked up by the bubbles or the descending clusters and move accordingly at a higher velocity. As a result of this, the distribution of the particles in the emulsion phase, where the velocity is close to zero, decreases. Therefore, at higher temperatures, the hold-up of solid particles decreases in the emulsion phase and increases in the bubble phase. This finding is consistent with the aforementioned result reported by Cui and Chaouki (2004)

By increasing the probability of solid particles being caught by the bubbles, one then could expect an increase in the ascending and descending velocity. A behavior, which can be observed in the ensemble average velocity of the countercurrent phases as reported in the Table 6.1. Thus, one also could conclude that the axial mixing of the solid particles is enhanced by increasing the temperature.

The ascending and descending velocity of the particles in the bed, reported in Table 6.1 and being used in solving the model's equations (Equations (6.1) and (6.2)), is calculated by dividing the bed into imaginary cells of equal size. Every time the tracer is entering a particular cell, its velocity is calculated. Finally, for all the cells in a certain elevation a mean velocity is calculated and is assigned to that specific cell. In order to prevent the cancellation of positive (ascending) and negative (descending) velocities, the mean upward and downward velocities were calculated separately at each elevation in the bed. A height dependent velocity profile was thus established

throughout the bed. The same procedure was applied to estimate the fraction of each countercurrent phase at different heights. Table 6.1 also reports fraction of bed in ascending phase (f_{as}) derived from the experimental result and calculated from the mass balance (i.e.: $U_{as} \times f_{as} = U_{ds} \times (1-f_{as})$). Figure 6.5 shows the axial velocity profile of the ascending and descending phases as a function of bed height.

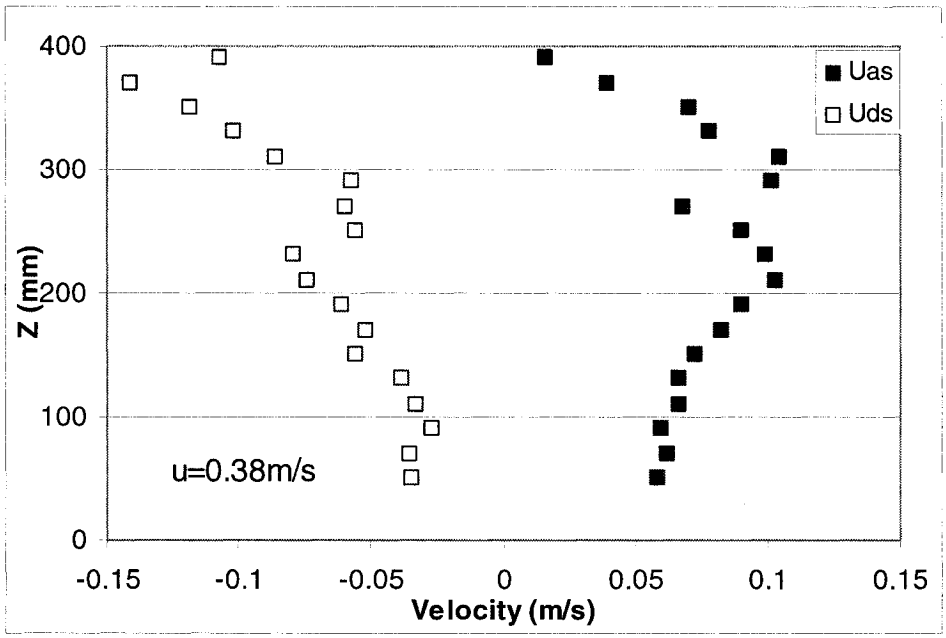

Figure 6.5: Mean ascending and descending velocity of the particle as a function of bed height (u=0.38 m/s)

6.2.5.2 Mixing Dynamics

In order to study the mixing dynamics in the bed, a large number of tracer particles must be injected into the bed. RPT experiments, however, result in instantaneous position of a single particle. The ergodicity theory enables us to virtually inject a large number of virtual particles at the same time and at a certain location in the bed. Details of the ergodicity theory and treatment of the experimental result to provide the injection of a large number of particles can be found elsewhere (Cassanello et al., 1996; Mostoufi and Chaouki, 2001; Larachi et al., 2003). The follow up of the movement of the tracers in the bed provides information on the concentration of tracers in different locations of the bed and at different times.

Five thousands tracer particles are injected at Z=200 mm (Z/H=0.5) from the distributor. The movement of the tracers is followed up for one thousands consecutive data points (20 seconds of experimental time). The long sampling time assures mixing in the bed until the equilibrium point. Figure 6.6 shows the dispersion of the particles in the bed for one experiment. The axial concentration profile of the tracer is then calculated by counting the number of particles in each cell in the bed and normalizing it by the total number of particles injected into the bed. Figure 6.7 shows the typical

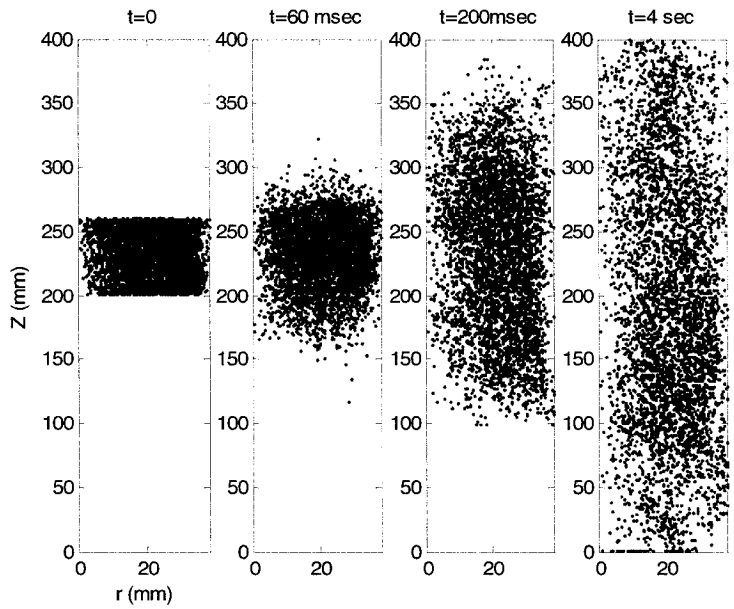

Figure 6.6: Dispersion of 5000 solid particles in the bed (u=0.38 m/s)

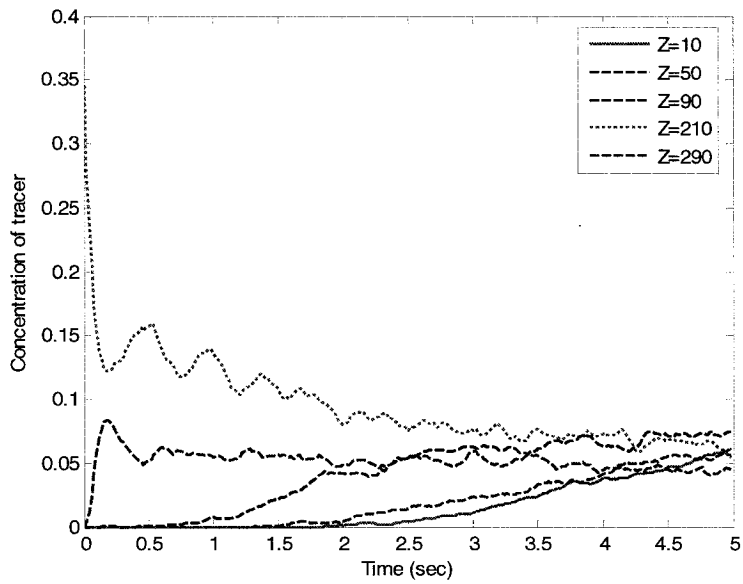

Figure 6.7: Concentration profile of the solid tracers at different heights of the bed (u=0.38 m/s)

concentration profile at different heights of the bed found for one of the experiments. The height of the bed indicated in Figure 6.7 and used in this work is the height of the center of each imaginary cell with respect to the distributor. The oscillations found in the concentration profile, as shown in the Figure 6.7, are common behavior in pulse injection to bubbling fluidized beds and have been reported by other investigators (Lim et al., (1991), Hull et al., (1999)). In fact, these oscillations reveal the existence of back mixing in the fluidized bed and prove the CCBM model to be a more robust model than the dispersion one.

6.2.5.3 Model Prediction and Parameter Estimation

Partial differential equations presented by Equations (6.1) and (6.2) were discretized and solved numerically for all the imaginary compartments in the bed. An optimization algorithm based on the Nelder-Mead direct search method was used to calculate the value of the exchange coefficient (K_w) as the only adjustable parameter in the model. Solid particles concentration predicted by CCBM model was fitted to the experimental concentration for all the height in the bed to obtain an optimum value for K_w. The correlation coefficients for different experiments were between 0.85-0.9. The model was solved for different experiments at different superficial gas velocities and bed temperatures. Figure 6.8 compares the model predictions with the experimental data for one of the experiments. Table 6.1 summarizes all the calculated K_w values for all the experiments.

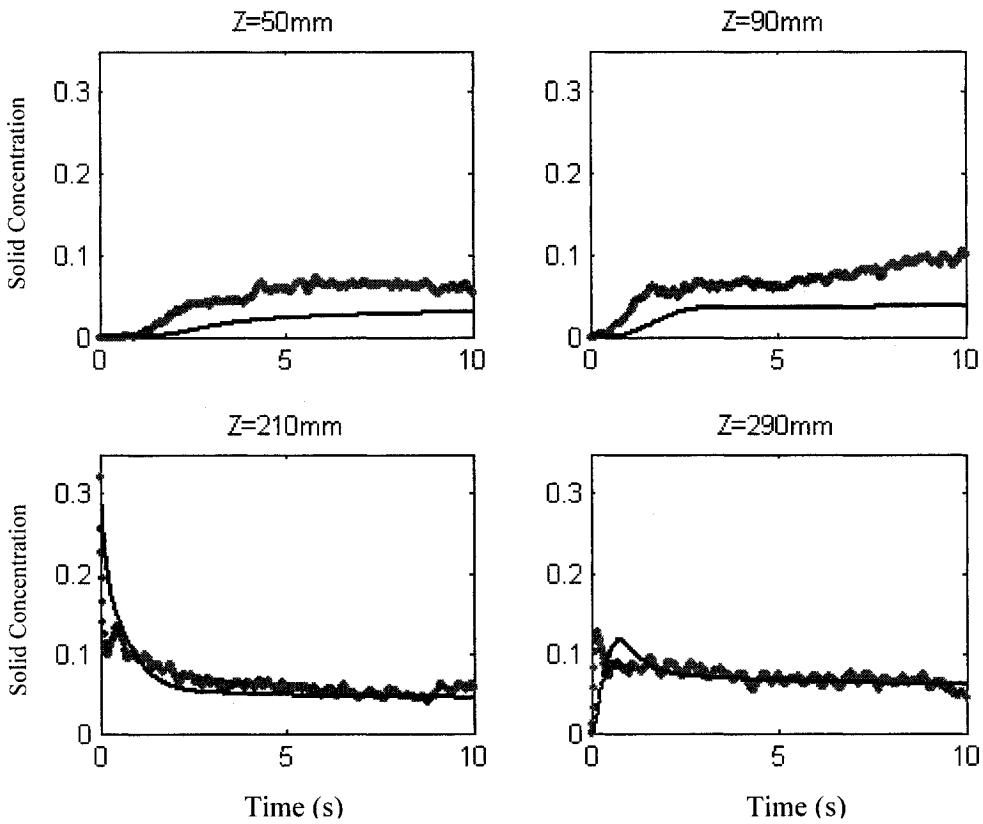

Figure 6.8: Typical concentration profile of the tracer after a pulse injection as a function of time, line for the model and dots for the experimental data, u=0.29, T=400°C

Table 6.2: Correlations for solid exchange coefficient and hydrodynamic parameters

Parameter	**Correlation**	**Reference**
Wake exchange coefficient	$K_w = \frac{3}{1-(1-f_w)\delta_b}\frac{1-\varepsilon_{mf}}{\varepsilon_{mf}}\frac{u_{mf}}{d_b}$	Yoshida and Kunii, 1968
Wake exchange coefficient	$K_w = \frac{4u_{mf}}{\pi\varepsilon_{mf}d_b}$	Chiba and Kobayashi, 1977
Wake exchange coefficient	$K_w = 0.807\frac{u_b}{d_b}$	Kocatulum et al. 1991
Wake exchange coefficient	$K_w = \frac{0.075(u-u_{mf})}{u_{mf}d_b}$ *for* $u/u_{mf} < 3$ $K_w = \frac{0.15}{d_b}$ *for* $u/u_{mf} > 3$	Lim et al., 1993
Wake exchange coefficient	$K_w = \frac{0.081}{2\varepsilon_{mf}d_b}$	Hoffmann et al., 1993
Minimum Fluidization velocity	$\mathrm{Re}_{p,mf} = \left[(27.2)^2 + 0.0408Ar\right]^{0.5} - 27.2$	Grace, 1982
Bubble Diameter	$d_b = d_{bm} + (d_{b0} - d_{bm})e^{-0.3Z/d_t}$ $d_{bm} = 0.65\left(\pi/4d_t^2(u_0 - u_{mf})\right)^{0.4}$ $d_{b0} = 1.3/g^{0.2}(u_0 - u_{mf}/N_{or})^{0.4}$	Mori and Wen, 1975
Bubble velocity	$u_b = u_0 - u_{mf} + u_{br}$ $u_{br} = 0.711(gd_b)^{0.5}$	Davidson and Harrison, 1963
Bubble fraction	$\delta_b = \frac{u_0 - u_{mf}}{u_b - u_{mf}}$	Kunii and Levenspiel, 1991

6.2.5.4 Comparison with Correlations

An increase in temperature not only changes the physical properties of the gas but also modifies the inter-particle forces involved in the fluidization of particles. However, the correlations that have been developed to estimate various hydrodynamic parameters, including K_w, take into account only the physical property changes of the gas phase at different temperatures. Therefore, these correlations are not necessarily accurate at higher temperatures.

A handful of correlations exist in the literature for the exchange coefficient between the wake and emulsion phase. The exchange coefficient varies directly with the minimum fluidization velocity and inversely with bubble velocity. Recent research, however, shows that the exchange coefficient is invariant with minimum velocity, but bubble velocity has a reverse impact on that. Lim et al. (1993) have shown that the correlations presented by both Yoshida and Kunii (1968) and Chiba and Kobayashi (1977) overestimate the exchange coefficient by one order of magnitude. The correlation presented by Lim et al. (1993), however, seems to predict more satisfactorily the exchange coefficient. Table 6.2 represents some correlations for the prediction of wake exchange coefficient as well as other required hydrodynamic parameters used in this work.

Figure 6.9 compares the K_w obtained in this work at T=25°C and T=200°C and different superficial gas velocities with those predicted by the correlations listed in Table 6.2. At ambient temperature, all the correlations overestimate the value of the exchange coefficient (K_w). The correlation developed by Hoffmann et al. (1993) and Lim et al. (1993), however, are the closest to the value obtained in this work. At higher superficial gas velocity (u/u_{mf}>5) the agreement between the aforementioned correlation and the obtained K_w is more satisfactory. As pointed out earlier, all the correlations listed in Table 6.2 have been developed at ambient temperature and in 2-D fluidized beds. This explains one reason for the deviation between the model and correlations even at ambient temperature. The correlations presented by Chiba and Kobayashi (1977) and Yushida and Kunii (1968) clearly overestimate the K_w. This agrees with previous studies (Lim et al., 1993).

At 200°C, even at higher gas superficial velocities (u/u_{mf}>5), less agreement is observed between the model and estimated value given by Lim's correlation. The simple correlation given by Hoffmann et al. (1993) in this case gives the best agreement with the experimental results.

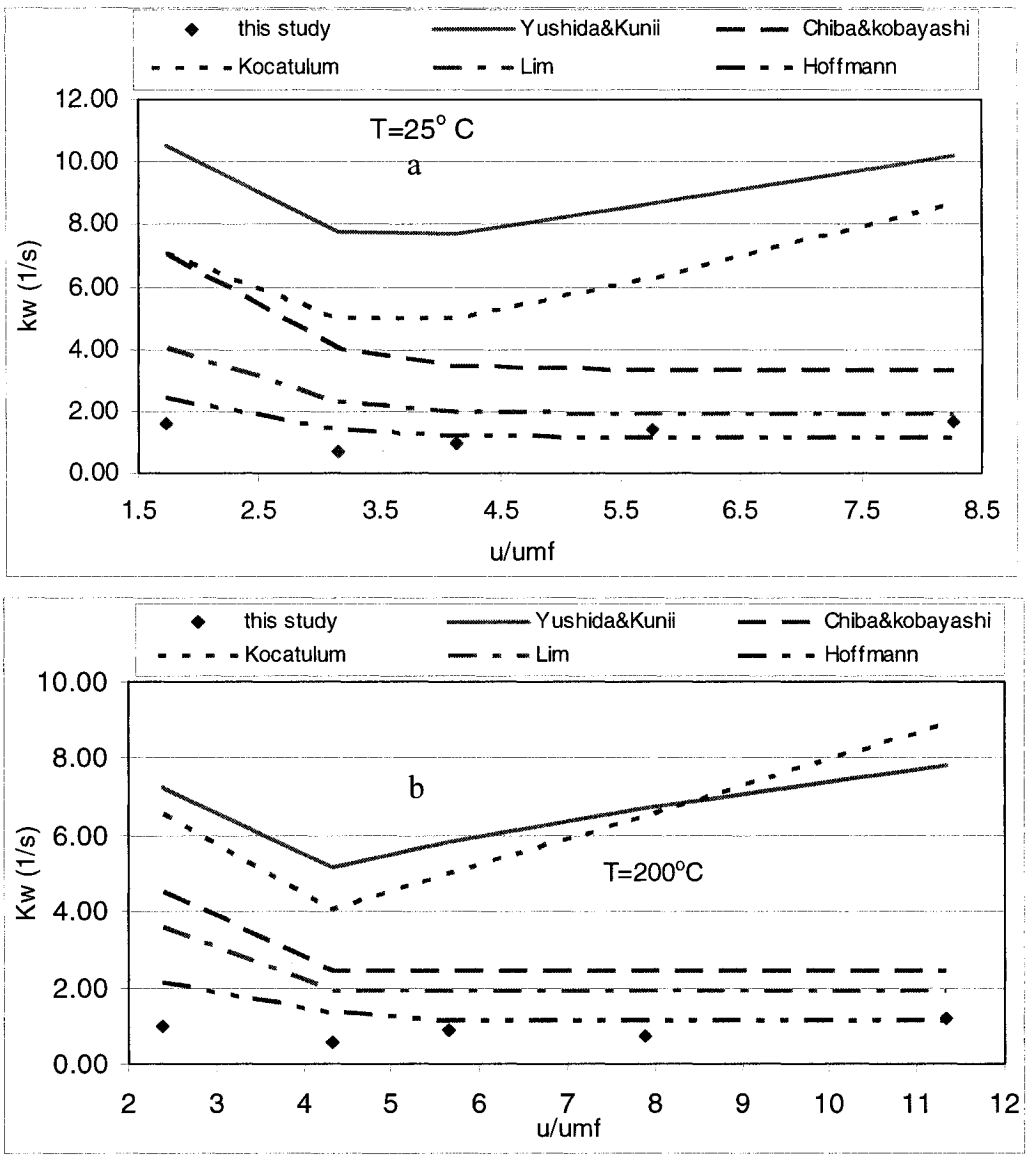

Figure 6.9: K_w value at different superficial gas velocities (a) T=25°C (b) u=0.38 m/s

The decrease in the value of K_w can be explained by the change that has occurred in the phases dynamics. As mentioned before, by increasing the temperature, more solids are caught by the bubbles and, thus, the velocity of the ascending phase increases. By increasing the ascending phase velocity the velocity of the descending phase also

increases to compensate for the higher upward solid mass flux. This causes more axial mixing in the bed. However, at the same time, when the particles spends more time in the dilute phase (ascending or descending) the mass transfer between the phases decreases. This is consistent with the sensitivity analysis done on the model, which shows that increasing the K_w has an inverse impact on the axial mixing. As a matter of fact, by increasing the K_w lateral mixing is enhanced while axial mixing diminishes. On the other hand, by increasing the wake velocity one expects an increase in the bubble size, which according to various studies has an inverse effect on the value of K_w in the bed.

6.2.6 CONCLUSIONS

The CCBM model was used to model solids mixing in the fluidized bed of sand particles at high temperatures. The effect of temperature on the phase dynamic shows more solids are present in the dilute phase at higher temperatures. This, in turn, affects the global mixing of solids in the bed. The dynamic parameters, i.e., ascending and descending velocities of the phases and the fraction of each phase in the bed, were found using the instantaneous position of a tagged particle in the bed in the RPT experiments. The only adjustable parameter when fitting the model to the concentration response from a pulse injection was the exchange coefficient between the phases. K_w was found to be in the range of 0.7-1.6 s^{-1} for different experiments. A decrease in the value of K_w by increasing the temperature was found and justified based on the dynamic changes in the bed.

6.2.7 NOTATIONS

C	concentration of particles
d	diameter, m
f	fraction of the ascending/descending phase in the bed
H	height of the bed, m
K	exchange coefficient between the countercurrent phases, 1/s
Re	Reynolds number
U	velocity of the particles in the ascending or descending phases, m/s
u	gas velocity, m/s

Greek letters

ε	voidage
δ	bubble fraction in bed

Subscripts

as	ascending phase
b	bubble
ds	descending phase
m	maximum
mf	minimum fluidization
w	wake

6.2.8 REFERENCES

Basesme, E. A.; Levy, E. K., "Solids exchange between the bubble wake and the emulsion phase in a two-dimensional gas-fluidized bed", Powder Technology, Vol.72, No. 1, 45-50 (1992).

Cassanello, M.; Larachi, F.; Guy, C.; Chaouki, J., "Solids mixing in gas-liquid-solid fluidized beds: experiments and modeling", Chem. Eng. Sci., Vol. 51, No.10, 2011-2020 (1996).

Chiba, T.; Kobayashi, H., "Solid Exchange between the bubble wake and the emulsion phase in a gas-fluidized bed" Journal of chemaical engineering of Japan, Vol.10, No. 3, 206-210 (1977).

Cui, H.; Chaouki, J., "Effects of temperature on local two-phase flow structure in bubbling and turbulent fluidized beds of FCC particles", Chem. Eng. Sci., Vol. 59, No.16, 3413-3422 (2004).

Davidson J.F and Harrison D.," Fluidized particles", Cambridge University Press, New York (1963).

Dechsiri, C.; Van Der Zwan, E. A.; Dehling, H. G.; Hoffmann, A. C., "Dispersion of particle pulses in fluidized beds measured by positron emission tomography", AIChE Journal, Vol. 51, No. 3, 791-801(2005).

Formisani, B.; Girimonte, R.; Pataro, G., "The influence of operating temperature on the dense phase properties of bubbling fluidized beds of solids", Powder Technology, Vol.125, No.1, 28-38 (2002).

Grace, J.R. in Handbook of multiphase systems, G. Hetsroni; p.8-1, Hemisphere, Washington, (1982).

Grasa, G.; Abanades, J. C., "The use of two different models to describe the axial mixing of solids in fluidised beds", Chem. Eng. Sci., Vol. 57, No. 14, 2791-2798 (2002).

Hoffmann, A.C.; Janssen, P. B. M., Prins, J. "Praticle Segregation in fluidized binary mixtures", Chem. Eng. Sci., Vol. 48, No. 9, 1583-1993 (1993).

Hull, A. S.; Chen, Z.; Fritz, J. W.; Agarwal, P. K., "Influence of horizontal tube banks on the behavior of bubbling fluidized beds. 1. Bubble hydrodynamics", Powder Technology, Vol.103, No. 3, 230-242 (1999).

Kocatulum, B.; Basesme, E. A.; Levy, E. K.; Kozanoglu, B. "In Particle motion in the wake of a bubble in a gas-fluidized bed", Annual Meeting of the American Institute of Chemical Engineers, Nov 17-22 1991, Los Angeles, CA, USA, 40-50 (1991).

Kunii D.and Levenspiel O.,. "Fluidization engineering" 2nd ed. MA, Butterworth-Heinemann series in chemical engineering (1991).

Lakshmanan, C. C.; Potter, O. E., "Numerical simulation of the dynamics of solids mixing in fluidized beds", Chem. Eng. Sci., Vol. 45, No. 2, 519-528 (1990).

Larachi, F.; Grandjean, B. P. A.; Chaouki, J., "Mixing and circulation of solids in spouted beds: Particle tracking and Monte Carlo emulation of the gross flow pattern", Chem. Eng. Sci., Vol. 58, No. 8, 1497-1507 (2003).

Lim, K. S.; Gururajan, V. S.; Agarwal, P. K., "Mixing of homogenous solids in bubbling fluidized beds: theoretical modelling and experimental investigation using digital image analysis", Chem. Eng. Sci., 48, (12), 2251-2265 (1993).

Lim, K. S.; Zhu, J. X.; Grace, J. R., "Hydrodynamics of gas-solid fluidization", International Journal of Multiphase Flow, Vol. 21, (Suppl), 141-193 (1995).

May, W.G., "Fluidized bed reactor studies", Chemical Engineering Progress, Vol. 55, No. 12, 49-56, (1959).

Mori, S.; Wen, C. Y., "imation of bubble diameter in gaseous fluidized beds", Vol. 21, No. 1, 109-115 (1975).

Mostoufi, N.; Chaouki, J., "Local solid mixing in gas-solid fluidized beds", Powder Technology, Vol. 114, No.1-3, 23-31 (2001).

Mostoufi, N.; Chaouki, J., "Flow structure of the solids in gas-solid fluidized beds", Chem. Eng. Sci., Vol. 59, No. 20, 4217-4227 (2004).

Shen, L.; Zhang, M., "Effect of particle size on solids mixing in bubbling fluidized beds", Powder Technology, Vol. 97, No. 2, 170-177 (1998).

Sitnai, O., "Solids mixing in a fluidized bed with horizontal tubes", Ind. Eng. Chem. Process Des. Dev. Vol. 20, No. 3, 533-538 (1981).

Stein, M.; Ding, Y. L.; Seville, J. P. K.; Parker, D. J., "Solids motion in bubbling gas fluidized beds" Chem. Eng. Sci., Vol. 55, No. 22, 5291-5300 (2000).

van Deemter, J. J, "The countercurrent flow model of a gas-solids fluidized bed", in proceeding of international symposium on fluidization, Netherland university press, Amsterdam (1967).

Yoshida, k.; Kunii, D., "Stimulus and response of gas concentration in bubbling fluidized beds", Journal of Chemical Engineering of Japan, Vol. 1, No. 1, 11(1968).

CHAPTER 7

SOME CHARACTERISTICS OF GAS-SOLID FLUIDIZATION AT HIGH TEMPERATURES*

7. 1 Presentation of the Article

Solids mixing at high temperature was addressed in the preceding chapter. Some other important characteristics of fluidization at elevated temperatures are the subject of the third article, which is presented in this chapter. Radioactive Particle Tracking (RPT) is used to study fluidized bed hydrodynamics in a temperature range of 25-700°C and a superficial gas velocity of 0.16-0.78 m/s. Two different solid particles, both belong to Group-B Geldart classification, are used as bed materials. Fluidized bed combustion and gasification of different solid fuels take place at the temperature range of 800-1000°C. The bed particles in these processes are usually inert particles, which belong to Group-B Geldart classification. Therefore, the hydrodynamic study presented in this work is relevant to fluidized bed *combustion* and *gasification.*

*This article was submitted to Powder Technology

7.2 Some Characteristics of Gas-Solid Fluidization at High Temperatures

Ramin Radmanesh, Jamal Chaouki*, Christophe Guy
Department of Chemical Engineering, École Polytechnique,
P.O. Box 6079, Station Centre-ville, Montréal, QC H3C 3A7, Canada
Fax*: 514 340 4159; e-mail: *jamal.chaouki@polymtl.ca*

7.2.1 ABSTRACT

Radioactive Particle Tracking (RPT) is used for the first time at elevated temperatures to investigate the effect of temperature on characteristics of fluidization in a bubbling regime. Silica sand particles with a solid density of 2650 kg/m^3 and a mean size of 250 μm and alumina particles with a solid density of 3400 kg/m^3 and a mean size of 150 μm, both of which belong to Group-B Geldart classification, are used in this study. Bubble (wake) velocity, jump time (and frequency), granular temperature and cycle time (and frequency) have been studied It is shown that correlations can predict bubble (wake) velocity as long as temperature does not affect surface properties of powders and consequently interparticle forces. However, when temperature affects the surface, as in the case of silica sand powders, the correlations for bubble velocity that only take into account gas phase property changes cannot predict the bubble velocity. It is also found that characteristics time for silica sand particles fluidization changes with changing temperatures, but those of alumina do not show significant changes.

KEYWORDS: Fluidization, Hydrodynamics, High temperature, Bubble velocity

7.2.2 INTRODUCTION

In past decades, chemical, petrochemicals and metallurgical industries have benefited from some unique aspects of gas-solid fluidized beds. Good solid mixing and fair mass and heat transfer are some of the advantages of fluidized beds in comparison to fix beds. Solids and bubbles motions and interactions play a key role in the performance of fluidized bed reactors. Bubble motion in the fluidized bed creates solids mixing and circulation. This, in turn, is very influential, especially when dealing with fast catalytic reactions or extremely exothermic reactions.

Along with new improvements in Computational Fluid Dynamics (CFD) and Discrete Element Method (DEM) modeling, pioneer measuring techniques have also been developed in the last few years to investigate fluidization. Positron Emission Particle Tracking (PEPT), Electrical Capacitance Tomography (ECT) and Radioactive Particle Tracking (RPT) are some of these methods. Stein *et al.* [1] and Stein *et al.* [2] at the University of Birmingham have used PEPT to study solids motion in fluidized bed reactors. Stein *et al.* [2] have been able to follow a tagged radioactive particle with a diameter of 600 μm in a fluidized bed of sand particles. They have measured many interesting characteristics of fluidization, such as jump, relaxation and idle time, as well as circulation frequency in a fluidized bed of 141 mm and 70 mm in diameters. Their results, determined by this non-intrusive technique, have showed good agreement with the previous published data.

Dechsiri *et al.* [3, 4] have used PET to study mixing and dispersion of particles in a fluidized bed. Their technique allows them to label bed particles with ^{18}F and study the dispersion of a group of labeled particles in the bed. The whole reactor is encircled in this case by a PET scanner. The labeling technique used by these authors overcomes some still challenging issues in particle tracking techniques, such as the possibility of having a tracer with a very low particle size (<200 μm) and a low density (<1600 kg/m^3). The technique, however, has the drawback of the reactor being encircled by a block of detector arrays. Moustoufi and Chaouki have used RPT to study local [5], and global [6] solids mixing, as well as the structure of the solid phase [7] in fluidized beds. They have used tracer particles as small as 400 μm. Although RPT leads to spatial coordination of a single tracer particle, experiments carried out over a sufficient length of time can be inferred as a pulse injection of a large number of tracer particles based on the ergodicity theory [8]. Solid diffusivities have been calculated locally in this way and have been presented as a function of radius of the reactor in bubbling and turbulent regimes [5]. Their study on global solid mixing shows that particles in fluidized beds move in the form of downward or upward clusters [6].

Most industrial units operate at elevated temperatures. Temperatures at the exit of risers in Fluid Catalytic Cracker (FCC) units are in the range of 495-550°C. Many catalytic reactions take place in this range of temperature. Fluidized bed combustion and gasification take place at the higher temperature range of 800°C-1000°C. Most studies on the fluidized bed hydrodynamics, however, have been carried out at ambient

temperature. There is certainly a lack of data at high temperatures. The few experimental studies at high temperatures have mostly focused on the effect of temperature on minimum fluidization velocity and bubble size. Pressure drop measurement or visual and x-ray monitoring have been used in most cases.

Geldart and Kapoor [9] have studied the effect of temperature on minimum bubbling velocity and bubble diameter for Group-A particles. They have found a small reduction in bubble size and u_{mb} with increasing temperature from ambient to 200°C. No significant changes, however, was reported at T=300°C. Kia and Furusoki [10] found the same trend for bubble size in the fluidization of FCC and alumina particles, both of which belong to group-A particles in a temperature range of 280-400 K. Unlike group-A particles, Hatate *et al.* [11] have reported a rise in bubble size by increasing temperature from ambient to 600 K in fluidization of Group-B particles. This difference, however, was diminished at higher superficial gas velocities. It is worth noting that the correlations predict an increase in bubble diameter and a reduction in minimum fluidization velocity by increasing temperature. This means more fluidity of particles by increasing temperature, which is a result of the increase in gas viscosity. If for any reason there would be a change in dominant forces from hydrodynamics to interparticles forces, the deviation between correlations, which rely merely on gas physical properties and actual bubble diameter or velocity increases. Lettieri *et al.* [12, 13] have demonstrated a case, where interparticle forces can dominate hydrodynamic forces. They have studied the fluidization of fresh and used (e-cat) FCC catalysts at

temperatures up to 650°C. The large deviation between calculated and measured pressure drop for e-cat used FCC catalysts and also doped silica catalysts at T=200°C shows that the interparticle forces dominate hydrodynamic forces at this temperature. In fact, the heavy hydrocarbons, already inside the pores of e-cat catalysts, start expelling at higher temperatures, which significantly modifies interactions between particles.

Previous studies in our laboratory demonstrate the effect of temperature on solid phase mixing and phase dynamics of Group-A and B particles in the temperature range of 25-400°C [14,15,16]. RPT has the capacity of being easily adopted for harsher experimental conditions at higher temperatures and pressures. In the present study, the experiments are extended to higher temperatures (700°C) and the effect of temperature on characteristics of solid phase is discussed. As already mentioned, fluidized bed combustion and gasification of different solid fuels take place at the temperature range of 800-1000°C. The bed particles in these processes are usually inert sand particles which belong to Group-B Geldart classification. Therefore, the hydrodynamic study presented in this work is relevant to fluidized bed combustion and gasification.

7.2.3 EXPERMIMENTAL

Figure 7.1 shows a schematic presentation of the reactor and detectors around the bed. The fluidized bed column is made of stainless steel that withstands high temperatures. It consists of a bed and freeboard of 78 ID mm and 750 mm in height, a windbox, which also serves as a pre-heater, and a disengagement zone of 150 ID mm and 900 mm in height. The external surface of the windbox and bed are wrapped with 6 KW heating bands. This allows temperatures as high as 800°C to be achieved in the bed.

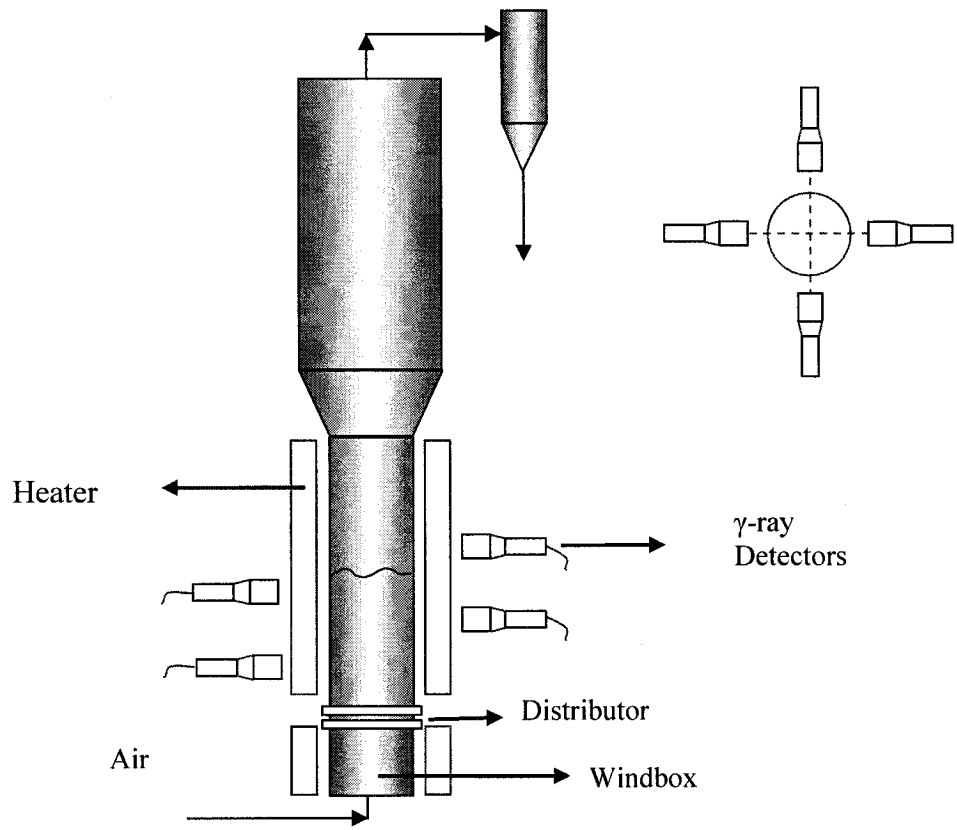

Figure 7.1: Schematic illustration of fluidized bed reactor and detectors

The gas flow rate to the reactor is measured by means of rotameter, at low gas velocities, and an orifice plate, at high gas velocities. The fluidizing gas in all the experiments was air.

Air at ambient temperature first passes through the windbox or preheating zone and then enters the bed through a distributor. The distributor is a perforated plate made up of 1-mm holes and a total free area of 0.5%. The temperatures in the bed and at various locations in the freeboard are measured using the thermocouples. A controller was used to maintain the temperature in the bed at the desired set point value. Two types of solid particles were used in the experiments. Silica sand particles with an average particle size of d_p=250μm and solid density of ρ_p=2650 kg/m^3 and alumina particles with d_p=150μm ρ_p=3400 kg/m^3. The settled bed height above the distributor was 20 cm for all the experiments. Experiments were carried out at different temperatures and superficial gas velocities. When changing the temperature from one experiment to the other, the flow rate of the air was readjusted to maintain the same superficial gas velocity at the bed temperature. The range of temperature in these experiments was 25-700°C and that of superficial gas velocity was 0.16-0.78 m/s. No sintering or agglomeration of sand/alumina particles were observed in the range of temperature used in these experiments. Table 7.1 lists the experimental conditions.

Table 7.1: Experimental conditions and velocity of bubbles (wakes) calculated using RPT data

Run	Bed material	u_g (m/s)	T (^{0}C)	u_{mf} (m/s)	u_w (m/s)
1	Sand	0.16	25	0.09	0.43
2	Sand	0.29	25	0.09	0.38
3	Sand	0.38	25	0.09	0.42
4	Sand	0.52	25	0.09	0.51
5	Sand	0.16	200	0.067	0.38
6	Sand	0.29	200	0.067	0.37
7	Sand	0.38	200	0.067	0.49
8	Sand	0.52	200	0.067	0.62
9	Sand	0.16	300	0.058	0.44
10	Sand	0.29	300	0.058	0.46
11	Sand	0.38	300	0.058	0.5
12	Sand	0.52	300	0.058	0.66
13	Sand	0.29	400	0.052	0.43
14	Sand	0.38	400	0.052	0.48
15	Sand	0.52	400	0.052	0.63
16	Sand	0.16	500	0.047	0.39
17	Sand	0.29	500	0.047	0.35
18	Sand	0.38	500	0.047	0.4
19	Sand	0.52	500	0.047	0.55
20	Sand	0.16	600	0.043	0.37
21	Sand	0.29	600	0.043	0.35
22	Sand	0.38	600	0.043	0.42
23	Sand	0.52	600	0.043	0.51
24	Sand	0.29	700	0.04	0.40
25	Sand	0.38	700	0.04	0.44
26	Sand	0.52	700	0.04	0.56
27	Alumina	0.29	25	0.054	0.46
28	Alumina	0.53	25	0.054	0.63
29	Alumina	0.87	25	0.054	0.92
30	Alumina	0.29	200	0.039	0.47
31	Alumina	0.53	200	0.039	0.70
32	Alumina	0.87	200	0.039	0.94
33	Alumina	0.29	400	0.030	0.49
34	Alumina	0.53	400	0.030	0.68
35	Alumina	0.87	400	0.030	0.94
36	Alumina	0.29	600	0.025	0.41
37	Alumina	0.53	600	0.025	0.59
38	Alumina	0.87	600	0.025	0.93

The tracer was made of scandium oxide with a density and size close to those of the bed material. It was activated to 300 μC_i in the SLOWPOKE nuclear reactor at École Polytechnique de Montréal. The long half life of scandium made it possible to run continuously for long period of time. Eight detectors were located around the fluidized bed to track the particle in the hot bed of sand. The sampling time in the experiments was 20 m s. Each experiment lasted at least 4 hours. Details of RPT experiments and the tracer position reconstruction can be found elsewhere [17].

7.2.4 RESULTS AND DISCUSSION

7.2.4.1 Bubble wakes velocity

Two ascending solid phases can be distinguished in bubbling fluidized beds: the wake phase that accompanies the bubbles with a velocity that is very close to that of the bubbles and the drift phase. The drift phase is the result of the wake phase shedding into the emulsion phase and, therefore, has a velocity less than the wake phase, but significantly higher than the emulsion phase. In the RPT experiments, when the tracer gets caught in a bubble its axial velocity boosts substantially. These higher velocities resulting from the upward movement of the tracer with the bubbles, if filtered from the other velocities corresponding to the drift and emulsion phase give rise to wake (bubble) velocity. Mostoufi and Chaouki [7] have proposed a method to filter out axial velocity signals related to the wake phase from the drift and emulsion phases. All the data points are scanned and all the consecutive data points with a constant axial

velocity for 10 or more consecutive data points are put aside. All the 10 consecutive data points with correlation coefficient (R) less than 0.98 are rejected. The result of such treatment is shown in Figure 7.2. Figure 7.2-a shows the tracer velocity distribution for all the data points at T=700^{o}C and u_g=29 cm/s. The distribution is a Gaussian function with the average velocity very close to zero. Figure 7.2-b shows the velocity distribution of the tracer after filtering corresponding to the times when it moves in a constant axial (upward/downward) velocity at the same operating condition. The negative side of the velocity, as explained by Mostoufi and Chaouki [7], represents the downward movement of particles (stable clusters) in the emulsion phase. The positive velocities are associated with the times when the tracer is caught in bubbles that have reached their stable velocities and moves upwardly with a higher velocity than the drift or emulsion phase. This may occur at different height of the bed and, correspondingly, there is a distribution of wake velocity. The time average of the upward velocities shown in Figure 2-b gives rise to mean wake (bubble) velocities. The wake velocity calculated in this manner is considered as the average of the wake velocity for the conditions of the bed. The average calculated wake velocities for different superficial gas velocities and bed temperatures are shown in Figure 7.3a-b. The lines in these figures represent the bubble velocity given by the correlations and the symbols are the experimental values of wake velocities determined using the mentioned method. Table 7.2 shows the

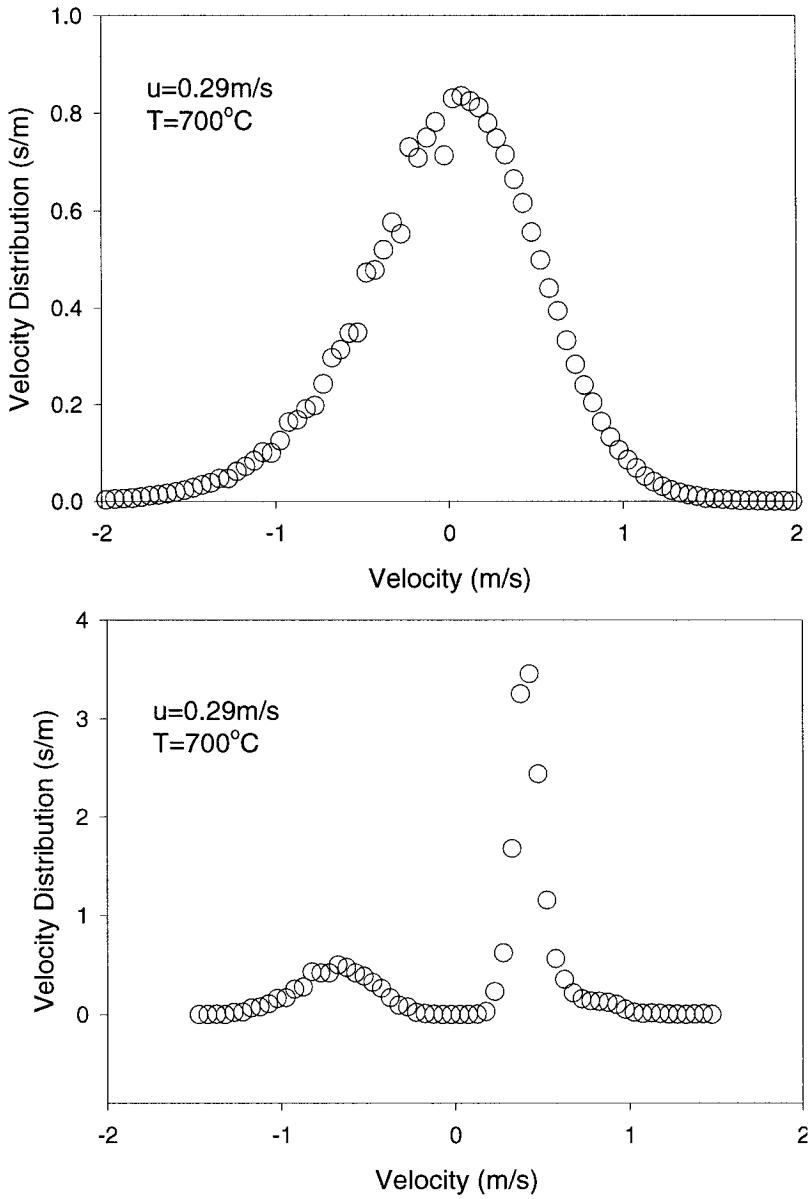

Figure 7.2: Velocity distribution of tracer in bed of sand particles. a) total velocity distribution b) velocity distribution of particle with constant velocity in 10 or more consecutive sampling time (t≥200ms)

correlations used in this study to calculate the wake velocity. The wake velocity was calculated at the middle of the bed height. Figures 7.3-a and 7.3-b portray calculated and measured wake velocities at the temperature range of 25-400°C and 500-700°C, respectively. Figure 7.3-a indicates a relatively good agreement between the correlation and experiments. However, by increasing the bed temperature there is a deviation between the calculated and measured bubble velocities. This is shown in Figure 7.3b where for T>400°C the correlations overestimate the wake velocities. It must be noted that the correlation only takes into account the changes in the viscosity and density of gas with temperature. The trend shown in Figure 7.3b cannot, however, be exclusively explained by gas property changes. The temperature might affect and change the surface properties of the sand particles as well and, thus, would change the interparticle forces. This, in turn, would affect the fluidity of the solid and characteristics of fluidization. This might be a peculiarity of the silica sand used in these experiments. As it is shown in Figure 7.4 a good agreement is demonstrated by alumina particles. The agreement is even excellent at the high temperature of 600°C.

In order to investigate the effect of temperature on solid particles surface, Scanning Electron Microscopy (SEM) of the surface of both silica sand and alumina particles was performed. The particles were fluidized at ambient and the high temperature of T=700°C for 2 hours. Samples from ambient and high temperature fluidization were collected for SEM experiments. The SEM results, presented in Figure 7.5, demonstrate a change on the surface of the silica sand particle after fluidization at high

temperatures. There exists no change on the surface of the alumina particles after being fluidized at higher temperatures.

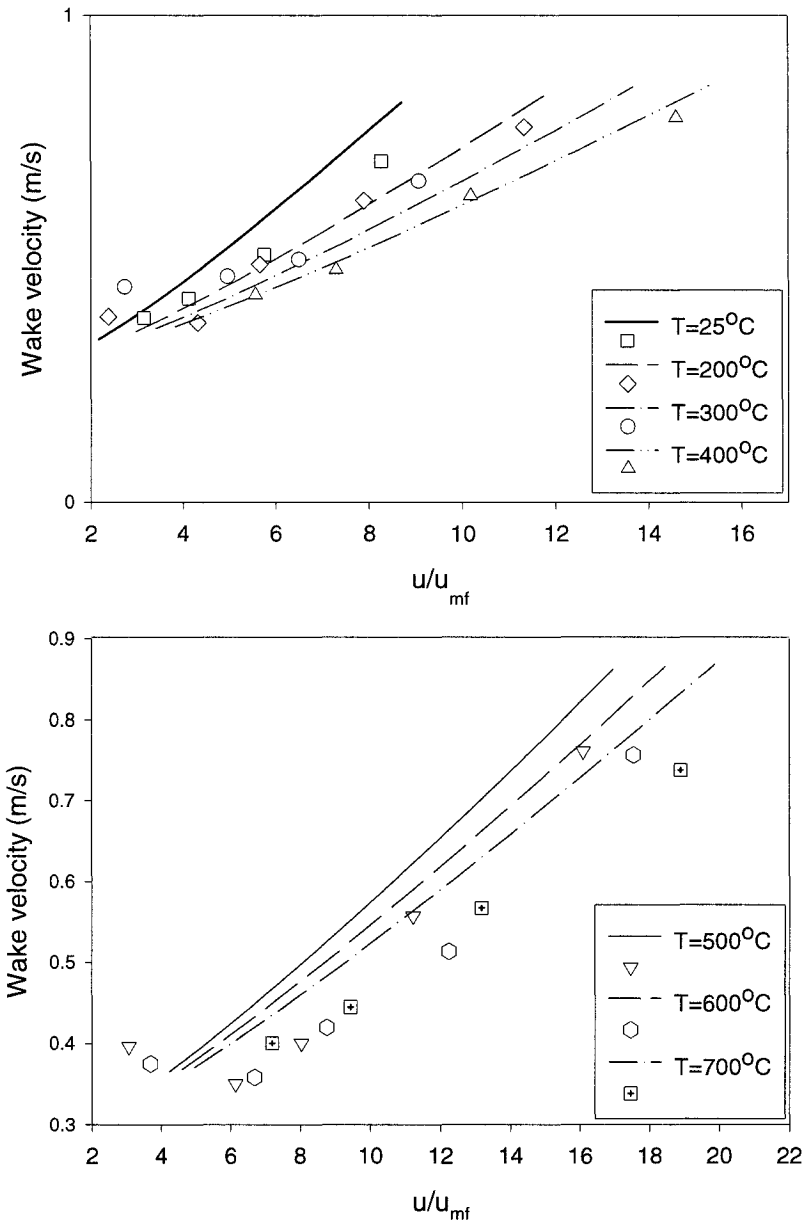

Figure 7.3: The wake velocity for sand particles calculated from RPT results at high temperature verses wake velocity given by the correlations (see Table 2). Symbols represent calculated values and lines are for the correlation

Table 7.2: Hydrodynamic correlations used to calculate wake velocity

Parameter	Correlation	Reference
Minimum fluidization velocity	$Re_{p,mf}=\left[(27.2)^2+0.0408Ar\right]^{0.5}-27.2$ $Ar=\frac{d_p^3\rho_g(\rho_s-\rho_g)g}{\mu^2}$	[18]
Bubble Diameter	$d_b=d_{bm}+(d_{b0}-d_{bm})e^{-0.3Z/d_t}$ $d_{bm}=0.65\left(\pi/4d_t^2(u_0-u_{mf})\right)^{0.4}$ $d_{b0}=1.3/g^{0.2}(u_0-u_{mf}/N_{or})^{0.4}$	[19]
Bubble velocity	$u_b=u_0-u_{mf}+u_{br}$ $u_{br}=0.711(gd_b)^{0.5}$	[20]
Wake velocity	$u_w=u_b$	[20]
Bubble fraction	$\varepsilon_b=\frac{u_0-u_{mf}}{u_b-u_{mf}}$	[20]

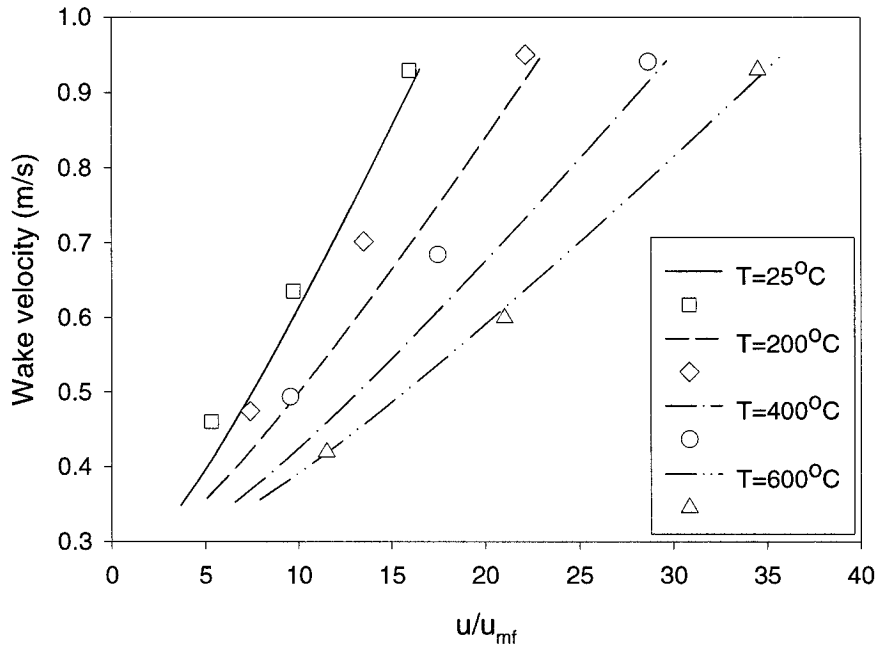

Figure 7.4: The wake velocity for alumina particles calculated from RPT results at high temperature verses wake velocity given by the correlations (see Table 7.2). Symbols represent calculated values and lines are for the correlation.

The color change of the sand particles after fluidization at high temperatures also suggest a change occurred in the structure of silica sand particles.. Pressure drop at different superficial gas velocity was measured across the bed as well. The minimum fluidization of sand particles, measured by recording the pressure drop at different gas velocity, remained unchanged after and before fluidization at high temperature. This suggests that there is no change in the size or density of the silica sand particles. The peculiar fluidization behavior of silica sand particles, therefore, can be related to the surface property changes. As a result of changes in the surface, the bubble velocity cannot be explained by gas property changes alone.

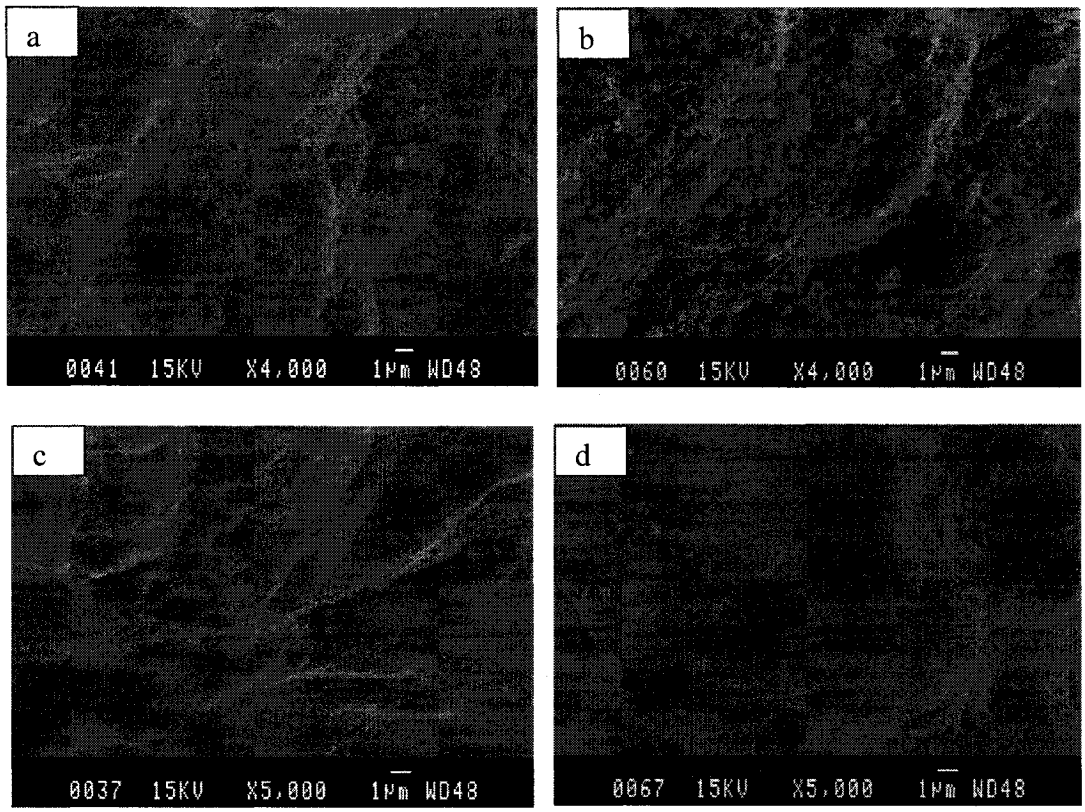

Figure 7.5: SEM results of silica sand and alumina particles before and after fluidization at high temperatures.

a) Surface of a silica sand particle before fluidizing at high temperature

b) Surface of a silica sand particle after fluidizing at T=700°C

c) Surface of a alumina particle before fluidizing at high

7.2.4.2 Jump Time Distribution

Jump time as proposed by Stein *et al.* [2] is the time that a particle spends in the wake of a bubble. The criteria presented by Stein *et al.* [1] were used to calculate the

distribution of jump times. Based on their criteria, a jump is defined as a vertical upward movement with a vertical velocity superior than 0.1 mm/s and a magnitude greater than 24 mm. Figure 7.6 shows the number of jumps in the fluidization of silica sand particles as a function of jump duration at a gas superficial velocity of 0.16 m/s and different bed temperatures. The average jump duration remains around 100 ms at all temperatures. The number of jumps, however, changes significantly with temperature at this gas velocity. It rises by increasing the temperature. The increase in the peak does not take place in a regular fashion. It reaches a maximum at the temperature close to 200°C and then from there it decreases continuously up to the temperature of 500°C. At higher temperatures (>600°C) again an increase in the peak number of jumps can be observed. Almost the same trend can be observed at other superficial gas velocities. However, the effect of temperature on the number of jumps is more evident at lower gas velocities.

The rise in the number of jumps can be explained by increasing the bubble diameter at high temperatures. This is in accord with experimental results of Hatate *et al.* [11]. They found that at low superficial gas velocities, bubble size in the fluidization of Group-B particles increases and by increasing gas velocity the difference in the bubble diameter diminishes. The increase in the number of jumps can also be related to the increase in bubble frequency, which has been reported by Mii *et al.* [21] on fluidization of Group-B graphite particles at temperatures up to 800°C. Yoshida *et al.* [22] have also reported that for the same type of particles, bubble frequency increases form 2 s^{-1}

at ambient temperature to 6 s^{-1} at 800°C at the same superficial gas velocity. This may be due to a drop in the minimum fluidization velocity by rising the temperature for this particle size [23]. By decreasing the minimum fluidization velocity, more gas flows as bubbles at the same superficial gas velocity.

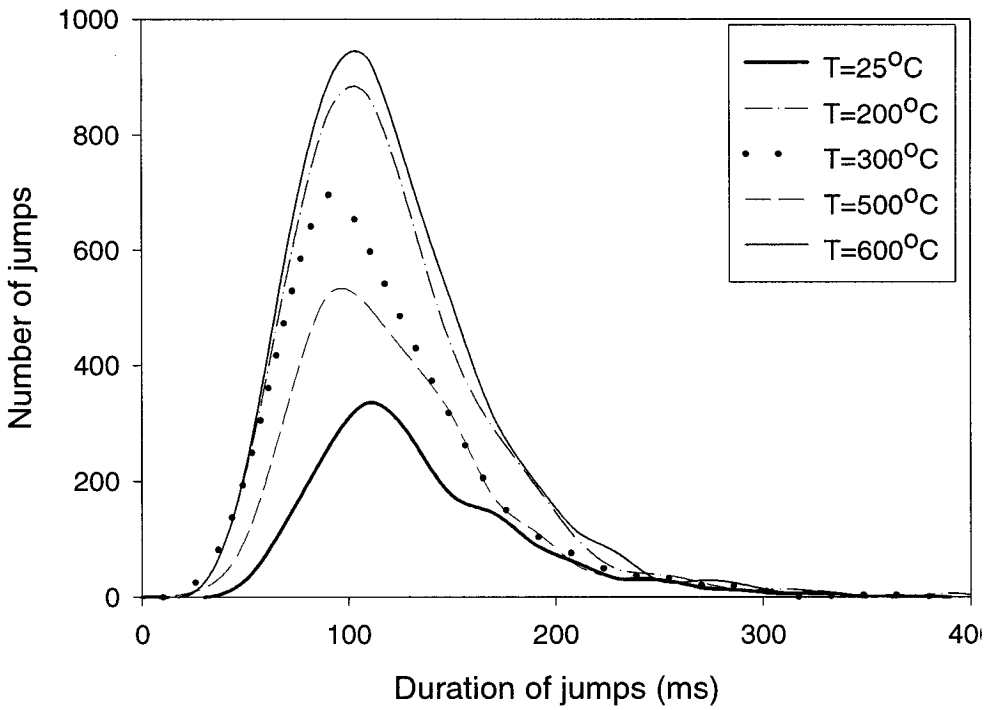

Figure 7.6: Effect of temperature on the number of jumps at superficial gas velocity of u=16cm/s for sand particles

Figure 7.7 shows the frequency of jumps for sand particles as a function of bed temperature and at different superficial gas velocities. Jump frequency is defined as the number of jumps in one second of an experiment. There is also an obvious increase in jump frequency by increasing superficial gas velocity. As mentioned before, the effect of temperature is more evident at lower gas velocities and this also can be observed in Figure 7.7.

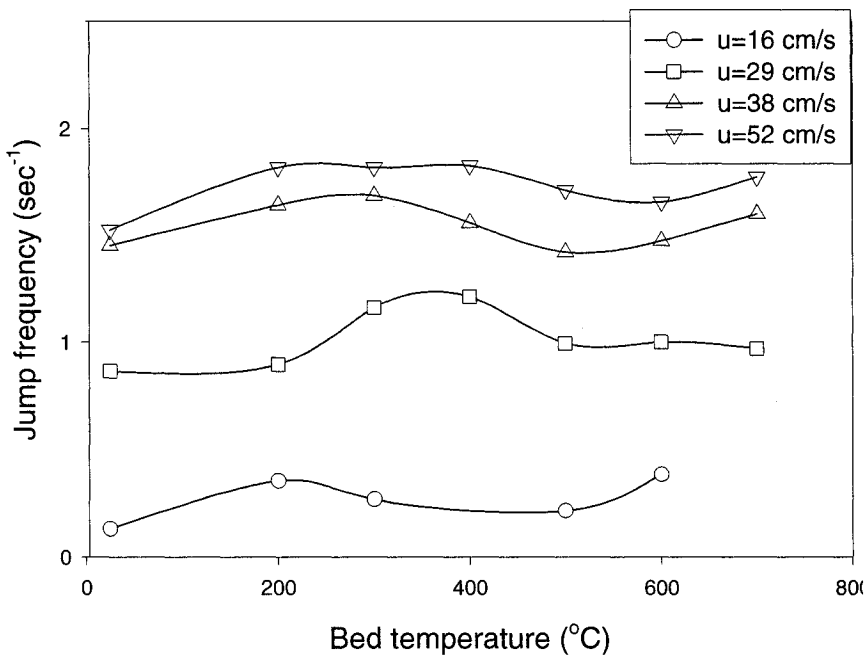

Figure 7.7: Effect of temperature on the jump frequency at different superficial gas velocities for sand particles

7.2.4.3 Cycle Time and Frequency

Circulation and, consequently, mixing of solids are caused by the upward motion of bubbles in fluidized beds. Bubbles carry solids upward in the wake drift phase. The upward movement of solid is compensated by the downward movement in emulsion and in the region close to the wall. Cycle time is thus a characteristic of axial solid mixing in the fluidized bed. The tracer cycle has been defined by Stein *et al.* [1] as the circulation of the tracer that takes place from below 30% to higher than 70% of the bed height and back. Figure 7.8 shows the probability distribution of cycle time for superficial gas velocity of 0.16 cm/s and at different temperatures. At higher temperatures, the peak in the cycle time distribution shifts toward shorter times, showing a higher solids circulation rates at higher temperatures. This is also in agreement with the increase in the number of jumps shown in Figure 7.6. A similar trend was observed for other superficial gas velocities. Figure 7.9-a and 7.9-b show the effect of temperature on the frequency of cycle and cycle time at different superficial gas velocities. Figure 7.9-a suggests a maximum cycle frequency at temperatures in the range of 250-300^{o}C. This is also reflected in jump frequency in Figure 7.7. As was mentioned in section 3.2, a higher frequency of jump and cycle suggests higher frequency in bubble formation that leads to more circulation of solids and, hence, promotes axial mixing in the bed.

Interestingly, the cycle time in the fluidization of alumina particles seems to be almost indifferent of temperature. While the cycle time increases significantly with superficial gas velocities, it remains unchanged with increasing temperature.

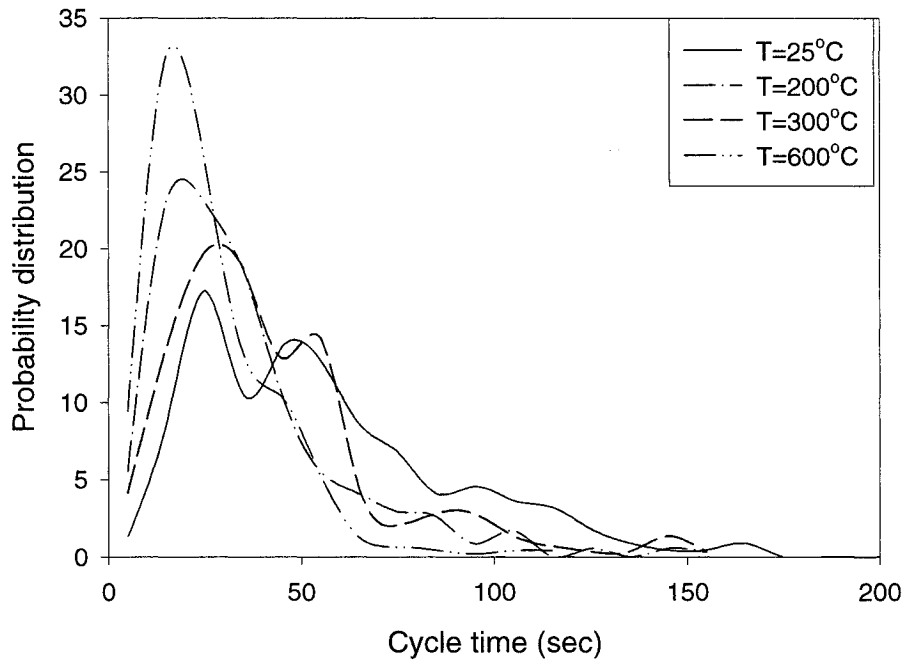

Fig. 7.8: Effect of temperature on the distribution of cycle time at superficial gas velocity of u=16cm/s for sand particles

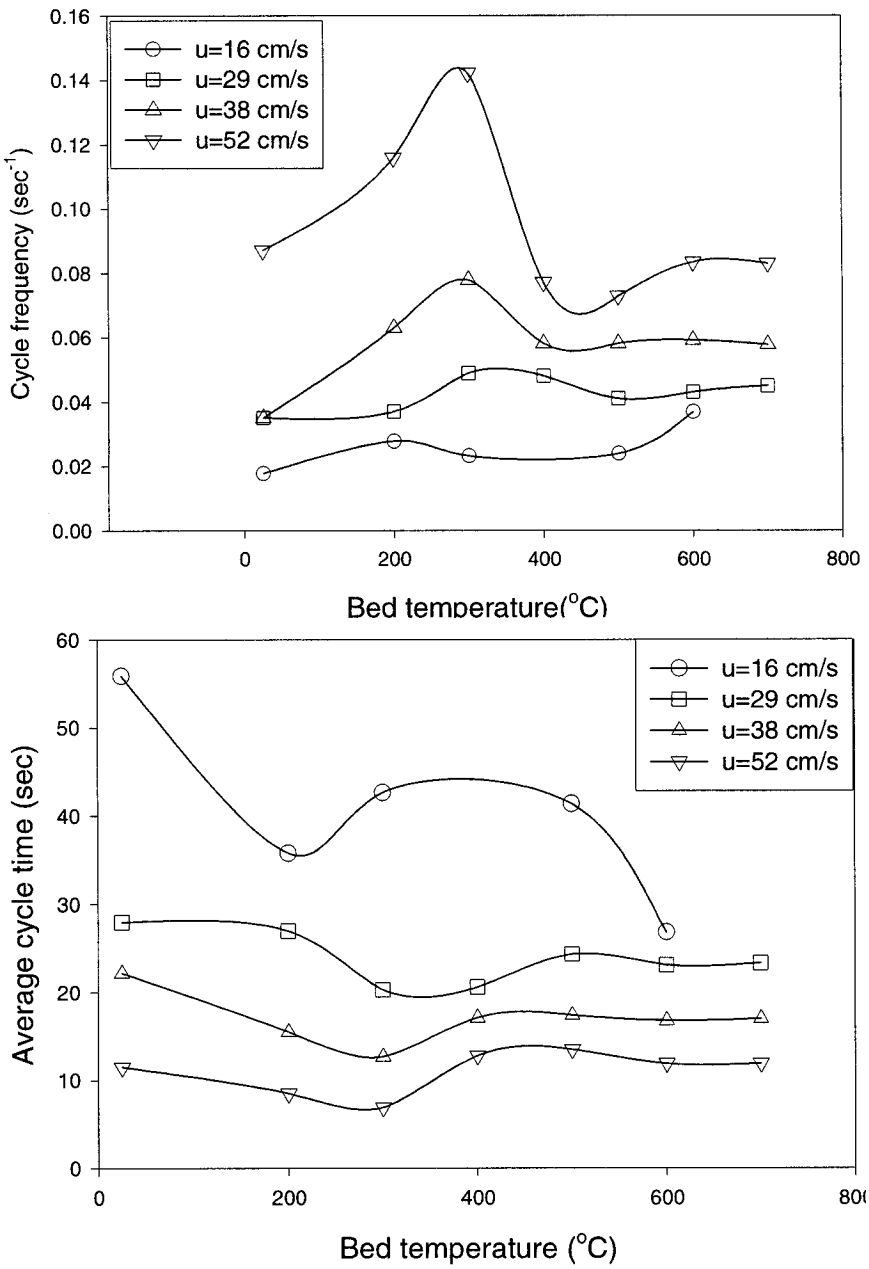

Fig. 7.9: Effect of temperature on the cycle frequency and time a) cycle frequency at different bed temperatures b) average cycle time at different

7.2.4.4 Granular Temperature

In an analogy to kinetic theory of gases, granular temperature is defined as:

$$\Theta = \frac{1}{3}\left(\sigma_\theta^2 + \sigma_r^2 + \sigma_z^2\right) \tag{7.1}$$

where, σ_θ, σ_r and σ_z are the variances of velocities in r z and θ direction. Granular temperature here is calculated for all the data points of each experiment. The objective is to understand how in the case of sand and alumina particles the variance of the velocity changes with temperature. It is also worth knowing how the granular temperature fits with other results, such as characteristic times that were discussed in sections 7.2.4.2 and 7.2.4.3. Moreover, the effect of surface changes, demonstrated in Figures 7.5, on the granular temperature can be tested. It should be noted that in the deep bed of these experiments the variance in the z direction is much higher than those in the direction of r and θ. Therefore, the values reported here essentially account for z direction, which is the dominant term in Equation 1 in these experiments.

Figure 7.10 presents granular temperature for sand and alumina particles at different bed temperatures. A maximum can be identified in case of sand particles at a temperature around 300°C. This is consistent with the jump and cycle frequency, which reach a maximum at around this temperature (see Figure 7.7 and 7.9). Interestingly, the granular temperature does not change significantly in the case of alumina particles. This can be explained by the fact that these two particles have shown different surface morphologies (see Figure 7.5) that also changes with temperature in the case of silica sand particles but remains unchanged in the case of alumina particles. Although both

silica sand and alumina particles belong to Geldart Group-B, the different surface morphologies in these two particles affect the nature of interparticle forces in their fluidization. This, consequently, results in two distinctive patterns of velocity fluctuations in fluidization of these two particles.

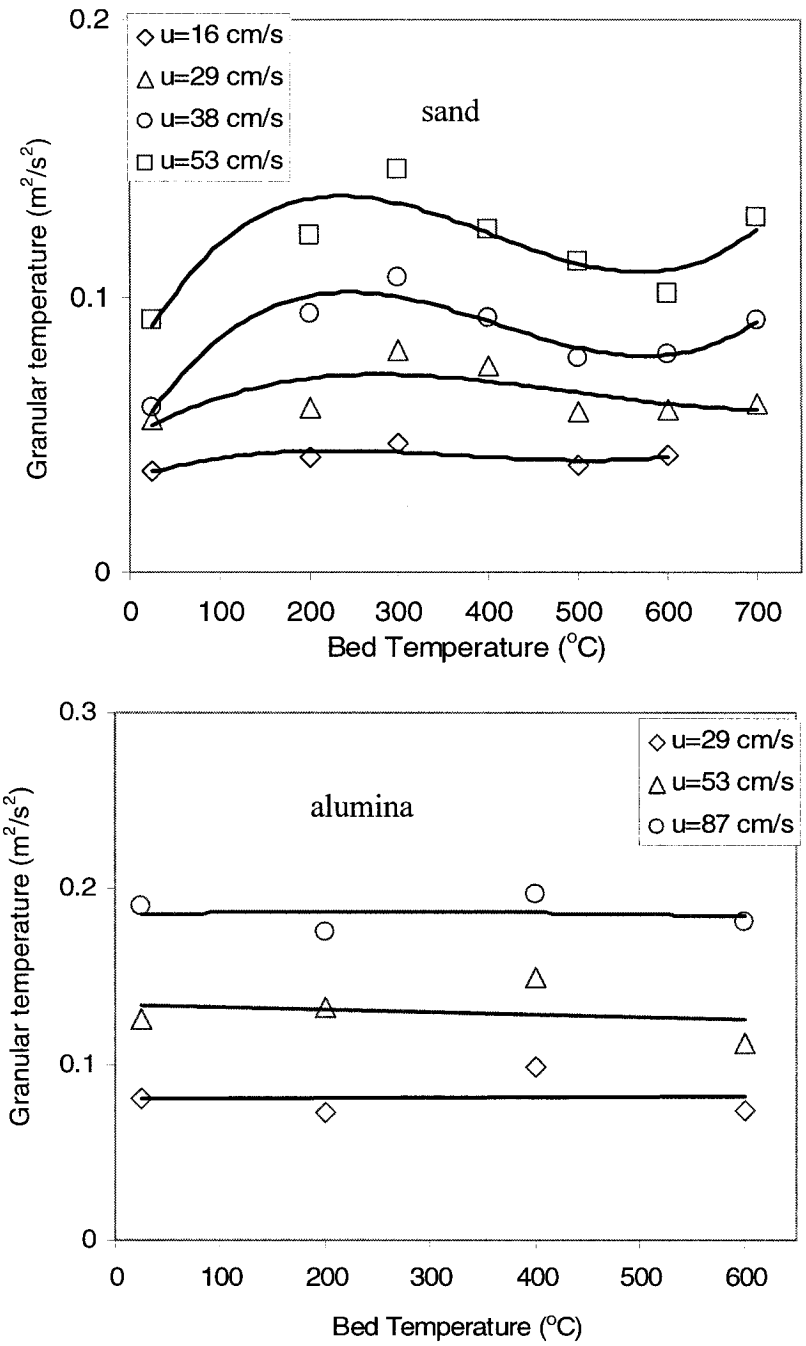

Fig. 7.10: Granular temperatures for sand and alumina particles at different bed temperatures and gas velocities. Symbols represent the calculated value from experiments and lines show the trends

7.2.5 CONCLUSION

Radioactive Particle Tracking (RPT) is used to study the hydrodynamic characteristics of a bubbling fluidized bed that operates at atmospheric pressure and different temperatures up to 700°C. The effect of temperature on several parameters relevant to bubbling mode of fluidization is investigated. It is shown that the bubble (wake) velocity at higher temperatures deviates from the correlation prediction if there is a change in solid surface, which influences the interparticle forces. If this is the case the bubble velocity cannot be explained merely by changes in interstitial gas properties. The effect of temperature on characteristic times of fluidization is also investigated. It is found that both characteristic times (i.e. jump time and cycle time) change with temperature. The number of jumps increases significantly at low superficial gas velocity by increasing temperature. The same trend is found for cycle time. There is no significant change in the characteristics times of alumina particles. Since both solid particles are essentially Geldart Group-B, the change in surface of silica sand particles was believed to be responsible for its different fluidization behavior compared to alumina particles.

7.2.6 ACKNOWLEDGEMENT

The authors would like to express their gratitude to Dr. Gregory Kennedy for his technical advice and Mr. St. Pierre and for the radiation of tracers.

7.2.7 NOTATIONS

Ar	Archimedes Number
u	Gas velocity (m/s)
d	bubble diameter (m)
Re	Reynolds number

Greek letter

Θ	Granular Temperature (m^2/s^2)
σ	Variance
ε	bubble fraction in bed

Subscript

mf	minimum fluidization condition
w	wake
g	interstitial gas
b	bubble

7.2.8 REFERENCES

[1] M. Stein, T.W. Martin, J.P.K. Seville, P.A. McNeil, D.J. Parker, Positron emission pticle tracking: particle velocities in gas fluidized beds, mixers and other applications, in J. Chaouki, , F. Larachi, , M.P.Dudukovic, Non-invasive monitoring of multiphase flows. Elsevier, chapter 10 (1997)309-333.

[2] M. Stein, Y.L. Ding, J.P.K. Seville, D.J. Parker, Solids motion in bubbling gas fluidized beds Chem. Eng. Sci. 55 (2000) 5291-5300.

[3] C. Dechsiri, A. Ghione, F.van de Wiel, H.G. Dehling, A.M.J. Paans, A.C. Hoffmann,Positron Emission Tomography applied to fluidization engineering, Can. j. Chem. Eng. 83 (2005) 88-96.

[4] C. Dechsiri, A. Van der Zwan, H.G. Dehling, A.C. Hoffmann, Dispersion of particle pulses in a fluidized beds measured by positron emission tomography, AIChE J. 51 (2005) 791-801.

[5] N. Mostoufi, J. Chaouki, Local solid mixing in gas-solid fluidized beds, Powder Technology. 14 (2001) 23-31.

[6] N. Mostoufi, J. Chaouki, On the axial movement of solids in gas-solid fluidized beds Source: Chem. Eng. Res. & Des. Part A Transactions of the Institute of Chemical Engineers. 78 (2000) 911-920.

[7] N. Mostoufi, J.Chaouki, Flow structure of the solids in gas-fluidized beds. Chem. Eng. Sci. (2004) 59 4217-4227.

[8] M. Cassanello, F. Larachi, C. Guy, J. Chaouki, Solids mixing in gas-liquid-solid fluidized beds: experiments and modeling, Chem. Eng. Sci. 51 (1996) 2011-2020.

[9] D. Geldart, D.S. Kapoor, Bubble sizes in a fluidized bed at elevated temperatures, 31 (1976) 842-843.

[10] T. Kai, S. Furusaki, Behavior of fluidized beds of small particles at elevated temperatures. Journal of chemical engineering of Japan. (1985) 18 113-118.

[11] Y. Hatate, K. Ohmagari, A. Ikari, K. Kondo, D.F. King, Behavior of bubbles in cylindrical fluidized bed at an elevated temperature. J. Chem. Eng. Japan. 21 (1988) 424-425.

[12] P. Lettieri, D. Newton, J.G. Yates, The influence of interparticle forces on fluidization behavior of some industrial materials at high temperature, Powder Technology. 110 (2000) 117-127.

[13] P. Lettieri, D. Newton, J.G. Yates, High temperature effects on the dense phase properties of gas fluidized beds, Powder Technology. 120 (2001) 34-40.

[14] H.Cui, P. Sauriol, J. Chaouki, High temperature fluidized bed reactor: measurements, hydrodynamics and simulation, Chem. Eng. Sci. 58 (2003) 3413-3422.

[15] H. Cui, J. Chaouki, Effects of temperature on local two-phase flow structure in bubbling and turbulent fluidized beds of FCC particles, Chem. Eng. Sci., 59 (2004) 3413-3422.

[16] R. Radmanesh, R. Mabrouk, J. Chaouki, C. Guy, The effect of temperature on solids mixing in a bubbling fluidized bed reactor, Inter. J. Chem. Reactor Eng. 3 (2005) A16 http://www.bepress.com/ijcre/vol3/A16/.

[17] F. Larachi, J. Chaouki, G. Kennedy, 3-D mapping of solids flow fields in multiphase reactor with RPT, AIChE J. 41 (1995) 439-443.

[18] J.R. Grace, in Handbook of multiphase systems, G. Hetsroni, Hemisphere, Washington, (1982).

[19] S. Mori, C.Y. Wen, Estimation of bubble diameter in gaseous fluidized beds, AIChE J. 21 (1975) 109.

[20] Kunii D., Levenspiel O. Fluidization engineering, 2nd ed. MA, Butterworth-Heinemann series in chemical engineering (1991).

[21] T. Mii, K. Youshida, D. Kunii, Temperature effect on characteristics of fluidized beds, J. Chem. Eng. Japan. 6 (1973) 100-102.

[22] K. Yoshida, S. Fujii, D. Kunii, Characteristics of fluidized beds at high temperatures, in Fluidization Technology, D.L. Keairns, Vol. 1 (1975) McGraw-Hill international book company, 43-48.

[23] T.M. Knowlton, Pressure and temperature effects in fluid-particle systems in fluidization, solids handling and processing, industrial application, Chapter 2, Edited by Wen-Ching Yang, Noyes Publications (1998) USA.

CHAPTER 8

BIOMASS GASIFICATION IN A BUBBLING FLUIDIZED BED REACTOR: EXPERIMENTS AND MODELING*

8. 1 Presentation of the Article

The fourth article is presented in this chapter. Kinetic models of biomass pyrolysis (presented in Chapter 5), as well as solid mixings parameters (presented in Chapter 6) are used in this chapter for modeling of biomass gasification in bubbling fluidized bed reactor. Gasification experiments have been also carried out and the results are compared with the model.

*This article was submitted to AIChE. Journal

8.2 Biomass Gasification in a Bubbling Fluidized Bed Reactor: Experiments and Modeling

Ramin Radmanesh, Jamal Chaouki*, Christophe Guy
Department of Chemical Engineering, École Polytechnique,
P.O. Box 6079, Station Centre-ville, Montréal, QC H3C 3A7, Canada
Fax*: 514 340 4159; e-mail: *jamal.chaouki@polymtl.ca*

8.2.1 Abstract

A model is presented for the gasification of beech wood particles in a bubbling fluidized bed gasifier (BFBG). The model encompasses the hydrodynamics of the solid and gas phases as well as the different reaction kinetics. It accounts also for the freeboard where additional homogeneous reactions take place. The influential impact of pyrolysis step on the final composition of produced fuel gas has been demonstrated by applying two different kinetic models for pyrolysis. Model results are compared with the experimental work of this study and other published results on wood gasification in BFBG. Effects of equivalence ratio (ER), steam to biomass ratio (SB), bed temperature, feed location and mass transfer between the counter-current phases (K_w) on the gas composition of product fuel gas are studied. The model shows good agreement with the experimental results.

8.2.2 Introduction

Gasification is the thermal conversion of solid carbonaceous materials to combustible fuel gas. Coal gasification, a fairly old process, has been widely used to harness energy

from coal in a more environmentally benign fashion. Biomass is indeed nothing but young coal and can be featured as an alternative to coal. Two main reasons for their boost as an alternative energy source can be recognized. Firstly, renewable energy sources mitigate greenhouse gas emission because CO_2 emitted from thermal conversion is naturally sequestered by photosynthesis. Secondly, biomass use as an energy resource relieves municipal and agricultural waste management from the burden of voluminous waste.

Coal gasifiers can be converted to biomass gasifiers by certain modifications. The difference between coal and biomass, however, mostly lies on the larger amount of volatile matter in biomass, which makes it more reactive compared to coal. This necessitates the need for biomass gasification studies. Many studies on the modeling of coal gasifers, in general, and coal gasification in bubbling fluidized beds, in particular, can be found in the literature. Nevertheless, modeling biomass gasification in bubbling fluidized beds has not been amply addressed. As recently indicated by Corella *et al.* (2005) only a few papers on the modeling of biomass bubbling fluidized bed gasifiers (BFBG) can be found in the literature.

In general, two different approaches can be identified in the modeling of biomass gasification in BFBG. The first approach is a kinetic-free equilibrium calculation to estimate the final composition of product gas (Bacon *et al.* 1985, Double *et al.* 1985, Ruggiero and Manfrida , 1999, Mansaray *et al.* 2000, Altafini *et al.* 2003, Li *et al.*

2004). The second approach, however, is more robust and takes into account the kinetics of the reactions along with the fluidized bed hydrodynamics (de Souza-Santos 1989, Hamel 2001, Fiaschi and Michelini, 2001). The first approach is not a dynamic modeling and does not take into account the underlying chemical and transport phenomena and particularly pyrolysis and tar formation.

Double *et al.* (1989) have classified the modeling of biomass gasification in BFBGs based on the equilibrium approach. In some studies, the whole gasification mechanism, including drying, primary and secondary pyrolysis, as well as the other chemical reactions in the gas and the solid phases, is considered as an equilibrium stage (Mansaray *et al.* 2000, Li *et al.* 2004) and, in other studies, only pyrolysis is the equilibrium stage (Bilodeau *et al.*, 1993, Sadaka *et al.* 2002). Mansaray *et al.* (2000) have used an ASPEN simulator to model rice husk gasification in a BFBG with a specially designed distributor. Bilodeau *et al.* (1993) and Sadaka *et al.* (2002) have used a semi-equilibrium model in which the gases resulting from pyrolysis have been accounted for through equilibrium calculations. These models can predict the variations of temperature and gas concentration in the reactor but they lack the tar formation and its cracking.

Kinetic non-equilibrium models that couple pyrolysis, homogeneous and heterogeneous reactions (including tar formation and cracking) with transport

phenomena in fluidized beds are few. Corella *et al.* (2005) have briefly reviewed the existing models for BFBGs.

In kinetic modeling of bubbling fluidized bed gasifiers (BFBGs), one needs hydrodynamics of the bed along with the kinetics of pyrolysis and various homogeneous and heterogeneous reactions. Hydrodynamics of the fluidized bed has been well studied. Most hydrodynamic properties of fluidized beds, however, have been derived at ambient temperature. Solids mixing in the fluidized bed was studied at high temperatures in our lab using radioactive particle tracking (RPT) (Radmanesh *et al.* 2005a). A two-phase counter-current back mixing model (CCBM) was used in that study to model mixing of solid particles. Pyrolysis of beech wood, also, was studied at moderate heating rates (Radmanesh *et al.* 2005b).

In the present study, the experimental results of beech wood gasification in a bubbling fluidized bed are used to evaluate a model for a BFBG. The presented model unifies the two previously studied aspects of the BFBG, i.e. hydrodynamics at high temperatures and pyrolysis, in a single model and evaluates the pyrolysis kinetic model derived at moderate heating rates. In order to underline the effect of the pyrolysis kinetic model on overall gas composition of the product gas, the previously kinetic model is compared with the one developed by Nunn *et al.* (1985) at very high heating rates. The model is also evaluated with other experimental data. The effect of feed location and gasifying agent are evaluated in this way.

8.2.3 Experimental

Beech wood particles with a diameter around 1-2 mm were used as biomass material in this study. The chemical properties of wood particles are presented in Table 8.1. An atmospheric fluidized bed reactor was designed and built to carry out biomass gasification experiments. Figure 8.1 shows a schematic of the reactor. The reactor is made of stainless steal and withstands temperatures as high as 900°C. It is 78 mm ID in the bed and freeboard area and 150 mm ID in the disengagement zone. Heights of the bed-freeboard and disengagement zones are 750 mm and 900 mm, respectively. The reactor consists of three heating zones. The temperature in each zone can be controlled separately. These zones include the preheating zone, where the fluidizing gas enters the reactor, the bed and the freeboard zone. Temperature in each zone was measured by means of several K-type thermocouples. The bed consisted of silica sand (Geldart-B classification) particles with an average particle size of 250 μm and a solid density of 2650 kg/m^3. The minimum fluidization velocity of sand particles at ambient temperature was u_{mf}=9 cm/s. The temperature difference between top and bottom of the bed was not more than 10°C in different experiments, which shows a good mixing in the bed.

Sampling ports are installed at 5 different locations of the reactor. The iso-kinetic sampling of product gas at different height of the reactor was carried out through a suitable sampling train of impingement bottles to separate tar and solid particulates from the gas. Product gases, after passing through the impingement bottles, entered the

Table 8.1 : Beech wood properties

Proximate Analysis	**Wt %**
Char	18
Volatile	81
Ash	0.8
Ultimate Analysis	
C	48.27
H	6.36
O	45.2
N	0.14
Wood Particle Size, d_a	1-2 mm

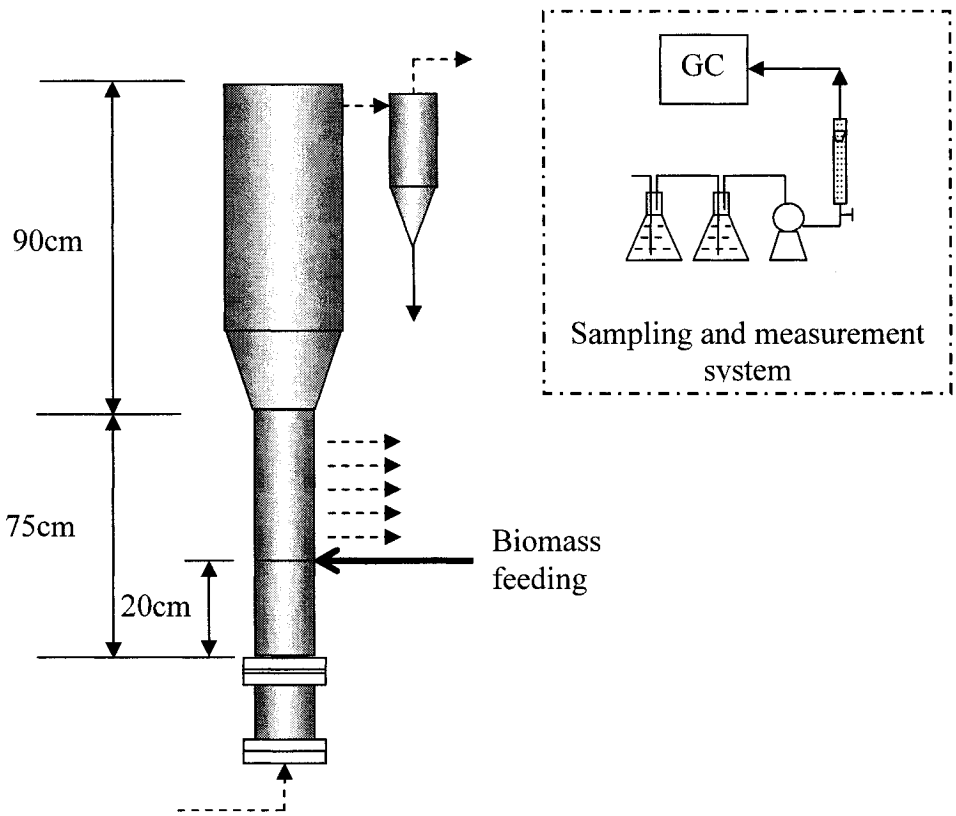

Figure 8.1: Schematic presentation of bubbling fluidized bed gasifier

GC. The GC was equipped with a thermal conductivity detector (TCD) and two columns. Molecular-sieve and Porapak columns were used simultaneously to separate the resulting gases. A rotameter was used in the sampling line to adjust the flow rate of the sampling gas. Beech wood particles were fed to the reactor through a screw feeder. The feeding rate of the wood during the experiments varied from 5-20 g/min. The wood particles in gasification experiments had essentially the same particle size as in the previous TGA/GC experiments, where the kinetics of pyrolysis was studied (Radmanesh *et al.*, 2005a).

The feeding point is located at the top of the bed and close to the bed surface, thus, the temperature at the feeding point is considered to be the same as the bed temperature. Air at ambient temperature was used as the gasifying agent. The flow rate of air was measured by means of a rotameter. The superficial gas velocity in the bed ranged from 0.13 m/s to 0.30 m/s at the bed condition (high temperature, atmospheric pressure). The reactor was operated at a bed temperature of 800°C. Temperature of the freeboard was kept in the range of 700°C-750°C. The residence time of gases in the freeboard was dependent on freeboard temperatures and varied from 2 to 4 seconds.

8.2.4 Model

A one-dimensional model is used to simulate the fluidized bed gasifier under isothermal conditions. The fluidized bed and consequently the model consist of two parts: the fluidizing bed and freeboard. Immediately after feeding the biomass

materials, due to instantaneous decomposition of carbonaceous material, the gaseous products of pyrolysis are released in the reactor. The major products of pyrolysis are char, tar and end-product stable gases such as CO, CO_2, CH_4, H_2 and H_2O.

The well-known two-phase model is employed to describe the fluidized bed. The bed is divided into a particle-lean bubble phase surrounded by a particle-rich emulsion phase. Heterogeneous and homogeneous reactions can take place in these phases. Mass transfer occurs between the bubble and emulsion phases. Solid phase (char) is modeled by the counter-current back mixing (CCBM) model. The main features and assumptions of the model can be summarized as follows:

1) Pyrolysis is considered to take place instantaneously in the feeding zone of the fluid-bed gasifier.
2) The yields of different products, including volatile products, char and tar, are determined based on the kinetic models developed earlier (Radmanesh *et al.*, 2005a).
3) Carbon is assumed to be the only constituent of char.
4) The bed is under isothermal condition. This is consistent with the experimental observation during biomass gasification.
5) The composition of products calculated in the pyrolysis stage is used as the boundary condition in the following step to solve mass balance equations in the bed and freeboard.

6) The CCBM model is used to describe char particles mixing in the fluidized bed (van Deemter, 1967). This model was applied by the authors to fluidized bed of sand particles at high temperatures (Radmanesh *et al.* 2005b). Figure 8.2 is a schematic representation of the CCBM model. The solid phase is where the heterogeneous reactions of char particles occur. Therefore, the reaction terms were included in the CCBM model. The parameters of CCBM model that were calculated at high temperatures in our previous work are used in this study to describe the mixing of char particles.
7) It is assumed that changes in the char particles size does not affect significantly the mass transfer coefficient between the ascending and descending phases.
8) Our earlier experiments and results reveal the importance of the freeboard area where other homogeneous reactions and especially tar cracking take place (Radmanesh *et. al.* 2005c). Thus, this zone is also considered in the modeling.
9) The voidage of the dense phase throughout the bed is equal to ε_{mf} (Kunii and Levenspiel 1991).
10) The volume fraction of solid in the bubble phase is taken to be 0.005 (Kunii and Levenspiel 1991).

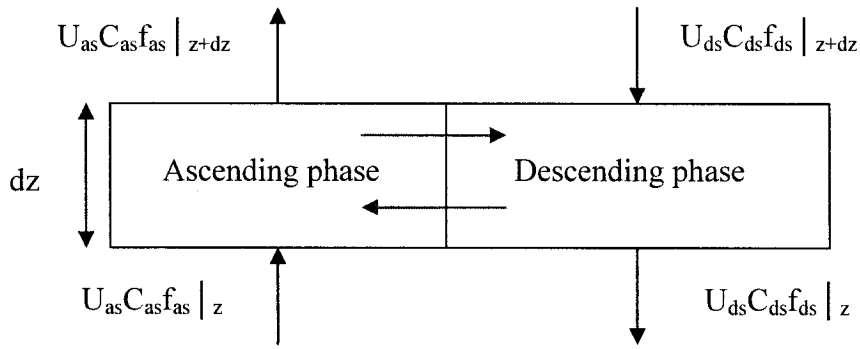

Figure 8.2: A demonstration of the CCBM model.

8.2.4.1 Energy balance for a single wood particle:

When the solid wood particles enter the hot bed of sands, they are subject to fast pyrolysis. The rate of temperature increase in the wood particles is important in calculating the final yield of different gases. Internal and external heat transfer resistances are negligible in the thin regime (Shin and Choi, 2000, van Den Arasen *et al.* 1982). Thus, the heat balance for a single particle can be written as follows:

$$\rho_p C_p V_p \frac{dT}{dt} = h_{conv.} A(T_b - T_p) + \sigma_{rad} \varepsilon_{rad} A(T_b^4 - T_p^4) \tag{8.1}$$

The convection heat transfer coefficient is calculated by the Ranz-Marshall correlation reported by Kunii and Levenspiel (1991):

$$\frac{h_{conv.} d_p}{k_g} = 2 + 0.6\,\mathrm{Re}^{1/2}\,\mathrm{Pr}^{1/3} \tag{8.2}$$

The effective emissivity in the condition of fluidized bed is calculated according to the correlation developed by Linjewile (1993):

$$\varepsilon_{rad} = \frac{1}{\varepsilon_p} + \frac{1}{\phi\left(\frac{1}{\varepsilon_{fb}} - 1\right)}, \phi = \left(1 + n_p \frac{d_i}{d_a}\right)^2 \tag{8.3}$$

where, ε_p is the emissivity, ε_{fb} is the effective emissivity of the fluidized bed, d_i and d_a are the diameters of the inert and active particles. The physical properties of the bed and wood particles are tabulated in Table 8.2. The density of wood particles changes during the course of pyrolysis. The change in the density was assumed to be proportional to the loss of the volatile matter in the particle which is defined as following:

$$\rho(t) = \rho_0\left(1 - \frac{V(t)}{V^*} X_{vm}\right) \tag{8.4}$$

where, X_{vm} is the volatile matter of the wood particles.

8.2.4.2 Kinetic models

8.2.4.2.1 Pyrolysis

The biomass particles undergo pyrolysis upon entering to the fluidized bed of hot sand particles. Pyrolysis is indeed the decomposition of biomass structure due to heat. In gasification and pyrolysis, the final composition of product fuel gas is important. This is because the final heating value of the gaseous product depends on its composition. In pyrolysis, therefore, kinetic models for both total devolatilization, which determines the

Table 8.2: Parameters used for energy balance

Parameter	Value	Reference
Wood Specific Heat	C_p=1112.0+4.85(T-273), J/kg K	Koufopanous *et al.* 1991
Density of the Wood	360, kg/m^3	Di Blasi 2004
ε_p for wood particles	0.95	Babu and Chaurasia, 2004
Effective Emissivity, ε_{fb}	0.8	Linjewile, 1993
Parameter in the Equation (8.6) n_p	5	Linjewile, 1993
Stephan Boltzmann Constant, σ	5.67×10^{-8} W/m^2 K^4	

extent of produced char, and individual gas release should be taken into consideration. The kinetic model which, is used for all the products, is a single-step first-order reaction. It can be described by the following equation:

$$\frac{dV_i}{dt} = k_{01i} e^{\left(-\frac{E_{1,i}}{RT_p}\right)} \left(V_i^* - V_i\right) \tag{8.5}$$

where, V_i and V_i^* are the instantaneous and total amount of volatile matter for the gaseous component presented as i.

Two different pyrolysis kinetic models are employed in this study and their performance in the overall modeling of BFBGs are compared. The first model is based on the work done by Nunn *et al.* (1985) on wood at high heating rates of 1000°C/s. The kinetics equation is the same as Equation (8.5).

The second model is based on our previous experiments on beech wood pyrolysis at moderate heating rates. A brief description of this model is presented here. The experimental results of a previous study (Radmanesh *et al.* 2005a) and also other pyrolysis studies (Bilbao *et al.*, 1995, González *et al.* 2003) show that the final yield of each gaseous product rises by increasing heating rate. Therefore, in order to account for the change of gas yields with heating rate, the first order kinetic model presented by Equation (8.5) was modified in a way that V* was a function of heating rate. This was done by using a simple first order model that related the change in the concentration of each gas precursor in the virgin biomass (V_i*) to heating rate. This can be described as follows:

$$\frac{dV^*}{d(1/\beta)} = -K_v V^* \qquad \text{or} \qquad V^* = V_\infty^* \exp(-K_v/\beta) \tag{8.6}$$

where, β is the rate of temperature increase in the particle (dT_p/dt) and. Tables 8.3 and 8.4 tabulate the kinetic parameters calculated by Nunn *et al.* (1985) at high heating rate and those of our previous work at moderate heating rates, respectively.

8.2.4.2.2 Secondary pyrolysis or tar cracking

The thermal cracking of tar, known also as secondary pyrolysis, is another important step. Since more than 60% of the primary pyrolysis product accounts for tar, this step has also an important impact on the accuracy prediction of final gas composition. The

Table 8.3: Kinetic parameters of primary pyrolysis (Nunn *et al.*, 1985)
(Model-1)

No.	Component	E_i (kcal/mol)	Log(k_{01}) (1/s)	V^*_i (kg/kg biomass)
1	Total devolatilization	16.5	4.53	92
	Total gas	11.8	4.53	41
2[+]	H_2	27	6.7	2.0
3	CH_4/C_2H_4 C_2H_6/C_3H_6	16.6	3.79	3.6
4	CO	14.6	3.36	17.0
5	CO_2	14.3	3.77	6.0
6	H_2O	11.5	3.35	5.14
7	Char=100-(total devolatilization)			
7	Tar= (total devolatilization)- (total gas release)			

[+]Hajaligol *et al.* (1982)

Table 8.4: Kinetic parameters of gas evolution during primary pyrolysis (Model-2)

No.	Component	Log(k_{01}) (1/s)	E_i (kJ/mol)	C_1		
Total devolatilization parameters for each pseudo-component						
1	Cellulose	13.9	192	0.61		
2	Hemicelloluse	10.2	133	0.27		
3	Lignin	3.1	86	0.11		
Individual gas kinetic parameters						
No.	**Component**	**Log(k_0) (1/s)**	**E_i (kJ/mol)**	**V^*_∞ Wt.%**	**V^***	**k_v**
1	H_2	1.7	85	1.2	-----	14.5
2	CH_4	1.1	45	1.1	------	8.2
3	CO	4.8	50	7.5	-----	11
4	CO_2	3.5	40	14	-----	5
5	H_2O	13.56	149	------	4.8	-----
6	Tar	12.0	113	------	63.8	-----

tar cracking takes place in the gas phase. Boroson *et al.* (1989) have studied the homogeneous cracking of tar resulting from sweet gum hard wood and developed a first order kinetic model. Their model was adopted by Roth *et al.* (2002) to calculate kinetic parameters for beech wood. This model is also used in this study:

$$tar(gas) \longrightarrow \upsilon_{H2} H_2(g) + \upsilon_{CH4} CH_4(g) + \upsilon_{CO} CO(g) + \upsilon_{CO2} CO_2(g) + \upsilon_{tar} tar_{inert} \quad (8.7)$$

The stoichiometric coefficients (υ_i) are presented in Table 8.5. The kinetic model is as follows (Boroson *et al.* 1989):

$$r_{cracking} = \upsilon_i 10^{4.98} \exp\left(-\frac{93}{RT}\right)(\rho_{tar}) \quad (8.8)$$

where, ρ_{tar} is the density of the tar in the gas stream and υ_i is the stoichiometric coefficient as presented in the Table 8.5.

8.2.4.2.3 Tar combustion

Tar material, like char and other combustibles, are subject to combustion. The kinetic model of Brydon *et al.* (1996) was used in this part for the combustion of tarry materials:

$$CH_{1.522}O_{0.0228} + 0.867O_2 \longrightarrow CO + 0.761H_2O$$
$$r_8 = M_{CH} 9.2\times10^6 T \exp(-9650/T) \quad (8.9)$$

Table 8.5: Stoichiometric coefficients for tar cracking (Wurzenberger *et al.*, 2002)

Component	υ_i
H_2	0.0173316
CH_4	0.0884052
CO	0.563316
CO_2	0.1109316
Secondary Tar	0.22

M_{CH} is the molecular mass of tar material and is M_{CH}=90 g/gmol according to the Brydon *et al.* (1966).

8.2.4.2.4 Homogeneous and heterogeneous reactions

Table 8.6 shows all the homogeneous and heterogeneous reactions involved in the gasification of biomass. These reactions take place after the primary pyrolysis of biomass in the bed and freeboard.

8.2.4.3 Mathematical description of the model

8.2.4.3.1 Fluidized bed

The following presents the mass balance for the gas phase in the bubble and the emulsion phases (Equations (8.10) and (8.11)) and mass balance for the char particles in the ascending and descending phases (Equations (8.12) and (8.13)):

Table 8.6: List of heterogeneous and homogenous reactions involved in gasifiers

NO	Chemical Reaction	Kinetic	Reference
R1	$\lambda C + O_2 \rightarrow 2(\lambda-1)CO + (2-\lambda)CO_2$	$r_1 = \frac{dX}{dt} = 1.5\times10^{6}.\exp(\frac{-13.078}{T_{par}}).p_{O2}.(1-X_c)^{1.2}$ $\lambda = 3\times10^{8}.\exp(\frac{-30178}{T_{par}})$	Wurzenberger *et al.*, 2002
R2	$C + H_2O \rightarrow CO + H_2$	$r_2 = \frac{k_2.p_{H2O}}{1+k_3.p_{H2O}+k_4.p_{H2}}$ 1/s $k_2 = 4.93\times10^{3}.\exp(\frac{-18522}{T_{par}})$ $k_3 = 1.11\times10.\exp(\frac{-3548}{T_{par}})$ $k_4 = 1.53\times10^{-9}\exp(\frac{25161}{T_{par}})$	Wurzenberger *et al.*, 2002
R3	$C + CO_2 \rightarrow 2CO$	$r_3 = 2\times10^{-8}\exp(\frac{-360065}{T_{par}})[CO_2]$ kmol/m^3/hr	Biba *et al.* 1978
R4	$CO + 1/2O_2 \rightarrow CO_2$	$r_5 = 10^{17.6}\exp(-20000/T_g)[CO][O_2]^{0.25}[H_2O]^{0.5}$ kmol m^{-3}s^{-1}	Bryden and Ragland, 1996
R5	$H_2 + 1/2O_2 \leftrightarrow H_2O$	$r_6 = 2.19\times10^{15}\exp(-13127/T_g)[H_2][O_2]$	Wurzenberger *et al.*, 2002
R6	$CH_4 + 2O_2 \rightarrow CO_2 + 2H_2O$	$r_7 = 1.58\times10^{16}\exp(-24343/T_g)[CH_4]^{0.7}[O_2]^{0.8}$	Wurzenberger *et al.*, 2002
R7	$CO + H_2O \rightarrow H_2 + CO_2$	$r_8 = 2.7\times10^{3}\exp(-\frac{1510}{T_g})\left[[CO][H_2O]-\left(\frac{[CO_2][H_2]}{K^*}\right)\right]$ $K^* = 0.0265\exp(\frac{3968}{T_g})$	Biba *et al.* 1978

Bubble phase:

$$-\delta_b \frac{d(\rho_g y_{i,b} u_b)}{dz} + K_{be}\rho_g (y_{i,e} - y_{i,b}) + \delta_b (1-\gamma_b)\sum_{g-g} \upsilon_{ij} R_i + \delta_b \gamma_b \sum_{g-s} \upsilon_{ij} R_i = 0 \tag{8.10}$$

Emulsion phase:

$$-(1-\delta_b)\varepsilon_{mf} \frac{d(\rho_g y_{i,e} u_e)}{dz} + K_{be}\rho_g (y_{i,b} - y_{i,e}) + (1-\delta_b)\varepsilon_{mf} \sum_{g-g} \upsilon_{ij} R_i + (1-\delta_b)(1-\varepsilon_{mf})\sum_{g-s} \upsilon_{ij} R_i = 0 \tag{8.11}$$

The gas density is calculated assuming an ideal gas behavior:

$$\rho_g = \frac{P}{RT}\left(\sum y_{i,g} M_i\right) \tag{8.12}$$

Char balance in ascending phase:

$$\omega_{as,0} \frac{dX_{as}}{dz} + K_w (C_{ds,c} - C_{as,c}) A f_{as} + A f_{as} \sum_{g-s} \upsilon_{i,c} R_i = 0 \tag{8.13}$$

Char balance in descending phase:

$$-\omega_{ds,0} \frac{dX_{ds}}{dz} + K_w (C_{as,c} - C_{ds,c}) A f_{as} + A(1-f_{as})\sum_{g-s} \upsilon_{i,c} R_i = 0 \tag{8.14}$$

Char concentration in counter-current phases:

$$C_{as,c} = \frac{\omega_{as,0}}{U_{as} f_{as} A}(1 - X_{as})$$
$$C_{ds,c} = \frac{\omega_{ds,0}}{U_{ds} f_{ds} A}(1 - X_{ds}) \tag{8.15}$$

Equations (8.10) and (8.11) give the gas concentration profile in the bed whereas, Equations (8.12) and (8.13) provide the char conversion profile in the bed, which is needed for char reaction kinetics. Thus, these equations must be solved simultaneously for all the gas species to obtain produced gas compositions and yields in the bed. The boundary condition for these equations is provided by the fluidizing gas composition at the distributor level and pyrolysis model at the feeding level.

Table 8.7 lists the hydrodynamic parameters used in the preceding equations along with the necessary correlations to estimate these parameters. The velocities of the ascending and descending phases are derived from the previous hydrodynamic studies in our lab (Radmanesh *et al.* 2005b). In the same study, it was shown that the K_w value given by Hoffmann *et al.* (1993) was in a good agreement with our experimental data at high temperatures. Therefore, this correlation, as shown in Table 7, is used in this study to calculate the transfer coefficient between the counter-current phases. It is assumed that the K_w calculated for the sand particles can be used for the char particles. This is justifiable by considering that K_w is more dependent on the bubble diameter.

8.2.4.3.2 Freeboard

The freeboard region above the bed provides a space not only for disengagement of solids but also further reactions. The gas that leaves the bed enters the freeboard section that behaves as a second reactor in series to the fluidized bed. Homogeneous and heterogeneous reactions as well as tar cracking continue in the freeboard region.

Table 8.7: Hydrodynamic parameters used in this study

Parameter	Correlation	Reference
Minimum Fluidization velocity	$\mathrm{Re}_{p,mf} = \left[(27.2)^2 + 0.0408 Ar\right]^{0.5} - 27.2$	Grace, 1982
Bubble Diameter	$d_b = d_{bm} + (d_{b0} - d_{bm}) e^{-0.3Z/d_t}$ $d_{bm} = 0.65\left(\pi/4 d_t^2 (u_0 - u_{mf})\right)^{0.4}$ $d_{b0} = 1.3/g^{0.2} (u_0 - u_{mf}/N_{or})^{0.4}$	Kunii and Levenspiel, 1991
Bubble velocity	$u_b = u_0 - u_{mf} + u_{br}$ $u_{br} = 0.711(g d_b)^{0.5}$	Davidson and Harrison, 1963
Bubble fraction	$\delta_b = \frac{u_0 - u_{mf}}{u_b - u_{mf}}$	Kunii and Levenspiel, 1991
Bubble-could transfer coefficient	$K_{bc} = 4.5\left(\frac{u_{mf}}{d_b}\right) + \frac{5.85 D^{0.5} g^{0.25}}{d_b^{1.25}}$	Kunii and Levenspiel, 1991
Cloud-emulsion transfer coefficient	$K_{ce} = 6.77\left(\frac{D\varepsilon_{mf} u_{br}}{d_b^3}\right)^{0.5}$	Kunii and Levenspiel, 1991
Bubble-emulsion transfer coefficent	$\frac{1}{K_{be}} = \frac{1}{K_{bc}} + \frac{1}{K_{ce}}$	Kunii and Levenspiel, 1991
f_{as}	$0.45 < f_{as} < 0.5$	Radmanesh *et al.* ,2005b
U_{as} (m/s)	$0.03 < U_{as} < 0.07$	Radmanesh *et al.*, 2005b
U_{ds} (m/s)	$0.05 < U_{ds} < 0.07$	Radmanesh *et al.* ,2005b
Wake exchange coefficient	$K_w = \frac{0.081}{2\varepsilon_{mf} d_b}$	Hoffman *et al.* (1993)
Wake exchange coefficient	$K_w = 0.807 \frac{u_b}{d_b}$	Kocatulum *et al.*(1991)

Models to predict the entrainment of particles from the bed are available in the literature (Yates 1983). As was mentioned earlier, biomass materials contain low proportion of char and large proportion of volatile matter (see Table 8.1). As a result, it

is assumed that the char particles are consumed in the bed and thus the entrainment of the char is negligible.

A plug flow model in this condition of low solids concentration and gas velocity is reasonable. Tar cracking and water gas shift reactions are the most important reactions that take place in this region. Depending on the biomass feeding location, other combustion reactions may also occur in the freeboard. The mass balance for each species in this region is given by the following differential equation:

$$\frac{d\left(u_f \rho_{i,g}\right)}{dz} = \sum_{g-g} \upsilon_{ij} R_i \tag{8.16}$$

where, u_f is the gas velocity in the freeboard, ρ_i is the density of different gas species and R_i is the gas phase reaction rates determined by the kinetics presented in Table 8.6.

8.2.5 Results and Discussion

8.2.5.1 Model comparison with experiments

The experimental data in this study have been collected in a fluidized bed gasifier with a top feeding of biomass close to the bed surface (see Figure 8.1). As it was shown by Corella *et al.* (1988), the location of biomass feeding (from the top or bottom of the bed) affects the distribution of gaseous products. In feeding from the bottom, pyrolysis products pass through the bed and thus there is a better mixing of the product gases

resulting from pyrolysis. Moreover, tar, in this case, is more prone to crack and the yield of stable gases increases as a result. Feeding into a bed of sand at a temperature of 800°C, however, is not always an easy task. Furthermore, as it will be shown in this work, feeding into the bottom of the bed, where there still exists oxygen, leads to the combustion of some combustible gases and may even reduce the final heating value of product fuel gas. In feeding from the top, the gas phase, including the tar, does not pass through the hot bed. The char particles in the bed undergo combustion and gasification (R1-R3). The resulting gases from these reactions (CO and CO_2) mix with the pyrolysis gas, which are calculated from the pyrolysis model. Homogeneous reactions especially tar cracking and shift reactions continue in the freeboard area of the reactor. The high temperature of the freeboard in these experiments favors the tar cracking reaction in this zone. However, depending on the flow rate of gasifying agent (i.e. air) and whether all the oxygen has been consumed in the bed, some gas phase combustion may also occur in this section.

Several experiments were performed with the beech wood in the bubbling fluidized bed reactor. The experiments were done at different equivalence ratios (ER). ER is an important parameter in the air-blown biomass gasification (Vriesman *et al.* 2000, Narvaez *et al.* 1996). It is defined as the air-to-fuel mass flow ratio used in the experiment divided by the air-to-fuel mass flow ratio required for a complete combustion. Table 8.8 summarizes the operating conditions in each gasification experiment and the resulting gas phase product composition.

Table 8.8: Experimental operating condition and product gas composition in dry basis

Run	T_{bed} (°C)	T_f (°C)	m_b (g/min)	u^* (m/s)	ER	Gas composition at exit (dry basis%)				
						H_2	CH_4	CO	CO_2	N_2
1	805	750	12	0.21	0.32	9.2	2.5	16.2	12.7	59.6
2	800	760	14	0.17	0.23	11.5	4.1	20.5	12.9	50
3	805	755	13	0.38	0.48	5.9	0.60	9.2	12.8	71
4	800	740	18	0.13	0.13	14.3	4.5	27.0	8.60	56
5	815	740	15	0.17	0.22	14.7	4.4	20.2	11.8	49
6	800	730	16	0.21	0.24	11.7	3.3	20	12.4	53
7	800	740	5.5	0.17	0.66	4.8	0.93	11	14	69

* air velocity at the bed condition

The profile of each gas along the height of the reactor is calculated by solving Equations (8.9) to (8.14) in the bed and freeboard. The boundary condition for the balance equations in the bed are given by the pyrolysis kinetic model. The pyrolysis kinetic model gives the composition of the gases, tar and char and these gas compositions serve as a boundary condition for the gasification in the bed. Two aforementioned kinetic models, presented in section 3.2.1, are used in this part. Gas composition calculated at $z=H_{bed}$ provides the boundary condition for the freeboard section.

Figure 8.3 portrays the concentration profile of the four major gases as a function of reactor height resulted from the first and second pyrolysis kinetic models (Tables 2 and 3) at a bed temperature of T=800°C and ER =0.32. It also compares two models with the experimental results of beech wood gasification at the same operating conditions.

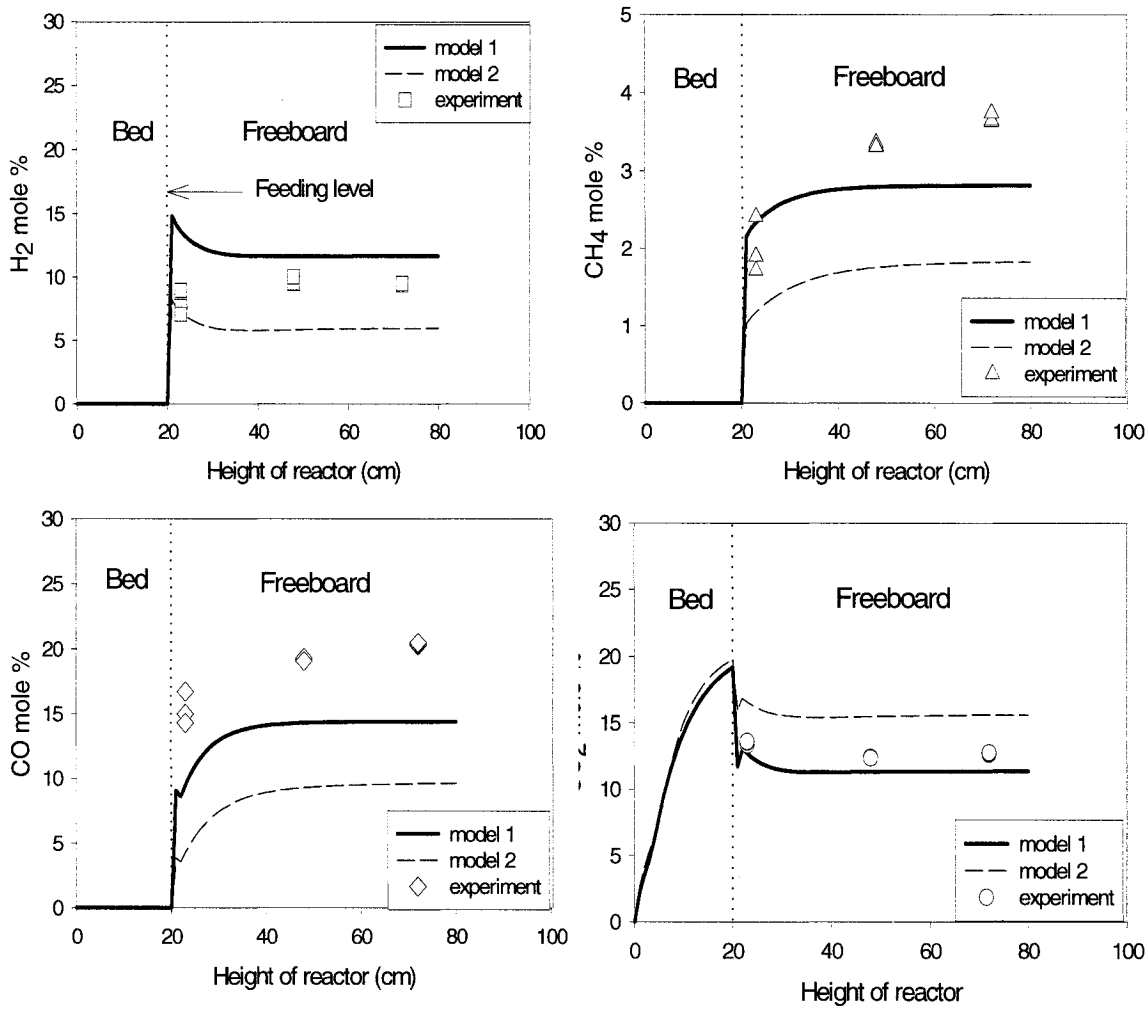

Figure 8.3: Concentration profiles of the gases along the reactor height, comparison of two pyrolysis kinetic models. T_{bed}=800°C , T_f=740°C and ER=0.32.

This figure demonstrates the importance of the pyrolysis step in final gas composition. As it shows, the first pyrolysis kinetic model, which was derived at higher heating rates can predict product gas composition satisfactorily. This, apparently, suggests a change in pyrolysis mechanism at very high heating rates, which forces a new distribution in the final product gas concentration. Therefore, the kinetic model derived at higher

heating rates estimates the final gas composition relatively better than the one derived at lower heating rates.

The dot lines in Figure 8.3 represents the feeding location, which is at top of the bed at height of z=20cm. Due to the sudden pyrolysis of wood in the feeding area, abrupt changes in the gas concentrations can be observed at that height. The model is able to predict the composition of product fuel gas. Figure 8.4 shows the same profile for the first pyrolysis kinetic model but at ER=0.13. Oxygen concentration is also shown in this figure. The concentration of oxygen drops from the bottom to the top of the bed and it almost disappears at the feeding point.

Figure 8.5-a compares total gas yield predicted by two pyrolysis kinetic models with the experiments at different ER values. The gas yield is defined as the total mass of gas produced at the exit of the reactor (top of the freeboard) divided by the mass of consumed biomass. The two models result in very close prediction of total yields. However, the distribution of gases, which is a determinant factor in heating value of the gas product, is entirely different. The Higher heating value (HHV) of the dry gas at the standard state can be estimated by the following equation (Li *et al.*, 2004):

$$HHV = (12.75[H_2] + 12.63[CO] + 39.82[CH_4])/100 \text{ Mj/Nm}^3 \quad (8.17)$$

This equation has been derived based on the heat of combustion of different gases. The gas concentration in Equation (8.17) is in mol%. Figure 8.5-b shows the HHV

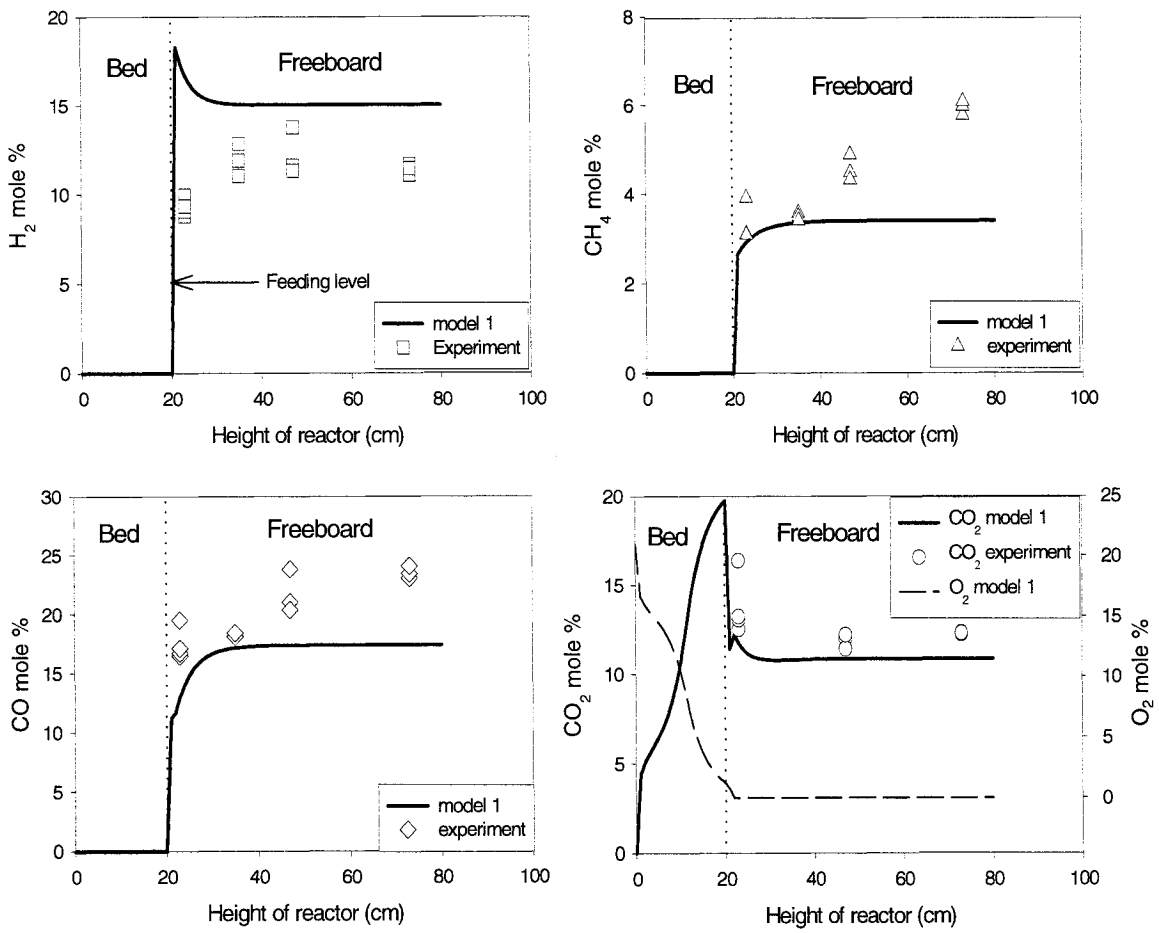

Figure 8.4: Concentration profiles of the gases along the reactor height, (T_{bed}=800°C, T_f=740°C, ER=0.13)

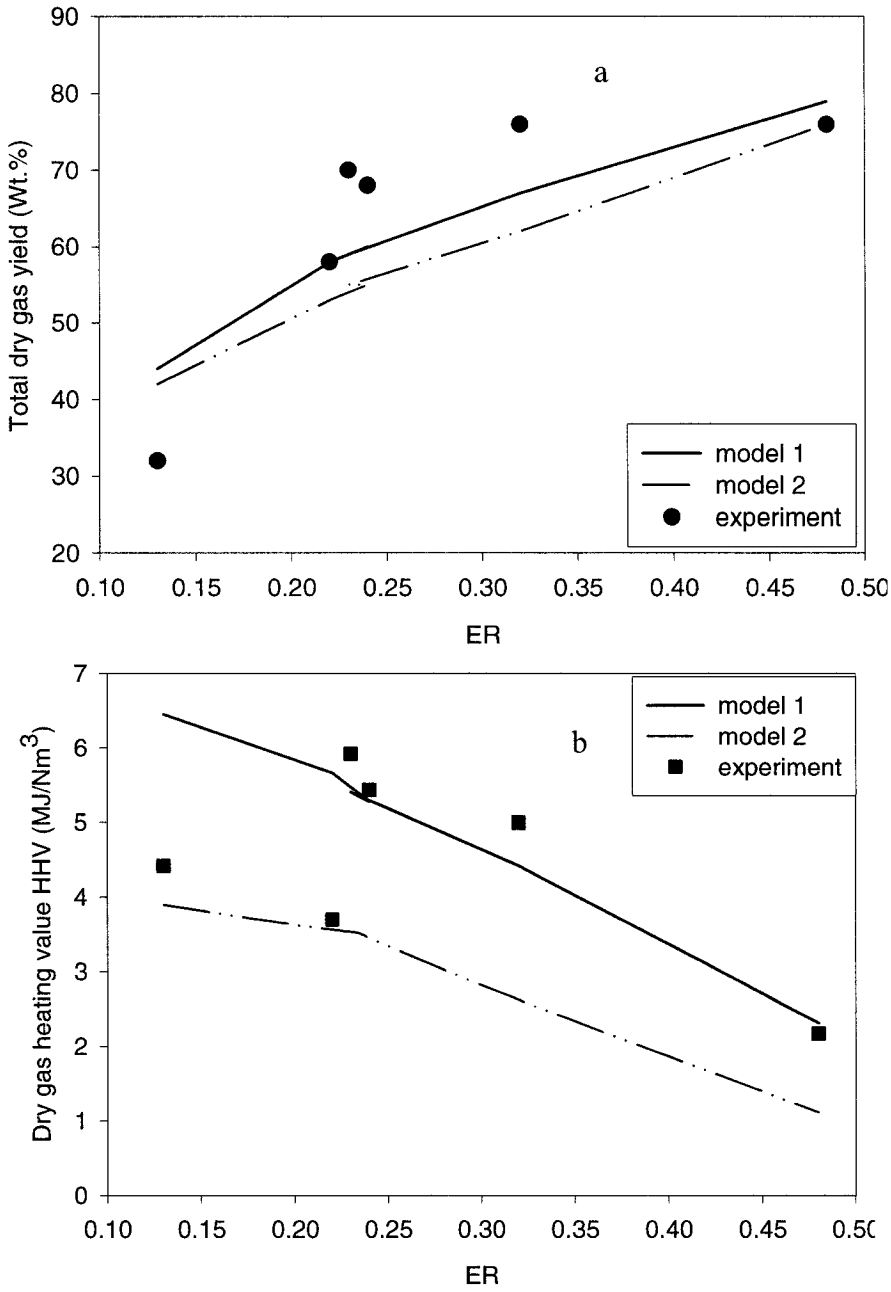

Figure 8.5: Total dry gas yield (kg of produced gas/kg of daf biomass) and heating value of the dry gas (MJ/Nm^3) at the exit of the reactor

estimated by Equation (8.17) for the product gas as a function of ER. The difference in the product distribution lays mainly on the prediction of CO and CO_2, where the second model always overestimates the yield of CO_2 and underestimates that of CO. Thus, the heating value of the gas predicted by the first model is lower than the second model and the experimental data. Figure 8.5-a also demonstrates an increase in the total gas yield by increasing ER. This is in accord with the previous studies (Narvaez *et al.*, 1995, Gil *et al.*, 1999). Both models are able to predict the gas yield increase with ER. The heating value of the product gas, however, decreases by increasing ER because of the larger contribution of CO_2 in the yield of gaseous product (Fiaschi and Michelini, 2001). This, in turn, is a result of a higher contribution of combustion (of char, tar and other combustible gases) and a lesser contribution of gasification in the overall reactions with increasing ER. The dilution of the product gas by N_2 also contributes to the lower HHV at higher ER.

The effect of ER on dry gas composition and yield of each individual gas are presented in Figures 8.6 and 8.7. The lines in these figures are the model resulted from first pyrolysis kinetic model (Nunn *et al.* 1985) and symbols are the experimental data. An increase in ER brings about a decrease in the concentration of H_2 and CO and a substantial increase in CO_2 concentration in dry gas product. This is because of the increasing role of the char combustion in the bed compared to its gasification reaction, which results in lower concentration of combustible gases and higher CO_2. These results are in agreement with the previous result published by Gil *et al.* (1999). Lim *et*

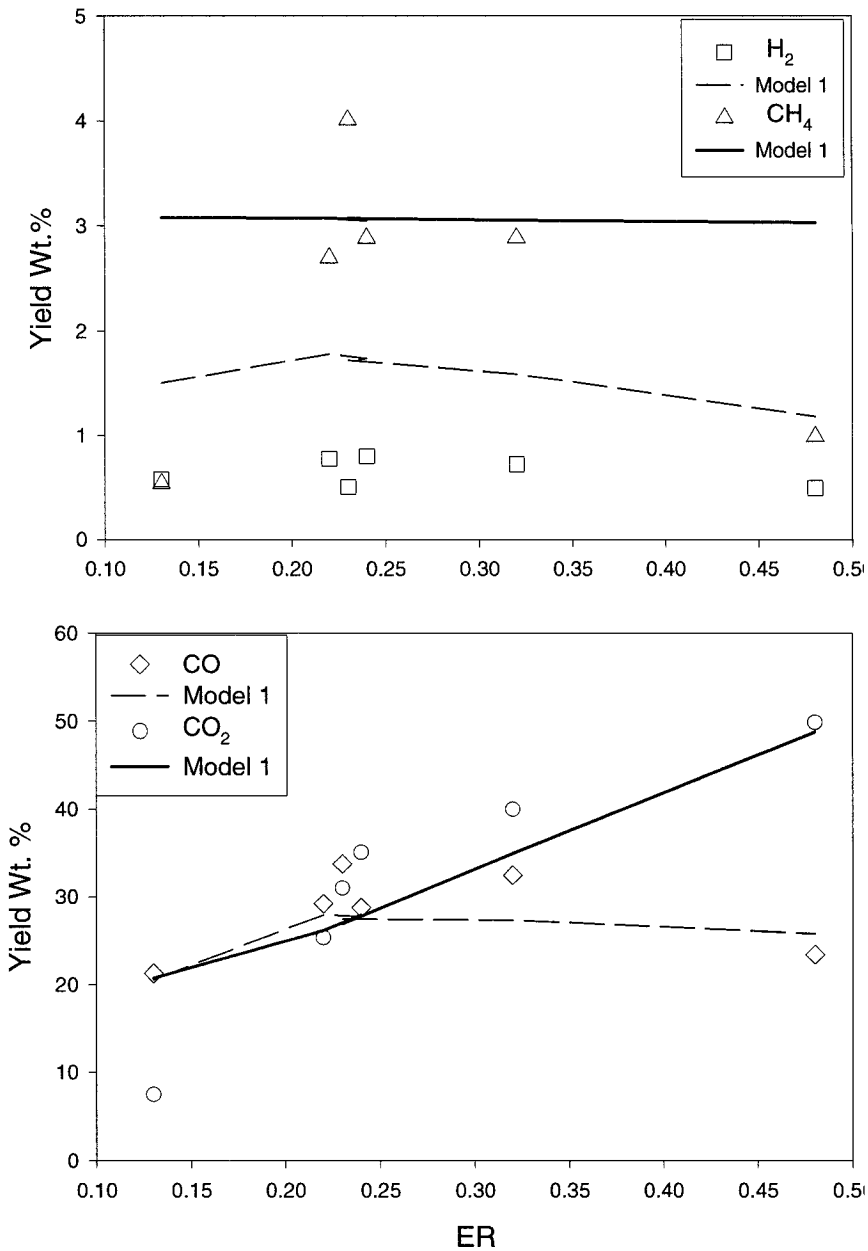

Figure 8.6: Individual dry gas yield at different ER and T_{bed}=800°C. Comparison of model with experiments (top-feeding).

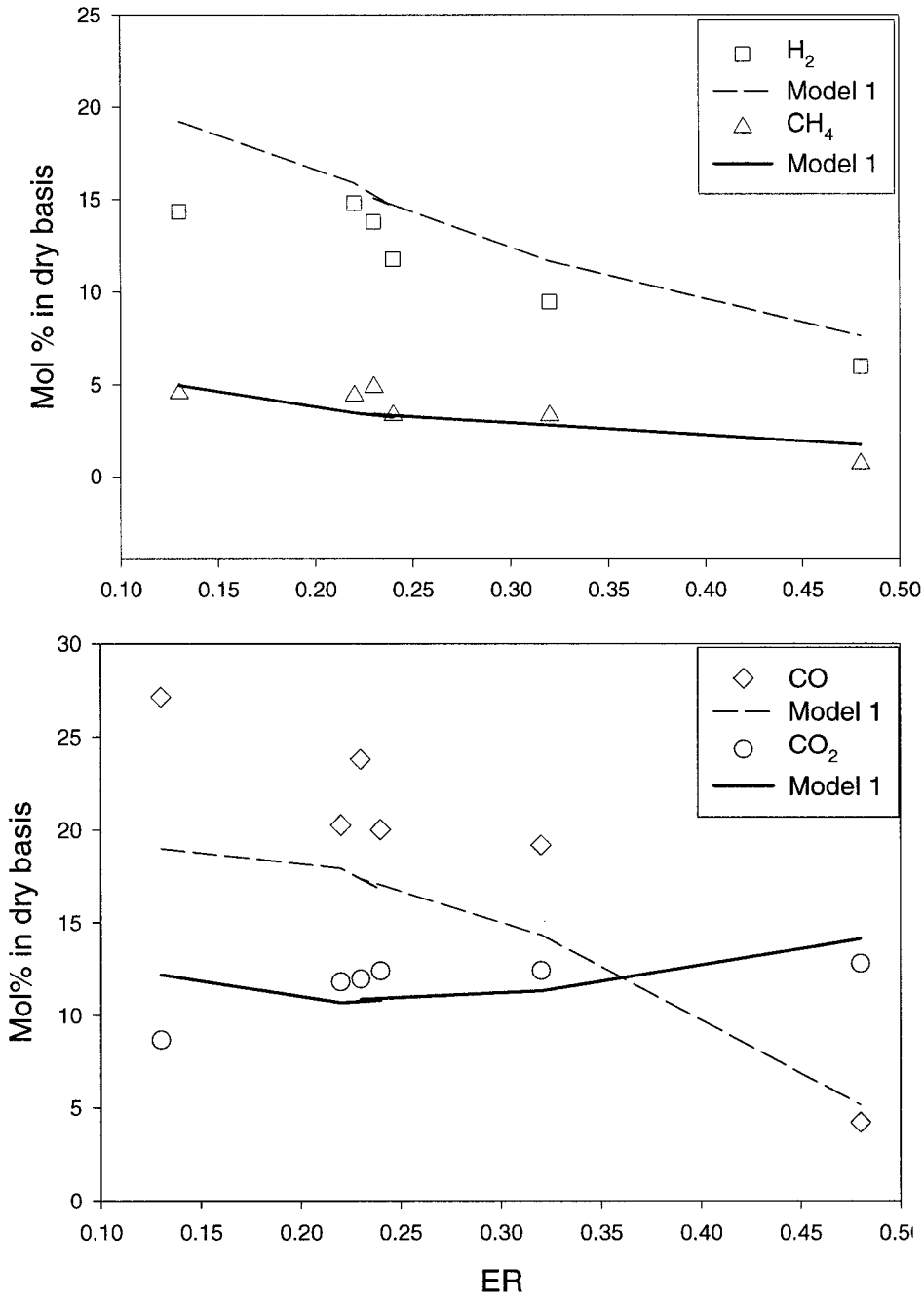

Figure 8.7: Concentration of individual gases in dry basis at different ER and T_{bed}=800°C. A comparison of the model with experiments (top-feeding).

al. (2004) have reported the same trend of gas composition changes with air ratio (ratio of actual air to stoichiometric required air) in a circulating fluidized bed.

8.2.5.2 Sensitivity analysis

The model shows considerable agreement with the experimental work of this study. The model also enables to study the influence of operating and hydrodynamics variables. The variables selected for the analysis are feeding point of the biomass (i.e. top- and bottom-feeding), ER, bed temperature, type of gasifying agent and K_w or the transfer coefficient between the counter-current phases. Model predictions in each case are compared with other experimental data that was carried out at the bubbling fluidized bed with different diameters. The model is also extrapolated to higher flow rate of gasifying agent and the effect of superficial gas velocity is considered on the heating value of the gaseous product.

8.2.5.2.1 Air-blown BFBG

8.2.5.2.1.1 Effect of feed location

Corella and co-workers have done extensive experimental work on biomass gasification in bubbling fluidized bed reactors (Corella *et al.* 1991, Herguido *et al.* 1992, Narvaez *et al.* 1996, Gil *et al.* (1999)). Since the size of the fluidized bed used in this study is very close to the one used by these authors, their experimental results are compared to the model. This allows investigating the effect of feeding location on gas

compositions as well. Narvaez *et al.* (1996) have studied air gasification of pine sawdust in a bubbling fluidized bed of 6 cm ID. Contrary to our experimental work, the wood particles feeding in their experiments takes place at the bottom of bed (i.e. 5 cm above the distributor). The model was adapted to a bottom-feeding of wood particles. The superficial gas velocities in both experiments are almost in the same ranges ($u=(2-3)\times u_{mf}$). Therefore, the same range of parameters for char mixing in the bed was assumed to be applicable here as well. Moreover, back mixing of the product gases has minor importance due to the low superficial gas velocities.

Figure 8.8 compares the model results with the experimental work of Narvaez *et al.* (1996). Figure 8.8-a shows the effect of ER and bed temperature on the dry gas composition of the product fuel gas. The effect of ER on gas concentrations is almost the same as the top-feeding presented in Figure 8.7. The effect of bed temperature at constant value of ER=0.3 is presented in Figure 8.8-b. High temperature greatly favors the gasification reactions (R2 and R3 in Table 8.6) and as a result of that the heating value of the product fuel gas increases. This is reflected in Figure 8.8-b where the concentration of H_2 and CO has increased substantially from 700°C to 800°C.

Both model and experimental data show a difference on the distribution of product gases between top- and bottom-feeding. In the bottom-feeding, the product gases form the pyrolysis step enters directly into the region of the bed where the concentration of oxygen is high. As a result, light gases, such as H_2 and CO, as well as tar, are prone to

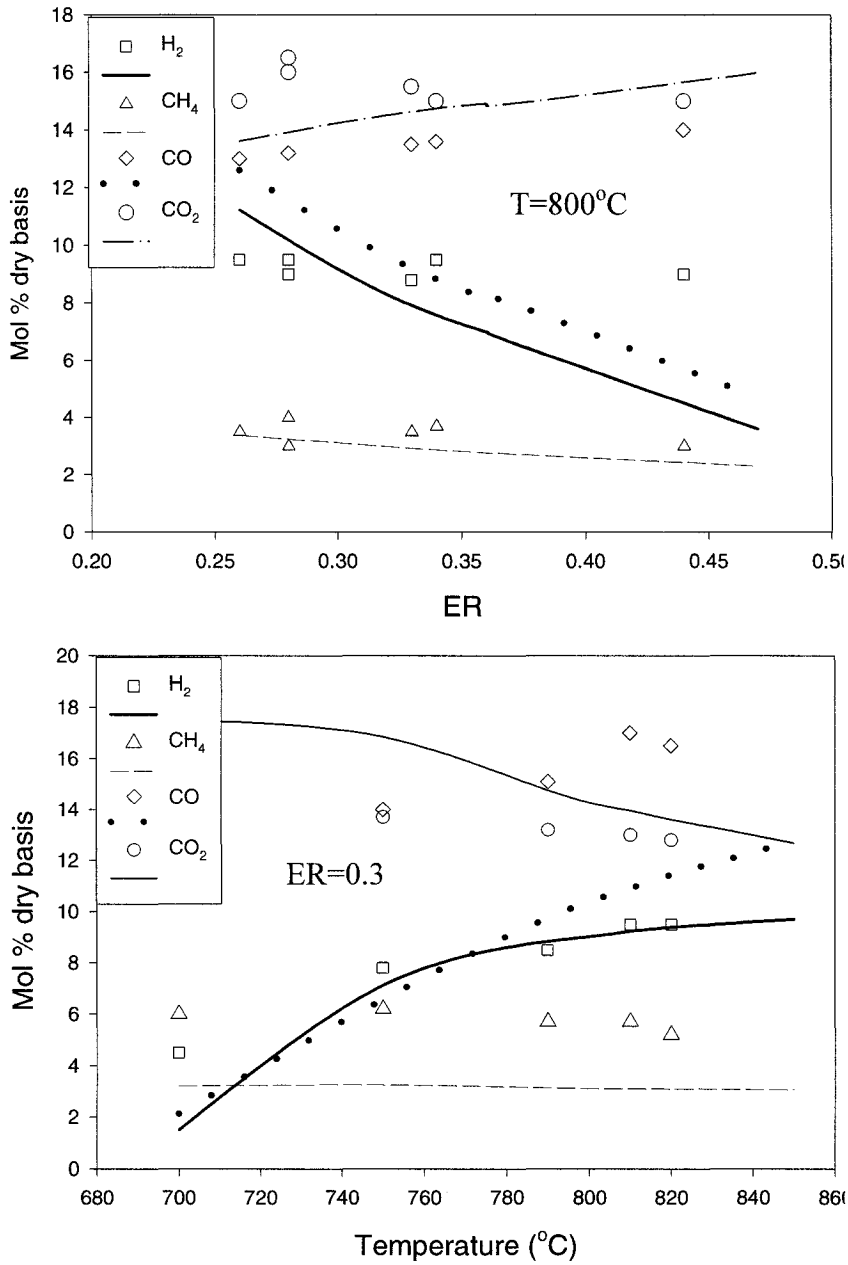

Figure 8.8: Model versus experiments (Narvaez *et al.* 1996) in air-blown BFBG with bottom-feeding.

a) Effect of ER on concentration at T=800°C.

b) Effect of temperature on concentration at ER=0.3

combustion in the bed. In the top-feeding, on the other hand, the gas product from pyrolysis step enters in a region that has already become depleted of oxygen mainly through the char combustion in the bed. Consequently, the concentration of H_2 and CO is higher in the top-feeding. This is also reflected in Figures 8.9-a and 8.9-b that show the effect of temperature and ER on HHV of the product gas. A comparison between this figure and Figure 8.5-b shows a lower heat content of the gaseous product in this case. The HHV of the product gas resulting from top-feeding, however, is disfavored by the higher quantity of tar, which is less prone to cracking and combustion in top-feeding.

8.2.5.2.1.2 Effect of gas velocity

The model is also extrapolated to higher superficial gas velocities. Table 8.9 presents gas velocities and other corresponding parameters used in the extrapolation. The bubble velocity and K_w presented in this table are those which were based on the RPT measurements at elevated temperatures. The extrapolation is carried out in a reactor with the same size and solid particles as in this study (see Figure 8.1) Changes on the superficial gas velocity have an impact on the hydrodynamics of the bed. Hydrodynamic changes take place mainly by changing bubble diameter and velocity. It also affects the residence time of the gas phase and, consequently, fuel gas distribution. Figure 8.10 shows the effect of superficial gas velocity on the fuel gas composition at two different ER values. The concentration of H_2 and CH_4 drops by increasing air superficial velocity, which results in a slightly lower HHV value by increasing gas

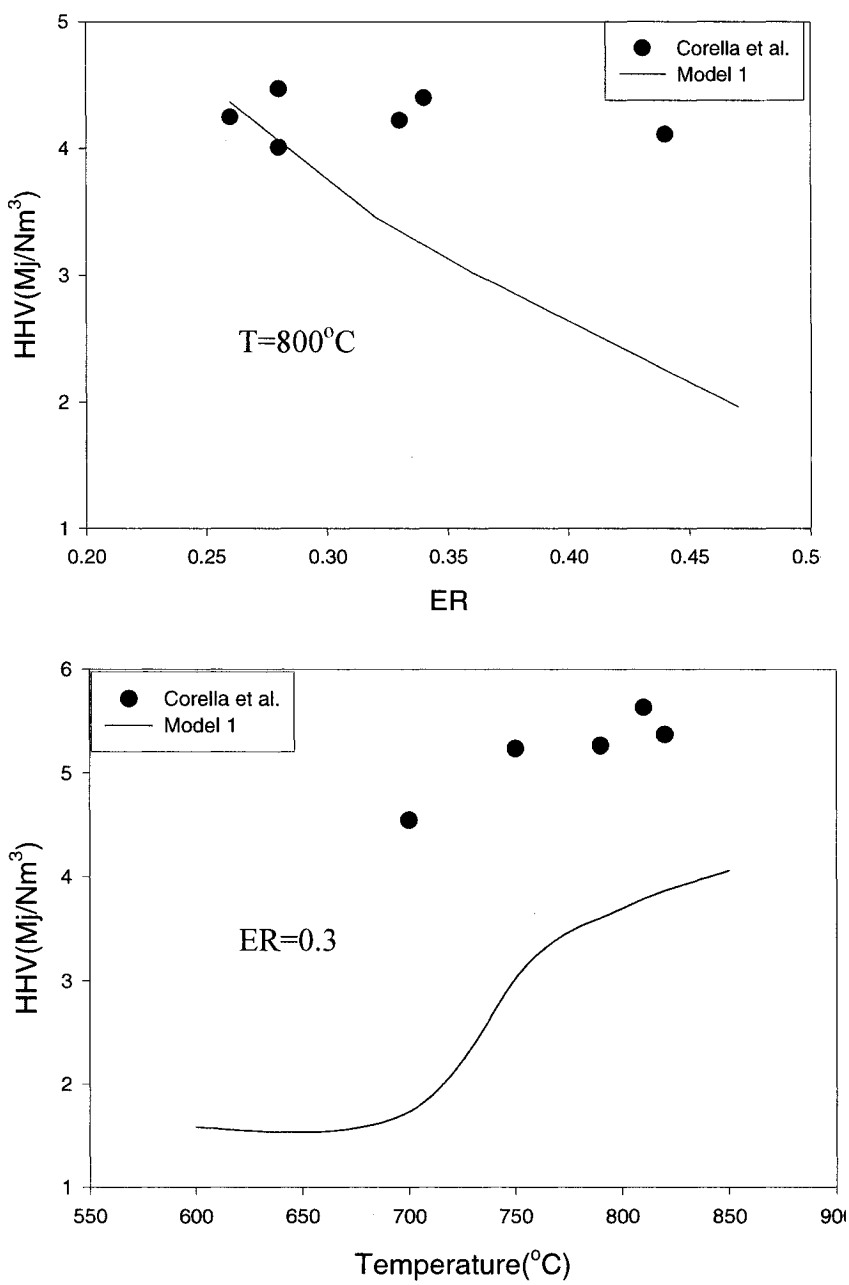

Figure 8. 9: Higher heating value of gas at different ER and bed temperature. Lines are the result of the model and symbols represent the experimental work (Narvaez *et al.* 1996).

Table 8.9: Gasification condition in the extrapolation of the model. T_{bed}=800°C, T_f=540°C, bottom-feeding

Air velocity (m/s)	ER	m_b (g/min)	u_b (m/s)	K_w (s^{-1})
0.29	0.25	23	0.4	0.64
0.38	0.25	30	0.45	0.85
0.53	0.25	42	0.56	0.86
0.76	0.25	60	0.73	1.2

velocity. The flow rate of gas which flows in the bubble phase is proportional to $u-u_{mf}$. By increasing gas velocity more gas flows in the bubble phase and, consequently, more oxygen is available in the bubble phase. As a result, more gases are prone to combustion in this phase. Since the combustion of H_2 is very rapid compared to the others, a larger reduction in concentration of this gas can be observed in the product gas.

8.2.5.2.1.2.3 Effect of K_w

In our previous study, the transfer coefficient between the counter-current phases (K_w) was found to be in the range of 0.6-1.7 s^{-1} for different superficial gas velocities and bed temperatures[14]. Among all the correlations for K_w, the one given byHoffmann *et al.* (1993) shows a better agreement with the experimental data at high temperatures. All the other correlations, including the one given by Kocatulum *et al.* (1991), shows higher discrepancies with the experimental data of solids mixing at high temperatures.

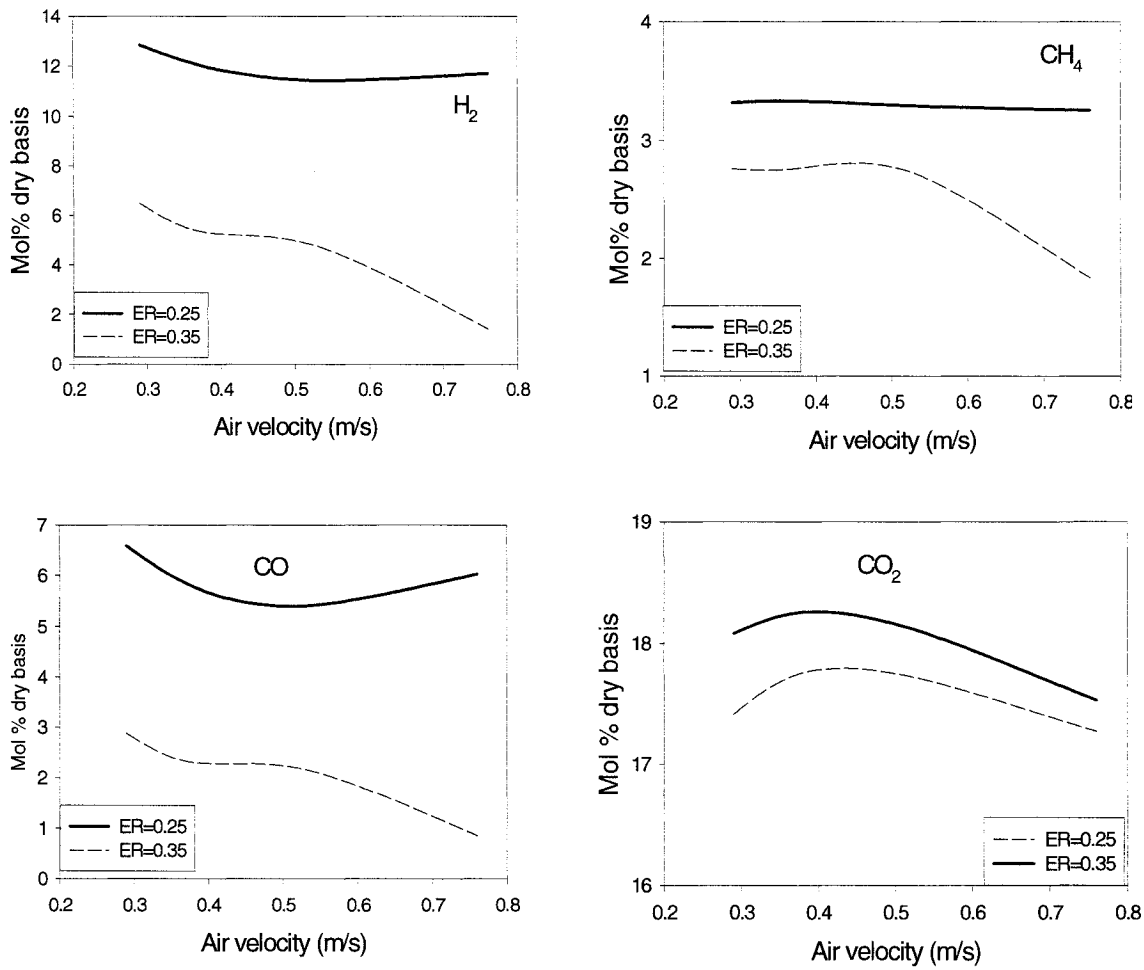

Figure 8.10: Gas composition versus air superficial velocity at two different ER. Extrapolation of the model to higher gas velocities. T_{bed}=800°C, T_f=540°C.

To investigate the effect of K_w on the final composition and heating value of product gas, this correlation, as presented in Table 8.7, is selected. The model was solved for a air-blown gasifier with a bottom-feeding condition using the new value of K_w. Figure 8.11 presents the simulation results at a bed temperature of T=800°C and different ER values using a K_w given by Kocatulum's correlation. The experimental conditions are

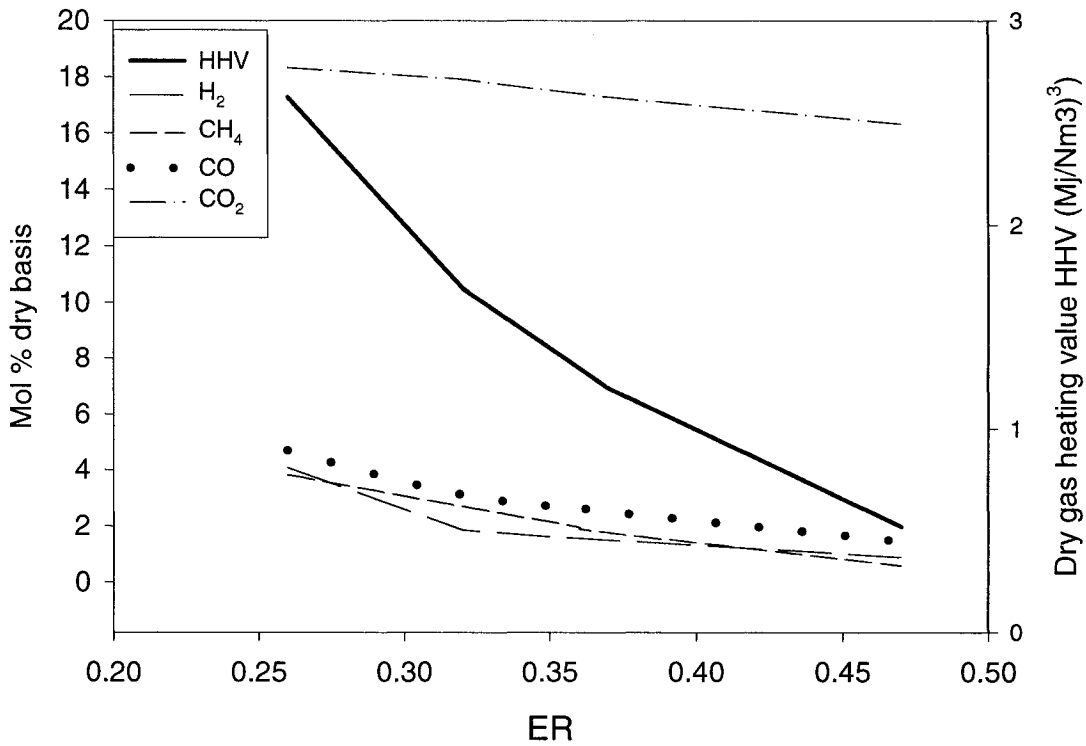

Figure 8.11: Gas composition and heating value of the product gas predicted by the model using a K_w given by Kocatulum *et al.* (1991).

the same as presented by Narvaez *et al.* (1996). The K_w calculated by Kocatulum's correlation in this condition is K_w=5 s^{-1}. As Figure 8.11 shows, heating value of the product gas is lower than that of evaluated based on K_w given by Hoffmann *et al.*[35]and experimental data of biomass gasification in a bubbling fluidized bed given by Narveaz *et al.*[40] (see for example Figure 8.9). This is due to the lower concentration of H_2 and higher concentration of CO_2 in the product gas. The competitive fast combustion of char and H_2 in solid and gas phases are affected by the hydrodynamics of the bed. A larger K_w promotes radial mixing in the solid phase but at the same time decreases the

contribution of oxygen consumption through char combustion reaction, which results in a higher contribution for the H_2 combustion. Interestingly, the agreement between simulation results and experimental data are more satisfactory when using a K_w close to the calculated range in solids mixing study at high temperatures (Radmanesh *et al.*, 2005b). This reveals the sensitivity of the model to the transfer coefficient between the counter-current phases.

8.2.5.2.2 Steam-blown BFBG: effect of gasifying agent

In this stage, the BFBG model is applied to steam gasification of wood. The same strategy, as was presented for air-blown gasification without any adjustable parameters, is used for steam-blown gasification in this section. Experimental results of Herguido *et al.* (1992) have been carried out in a 15 ID cm fluidized bed with bottom-feeding. Figure 8.12 compares their experimental results for steam gasification of saw dust with the model. Figure 8.12-a and 8.12-b show the effect of steam to biomass mass ratio (SB) and bed temperature on the gas composition of the product gas, respectively. Unlike air gasification where the product fuel gas is rich in CO_2 and CO, steam gasification results in H_2–rich gas. The model is capable of predicting the composition of the hydrogen in the final product gas.

The concentration of both H_2 and CO_2 increases by increasing SB. This can be explained by the shift reaction where the higher water concentration favors the CO_2 and H_2 production. Gil *et al.* (1999) have reported the same trend in concentration of gases

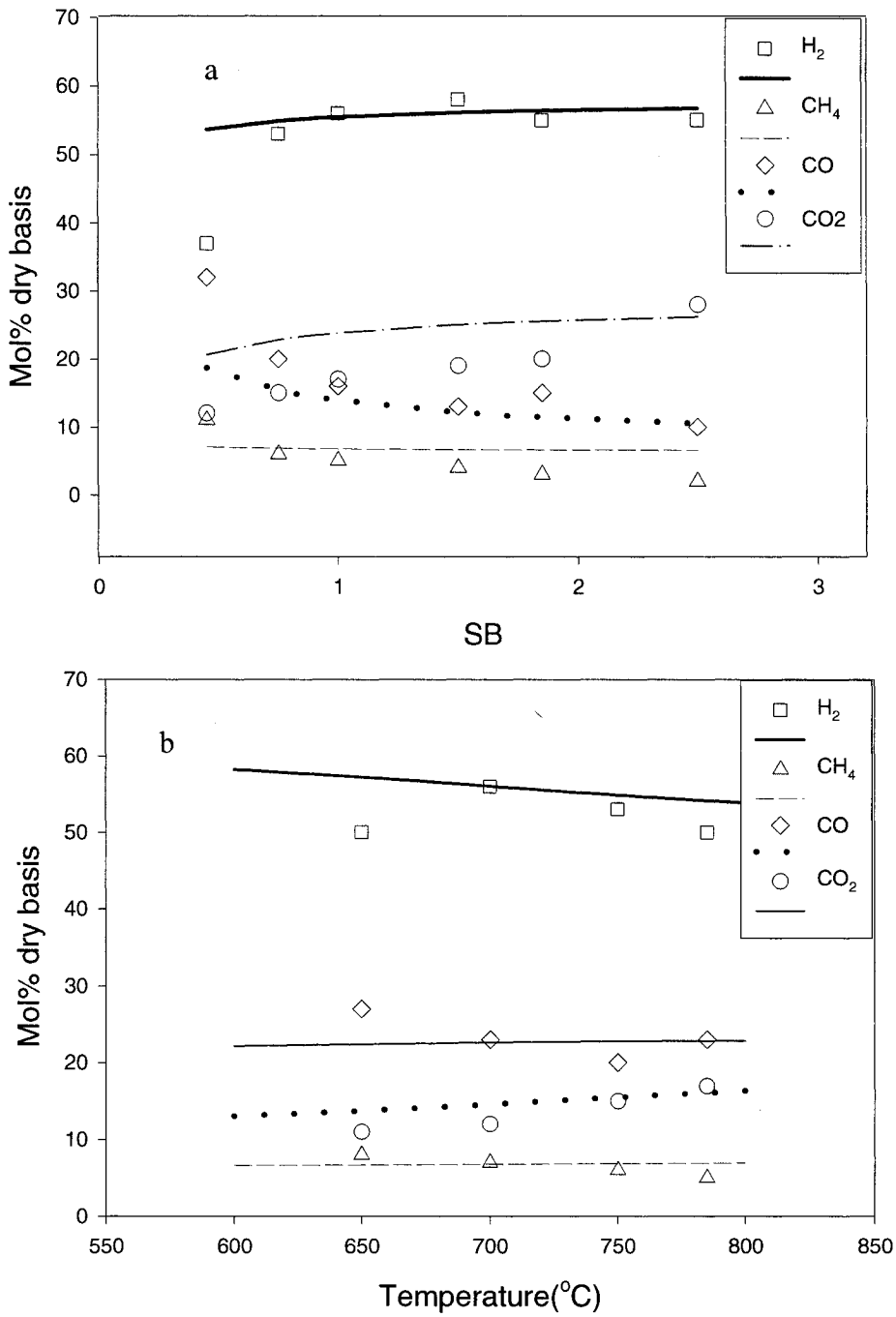

Figure 8.12: Model versus experiments (Herguido *et al.*, 1992) in steam-blown BFBG with bottom-feeding.

a) Effect of SB on concentration at T=750°C.

b) Effect of temperature on concentration at SB=0.75

in steam gasification of wood in BFBG. It is worth noting that biomass gasification using steam as the only gasifying agent does not correspond to industrial reality because of its lack of autothermicity. In reality, it is always necessary to use some air in order to provide the required energy for the endothermic reactions involved in steam gasification.

8.2.6 Conclusions

- A model was developed for biomass gasification in a bubbling fluidized bed reactor. The model takes into account the pyrolysis and various heterogeneous and homogeneous reactions kinetics as well as the hydrodynamics of the bed and freeboard. The model consists of no adjustable parameters.
- A two-phase model was used to describe the gas phase in the bed whereas a CCBM model was applied for the char mixing in the bed.
- It was shown that pyrolysis is an important step in the overall gasification model which can determine the distribution of products and thus the heating value of product fuel gas.
- Better results were obtained when using the pyrolysis model developed by Nunn *et al.*[15], which was developed at higher heating rates.
- The gasification models, developed based on the first and second pyrolysis kinetic models, were both able to predict the variation of total gas yield with

ER. However, the first kinetic model could follow the distribution of gases and thus the heating value of the product fuel gas more satisfactory.

- The model of BFBG also showed a good agreement with experiments on steam gasification of wood, where by increasing SB, H_2 and CO_2 concentration rises and that of CO drops.

8.2.7 Notations

C_i	contribution coefficient of each pseudo component in biomass, (Table 8.4)
C_p	heat capacity, J/kg K
d	diameter, m
E	activation Energy, kJ/mol
h_{conv}	convective heat transfer coefficient, W/m^2 K
K_g	thermal conductivity of gas, W/m K
$k_{0,i}$	frequency factor for component i, 1/s
K	transfer coefficient, 1/s
M_i	molecular weight of component I, kg/kmol
n_p	parameter in Equation (8.3)
R_i	rate of reaction for component i
Re	Reynolds number
Pr	Prandtl number

T_{bed}	bed temperature, K
T_p	particle temperature, K
u	gas velocity, m/s
U	counter-current phases, m/s
V_i	release volatile matter, wt%
V_i^*	ultimate final yield for component i in pyrolysis
X	conversion of char
X_{vm}	volatile content in the wood, wt%
y_i	weight fraction of component i in the gas
z	height of the freeboard, m

Subscripts:

b	bubble
p	particle
i	gaseous components in the product gasj
j	reaction index
as	ascending phase
ds	descending phase
c	char
f	freeboard

w	wake
bc	bubble-cloud
be	bubble-emulsion

Greek:

ε	emissivity coefficient
φ	Parameter in Equation (8.3)
ε_{mf}	minimum fluidization velocity, m/s
ρ_i	density of component i, kg/m^3
υ_i	stoichiometric coefficient of component i
δ_b	fraction of bed in bubble
γ_b	fraction of solid in bubble, m^3/m^3

8.2.8 Reference

Altafini, C.R., Wamder, P.R., Barreto, R.M., 2003. Prediction of working parameters of a wood waste gasifier through an equilibrium model. Energy Conversion & Management 44, 2763-2777.

Babu, B.V. and Chaurasia, A.S., 2004. Dominant design variables in pyrolysis of biomass particles of different geometries in thermally thick regime. Chemical Engineering Science 59, 611-622.

Bacon, D.W., et al., 1985. Modeling of Fluidized Bed Gasifiers. In Fundamentals of Thermochemical Biomass Conversion. ed. T.A. Milne and K.L. Mudge. Elsevier Applied Science. 717-732.

Biba, V., Macak, J., Klose, E. Malecha, J., 1978. Mathematical modeling for the gasification of coal under pressure. Industrial & Engineering Chemistry Process Design and Development 17-92-98.

Bilbao, R., Arauzo, J., Salvador, M.L., 1995. Kinetics and modeling of gas formation in the thermal decomposition of powdery cellulose and pine sawdust Industrial & Engineering Chemistry Research 34, 786-793.

Bilodeau, J.F. Thérien, N., Proulx, P., Czernik, S., Chornet, E., 1993. A mathematical model of fluidized bed biomass gasification. The Canadian Journal of Chemical Engineering 71, 549-557.

Boroson, M.L., Howard, J. B., Longwell, J.P., Peters, W.A, 1989. Product yields and kinetics from the vapor phase cracking of wood pyrolysis Tars. AIChE J. 35, 120-128.

Bryden, K.M., Ragland, K., 1996. Numerical modeling of deep fixed bed combustor. Energy & Fuel 10, 269.

Corella J., Sanz A., 2005. Modeling circulating fluidized bed biomass gasifiers. A pseudo-rigorous model for stationary state. Fuel Processing Technology 86, 1021-1053.

Corella, J. Herguido, J. Alday, F.J. 1988. Pyrolysis and steam gasification of biomass in fluidized beds: influence of the type and location of the biomass feeding point on the product distribution. In research in thermochemical biomass conversion. Bridgwater, A.V, Kuester, J. L. Editor Elsevier Applied Science Ondaon 384.

Corella, J., M.P. Aznar, J. Delgado, Aldea, E., 1991. Steam gasification of cellulosic wastes in a fluidized bed with downstream vessels. Industrial & Engineering Chemistry Research 30, 2252-2262.

Davidson J.F and Harrison D.,1963. Fluidized particles. Cambridge University Press, New York.

de Souza-Santos, M.L., 1989. Comprehensive modeling and simulation of fluidized bed boilers and gasifiers. Fuel 68, 1507-1521.

Di Blasi, C., 2004. Modeling wood gasification in a countercurrent fixed-bed reactor. AIChE J. 50, 2306-2319.

Double, J.M., Smith E.L., Bridgwater A.V., 1989. Computer modeling of fluidized bed gasifier. process and gasification, ed. Ferrero, G.L., Maniatis, K., Buekens, A. Elsevier Applied Science. 651-655.

Fiaschi D., Michelini M., 2001. A two-phase one-dimensional biomass gasification kinetic model. Biomass and Bioenergy 21, 12-132.

Gil, J., Corella, J. Aznar, M.P., Caballero, M.A., 1999. Biomass gasification in atmospheric and bubbling fluidized bed: effect of the type of gasification agent on the product distribution. Biomass and Bioenergy 17, 389-403.

Grace, J.R., 1982. In Handbook of multiphase systems, Hetsroni, G., Hemisphere, Washington, 8-1

González JF., Encinar JM, Canito JL, Sabio E, Chacon M. 2003. Pyrolysis of cherry stones: Energy uses of the different fractions and kinetic study. Journal of Analytical and Appllied Pyrolysis 67, 165-190.

Hajaligol, M. R., Howard, J. B., Longwell, J. P., Peters, W. A. 1982. Product compositions and kinetics for rapid pyrolysis of cellulose. Industrial & Engineering Chemistry Process design and development, 21:3, 457-465.

Hamel, S., Wolfgang, K., 2001. Mathematical modeling and simulation of bubbling fluidized bed gasifiers. Powder Technology 120. 105-112.

Herguido, J., Corella, J., Gonzalez-saiz, J., 1992. Steam gasification of lignocellulosic residues in a fluidized bed at a small pilot scale. Effect of the type of the feedstock. Industrial & Engineering Chemistry Research 31, 1274-1282.

Hoffmann, A.C.; Janssen, P. B. M., Prins, J., 1993. Particle Segregation in fluidized binary mixtures, Chemical Engineering Science, 48:9, 1583-1993.

Kocatulum, B., Basesme, E. A., Levy, E. K., Kozangolu, B. 1991. Particle motion in the wake of a bubble in a gas-fluidized bed, Annual Meeting of the American Institute of Chemical Engineers, Nov 17-22. 1991. Los Angeles, CA, USA, 40-50.

Koufopanous, C.A., Papayannakos N., Maschio G., Lucchesi A., 1991. Modeling of pyrolysis of biomass particles. Studies on kinetic, thermal and heat transfer effects. Canadian Journal of Chemical Engineering 69, 907.

Kunii D., Levenspiel O., 1991. Fluidization engineering. 2nd ed. MA, Butterworth-Heinemann series in chemical engineering.

Li, X., Grace, J.R., Watkinson, P., Lim, C.J. , Ergudenler, A., 2001. Equilibrium modeling of gasification: a free energy minimization approach and its application to a circulating fluidized bed coal gasifier. Fuel 80, 195-207.

Li, X., Grace J.R., Lim, C.J, Watkinson A.P., Chen H.P., Kim, J.R., 2004. Biomass gasification in a circulating fluidized bed. Biomass and Bioenergy 26,171-193.

Linjewile, T.M., 1993. Temperature of burning carbonaceous particles in a fluidized bed combustor, Thesis (PhD). The University of Adelaide.

Mansaray, K.G., Al-Taweel, A.M., Ghaly, A.E., Hamdullahpur, F., Ugursal, V.I., 2000. Mathematical modeling of a fluidized bed rice husk gasifier: Part I -model development. Energy Sources 22, 83-98.

Narvaez, I., Orio, A., Aznar, M.P., Corella, J., 1996. Biomass gasification with air in an atmospheric bubbling fluidized bed. Effect of six operational variables on the quality of the produced raw gas. Industrial & Engineering Chemistry Research 35, 2110-2120.

Nunn TR, Howard JB, Longwell JP, Peters WA. 1985. Product Compositions and Kinetics in the Rapid Pyrolysis of Sweet Gum Hardwood. Industrial & Engineering Chemistry Process Design & Developments 24, 836-844.

Radmanesh, R., Chaouki, J., Guy, C. 2005a. A unified lumped approach in kinetic modeling of biomass pyrolysis. Accepted in Fuel.

Radmanesh, R., Mabrouk, R., Chaouki, J., Guy, C. 2005b. The effect of temperature on solids mixing in a bubbling fluidized bed reactor. International Journal of Chemical Reactor Engineering Vol. 3, A16.

Radmanesh, R., Chaouki, J., Guy, C., July 2005c. Modeling biomass pyrolysis in a bubbling fluidized bed reactor. 7th world congress of chemical engineering, Glasgow, Scotland, Sustainable and Clean Technologies - Alternative Feeds.

Ruggiero, M., Manfrida, G., 1999. An equilibrium model for biomass gasification process. Renewable Energy 16, 1106-1109.

Roth, J., Steiner, G., Wolfinger, M.G., Staudinger, G., 2002, Tar cracking from fast pyrolysis of large beech wood particles. Journal of Analytical and Applied Pyrolysis 62(1), 83-92.

Sadaka, S.S., Ghaly, A.E., Sabbah, M.A. 2002. Two phase biomass air-steam gasification model for fluidized bed reactors: Part I---model development. Biomass and Bioenergy, 22, 439-462.

Shin, D., Choi, S., 2000. Combustion of simulated waste particles in a fixed bed, Combustion & Flame, 121(1), 167-180.

Vriesman, P., Heginuz, E., Sjostrom, K., 2000. Biomass gasification laboratory-scale AFBG: influence of the location of the feeding pint on the fuel-N conversion. Fuel 79, 1371-1378.

Van Den Aarsen, F.G., Beenackers, A.C.M., van Swaaij, W. P. M., 1982. Wood pyrolysis and carbon dioxide char gasification in a fluidized bed, In: fundamentals of thermochemical biomass conversion. Elsevier applied science publisher, 691.

van Deemter, J. J. 1967. The countercurrent flow model of a gas-solids fluidized bed, in proceeding of international symposium on fluidization, Netherlands university press, Amsterdam.

Wurzenberger, J.C, Wallner S., Raupenstrauch, H., Khinast, J.G, 2002. Thermal conversion of biomass: comprehensive reactor and particle modeling. AIChE J., 48(10), 2398-2411.

Yates, J. G., 1983. Fundamentals of fluidized-bed chemical processes. London: Butterworths.

CHAPTER 9

GENERAL DISCUSSION

Biomass gasification is a sustainable route toward energy and chemical production. The recent sensitivities over the climate changes and gas emissions have given a new momentum to gasification. This work is an attempt to address some important issues involved in the gasification of biomass materials.

As presented in Chapter 2, many reactions are involved in gasification. These reactions can be summarized as primary pyrolysis, secondary pyrolysis or tar cracking and different homogeneous and heterogeneous reactions. In a fluidized bed, these reactions should be taken into consideration in conjunction with the heat and mass transfers that take place in the bed and freeboard. Primary pyrolysis is the first step that takes place instantaneously, compared to the other chemical reactions involved in gasification. The volatile matter, char and tar released during the pyrolysis are subject to other chemical reactions in the fluidized bed or the freeboard of the reactor. The understanding of the biomass kinetics and bed hydrodynamics are hence essential in modeling and predicting the produced fuel gas composition from a bubbling fluidized bed gasifier (BFBG).

Thermogravimetry analysis (TGA) and gas chromatography (GC) are used simultaneously in this work to explore pyrolysis of biomass. The former leads to the overall devolatilization of biomass, whereas the latter provides the evolution of the gases during the pyrolysis. The evolution of four main gases, i.e H_2, CH_4, CO and CO_2 can be detected by GC; these are the most abundant gases produced during the pyrolysis. Tar and water, which are the condensable part of the product and cannot be detected by GC, are determined through a mass balance in the system. Therefore, a complete picture of biomass pyrolysis is provided using the system of TGA/GC.

The TGA/GC experiments are carried out at different moderate heating rates (10, 20, 30, 50 K/min). These heating rates are very relevant to biomass gasification in moving bed reactors, where the rate of temperature increase in the particles is slow. In fluidized bed gasification the average heating rate in biomass particles are higher. In fact, particle dynamic in this case are very affected by convective transport of volatile products and particle size. In practical application of fluidized bed biomass gasification, the biomass particle sizes may vary from few millimetres to few centimetres. The heating rate in this condition, where internal heat transfer limitation is important and also where endothermic and exothermic reactions (due to primary and secondary pyrolysis) take place inside biomass particles, is again low. Table 9.1 shows the effect of wood particle diameter on heating rate at the centre of a wood particle and at different solid mass fractions (Di Blasi, 2000). At a higher particle size the heating rate is lower at the center of a wood particle fed to a fluid-bed of sand particles at

T=800 K. This is a clear indication of the importance of particle size and internal heat transfer resistances.

Table 9.1: Heating rate of wood particles at different particle size and solid mass fractions, T_{bed}=800 K (Di Blasi, 2000)

Y	d_p=0.2 mm	d_p=2 mm	d_p>4 mm
0.8	1086 K/s	43 K/s	≤15 K/s
0.5	548	18	
0.2	340	10	≤4.5

As our experimental data of wood gasification at a fluidized bed reactor shows, the heating value of the produced gas is slightly higher in top-feeding, where the biomass is fed in the freeboard. In industrial application, biomass feeding into the freeboard is more practical. In this condition, the external heat transfer coefficient is lower compared to feeding into the bed. This, again, slows down the rate of temperature increase in biomass particles.

In the hydrodynamics study of the fluidized bed, for the first time, Radioactive Particle Tracking (RPT) technique is used at high temperature to study solids mixing and some hydrodynamic characteristics of fluidization at high temperatures. In the first step, solids mixing was studied by a counter-current back mixing model (CCBM) (May 1950) at a temperature range of 25-400°C. The experiments and analysis were then extended to temperatures as high as 700°C. This temperature was the maximum temperature that allowed the safe operation of NaI scintillation detectors. The

experiments carried out in this part are relevant to the hydrodynamic studies of fluidized bed gasification or combustion.

A model for BFBG of biomass material is developed. Gasification and pyrolysis experiments were carried out in bubbling fluidized bed reactor to verify the model. The gas velocity in gasification experiments ranged from 0.13 to 0.35 m/s. The bed and freeboard temperature were 800 and 740 ^{o}C, respectively.

The following is a discussion on some of the results obtained in this work.

9.1 Effect of pyrolysis kinetics on gasification

The results of the model presented in Chapter 8 demonstrate the importance of the pyrolysis step in the final gas composition. As it shows, the first pyrolysis kinetic model, which was derived at higher heating rates can predict product gas composition satisfactorily. This, apparently, suggests a change in pyrolysis mechanism at very high heating rates, which forces a new distribution in the final product gas concentration. Therefore, the kinetic model derived at high heating rates estimates the final gas composition relatively better than the one derived at lower heating rates.

9.2 Effect of temperature on fluidization

It is shown that the bubble (wake) velocity at higher temperatures deviates from the correlation prediction and that the trend cannot be explained merely by changes in

interstitial gas properties. This is explained and justified based on the surface changed observed in the SEM results of silica sand particles. Two characteristic time (i.e. jump time and cycle time) change with temperature. The number of jumps increases significantly at low superficial gas velocity by increasing temperature. The same trend is found for cycle time. There is no significant change in the characteristic times of alumina particles. Since both solid particles belong to Group-B Geldart classification, the change in surface of silica sand particles was believed to be responsible for its different fluidization behavior compared to alumina particles.

9.3 Effect of Kw on gasification modeling

In Chapter 6 of this thesis, transfer coefficient (K_w) between the counter-current phases in the CCBM model is calculated at high temperatures and compared with available correlations in the literature. It is shown that most correlations overestimate the K_w value. The correlation presented by Hoffmann *et al.* (1993), however, shows a good agreement with the RPT data at high temperatures. Therefore, in Chapter 8, the K_w given by Hoffmann's correlation is used in the modeling of a BFBG. To investigate the effect of K_w on the gas composition of product gas in the same chapter, correlation presented by Kocatulum *et al.* (1991), with a higher discrepancy with calculated K_w from the RPT data, is also used in the modeling. It is found that there exists a better agreement between the gas composition predicted by the gasification model and experimental data of beech wood gasification in a BFBG, when using Hoffmann's

correlation. This is also an interesting way in which, the hydrodynamic results are verified through gasification data in a bubbling fluidized bed reactor.

CHAPTER 10

CONCLUSION AND RECOMMENDATIONS

10.1 General Conclusion

The primary objective of this research was to provide a comprehensive model for bubbling fluidized bed gasifiers (BFBGs) of biomass materials. The following important aspects were considered in the modeling of BFBGs:

1. *The kinetics of pyrolysis*: It is shown in Chapter 2 that pyrolysis is an influential step in predicting fuel gas composition in the fluidized bed gasification of biomass materials. It determines the yields of different gases and char. The larger volatile content of biomass materials (c.a 75-85%) necessitates a kinetic model that accounts for the formation of different gases during pyrolysis.

2. *The hydrodynamics of bed at elevated temperatures*: Fluidized bed gasification and combustion take place at high temperatures ($T \geq 800^{o}C$). Despite this fact, it is shown in Chapter 2 that few investigations have been reported on the temperature dependence on fluidization. There is a lack of information in the hydrodynamic study of fluidized beds at high temperatures.

Pyrolysis of three biomass materials was studied in a system consisting of a thermobalance and a gas chromatograph. A map of different products during the pyrolysis of biomass materials was demonstrated at moderate heating rates. This included the char, H_2, CH_4, CO, CO_2 and liquids (tar and water). CO_2 and CO were identified as the most abundant gases resulting from pyrolysis. Suitable kinetic models were also developed for all the range of products. It was shown that the heating rate had an impact on the final attainable gas yields. The kinetic models were improved in order to extend their applicability to other heating conditions. This makes the model more versatile especially in applying it to different reactors where the operating conditions are different from the thermobalance.

Hydrodynamics of a fluidized bed was studied using Radioactive Particle Tracking (RPT) technique in a temperature range of 25-700°C and a velocity range of 0.16-0.78 m/s. Two types of particle (i.e. silica sand and alumina particles), both of them belonging to Group-B Geldart powders, were used as the bed material. The temperature range and type of particles used in this part of work were very relevant to fluidized bed gasification and combustion. The effect of temperature on several parameters of fluidization was investigated. It was shown that the bubble (wake) velocity for silica sand particles at higher temperatures deviates from the prediction of correlations and that the trend could not be explained merely by changes in interstitial gas properties. This was justified by the changes observed on the surface of silica sand particles in Scanning Electron Microscopy (SEM) results. For alumina particles, the correlation

could predict the bubble velocity even at high temperatures. The SEM results of alumina particle surface showed no changes on the morphology of the surface. The characteristic times of fluidization which were investigated in this study (i.e. jump time and cycle time) showed variations by changing the temperature at the same superficial gas velocities. The number of jumps increased significantly at low superficial gas velocity by increasing temperature. The same trend was found for cycle time. There was no significant change in the characteristics times of alumina particles. Since both solid particles belong to Group-B Geldart powders, the change in surface of silica sand particles was believed to be responsible for its different fluidization behavior compared to alumina particles.

RPT results at high temperature were also used to study solids mixing at elevated temperatures. This is another aspect of fluidization which is relevant to fluidized bed gasification and combustion as well. Solids mixing was studied using a counter-current back mixing (CCBM) model, which was applied to fluidization of silica sand particles at high temperatures. The effect of temperature on the phase dynamics showed more solids are present in the dilute phase at higher temperatures in a temperature range of 25-400^{o}C. This, in turn, affects the global mixing of solids in the bed. The transfer coefficient between the counter-current phases (K_w) was found to be in the range of 0.6-1.7s^{-1} in different experiments.

The CCBM solids mixing model and bubble velocity calculated at high temperatures using RPT experiments, as well as the pyrolysis kinetic models developed in this work, were used in Chapter 8 in the modeling of a BFBG. Two kinetic models for pyrolysis were used (Chapter 5 and Nunn *et al.* 1985) and compared in this work. It was found that the prediction of fuel gas composition strongly depends on the kinetic models of primary pyrolysis. The kinetic model of Nunn *et al.* (1985) developed at fairly high heating rates showed more promising results, in comparison to the kinetic model developed in this work at moderate heating rates.

10.2 Recommendations

10.2.2 Kinetics of pyrolysis

The kinetic model presented in this thesis can be extended to higher heating rates. The results of the model presented in Chapter 8 show that there must be a change in pyrolysis mechanism that leads to less satisfying results when extrapolating from moderate and low heating rates to very high heating rates. An understanding of this mechanism can result in more robust kinetic models for biomass gasifiers.

10.2.1 Tar removal

The main hurdle in the route from biomass to electricity through gasification remains in the gas cleaning and tar removal. The sticky and noxious tar material, as an undesired by-product in gasification, causes many operating problems, especially, when the end-

product gas is supposed to be used in a gas turbine. The main challenge in tar cracking is to find a cheap but effective catalyst, which can be preferably used in the gasifier bed.

10.2.2 Nitrogen elimination

Gasification is an autothermal process, which means that the heat required for drying, pyrolysis and other endothermic reactions is provided through combustion reactions. This necessitates the use of air or oxygen. Even in steam gasification, air or oxygen is needed for the autothermicity of the process. The use of pure oxygen is, however, disfavored by the required separation step, which increases the fixed and operating costs. The use of air as a gasifying agent, on the other hand, has the drawback of diluting the produced fuel gas with a large quantity of nitrogen (i.e. 55-60% N_2 depending on the ER value). A simple but effective solution which avoids the dilution of produced fuel gas by nitrogen is to use oxygen-carrier catalysts, such as NiO_2 or MoO, instead of air. Figure 10.1 portraits a schematic presentation of this so called Chemically Looped Gasifier (CLG). This process also can be carried out in an internally circulating fluidized bed (ICFB) reactor, where oxidation reactions take places in the riser and reduction reactions in the downcomer annulus.

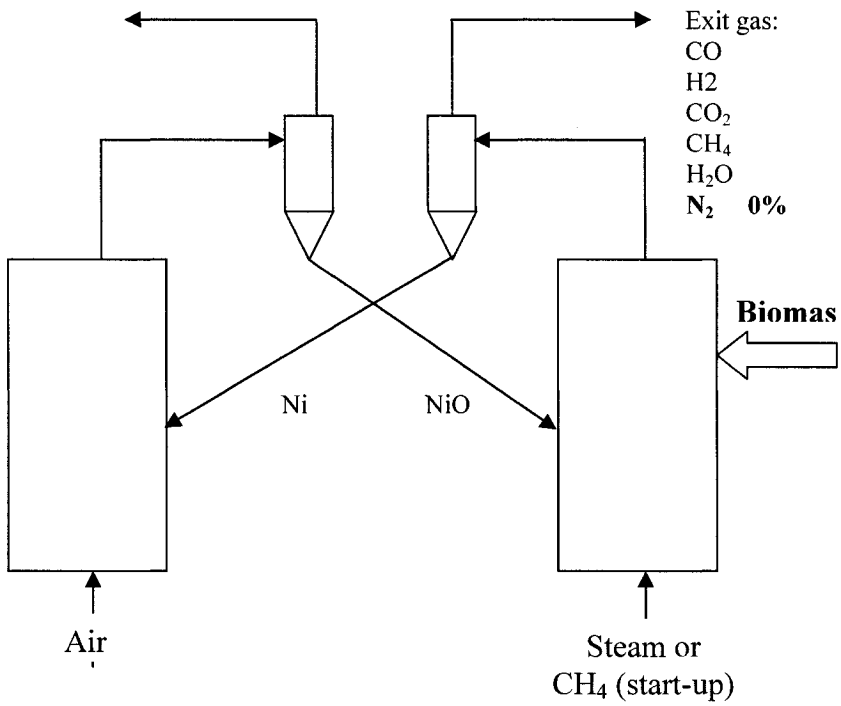

Figure 10.1 Chemical Looping Gasification

10.2.3 The Hydrodynamics of bed at high temperature

Much more work is still required to explore the effect of temperature on bed hydrodynamics. The RPT technique can be modified for smaller particles, namely Geldart Group-A powders. This work showed how a change on the surface of particles can affect the characteristics of fluidization. Experiments can be extended to particles that are prone to severe surface or physical property changes. This will provide more information on the effect of the surface or physical properties changes of solid particles on the hydrodynamic characteristics of fluidization.

REFERENCES

ALTAFINI, C.R., WAMDER, P.R., BARRETO, R.M. (2003). Prediction of working parameters of a wood waste gasifier through an equilibrium model. Energy conversion and management, 44, 2763-2777.

ANDRÉ, R.N., PINTO, F., FRANCO, C., DIAS, M., GULYURTLU, I., MATOS, M.A.A., CABRITA, I. (2005). Fluidized bed co-gasification of coal and olive oil industry wastes. Fuel, 84, 1635-1644.

ANTAL, M.J., VARHEGYI, G. (1995). Cellulose pyrolysis kinetics: The current state of knowledge, Industrial &. Engineering. Chemistry. Research, 34, 703.

ANTHONY, D., HOWARD, B. (1976). Coal devolatilization and hydrogasification. AIChE J., 22, 625-656.

ARAUZO, J., RADLEIN, D., PISKORZ, J., SCOTT, D.S. (1997). Catalytic pyrogasification of biomass. Evaluation of modified Nickel catalysts. Industrial & Engineering Chemistry Research. 36, 67-75.

AZNAR, M.P., CORELLA, J., DELGADO, J., LAHOZ, J. (1993). Improved steam gasification of lignocellulosic residues in a fluidized bed with commercial steam reforming catalyst. Industrial & Engineering Chemistry Research, 32, 1-10.

BABU, B.V., CHAURASIA, A.S. (2004). Dominant design variables in pyrolysis of biomass particles of different geometries in thermally thick regime. Chemical Engineering Science, 59:3, 611-622.

BACON, D.W., DOWNIE, J., HSU, J.C., PETERS J. (1985). Modeling of Fluidized Bed Gasifiers. In Fundamentals of Thermochemical Biomass Conversion, ed. T.A. Milne and K.L. Mudge. Elsevier Applied Science. 717-732.

BAKER, E.G., MUDGE, L.K., BROWN, M.D. (1987). Steam gasification of biomass with Nickel secondary catalysts. Industrial & Engineering Chemistry Research, 26, 1335-1339.

BANYASZ, J. L., LYONS-HART, J., SHAFER, K. H. (2001). Gas evolution and the mechanism of cellulose pyrolysis. Fuel, 80, 1757-1763.

BASESME, E. A.; LEVY, E. K. (1992). Solids exchange between the bubble wake and the emulsion phase in a two-dimensional gas-fluidized bed. Powder Technology, 72:1. 45-50.

BECK, S.R., HUFFMAN, W.J., LANDEENE, B.L., HALLIGAN, E. (1979). Pilot plant results for partial oxidation of cattle feedlot manure. Industrial & Engineering Chemistry Process Design and Development, 18:2, 328-332.

BECK, S.R., WANG, W. (1980). Wood gasification in a fluidized bed. Industrial & Engineering Chemistry Research, 19, 312-317.

BEENACKERS, A.A.C.M. (1999). Biomass gasification in moving beds: A review of European technology. Renewable Energy, 16, 1180-1186.

BIBA, V., MACAK, J., KLOSE, E. MALECHA, J. (1978). Mathematical Modeling for the Gasification of Coal under Pressure. Industrial & Engineering Chemistry Process Design and Development, 17, 92-98.

BILBAO, R., ARAUZO, J., MURILLO, M. B., SALVADOR, M. L. (1997). Gas formation in the thermal decomposition of large spherical wood particles. Journal of Analytical and Applied Pyrolysis, 43:1, 27-39.

BILBAO, R., ARAUZO, J., SALVADOR, M. L. (1995). Kinetics and modeling of gas formation in the thermal decomposition of powdery cellulose and pine sawdust. Industrial & Engineering Chemistry Research, 34:3, 786-793.

BILODEAU, J.F. THÉRIEN N., PROULX, P. CZERNIK S., CHORNET, E. (1993). A mathematical model of fluidized bed biomass gasification. The Canadian Journal of Chemical Engineering, 71, 549-557.

BLANCO LOPEZ, M.C., BLANCO, C.J., MARTINEZ-ALONSO, A., TASCON, J.M.D. (2002). Composition of gases released during olive stone pyrolysis. Journal of Analytical and Applied Pyrolysis, 65, 313-322.

BOROSON, M.L., HOWARD, J. B., LONGWELL, J.P., PETERS, W.A. (1989). Product yields and kinetics from the vapor phase cracking of wood pyrolysis tar. AIChE J., 35:1, 120-128.

BRADBURY, A., SAKAI, Y., SHAFIZADEH, F. (1979). Kinetic model for pyrolysis of cellulose. Journal of Applied Polymer Science, 23, 3271-3280.

BRANCA, C., Di BLASI, C. (2003). Kinetics of the isothermal degradation of wood in the temperature range 528-708 K. Journal of Analytical and Applied Pyrolysis, 67:2, 207-219.

BRYDEN, K.M., RAGLAND K. (1996). Numerical modeling of deep, fixed bed combustor. Energy & Fuel, 10, 269.

CABALLERO, M., AZNAR, M.P., GIL, J., MARTIN, J.A. (1997). Commercial steam reforming catalysts to improve biomass gasification with steam oxygen mixtures 1. hot gas upgrading by the catalyst reactor. Industrial & Engineering Chemistry Research. 36. 5227-5239.

CABALLERO, M., CORELLA, J., AZNAR, M.P., GIL, J. (2000). Biomass gasification with air in fluidized bed. Hot gas cleanup with selected commercial and full-size Nickle-based catalyst. Industrial & Engineering Chemistry Research. 39. 1143-1154.

CASSANELLO, M., LARACHI, F., GUY, C., CHAOUKI, J. (1996). Solids mixing in gas-liquid-solid fluidized beds: experiments and modeling. Chemical Engineering. Science, 51:10. 2011-2020.

CHANG, W.R., KELBON, M., KRIEGER-BROCKETT, B. (1988). Single-particle biomass pyrolysis: correlations of reaction products with process conditions. Industrial & Engineering Chemistry Research, 27:12, 2261-2275.

CHAUDHARI, S.T., BEJ, S.K., BAKHSHI, N.N., DALAI, A. K. (2001). Steam gasification of biomass-derived char for the production of carbon monoxide-rich synthesis Gas. Energy & Fuel, 15, 736-742.

CHAOUDHARI, S.T., DALAI, A.K., BAKHSHI, N.N. (2003). Production of hydrogen and or syngas (H_2 + CO) via steam gasification of biomass derived chars. Energy & Fuels. 17. 1062-1067.

CHIBA, T., KOBAYASHI, H. (1977). Solid Exchange between the bubble wake and the emulsion phase in a gas-fluidized bed. Journal of chemical engineering of Japan, 10: 3, 206-210.

CIFERNO, J.P., MARANO, J.J. (2002). Benchmarking biomass gasification technologies for fuels, chemicals and hydrogen production. U.S. Department of energy national energy technology laboratory.

CORELLA, J., SANZ, A. (2005). Modeling circulating fluidized bed biomass gasifiers. A pseudo-rigorous model for stationary state. Fuel processing technology, 86, 1021-1053.

CORELLA, J., TOLEDO, J.M., PADILLA, R. (2005). Catalytic hot gas cleaning with monoliths in biomass gasification in fluidized beds 1. their effectiveness for tar elimination . Industrial & Engineering Chemistry Research, 43, 2433-2445

CORELLA, J., ORIO, A., AZNAR, M.P. (1998). Biomass Gasification with air in a fluidized bed: reforming of the gas composition with commercial steam reforming catalysts. Industrial & Engineering Chemistry Research. 37. 4617-4624.

CORELLA, J., AZNAR, M.P., GILL, J., CABALLERO, M. (1999). Biomass Gasification in Fluidized Bed: Where to locate the Dolomite to Improve Gasification? Energy & Fuel, 13, 1122-1127.

CORELLA, J. HERGUIDO, J. ALDAY, F.J. (1988). Pyrolysis and steam gasification of biomass in fluidized beds: influence of the type and location of the biomass feeding point on the product distribution. In: Research in thermochemical biomass conversion. BRIDGWATER, A.V, KUESTER, J. L.; Editor Elsevier Applied Science: Ondaon. 384.

CORELLA, J., M.P. AZNAR, J. DELGADO, ALDEA, E. (1991). Steam gasification of cellulosic wastes in a fluidized bed with downstream vessels. Industrial & Engineering Chemistry Research, 30, 2252-2262.

COURBARIAUX, Y. (2004). Étude et mis au point d'un procédé de traitment des brasques de l'industrie de l'aluminium. Thèse de Doctorat, École polytechnique de Montréal, Canada.

COZZANI, V., NICOLELLA, C., PETARCA, L., ROVATTI, M., TOGNOTTI, L., (1995). A Fundamental study on Conventional Pyrolysis of a Refused-Derived Fuel. Industrial & Engineering Chemistry Research, 34, 2006-2020.

COZZANI, V., LUCCHESI, A., STOPPATO, G., MASCHIO, G. (1997). A new method to determine the composition of biomass by thermogravimetric analysis. The Canadian journal of chemical engineering, 75, 127-133.

CUI, H.; CHAOUKI, J. (2004). Effects of temperature on local two-phase flow structure in bubbling and turbulent fluidized beds of FCC particles. Chemical Engineering Science, 59:16, 3413-3422.

CUI, H.; SAURIOL, P., CHAOUKI, J. (2003). High temperature fluidized bed reactor: measurements, hydrodynamics and simulation. Chemical Engineering Science. 58. 3413-3422.

DAVIDSON, J.F and HARRISON, D. (1963). Fluidized particles. Cambridge University Press. New York.

DELGADO, J., AZNAR, M.P., CORELLA, J. (1996). Calcined Dolomite, magnetite, and calcite for cleaning hot gas from a fluidized bed biomass gasifier with steam: life and usefulness. Industrial & Engineering Chemistry Research, 35, 3637-3643.

DE SOUZA-SANTOS, M.L. (1989). Comprehensive Modeling and Simulation of Fluidized Bed Boilers and Gasifiers. Fuel, 68, 1507-1521.

DECHSIRI, C., GHIONE, A., VAN de WIEL, F., DEHLING, H.G., PAANS, A.M.J., HOFFMANN, A.C. (2005). Positron Emission Tomography applied to fluidization engineering. The Canadian journal of chemical engineering, 83, 88-96.

DECHSIRI, C., VAN DER ZWAN, A., DEHLING, H.G., HOFFMANN, A.C. (2005). Dispersion of particle pulses in a fluidized beds measured by positron emission tomography. AIChE. J., 51:3. 791-801.

DI BLASI, C. (1996a). Kinetic and heat transfer control in the slow and flash pyrolysis of solid. Industrial & Engineering Chemistry Research, 35, 37-46.

DI BLASI, C. (1996b). Heat, Momentum and Mass Transfer Through a Shrinking Biomass Particle Exposed to Thermal Radiation. Chemical Engineering Science, 51:7, 1121-1132.

DI BLASI, C. (1997). Influence of Physical Properties on Biomass Devoletalization Characteristics. Fuel, 76:10, 975-964.

DI BLASI, C. (1998). Comparison of semi-global mechanisms for primary pyrolysis of lignocellulosic. Journal of Analytical and Applied Pyrolysis, 47:1, 43-64.

DI BLASI, C. (2000). Modeling of fast pyrolysis of cellulosic particles in fluid-bed reactor. Chemical Engineering Science, 55, 5999-6013.

DI BLASI, C., BRANCA, C. (2001). Kinetics of primary product formation from wood pyrolysis. Industrial and Engineering Chemistry Research, 40:23, 5547-5556.

DI BLASI, C. (2002). Modeling extra and intera-particle processes of wood fast pyrolysis. AIChE J., 48:10, 2386-2397.

DI BLASI, C., BRANCA, C. (2003). Temperature of wood particles in a hot sand bed fluidized by nitrogen. Energy & Fuel, 17, 247-254.

DI BLASI, C. (2004). Modeling wood gasification in a countercurrent fixed-bed reactor. AIChE. J., 50:9, 2306-2319.

DI FELICE, R., COPPOLA, G., RAPAGNA, S., JAAND, N. (1999). Modeling of biomass devolatilization in a fluidized bed reactor. The Canadian Journal of Chemical Engineering. 77, 325-332.

DOUBLE, J.M., SMITH E.L., Bridgwater A.V. (1989). Computer Modleing of Fluidized Bed Gasifier. Process and Gasification, ed. G.L. Ferrero, K. Maniatis, and A. Buekens.: Elsevier Applied Science. 651-655.

EIDE, L.I, ANHEDEN, M., LYNGFELT, A., ABANADES, C., YOUNES, M., CLODIC, D., BILL, A.A., FERON, P.H.M., ROJEY, A., GIROUDIÉRE, F. (2005). Novel capture processes oil and gas science and technology. Oil and gas science and technology Rev. IFP, 60, 497-508.

ENCINAR, J.M., GONZALEZ, J.F., GONZALEZ, J. (2000). Fixed bed pyrolysis of cynara cardunculus L. Product yields and compositions. Fuel processing technology. 68. 209-222.

FANG, Y., HUANG, J., WANG, Y., ZHANG, B. (2001). Experimental and Mathematical Modeling of a Bench-Scale Circulating Fluidized bed Gasifier. Fuel Processing Technology. 69. 29-44.

FIASCHI, D., MICHELINI, M. (2001). A two-phase one-dimensional biomass gasification kinetic model. Biomass and Bioenergy, 21, 12-132.

FORMISANI, B., GIRIMONTE, R., PATARO, G. (2002). The influence of operating temperature on the dense phase properties of bubbling fluidized beds of solids. Powder Technology, 125:1, 28-38.

GELDART, D., KAPOOR, D.S. (1976). Bubble sizes in a fluidized bed at elevated temperatures. Chemical Engineering Science, 31, 842-843.

GEYER, W.A., DEWYKE, J., WALWENDER W.P. (2000). Biomass and gasification properties of young populus clones. Wood and Fiber Science, 32 :2, 375-384.

GIL, J., CORELLA, J. AZNAR, M.P., CABALLERO, M.A. (1999). Biomass gasification in atmospheric and bubbling fluidized bed: effect of the type of gasification agent on the product distribution. Biomass and Bioenergy, 17, 389-403.

GONZALEZ J.F., ENCINAR J.M., CANITO, J.L., SABIO, E., CHACON M. J. (2003). Pyrolysis of cherry stones: Energy uses of the different fractions and kinetic study. Journal of Analytical and Applied Pyrolysis, 67:1, 165-190.

GONZALEZ, J. F., RAMIRO, A., GONZALEZ-GARCIA, C. M., GANAN, J., ENCINAR, J. M., SABIO, E., RUBIALES, J. (2005). Pyrolysis of Almond Shells. Energy Applications of Fractions. Industrial & Engineering Chemistry Research. 44:9. 3003-3012.

GRACE, J.R. (1982). In Handbook of multiphase systems. G. HETSRONI. Hemisphere. Washington.

GRANITE, E.J., O'BRIEN, T. (2005). Review of novel methods for Carbon dioxide separation from flue and fuel gases. Fuel Processing Technology, 86, 1423-1434.

GRASA, G., ABANADES, J. C. (2002). The use of two different models to describe the axial mixing of solids in fluidized beds. Chemical Engineering Science, 57:14, 2791-2798.

GRONLI, M.G., VARHEGYI, G., DI BLASI, C. (2002). Thermogravimetric analysis and devolatilization kinetics of wood. Industrial & Engineering Chemistry Research, 41:17, 4201-4208.

GRONLI, M., ANTAL, M. J. J., VARHEGYI, G. (1999). Round-robin study of cellulose pyrolysis kinetics by thermogravimetry. Industrial & Engineering Chemistry Research, 38:6, 2238-2244.

HAJALIGOL, M. R., HOWARD, J. B., LONGWELL, J. P., PETERS, W. A. (1982). Product compositions and kinetics for rapid pyrolysis of cellulose. Industrial & Engineering Chemistry Process design and development, 21:3, 457-465.

HAMEL, S., WOLFGANG, K. (2001). Mathematical modeling and simulation of bubbling fluidized bed gasifiers. Powder Technology, 120, 105-112.

HATATE, Y., OHMAGARI, K. IKARI, A., KONDO, K., KING, D.F. (1988). Behavior of bubbles in a cylindrical fluidized bed at an elevated temperature. Journal of chemical engineering of Japan, 21, 424-425.

HERGUIDO, J., CORELLA J., GONZALEZ-SAIZ, J. (1992). Steam gasification of Lignocellulosic residues in a fluidized bed at a small pilot scale. Effect of the type of the feedstock. Industrial & Engineering Chemistry Research, 31, 1274-1282.

HOFFMANN, A.C., JANSSEN, P. B. M., PRINS, J. (1993). Particle Segregation in fluidized binary mixtures. Chemical Engineering Science, 48:9, 1583-1993.

HOVELAND, D.A., WALAWENDER, W.P., FAN, L.T. (1985). Steam gasification of pure cellulose. 2. Elevated freeboard temperature. Industrial & Engineering Chemistry Process Design and Development, 24, 818-821.

HULL, A. S., CHEN, Z., FRITZ, J. W., AGRAWAL, P. K. (1999). Influence of horizontal tube banks on the behavior of bubbling fluidized beds. 1. Bubble hydrodynamics. Powder Technology, 103:3, 230-242.

KAI, T., FURUSAKI, S. (1985). Behavior of fluidized beds of small particles at elevated temperatures. Journal of chemical engineering of Japan, 18, 113-118.

KNOWLTON, T.M. (1998). Pressure and temperature effects in fluid-particle systems in fluidization, solids handling and processing, industrial application. Chapter 2, Edited by WEN-CHING YANG, Noyes Publications USA,.

KOCATULUM, B., BASESME, E. A., LEYV, E. K., KOZANOGLU, B. (1991). Particle motion in the wake of a bubble in a gas-fluidized bed, Annual Meeting of the American Institute of Chemical Engineers, Nov 17-22. 1991. Los Angeles, CA, USA, 40-50.

KOOUFOPANOS, C. A., MASHIO, G., LUCCHESI, A. (1989). Kinetic modeling of pyrolysis of biomass and biomass components. Canadian Journal of Chemical Engineering, 67:1. 75-84.

KOUFOPANOUS, C.A., PAPAYANNAKOS, N., MASCHIO G., LUCCHESI, A. (1991). Modeling of the pyrolysis of biomass particles, studies on kinetic, thermal and heat transfer effect Canadian Journal of chemical engineering. 69. 907-915

KUNII, D., LEVENSPIEL, O., (1991). Fluidization Engineering. 2nd ed. MA, Butterworth-Heinemann series in chemical engineering.

LAKSHMANAN, C. C.; POTTER, O. E. (1990). Numerical simulation of the dynamics of solids mixing in fluidized beds. Chemical Engineering Science, 45:2, 519-528.

LARACHI, F., CHAOUKI, J., KENNEDY, G. (1995). 3-D Mapping of solids flow fields in multiphase reactor with RPT. AIChE J., 41, 439-443.

LARACHAI, F.; GRANDJEAN, B. P. A.; CHAOUKI, J. (2003). Mixing and circulation of solids in spouted beds: Particle tracking and Monte Carlo emulation of the gross flow pattern. Chemical. Engineering. Science, 58:8, 1497-1507.

LETTIERI, P., NEWTON, D., YATES, J.G. (2001). High temperature effects on the dense phase properties of gas fluidized beds. Powder Technology, 120, 34-40.

LETTIERI P., NEWTON, D., YATES, J.G. (2000). The influence of interparticle forces on fluidization behavior of some industrial materials at high temperature. Powder Technology, 110, 117-127.

LEVENSPIEL, O. (2005). What will come after petroleum. Industrial & Engineering Chemistry Research, 44, 5073-5078.

LI, X., GRACE, J.R., LIM, C.J, WATKINSON, A.P., CHEN, H.P., KIM, J.R. (2004). Biomass gasification in a circulating fluidized bed. Biomass and Bioenergy, 26, 171-193.

LI, X., GRACE, J.R., WATKINSON, P., LIM, C.J., ERGUDENLER, A. (2001). Equilibrium Modeling of Gasification: a Free Energy Minimization Approach and its Application to a Circulating Fluidized Bed Coal Gasifier. Fuel, 80, 195-207.

LIANG, XT., KOZISKI, J.A. (2000). Numerical modeling of combustion and pyrolysis of cellulose biomass in thermogravimetric system. Fuel, 79, 1477-1486.

LIDEN, A.G., BERRUTI, F., SCOTT. D.S. (1988). A kinetic model fro product of liquids from the flash pyrolysis of biomass. Chemical Engineering Communications, 65, 207-221.

LIM, K. S., GURURAJAN, V. S., AGARWAL, P. K. (1993). Mixing of homogenous solids in bubbling fluidized beds: theoretical modeling and experimental investigation using digital image analysis. Chemical Engineering. Science, 48:12, 2251-2265.

LIM, K. S., ZHU, J. X., GRACE, J. R. (1995). Hydrodynamics of gas-solid fluidization, International Journal of Multiphase Flow, 21(Suppl). 141-193.

LINJEWILE, T.M. (1993). Temperature of burning carbonaceous particles in a fluidized bed combustor. Thesis (PhD). The University of Adelaide.

LLOP, M., CSAL, J. ARNALDOS, J. (2000). Expansion of gas-solid fluidized beds at pressure and high temperature. Powder Technology, 107, 212-225.

MANSARAY, K.G., AL-TAWEEL, A.M., GHALY, A.E., HAMDULLAHPOUR, F., UGURSAL, V.I. (2000). Mathematical modeling of a fluidized bed Rice Husk gasifier: Part I -model development. Energy Sources, 22, 83-98.

MANSARAY, K.G., GHALY, A.E., AL-TAWEEL, A.M., HAMDULLAHPUR, F., UGURSAL, V.I. (1999). Air gasification of rice husk in a dual distributor type fluidized bed gasifier. Biomass and Bioenergy, 17, 315-332.

May, W.G. (1959). Fluidized bed reactor studies. Chemical Engineering Progress, 55:12. 49-56.

MANIATIS, K., MILLICH, E. (1998). Energy from biomass and waste: the contribution of utility scale biomass gasification plants. Biomass and Bioenergy, 15:3, 195-200.

MCLENDON, T.R., LUI, A.P., PINEAULT, R.L., BEER, S.K., RICHARDSON, S.W. (2004). High-pressure co-gasification of coal and biomass in a fluidized bed. Biomass and Bioenergy, 26. 377-388.

MESZAROS, E., VARHEGYI, G., JAKAB, E., MAROSVOLGYI, B. (2004). Thermogravimetric and reaction kinetic analysis of biomass samples from an energy plantation. Energy & Fuels, 18:2, 497-507.

MII, T.,YOUSHIDA, K., KUNII, D. (1973). Temperature effect on characteristics of fluidized beds. Journal of chemical engineering of Japan, 6, 100-102.

MILLER, R.S., BELLAN, J. (1997). A generalized biomass pyrolysis model based on superimposed cellulose, hemicellulose and lignin kinetics. Combustion Science & Technology, 176, 97-137.

MORI, S., WEN, C. Y. (1975). Estimation of bubble diameter in gaseous fluidized beds. AIChE. J., 21:1, 109-115.

MOSTOUFI, N., CHAOUKI, J. (2004). Flow structure of the solids in gas-fluidized beds. Chemical Engineering Science, 59, 4217-4227.

MOSTOUFI, N., CHAOUKI, J. (2000). On the axial movement of solids in gas-solid fluidized beds Source. Chemical Engineering Research and Design, Transactions of the Institute of Chemical Engineers, Part A. 78:6, 911-920.

MOSTOUFI, N., CHAOUKI, J. (2001). Local solid mixing in gas-solid fluidized beds. Powder Technology, 114:1-3, 23-31.

NARVAEZ, I., ORIO, A., AZNAR, M.P., CORELLA, J. (1996). Biomass gasification with air in an atmospheric bubbling fluidized bed. Effect of six operational variables on the quality of the produced raw gas. Industrial & Engineering Chemistry. Research, 35, 2110-2120.

NARVAEZ, I., CORELLA, J., ORIO, A. (1997). Fresh tar (from a biomass gasifier) elimination over a commercial steam-reforming catalyst, kinetics and effect of different variables of operation. Industrial & Engineering Chemistry Research, 36, 317-327.

NUNN, T.R., HOWARD, J.B., LONGWELL, J.P., PETERS, W.A. (1985). Product Compositions and Kinetics in the Rapid Pyrolysis of Sweet Gum Hardwood. Industrial and Engineering Chemistry Process Design & Development, 24, 836-844.

ORFAO, J. J. M.; ANTUNES, F. J. A.; FIGUEIREDO, J. L. (1999). Pyrolysis kinetics of lignocellulosic materials - three independent reactions model. Fuel, 78:3, 349-358.

OLIVARES, A., AZNAR, M.P., CABALLERO, M.A., GIL, J., FRANCÉS, E., CORELLA, J. (1997). Biomass Gasification: Produced Gas Upgrading by in-Bed Use of Dolomite. Industrial & Engineering Chemistry Research, 36:12, 5220-5226.

PAISLEY, M.A., LITT, R.D. CREAMER, K.S. (1990). Gasification of Refused-Derived Fuel in a High Throughput Gasification System. Energy From Biomass and Wastes: Columbus, Ohio.

PANIGRAHI, S., DALAI, A.K., CHAUDHARI, S.T., BAKHSHI, N.N. (2003). Synthesis gas production from steam gasification of biomass-derived oil. Energy & Fuels, 17, 637-642.

PADBAN , N., WANG, W., YE, Z., BJERLE, I, ODENBRAND, I. (2000). Tar formation in pressurized fluidized bed air gasification of woody biomass. Energy & Fuel, 14, 603-611.

PARIKH, J., CHANNIWALA, S.A., GHOSAL, G.K. (2005). A correlation for calculating HHV from proximate analysis of solid fuels. Fuel, 84, 487-494.

PERRY, R.H. , CHILTON, C.H. (1973). Chemical engineer's handbook. 5th .edition Tokyo.

PYLE, D. L., ZAROR, C.A. (1984). Heat transfer and kinetics in the low temperature pyrolysis of solids. Chemical Engineering Science, 39:1, 147-158.

RADMANESH, R., CHAOUKI, J., GUY, C. (2005a). A unified lumped approach in kinetic modeling of biomass pyrolysis. Accepted in Fuel. .

RADMANESH, R., MABROUK, R., CHAOUKI, J., Guy C. (2005b). The effect of temperature on solids mixing in a bubbling fluidized bed reactor. International journal of chemical reactor engineering, 3, A16, http://www.bepress.com/ijcre/vol3/A16/..

RADMANESH R., CHAOUKI, J., GUY, C. (2005c, July). Modeling biomass pyrolysis in a bubbling fluidized bed reactor. 7th World Congress of Chemical Engineering, Glasgow, Scotland, Sustainable and Clean Technologies - Alternative Fuels.

RAPAGNA, S., JAND, N., KIENNEMANN, A., FOSCOLO, P.U. (2000). Steam-gasification of biomass in a fluidized-bed of olivine particles. Biomass and Bioenergy. 19. 187-197.

REINA, J., VELO, E.; PUIGJANER, L. (1998). Kinetic study of the pyrolysis of waste wood. Industrial & Engineering Chemistry Research, 37:11, 4290-4295.

ROSS, D.P., HEIDENREICH, C.A., ZHANG, D.K. (2000). Devolatilization times of coal particles in a fluidized bed. Fuel. 79. 873-883.

ROTH, J., STEINER, G., WOLFINGER, M.G., STAUDINGER, G. (2002). Tar cracking from fast pyrolysis of large beech wood particles. J. Analytical and Applied Pyrolysis, 62:1, 83-92.

RUGGIERO, M., MANFRIDA, G. (1999). An equilibrium model for biomass gasification process. Renewable Energy, 16, 1106-1109.

SADAKA, S.S., GHALY, A.E., SABBAH, M.A. (2002). Two Phase Biomass Air-Steam Gasification Model for Fluidized Bed Reactors: Part I-Model Development. Biomass and Bioenergy, 22, 439-462.

SETT, A., BHATTACHARAYA, S.C. (1988). Mathematical modeling of a fluidized bed charcoal gasifier. Applied Energy, 30:3, 161-186.

SHAFIZADEH, F., CHIN, P.P.S. (1977). Thermal deterioration of wood. ACS symposium series, 43, 57-81.

SHEN, L., ZHANG, M. (1998). Effect of particle size on solids mixing in bubbling fluidized beds. Powder Technology, 97:2, 170-177.

SHIN, D., CHOI, S. (2000). Combustion of simulated waste particles in a fixed bed. Combustion & Flame, 121:1, 167-180.

SIMMONS, G., GENTRY, M. (1986). Kinetic formation of CO CO_2 H_2 and light hydrocarbon gases from cellulose pyrolysis. Journal of Analytical and Applied Pyrolysis, 10. 129-138.

SITNAI, O. (1981). Solids mixing in a fluidized bed with horizontal tubes. Industrial & Engineering Chemistry Process Design & Development, 20:3, 533-538.

SORUM L., GRONLI, M.G., HUSTAD, J.E. (2001). Pyrolysis characteristic and kinetic of municipal solid wastes. Fuel, 80:9, 1217-1227.

STEIN M., DING, Y.L. SEVILLE, J.P.K., PARKER, D.J. (2000). Solids motion in bubbling gas fluidized beds. Chemical Engineering Science, 55, 5291-5300.

STEIN, M., MARTIN, T.W., SEVILLE, J.P.K., MC NEIL, P.A., PARKER, D.J. (1997). Positron emission particle tracking: particle velocities in gas fluidized beds, mixers and other applications. In Non-invasive monitoring of multiphase flows, CHAOUKI, J., LARACHI, F., DUCUKOVIC, M.P. Elsevier. Chapter 10. 309-333.

STEIN, M., DING, Y. L., SEVILLE, J. P. K., PARKER, D. J. (2000). Solids motion in bubbling gas fluidized beds. Chemical Engineering. Science, 55:22, 5291-5300.

SUUBERG, E.M., PETERS, W.A., HOWARD, J.B. (1978). Product composition and kinetics of lignite pyrolysis. Industrial & Engineering Chemistry Process Design and Development, 17:1, 37.

TENG, H., WEI, Y.-C. (1998). Thermogravimetric studies on the kinetics of rice hull pyrolysis and the influence of water treatment. Industrial & Engineering Chemistry Research, 37:10, 3806-3811.

THURNER, F., MANN, U. (1978). Kinetic investigation of wood pyrolysis. Industrial & Engineering Chemistry Process Design & Development, 17, 37.

VAMVUKA, D., KAKARAS, E., KASTANAKI, E., GRAMMELIS, P. (2003). Pyrolysis characteristics and kinetics of biomass residuals mixtures with lignite. Fuel, 82:(15-17), 1949-1960.

VAN DEEMTER, J. J. (1967). The countercurrent flow model of a gas-solids fluidized bed. in proceeding of international symposium on fluidization. Netherland university press, Amsterdam.

VAN DEN ARSEN F.G., BEENACKERS, A.C.M., VAN SWAAIJ, W. P. M. (1982). Wood pyrolysis and carbon dioxide char gasification in a fluidized bed. In: fundamentals of thermochemical biomass conversion, Elsevier applied science publisher, 691.

VAN DER DRIFT, A., VAN DOORN, J., VERMEULEN, J.W. (2001). Ten Residual Biomass Fuels for Circulating Fluidized Bed Gasification. Biomass and Bioenergy, 20, 45-56.

VARHEGYI, G., ANTAL, M. J. J., JAKAB, E., SZABO, P. (1997). Kinetic modeling of biomass pyrolysis. Journal of Analytical and Applied Pyrolysis, 42:1, 73-87.

VARHEGYI, G., ANTAL, M. J. J., SZEKELY, T., SZABO, P. (1989). Kinetics of the thermal decomposition of cellulose, hemicellulose, and sugar cane bagasse. Energy & Fuels, 3:3, 329-335.

VARMA, A., DIAKOV, V., SHAFIRVICH, E. (2005). Heterogeneous combustion: recent developments and new opportunities for chemical engineers. AIChE J., 51, 2876-2884.

VRIESMAN, P., HEGINUZ, E., SJOSTROM, K. (2000). Biomass gasification in laboratory-scale AFBG: influence of the location of the feeding pint on the fuel-N conversion. Fuel, 79, 1371-1378.

WALAWENDER, W.P., HOVELAND, D.A., FAN, L.T. (1985). Steam gasification of pure cellulose. 1. Uniform temperature profile. Industrial & Engineering Chemistry Research, 24. 813-817.

WANG, T., CHANG, J., LV, P. (2005). Novel catalyst for cracking of biomass tar. Energy & Fuels, 19, 22-27.

WURZENBERGER, J.C, WALLNER, S., RAUPENSTRAUCH, H., KHINAST, J.G, (2002). Thermal conversion of biomass: comprehensive reactor and particle modeling. AIChE J, 48:10, 2398-2411.

YATES, J. G. (1983). Fundamentals of fluidized-bed chemical processes. London: Butterworths.

YOSHIDA, K., KUNII, D. (1968). Stimulus and response of gas concentration in bubbling fluidized beds. Journal of Chemical Engineering of Japan, 1:1, 11.

YOSHIDA, K., FUJII S., KUNII, D. (1975). Characteristics of fluidized beds at high temperatures. In Fluidization Technology, KEAIRNS, D.L., Vol. 1, McGraw-Hill international book company, 43-48.

ZANZII, R.; SJOSTROM, K., BJORNBOM, E. (2002). Rapid pyrolysis of agricultural residues at high temperature. Biomass & Bioenergy, 23, 357-366.

APPENDIX A

Modeling of Biomass Pyrolysis in a Bubbling Fluidized Bed Reactor

Ramin Radmanesh, Jamal Chaouki, Christophe Guy
Dpt. Of Chemical Engineering, Ecole Polytechnique
PO Box 6079, St. CV, Montreal, Qc, Canada H3C 3A7
jamal.chaouki@polymtl.ca

Presented in 7th World Congress of Chemical Engineering

Abstract

A model is presented to develop mechanisms of fluidized bed wood pyrolysis and to predict the final gas composition in a fluidized bed reactor. As part of it, temperature response of wood particles and heat transfer were built on literature survey and pyrolysis kinetic was determined using the thermogravimetry-gas chromatography (TGA-GC) technique. Apart from pyrolysis, the water-gas shift reaction and tar cracking are also considered in the modeling of free board zone of the fluidized bed reactor. The model predictions reasonably follows the trend of gas concentration of the experimental results between 370-620°C in the bed and 500-600°C in the freeboard. The experimental works and the modeling result show the importance of the freeboard area of the fluidized bed reactor for the cracking of the tar.

A.1 Introduction

Pyrolysis is an important stage in the gasification and combustion of solid fuels. It has a strong impact on the final product gas composition and consequently the heating value of the resulting gas in gasification. It is even a more crucial stage for biomass materials such as wood and agricultural wastes, where the volatile content is considerably higher than other solid fuels. Thus, a suitable kinetic model of the pyrolysis is a key part for the overall modeling attempts of gasifiers and combustors. In this study, a Thermogravimetry analysis (TGA) was used to model the total devolatilization of biomass whereas a gas chromatography (GC) served to determine different kinetics of gas releases. The developed kinetic models were then applied to predict the final gas composition using the modeling of tar cracking in the freeboard of a fluidized bed reactor.

A.2. Model

Solid fuels are subject to pyrolysis upon entering the fluidized bed reactor. The products of pyrolysis are char, volatiles and ash. The volatile gases then travel through the freeboard while char and ash particles disperse into the bed. Some fine char particles also entrain into the freeboard zone. The gas products from primary pyrolysis are then subject to further reactions in the gas-solid phases. The main reactions in the reactor below 700^{o}C are thermal cracking of the tar or secondary pyrolysis and the water-gas shift reaction. Apart from the pyrolysis kinetic model, the temperature response of the wood particles is also needed to calculate the final yield of different

gases. The heating rate of the particle or its response to the temperature depends on the bed temperature, heat transfer coefficient in the bed and also physical properties of wood particles (Di Blasi and Branca, 2003, Ross *et al.*, 2000). Therefore, the pyrolysis kinetic model should be solved along with an energy balance for a single particle to calculate the final yield and composition of the gases resulting from pyrolysis.

In the free board, flows and reactions of gases were expressed using a subsequent arithmetic model. The boundary conditions for this freeboard model, which are the concentrations of different gases from pyrolysis in the bed, are provided by the pyrolysis kinetics.

A.2.1 Freeboard

A plug flow model is considered to describe mathematically the flow of the gases in the freeboard. As mentioned before, the reactions which are important and should be taken into account are tar cracking and water gas shift reactions. The mass balance for each species in this region is given by the following differential equations:

tar:

$$\frac{d(u\rho_{tar,g})}{dZ} = r_{tar}(X_{tar}\rho_g) \tag{A.1}$$

gases:

$$\frac{d(u\rho_{i,g})}{dZ} = r_{tar}\upsilon_i(X_{tar}\rho_g) + M_i r_{w-g} \tag{A.2}$$

N_2:

$$\frac{d(u\rho_{i,g})}{dZ} = 0 \tag{A.3}$$

Where, X_{tar} is the mass fraction of the tar in the gas stream, ρ_{tar} and ρ_i are the density of the tar and gas species, v_i is the stoichiometric coefficient for the tar cracking reaction as shown in Equation (A.14), r_{tar} and $r_{w\text{-}g}$ are the rate of the tar cracking and water gas shift reaction and u is the velocity of the gas stream in the freeboard.

A.2.2 Energy balance for a single wood particle

An energy balance is needed to calculate the temperature response of the wood particles when they are fed to the reactor. When the solid wood particles enter the hot bed of sand particles they are subject to fast pyrolysis. The rate of the temperature increase in the wood particles is essential in calculating the final yield of different gases. Internal and external heat transfers take place at this point. However, for the small wood particles the internal heat transfer resistance is negligible (Shin and Choi, 2000, Van Den Aarsen *et al.,* 1982). Thus, the heat balance for a single particle can be written as follows:

$$\rho_p C_p V_p \frac{dT}{dt} = h_{conv} A\left(T_b - T_p\right) + \sigma_{rad} \varepsilon_{rad} A\left(T_b^4 - T_p^4\right) \tag{A.4}$$

The convection heat transfer coefficient is calculated by the Ranz-Marshall correlation reported by Kunii and Levenspiel (1991):

$$\frac{h_{conv} d_p}{k_g} = 2 + 0.6\,\mathrm{Re}^{1/2}\,\mathrm{Pr}^{1/3} \tag{A.5}$$

The effective emissivity in the condition of fluidized bed is calculated according to correlation developed by Linjewile (1993):

$$\varepsilon_{rad} = \frac{1}{\varepsilon_p} + \frac{1}{\phi\left(\frac{1}{\varepsilon_{fb}} - 1\right)}, \phi = \left(1 + n_p \frac{d_i}{d_a}\right)^2 \tag{A.6}$$

Table A-1: Parameters used for energy balance

Parameter	Value	Reference
Wood Specific Heat	C_p=1112.0+4.85(T-273), J/kg K	Koufopanous *et al* 1991
Density of the Wood	360, kg/m^3	Di Blasi 2004
ε_p for wood particles	0.95	Babu and Chaurasia 2004
Effective Emissivity, ε_{fb}	0.8	Linjewile 1993
Parameter in the Equation (A.6) n_p	5	Linjewile 1993
Stephan Boltzmann Constant, σ	5.67×10^{-8} W/m^2 K^4	

Table A-2: Wood particle properties

Proximate Analysis	**Wt %**
Char	16.90
Volatile	80.34
Ash	2.70
Ultimate Analysis	
C	48.2
H	6.4
O	45.2
N	0.14
Wood Particle Size, d_a	1-2 mm

where, ε_p is the emissivity, ε_{fb} is the effective emissivity of the fluidized bed, d_i and d_a are the diameters of the inert and active particles. Table A-1 shows the parameters use in energy balance. The physical properties of the bed and wood particles are tabulated in Table A-2. The density of wood particles changes during the course of pyrolysis. The change in the density was assumed to be proportional to the loss of the volatile matter in the particle which is defined according to:

$$\rho(t) = \rho_0 \left(1 - \frac{V(t)}{V^*} X_{vm}\right) \tag{A.7}$$

where, X_{vm} is the volatile matter of the wood particles.

A.3 Kinetic

A.3.1 Total volatile release in primary pyrolysis

Different models have been proposed in the literature for the pyrolysis of wood. They range from empirical models to more sophisticated kinetic models based on underlying physicochemical process. The first approach, although less fundamental, is extremely useful in predicting the overall yield of devolatilization. A first order single step kinetic model has manifested a good prediction in modeling cellulose pyrolysis (Antal *et al* 1995). The wood consists of three components i.e. cellulose, hemicellulose and lignin. Accordingly, a first order single step kinetic model for each component has been proven to predict the total devolatilization rate satisfactorily (Gronli *et al.,* 2002). For each component a first order kinetic can be written:

$$\frac{d(Vi/V_i^*)}{dt} = k_{01i} \exp\left(-\frac{E_{1,i}}{RT_p}\right)\left(1 - \frac{Vi}{V_i^*}\right) \tag{A.8}$$

where V_i^* is the total amount of volatile matter for each component in the biomass. The total devolatilization is proportional to the contribution of each component:

$$\left(\frac{V}{V^*}\right)_{total} = \sum_{i=1}^{3} \alpha_i \times \left(\frac{V_i}{V_i^*}\right) \tag{A.9}$$

It is worth noting that in this model the sum of the contribution coefficient for the three components is equal to one ($\sum \alpha_i = 1$). This can be inferred from the fact that at t=∞ in the TGA experiments the ratio (V/V^*) must be equal to one.

This model was fitted to the TGA experimental work to obtain the best parameters which minimize the following objective function:

$$Obj = Min \sum \left(y_i^{cal} - y_i^{\exp}\right)^4 / N. \qquad (A.10)$$

Where, y_i^{cal} and $y_i^{\exp}$ are the total calculated and measured volatile yield, and N is the total number of data points in the TGA experiments. Table A-3 shows the kinetic parameters calculated for beech wood. The power 4 is chosen in the objective function instead of 2 to reduce the convergence time of the optimization calculations.

Table A-3: Total devolatilization parameters

components	Log(k_{0i}) 1/s	E_i (kJ/mol)	α_i
Cellulose	13.9	192	0.61
Hemicelloluse	10.21	133	0.28
Lignin	3.11	86	0.11

A.3.2 Evolution of individual volatile gases during primary pyrolysis

The experimental result of TGA can not be used alone to estimate the kinetic parameters for the evolution of different gases during the pyrolysis because the TGA experiments merely lead to total mass loss. However, a TGA linked to a gas chromatograph (GC) is can be used to measure the evolution of each gas species. The evolution of the four permanent gases (H_2, CH_4, CO and CO_2) was studied with this

system and the corresponding kinetic parameters were developed. A first order kinetic model was fitted to the experimental work. The model description for each gas is as follows:

$$\frac{dV_i}{dt} = k_i\left(V_i^* - V_i\right) \tag{A.11}$$

or after integration:

$$1 - yi = \frac{V_i^* - V_i}{V_i^*} = \exp\left(- \int_0^t k_{0i} \exp(-E_i / RT_P)dt \right), \tag{A.12}$$

where, V_i^* is the ultimate yield for a volatile matter available in the virgin biomass and V is the volatile matter which has been released. Tar and water are the other two major gas components released during the primary pyrolysis. Since the micro-GC used in this study could not detect the release of water, the results presented by Wurzenberger *et al.* (2002) was used for this component. Table A-4 shows the kinetic parameters calculated in this work and also the kinetic parameters for H_2O reported by Wurzenberger *et al.* (2002). It is worth mentioning that it was not possible to verify the complete mass balance closure due to difficulties in collecting the tar and detecting the water exiting from the TGA. In fact, the overall evolution rates of condensable vapors (tar and water) were calculated by subtracting the main gases evolution rates from the total devolatilization rate

Table A-4: Kinetic parameters for primary pyrolysis

No.	Component	Log(k_{01}) (1/s)	E_i(kJ/mol)	V^*_i(kg/kg biomass)
1	H_2	4.05	95	0.0065
2	CH_4	3.5	60	0.0064
3	CO	11.50	105	0.0383
4	CO_2	6	55	0.0972
5	H_2O	13.56	149	0.0480
6	Tar	12.0	113	0.6379

A.3.3 Tar cracking

Thermal cracking of the tar, known also as secondary pyrolysis after primary pyrolysis is another important step. Since more than 60% of the primary pyrolysis product accounts for the tar, this step has also an important impact on the accuracy of prediction of the final gas composition. The tar cracking mostly takes place in the homogeneous gas phase. Boroson *et al.* (1989) have studied homogeneous cracking of tar resulted from sweet gum hard wood. They developed a first order kinetic model. Their model was adopted by Roth *et al.* (2002) to calculate kinetic parameters for beech wood. This model is applied in this study (Wurzenberger *et al.*, 2002):

$$tar(gas) \longrightarrow \upsilon_{H2} H_2(g) + \upsilon_{CH4} CH_4(g) + \upsilon_{CO} CO(g) + \upsilon_{CO2} CO_2(g) + \upsilon_{tar} tar_{inert} \tag{A.13}$$

The stoichiometric coefficients (υ_i) are presented in Table A-5. The kinetic model as presented by Boroson *et al.* (1989) is as follows:

$$r_{cracking} = \upsilon_i 10^{4.98} \exp\left(-\frac{93}{RT}\right)(\rho_{tar}) \tag{A.14}$$

where ρ_{tar} is the density of the tar in the gas stream and υ_i is the stoichiometric coefficient as presented in the Table A-5.

Table A-5: Stoichiometric coefficients for tar cracking (Wurzenberger *et al.* 2002)

Component	υ_i
H_2	0.0173316
CH_4	0.0884052
CO	0.563316
CO_2	0.1109316
Secondary Tar	0.22

A.3.4 Water gas shift reaction

The water-gas shift reaction is considered to take place in the freeboard of the reactor:

$$CO + H_2O \leftrightarrow CO_2 + H_2 \tag{A.15}$$

The kinetics for this reaction was presented by Biba *et al.* (1978) and is used in this modeling:

$$r_{w-g} = 2.78\exp(-1513/T_g)\left(C_{CO}C_{H2O} - \frac{C_{CO2}C_{H2}}{KE}\right) \text{ mole/m}^3\text{.s}$$
$$KE = 0.02565\exp(3966/T_g) \tag{A.16}$$

A.4 Methodology

As mentioned before, the wood particles experience immediate pyrolysis upon entering to the bed. In order to determine gas compositions and yields of the main gases resulted from pyrolysis, Equation (A.4) for the wood particles' temperature response should be solved simultaneously with the kinetic modeling equations (see Equations (A.8), (A.9) and (A.12)). Pyrolysis stops when the maximum total devolatilization

$((V/V^*)_{total}=1)$ defined by Equation (A.9) is achieved. The concentrations or yields calculated from the pyrolysis stage serve as a set of boundary conditions in solving Equations (A.1) to (A.3) which lead to final gas compositions along the freeboard height of the reactor. The kinetic models in this part of reactor are tar cracking and the water-gas shift reaction defined by Equations (A.14) and (A.16).

A.5 Experimental

A.5.1 TGA/GC

A Mettler-Toledo thermobalance was hooked up to a Varian micro-GC to study the pyrolysis of biomass. Argon was used as the carrier gas in the TGA experiment. The exiting gases from TGA were sucked by the sampling pump of the GC. Ar, H_2, CH_4, CO and CO_2 were analyzed with the thermal conductivity detector of the GC. Molecular sieve and Porapak columns were used simultaneously to separate the resulting gases. The gas yield evolution was calculated by argon balance.

A.5.2 Bubbling fluidized bed reactor

A bubbling fluidized bed capable of withstanding high temperatures was designed to study biomass pyrolysis and gasification. The fluidized bed is 3 inches in

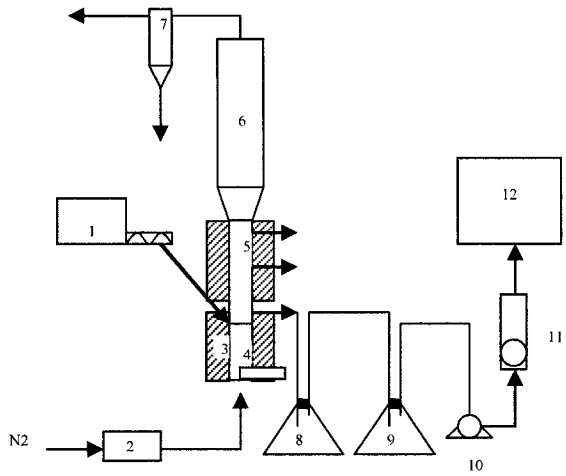

Figure A-1: Schematic presentation of bubbling fluidized bed reactor, 1-screw feeder, 2-preheater, 3-electrical heater around the bed and free board, 4- bed of sand particles, 5-freeboard, 6- Disengagement zone, 7-cyclone, 8, 9- gas impingers to trap solid and tar, 10-sampling pump, 11-rotamter, 12- GC

diameter, 20 inches in freeboard and 36 inches of disengagement zone. Figure A-1 presents a schematic of the reactor. The reactor consists of three heating zones. The temperature in each zone can be controlled separately. These zones include a preheating zone, where the fluidizing gas enters the reactor, a fluidized bed and a freeboard zone. Temperature of each zone is controlled and can be also monitored by means of several k-type thermocouples. Sampling ports in 5 different locations of the reactor have been installed. Gas sampling can be done via a suitable sampling train to separate the tar and solid from the gas. The clean gas then enters the GC. A rotameter is used in the sampling line to control the flow rate of the sampling gas. The beech wood particles are fed through a screw feeder to the reactor. The average feeding rate of the wood during the experiments was 2 g/min. The wood particles have essentially the same size as in the TGA/GC experiments. The feeding point is very close to the surface of the bed and thus the temperature at the feeding point is considered the same as the bed temperature. The flow rate of nitrogen is controlled by the rotameter. The superficial gas nitrogen is also controlled by a rotameter. The superficial gas velocity in the bed ranged from 0.13 m/s to 0.30 m/s depending on the temperature in the bed. The reactor was operated at different bed temperatures from 370 to 620°C. The temperature of the freeboard was kept different from the bed. In most experiments the temperature of the freeboard was 200°C higher than bed temperature with the maximum temperature of 600°C. The residence time of gases in the freeboard depends on freeboard temperatures and varies from 1 to 2 seconds.

A.5.3 Results and discussions

Figure A-2 presents the change in the total volatiles yield for the primary pyrolysis as a function of bed temperature. The result shows an increase in the total volatile yield by increasing the bed temperature. The same trend was observed in the TGA-GC experiments where the total volatiles yield increases with increasing heating rate in the thermo-balance. Figure A-3 shows the gas compositions of the permanent gases on a molar dry-tar-free basis from the sampling position close to the feeding point and thus the composition is considered compositions of gases of primary pyrolysis.

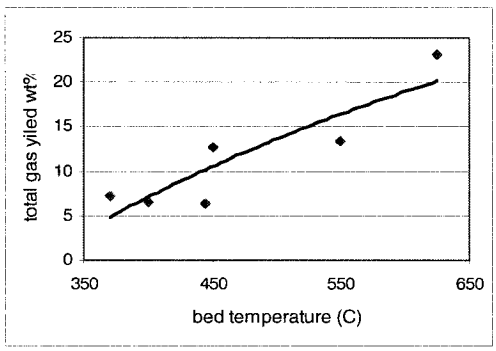

Figure A-2: Total volatile yield as a function of bed temperature

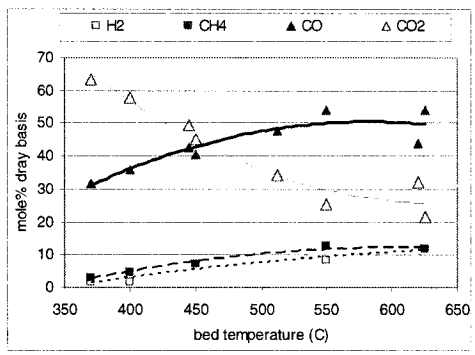

FigureA-3: Molar fraction of gases in tar free dry basis as a function of bed temperature

Reasonable agreements exist between the previous experimental results with TGA-GC and Figure A-3. In both cases, CO_2 is the most abundant component in the product gas.

The higher concentration of hydrogen at higher temperatures also agrees with TGA-GC results where the hydrogen release temperature was between 700-850°C. Li *et al.* (2001) have also reported the same trend for the change of CO_2, CO and H_2 concentration with temperature using an equilibrium model in gasification of coal. However, the trend for CH_4 seems to be different. The CH_4 concentration in the

product gas increases with temperature, which is contradictory to the drop in CH_4 concentration with temperature reported by Li *et al.* (2001).

Figure A-4 presents the experimental results and model prediction for CO2 and

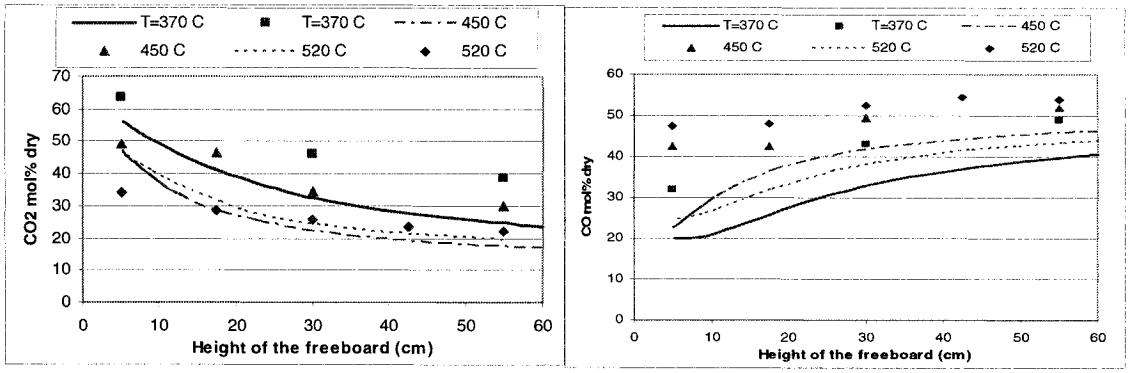

FigureA-4: Measured and calculated concentration of CO_2 and CO in dry basis at two different temperatures. Symbols for experimental and lines for calculated results.

CO. Figure A-5 shows the same type of results for the CH_4. The predicted and experimental concentrations of CO and CH_4 increase and that of CO_2 drops along the height of the freeboard. The concentration of H_2 also increases but very slightly along the freeboard. Sett and Bhattacharya (1988) have observed the same changes in the

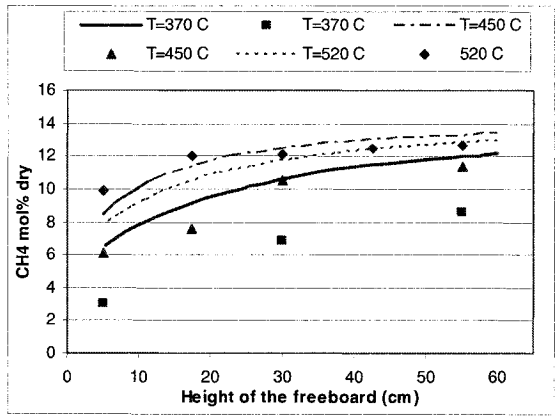

FigureA-5: Measured and calculated concentration of CH_4, Symbols for experimental and lines for

concentration in a charcoal fluidized bed gasifier. The drop in CO_2 concentration is related to the water-gas shift reaction and reveals the importance of this reaction. The gasification reaction or the reaction between char and H_2O can proceed very slightly at the bed and freeboard temperature and this can explain the slight increase of the H_2 concentration.

Although the model predicts the trend for each gas successfully, it can not accurately predict the concentrations. However, at lower temperatures (370°C and 450 °C) the deviations from the experimental results are larger. The tar cracking model developed by Boroson *et al.* (1989) is in the temperature range of 500-800°C. This paper adopted their model at lower temperatures. This can explain the larger deviation between predicted and measured values at lower temperature.

A.6 Conclusions

In this study, the kinetic model developed previously for the primary pyrolysis of beech wood was applied to a bubbling fluidized bed reactor. This complete model includes heat transfer, primary and secondary pyrolysis kinetics. The volatile gases and tar resulted from the primary pyrolysis take part in the tar cracking and water-gas shift reactions in the freeboard of the reactor. The experimental work reveals the important role of the freeboard in the cracking of tar and improving the gas composition. The model for the freeboard of a bubbling fluidized bed reactor predicts the concentrations trend of the main gases components in the freeboard.

Notation

C_i	concentration of component i, $kmol/m^3$
C_p	heat capacity, J/kg K
d	diameter, m
E	activation Energy, kJ/mol
h_{conv}	convective heat transfer coefficient, W/m^2 K
K_g	thermal conductivity of gas, W/m K
$k_{0,i}$	frequency factor for component i, 1/s
M_i	molecular weight of component I, kg/kmol
N	Total number of data points in TGA experiments
n_p	parameter in Equation (A.6)
r_i	rate of reaction for component i
r_{w-g}	water gas shift's reaction rate
Re	Reynolds number
Pr	Prandtl number
T_b	bed temperature, K
T_p	particle temperature, K
u	gas velocity in the freeboard, m/s
V_i	release volatile matter, wt%
V_i^*	ultimate final yield for component i in pyrolysis
V_p	volume of the wood particle, m^3
X_{tar}	mass fraction of the tar in the gas stream, wt%

X_{vm}	volatile content in the wood, wt%
y_i	total volatile yield for component i
Z	height of the freeboard, m

Greek letters

α_i	contribution coefficient in Equation (A.9)
ε	emissivity coefficient
φ	Parameter in Equation (A.6)
ρ_i	density of component i, kg/m^3
υ	stoichiometric coefficient

References

Antal, M.J., Varhegyi, G., 1995, Cellulose pyrolysis kinetics: The current state of knowledge, *Ind. Eng. Chem. Res.*, 34,703.

Babu, B.V. and Chaurasia, A.S., 2004, Dominant design variables in pyrolysis of biomass particles of different geometries in thermally thick regime, *Chem Eng Sci*, 59(3), 611-622.

Biba, V., Macak, J., Kolse, E.and Malecha, J., 1978, Mathematical model of gasification of coal under pressure, *Ind. Eng. Chem. Process Des. Dev,* 17, 92.

Boroson, M.L., Howard, J. B., Longwell, J.P.and Peters, W.A, 1989, Product yields and kinetics from the vapor phase cracking of wood pyrolysis Tars, *AIChE*, 35(1), 120-128.

Di Blasi, C.and Branca, C., 2003, Temperature of wood particles in a hot sand bed fluidized by Nitrogen. *Energy & Fuel,* 17(1), 247-254.

Di Blasi, C., 2004, Modeling wood gasification in a countercurrent fixed-bed reactor, *AIChE,* 50(9), 2306-2319.

Gronli, M.G., Varhegyi, G.and Di Blasi, C., 2002, Thermogravimetric analysis and devolatilization kinetics of wood, *Ind. Eng. Chem. Res.,* 41(17), 4201-4208.

Koufopanous, C.A., Papayannakos N., Maschio G.and Lucchesi A., 1991, Modeling of pyrolysis of biomass particles. Studies on kinetic, thermal and heat transfer effects, *Can J Chem Eng,* 69, 907.

Kunii D.and Levenspiel O., 1991. *Fluidization engineering.* 2nd ed. MA, Butterworth-Heinemann series in chemical engineering.

Li, X., Grace, J.R., Watkinson, A.P.and Ergudenler, A., 2001, Equilibrium modeling of gasification: a free energy minimization approach and its application to a circulating fluidized bed coal gasifier, *Fuel*, 80(2), 195-207.

Linjewile, T.M., 1993, *Temperature of burning carbonaceous particles in a fluidized bed combustor*, Thesis (PhD). The University of Adelaide.

Roth, J., Steiner G., Wolfinger, M.G.and Staudinger, G., 2002, Tar cracking from fast pyrolysis of large beech wood particles. *J. Anal. and Appl. Pyrolysis*. 62(1), 83-92.

Ross, D.P., Heidenreich, C.A.and Zhang, D.K., 2000, Devolatilization times of coal particles in a fluidized bed, *Fuel*, 79, 873-883.

Sett, A. and Bhattacharaya, S.C., 1988, Mathematical modeling of a fluidized bed charcoal gasifier, A*pplied energy*, 30(3), 161-186.

Shin, D.and Choi, S., 2000, Combustion of simulated waste particles in a fixed bed, *Combustion & Flame*, 121(1), 167-180.

Van Den Aarsen F.G., Beenackers; A.C.M.and van Swaaij, W. P. M., 1982, Wood pyrolysis and carbon dioxide char gasification in a fluidized bed, *In: fundamentals of thermochemical biomass conversion*. Elsevire applied science publisher, 691.

Wurzenberger, J.C, Wallner S., Raupenstrauch, H.and Khinast J.G, 2002, Thermal conversion of biomass: comprehensive reactor and particle modeling, *AIChE,* 48(10), 2398-2411.

APPENDIX B

DETAILS OF BUBBLING FLUIDIZED BED REACTOR

The drawings of the fluidized bed reactor used in this study for biomass gasification is presented in detail. The following drawings illustrate different parts of the fluidized bed reactor including windbox, bed section, freeboard zone, and disengagement zone.

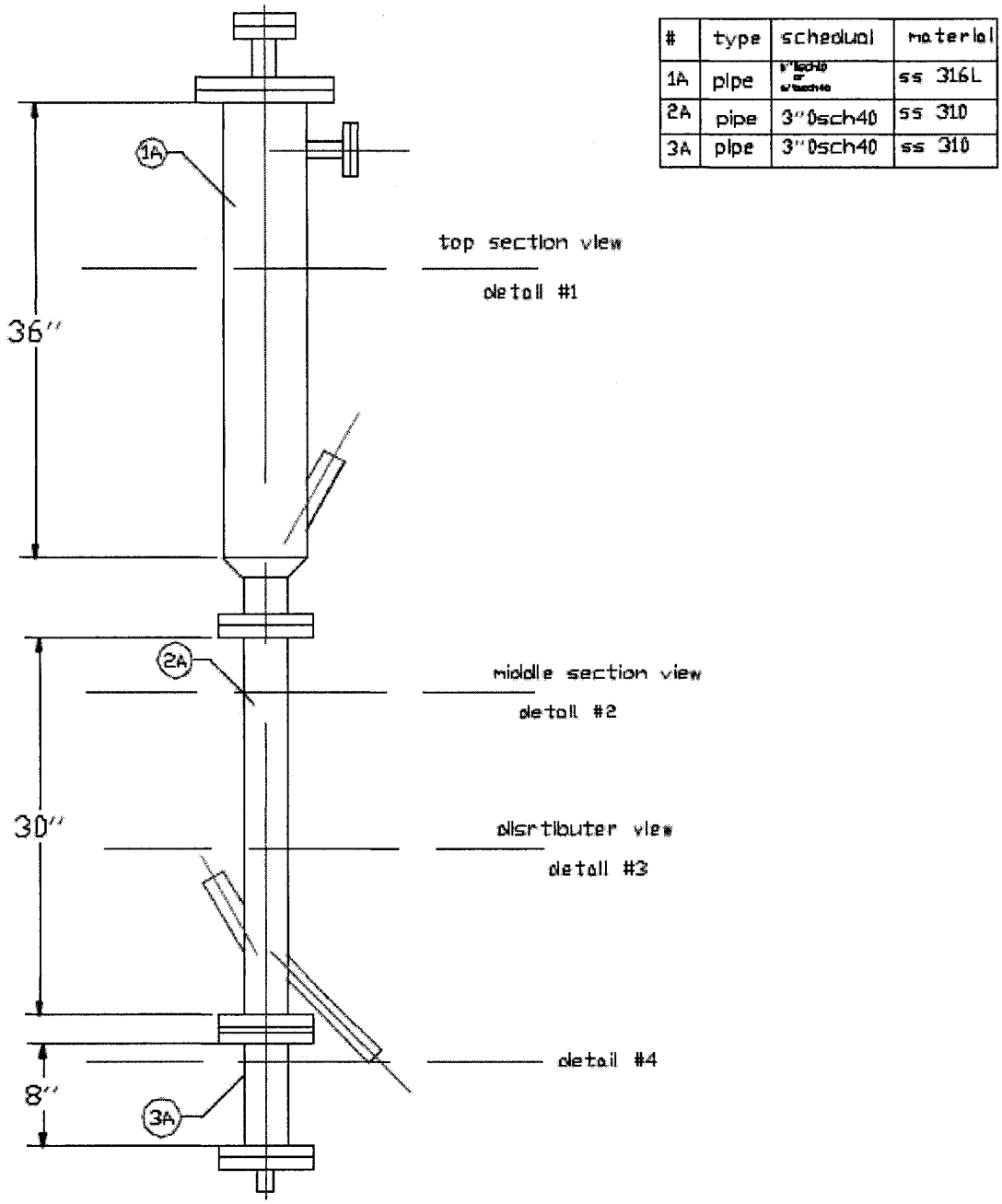

Figure B-1: Overall view and sizing of the reactor.

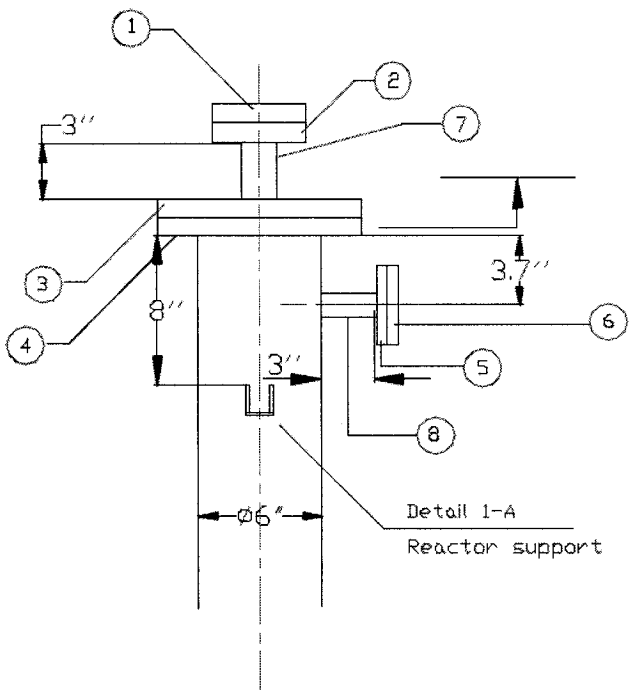

#	Qty	material	Item	standard
1	1	ss316L	flange	Blind ANSI 150, 1.5"
2	1	ss316L	flange	slip on ANSI 150, 1.5"
3	1	ss316L	flange	Blind ANSI 150, 6"
4	1	ss316L	flange	slip on ANSI 150, 6"
5	1	ss316L	flange	slip on ANSI 150, 1"
6	1	ss316L	flange	Blind ANSI 150, 1"
7	1	ss316L	pipe	OSCH40 1.5"
8	1	ss316L	pipe	OSCH40 1"

Figure B-2: The top view of disengagement zone and sizing.

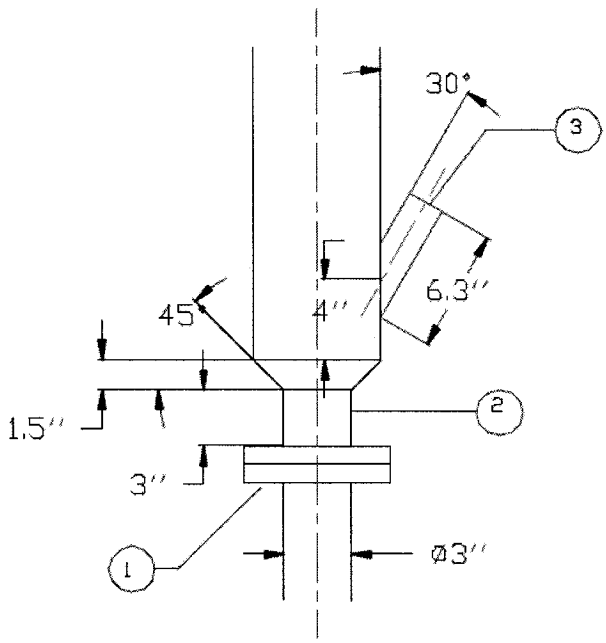

#	Qty	item	material	standad
1	2	flange	ss310	slip on ANSI 150 3"
2	1	pipe	ss316L	0SCH40 3"
3	1	pipe	ss316L	threaded 0SCH40 15"

Figure B-3: view of the bottom part of disengagement zone and sizing

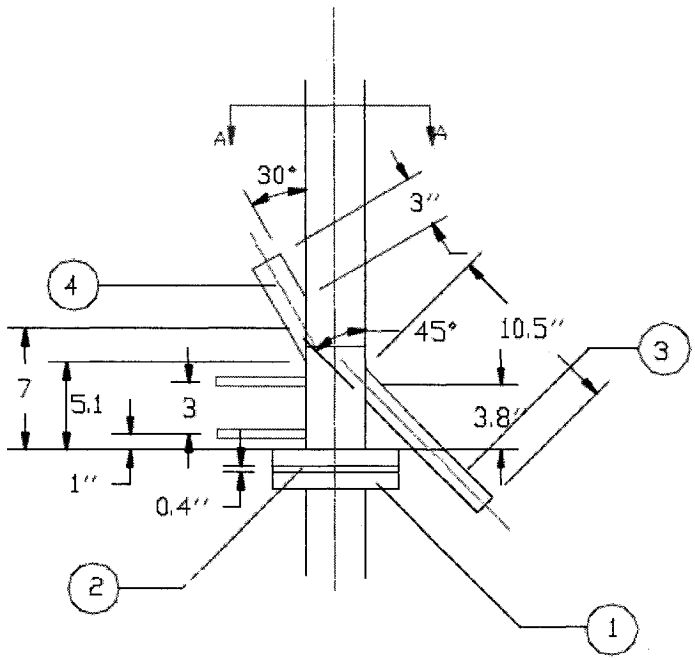

#	Qty	Item	material	standard
1	2	flange	ss310	slip on ANSI 150, 3"
2	1	distributor	ss310	according to drawing
3	1	pipe	ss310	15"OSDH40 Threaded
4	1	pipe	ss310	1" OSDH40 Threaded

Figure B-4: Detail of bed section

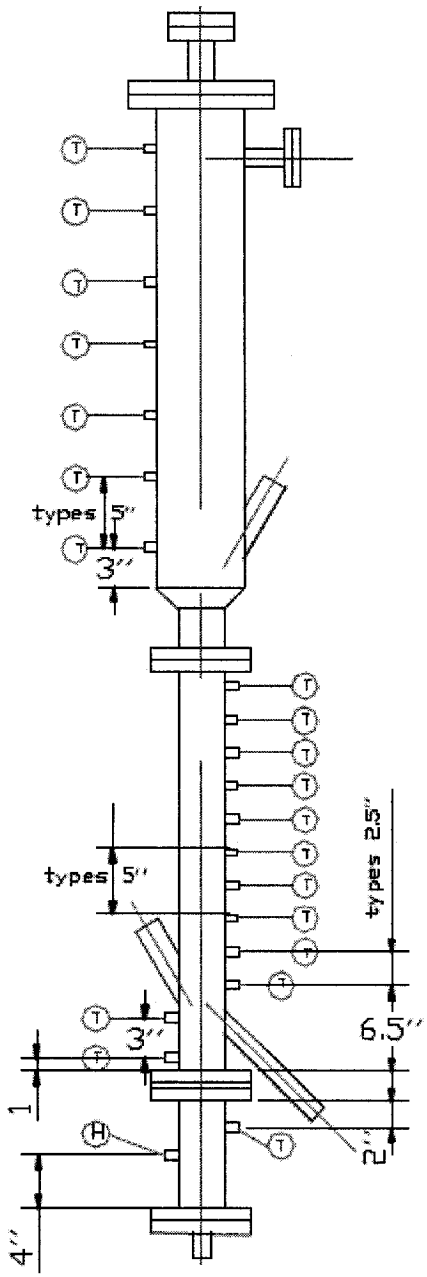

#	Item	Qty	material	standard
T	coupling	20	ss 316L	1/8 NPT female
H	coupling	1	ss 316L	3/4 NPT female

Figure B-5: Details location of thermocouples and sampling ports

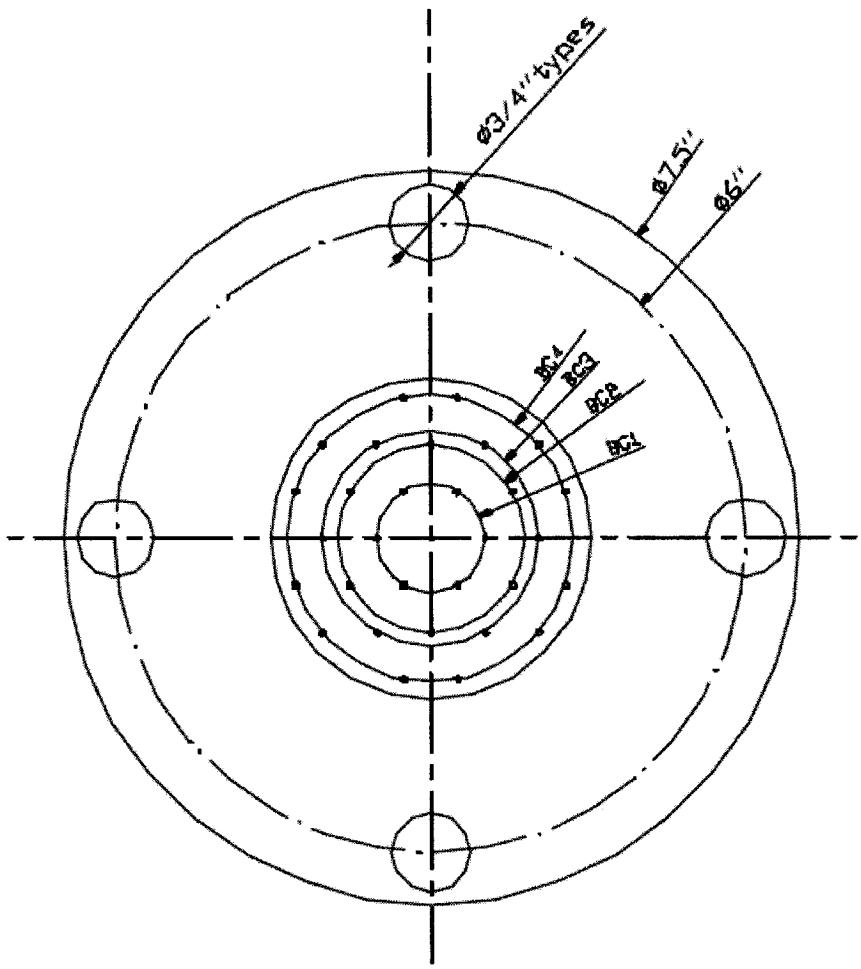

Distributor Dimensions			
Plate thickness	3/8 "		
Holes Diameter	3/64 "		
BCs Dimension	R	Angle	#Hole
BC1	1.031	30	6
BC2	1.785	0	6
BC3	2.062	30	6
BC4	2.729	10.8 49.1	6 6

Figure B-6: Details of distributor and supporting flanges.

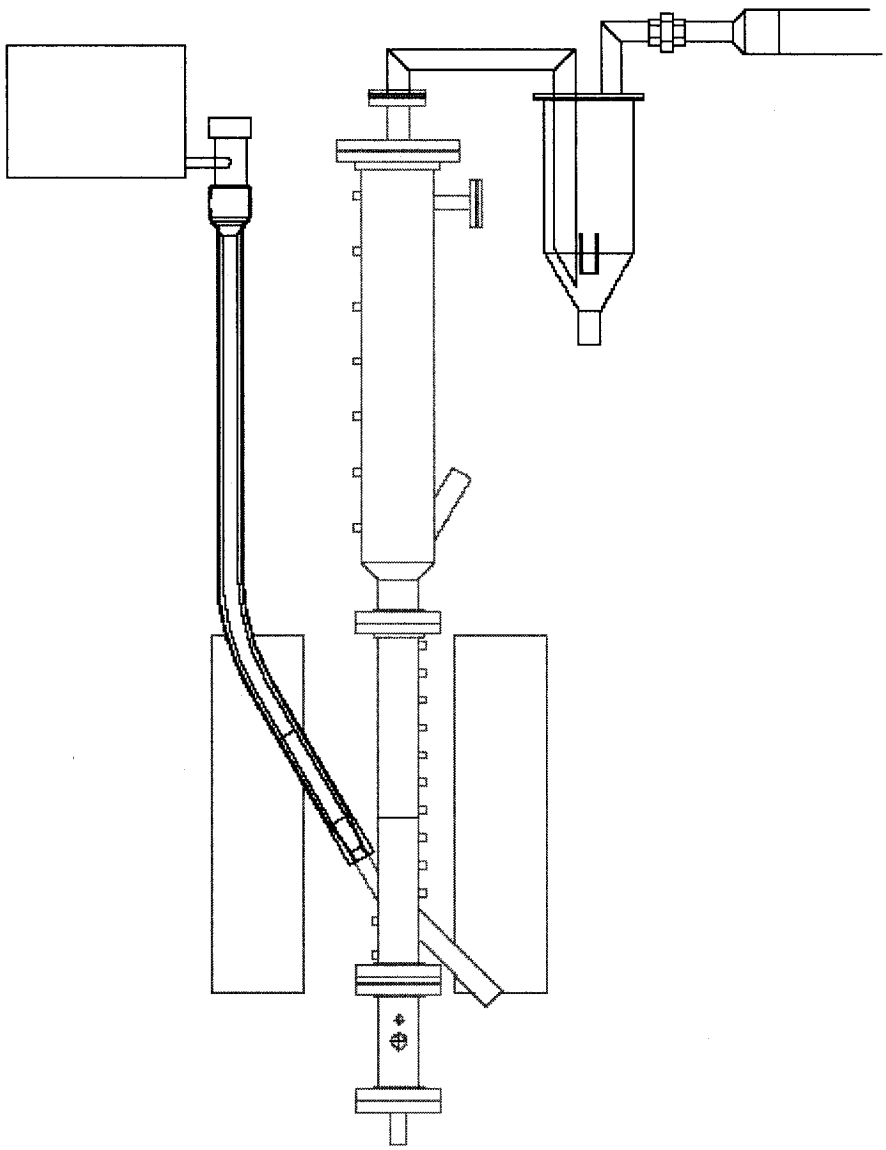

Figure B-7: Overall presentation of the reactor, heating elements ,solid feeder and cyclone

APPENDIX C

MASS SPECTROMETRY VERIFICATION OF GAS EVOLUTION DURING PYROLYSIS

Mass Spectrometer (MS) was used to verify quantitatively the evolution of gases during pyrolysis obtained by Gas chromatography (GC) in chapter 5. A good agreement was found between the results of MS and GC. Figure C1 shows the evolution of masses m/e=2, 15, 26, 44, which are related to H_2, CH_4, CO and CO_2, respectively, at two different heating rates. This figure also shows that gas yields (total surface area) increases by increasing heating rate. The intensity has been normalized based on initial sample size and the maximum detected peak during each experiment.

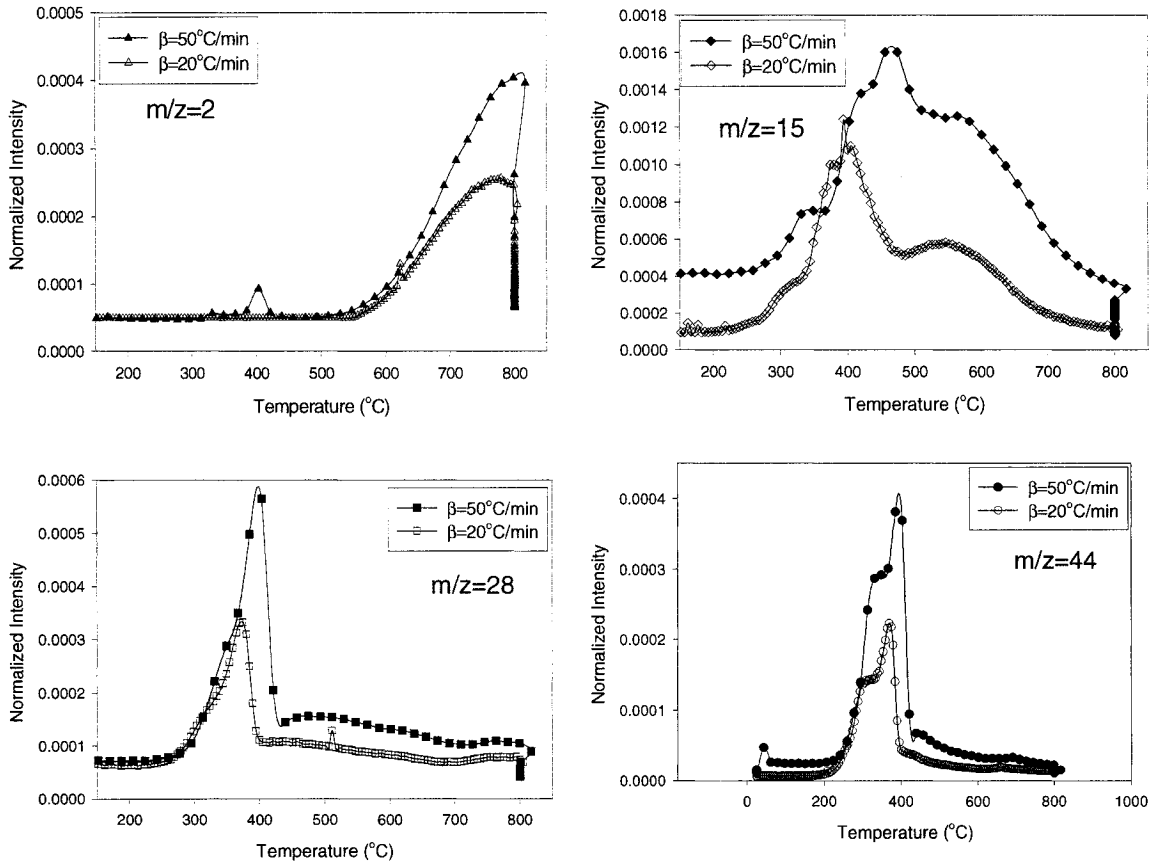

Figure C-1: Mass spectrometry results on gas evolution of beech wood particles at two different heating rates. The results are very quite comparable with the GC results and prove the accuracy of GC results.

APPENDIX D

HEATING VALUE CALCULATON FOR SOLID FUELS

The heating value of a fuel can be obtained using a calorimeter. If the calorimeter is not available, one needs the ultimate analysis of the fuel to calculate the high heating value using Dulong formula (Perry and Chilton 1973):

$$HHV(MJ/kg)=33.86 \times C + 144.4 \times (H-O/8) + 9.428 \times S$$

C, H, O and S are mass fraction obtained by ultimate analysis.

Recently, Parikh *et al.* (2005) have reviewed all the correlations for prediction of high heating values.

APPENDIX E

CALIBRATIONS OF ROTAMETERS AND ORIFICE PLATES

The following are the description of the manometers and orifice plates used in the experimental part of this study:

- A rotameter to measure air inlet flow rate to the reactor (FL-3840ST).
- A rotameter to measure gas outlet from the sampling ports (FL-3610ST).
- An orifice plate to measure air inlet flow rate to the reactor (installed on the ½'' tube).
- An orifice plate to measure air inlet flow rate to the reactor (installed on the ¾'' tube).

The calibration information of the above mentioned rotameters and orifice plates are presented in the following pages.

Table F-1: Calibration of rotameter FL-3840ST with air at 25 psig pressure

	*T→	25°C	100°C	200 °C	300 °C	400 °C	500 °C	600 °C	700 °C	800 °C
Opening %	Mass flow rate (kg/s)	**U_1 (m/s)	U_1 (m/s)	U_1 (m/s)	U_1 (m/s)	U_1 (m/s)	U_1 (m/s)	U_1 (m/s)	U_1 (m/s)	U_1 (m/s)
0	0	0	0	0	0	0	0	0	0	0
10	3.97E-05	0.0074942	0.0093	0.0118	0.01441	0.0169	0.0194	0.02195	0.0244	0.0269
20	9.24E-05	0.017444	0.0218	0.027	0.0335	0.039	0.0452	0.05110	0.0569	0.062
30	0.0001464	0.027645	0.0346	0.043	0.0531	0.062	0.0717	0.08098	0.0902	0.0995
40	0.0002018	0.038096	0.0476	0.0604	0.0732	0.086	0.0988	0.11160	0.1243	0.1371
50	0.0002585	0.048799	0.061	0.077	0.093	0.110	0.1265	0.14295	0.1593	0.1757
60	0.0003165	0.059751	0.0747	0.094	0.114	0.134	0.1549	0.17504	0.1950	0.2151
70	0.0003758	0.070954	0.0888	0.112	0.136	0.160	0.1840	0.20786	0.2316	0.2554
80	0.0004365	0.082408	0.1031	0.130	0.158	0.186	0.2137	0.24141	0.2690	0.2967
90	0.0004985	0.094113	0.1177	0.149	0.1809	0.212	0.2441	0.27570	0.3072	0.338
100	0.0005618	0.10607	0.1327	0.16	0.2039	0.2395	0.2751	0.31073	0.3463	0.3819
110	0.0006265	0.11827	0.1480	0.187	0.227	0.267	0.3067	0.34647	0.3861	0.4258
120	0.0006925	0.13073	0.1636	0.207	0.2513	0.295	0.3391	0.38297	0.4268	0.4707
130	0.0007598	0.14344	0.1795	0.227	0.275	0.324	0.3720	0.42021	0.4683	0.516
140	0.0008284	0.15639	0.1957	0.248	0.3007	0.353	0.4056	0.45814	0.5106	0.5631
150	0.0008984	0.1696	0.2122	0.269	0.3261	0.383	0.4399	0.49684	0.5537	0.6106

*T: Temperature in the bed.

**U_1 velocity of gas in the reactor at the condition of bed.

Table F-2: Calibration of rotameter FL-3610ST for product gas flow measurements in the sampling line

opening %	Mass flow rate (kg/s)	*U_2(m/s)
0	6.59E-07	0.017903
5	1.15E-06	0.031281
10	1.73E-06	0.047071
15	2.39E-06	0.064924
20	3.11E-06	0.084491
25	3.88E-06	0.10542
30	4.69E-06	0.12737
35	5.52E-06	0.14998
40	6.36E-06	0.17291
45	7.20E-06	0.19581
50	8.03E-06	0.21833
55	8.83E-06	0.24012
60	9.59E-06	0.26083
65	1.03E-05	0.28011

*U_2: gas velocity at the ambient temperature in a ¼'' sampling tube.

Table F-3: Calibration of orifice plate (½'' tube) with air at 25 psig pressure

	*T→	T=25°C	T=100 °C	T=200 °C	T=300 °C	T=400 °C	T=500 °C	T=600 °C	T=700 °C	T=800 °C
$\Delta P(In\ H_2O)$	Mass flow rate (kg/s)	U_1(m/s)	U_1 (m/s)	U_1 (m/s)	U_1 (m/s)	U_1 (m/s)	U_1 (m/s)	U_1 (m/s)	U_1 (m/s)	U_1 (m/s)
0.3	0.0007941	0.149	0.186	0.236	0.286	0.336	0.386	0.436	0.487	0.537
2.45	0.0015881	0.29	0.373	0.473	0.573	0.673	0.773	0.873	0.974	1.074
4	0.0020646	0.38	0.485	0.615	0.745	0.875	1.006	1.136	1.266	1.396
5	0.0022234	0.41	0.522	0.662	0.803	0.943	1.083	1.223	1.363	1.503
7.15	0.0028587	0.536	0.672	0.852	1.032	1.21	1.392	1.573	1.753	1.933
12.05	0.0033351	0.62	0.784	0.994	1.204	1.41	1.625	1.835	2.045	2.255
15.45	0.0038115	0.71	0.896	1.136	1.376	1.61	1.857	2.097	2.337	2.578
17.8	0.0041292	0.775	0.970	1.231	1.491	1.751	2.012	2.272	2.532	2.792
23.9	0.0047644	0.89	1.12	1.420	1.720	2.021	2.321	2.621	2.922	3.222
29.1	0.0053997	1.01	1.26	1.609	1.950	2.290	2.631	2.971	3.311	3.652
32.9	0.0057173	1.07	1.34	1.704	2.065	2.425	2.785	3.146	3.506	3.867
40.2	0.0063526	1.19	1.49	1.894	2.294	2.69	3.095	3.495	3.896	4.296
45.3	0.0066702	1.2	1.56	1.988	2.409	2.829	3.250	3.670	4.091	4.511
51	0.006829	1.28	1.60	2.036	2.466	2.897	3.327	3.758	4.188	4.619

*T: Temperature in the bed.

**U_1 velocity of gas in the reactor at the condition of bed.

Table F-4: Calibration of orifice plate (3/4'' tube) with air at 25 psig pressure

	*T→	T=25°C	T=100 °C	T=200 °C	T=300 °C	T=400 °C	T=500 °C	T=600 °C	T=700 °C	T=800 °C
ΔP(In H_2O)	Mass flow rate (kg/s)	**U_1(m/s)	U_1 (m/s)	U_1 (m/s)	U_1 (m/s)	U_1 (m/s)	U_1 (m/s)	U_1 (m/s)	U_1 (m/s)	U_1 (m/s)
0.7	0.0019058	0.357	0.4891	0.568	0.7513	0.80	0.928	1.04	1.16	1.28
1.4	0.002541	0.477	0.6521	0.757	1.0018	1.07	1.238	1.39	1.55	1.71
3.8	0.0038115	0.715	0.978	1.136	1.502	1.61	1.857	2.09	2.33	2.57
3.9	0.0041292	0.775	1.059	1.231	1.6280	1.75	2.01	2.27	2.53	2.792
5.7	0.0047644	0.894	1.222	1.420	1.8784	2.02	2.32	2.62	2.92	3.22
7.3	0.0057173	1.07	1.467	1.704	2.254	2.42	2.78	3.14	3.50	3.86
8.9	0.0060349	1.133	1.548	1.799	2.3793	2.56	2.94	3.32	3.70	4.08
10.9	0.0069878	1.312	1.793	2.083	2.7550	2.96	3.40	3.84	4.28	4.72
13.4	0.0073055	1.372	1.874	2.178	2.8803	3.09	3.55	4.02	4.48	4.94
15.8	0.0082583	1.551	2.119	2.462	3.256	3.50	4.02	4.54	5.06	5.58
19.8	0.0090524	1.7005	2.323	2.699	3.569	3.84	4.410	4.98	5.55	6.12
22.6	0.0095288	1.79	2.445	2.841	3.757	4.04	4.643	5.24	5.84	6.44
25.2	0.010323	1.939	2.649	3.077	4.0699	4.37	5.03	5.68	6.33	6.98
31.8	0.011435	2.14	2.934	3.409	4.508	4.85	5.57	6.29	7.01	7.73
34.5	0.01207	2.26	3.097	3.598	4.758	5.12	5.88	6.64	7.40	8.16
39.4	0.012546	2.35	3.220	3.740	4.94	5.32	6.11	6.90	7.69	8.48
40.1	0.012853	2.41	3.298	3.832	5.067	5.45	6.26	7.07	7.88	8.69
47	0.013591	2.55	3.488	4.052	5.358	5.76	6.62	7.47	8.33	9.19
48.9	0.013886	2.60	3.563	4.140	5.474	5.89	6.76	7.64	8.51	9.39
53.5	0.014624	2.74	3.753	4.360	5.76	6.20	7.12	8.04	8.96	9.89
56.6	0.015215	2.85	3.904	4.536	5.99	6.45	7.41	8.37	9.33	10.29

*T: Temperature in the bed.

U_1 velocity of gas in the reactor at the condition of bed.